Improved Time-Frequency Approaches for Characterization of Multiple Higher Order Chirp Waveforms with Applications in Radar Signal Processing

A thesis submitted in partial fulfillment of
the requirements for the degree of

Doctor of Philosophy

by

Peeyush Sahay
(Roll No. 133074009)

Supervisors:
Prof. Vikram M. Gadre and Shri P. Radhakrishna, LRDE

Department of Electrical Engineering
Indian Institute of Technology, Bombay
2019

This work is dedicated to my family. I am forever indebted to them for their continuous motivation and support. It would not be possible for me to continue my education after a long gap without their sacrifice.

I dedicate this work to my supervisors Prof.V.M.Gadre and P.Radhakrishna

Declaration of the Academic Ethics

I declare that this written submission represents my ideas in my own words and where others' ideas or words have been included, I have adequately cited and referenced the original sources. I declare that I have properly and accurately acknowledged all sources used in the production of this thesis.

I also declare that I have adhered to all principles of academic honesty and integrity and have not misrepresented or fabricated or falsified any idea/data/fact/source in my submission. I understand that any violation of the above will be a cause for disciplinary action by the Institute and can also evoke penal action from the sources which have thus not been properly cited or from whom proper permission has not been taken when needed.

Date: .....

Peeyush Sahay

(Roll No. 133074009)

Abstract

Non-stationary signals can be analyzed using time-frequency analysis for classification, characterization, and feature extraction purposes in many fields. Non-stationary signals such as higher order polynomial chirps are present in many practical systems like radar, sonar, and biomedical signal processing. This thesis focuses on higher order time-frequency methods and their applications in synthetic aperture radar (SAR) and conventional radar for representation, extraction, characterization, and parameter estimation of multicomponent frequency modulated signals. The proposed methods can be applied in different applications such as sonar and biomedical signal processing.

The first aim of the thesis is to focus on higher order time-frequency spectrogram for analyzing closely spaced multicomponent frequency modulated signals. The second aim of the thesis is to develop a technique for SAR ground moving target velocity and acceleration parameter detection and their imaging based on estimated parameters. The third aim of the thesis is to focus on the ambiguity function for analyzing multicomponent higher order radar waveform and its characterization. The fourth aim of the thesis is to focus on the joint estimation of parameters of time-delayed weak (low signal to noise ratio) moving target using a matched filtering approach in the case of conventional ground based radar.

Adaptive generalized fractional spectrogram and its application is the first contribution of this thesis (Chapter 2). According to literature, the generalized time-frequency transform (GTFT) is a powerful tool to analyze a large variety of frequency modulated signals. However, it is not adequate to represent the variation of frequency over time for non-stationary signals. There is a need to develop a high concentration, high resolution, cross term free time-frequency distribution for analyzing multicomponent frequency modulated signals. To solve this problem, short-time GTFT and short-time GTFT based adaptive generalized fractional spectrogram (AGFS)

are proposed in this thesis. It is also a generalization of the short-time Fourier transform based spectrogram and the short-time fractional Fourier transform based spectrogram. With the help of simulated and real data examples, the performance of AGFS is demonstrated in comparison to other time-frequency distributions for resolving, representing, and extracting individual components of multicomponent quadratic chirps.

SAR ground moving target detection and its imaging using AGFS based approach are presented as the second contribution of this thesis (chapter 3). SAR is used for taking the image of stationary targets, but it produces blurriness in the image in the presence of moving targets. Blurriness further increases, if moving targets have higher order motion. A novel approach is proposed for estimation of SAR ground moving target's radial velocity, tangential velocity, and tangential acceleration parameters, and SAR moving target imaging using AGFS based method. The performance of the proposed approach with AGFS is compared with GTFT based parameter estimation approach in terms of mean square error, signal to noise ratio gain, impulse responses, and region of convergence. Finally, SAR multiple ground moving targets imaging based on AGFS is presented.

Generalized fractional ambiguity function and its applications are the third contribution of this thesis (Chapter 4). According to literature, the ambiguity function is an essential time-frequency analysis tool to analyze the radar waveform properties in radar applications. It can be used effectively and reliably to analyze properties like the peak to side-lobe ratio, time delay resolution, Doppler resolution, and tolerance characteristic. However, it fails to analyze higher order chirp waveforms and is unable to estimate their parameters. To solve this problem, a GTFT based generalized fractional ambiguity function (GFAF), and generalized fractional Wigner-Ville distributions are proposed. GFAF is also a generalization of the Fourier transform based ambiguity function, and the fractional Fourier transform based ambiguity function. Examples are presented to demonstrate the performance of GFAF in analyzing cubic frequency modulated waveforms and estimating parameters of simulated as well as real multicomponent cubic frequency modulated signals. The superiority of GFAF over existing methods is demonstrated by comparing the mean square error and signal to noise ratio gain to existing time-frequency distributions.

GTFT based matched filtering, and its application for joint estimation of low signal to noise ratio moving target's parameters is presented as the fourth contribution of this thesis (chapter

5). The complete mathematical derivation of the GTFT domain matched filter detector for radar applications has been presented. In terms of signal to noise ratio gain, GTFT matched filtering is compared with time domain matched filtering, GTFT, and fractional Fourier transform transformation gain in case of time domain additive white Gaussian noise thus showing its advantage over current methods. As an application of GTFT matched filtering, signal to noise ratio gain degradation of a moving target is compared with conventional time domain matched filter performance in case of varying Doppler frequency. Finally, a new waveform named double quadratic chirp has been proposed to detect time delay, velocity, acceleration, and jerk of the moving target simultaneously using GTFT based matched filtering.

In summary, various techniques of representation, extraction, characterization, and parameter estimation of multicomponent frequency modulated signals are proposed in this thesis. Conclusion and future works are also suggested in this thesis (chapter 6).

Acknowledgments

I want to thank Prof.V.M. Gadre for giving me the opportunity to work on this topic. He has given me complete freedom to choose my technical path. He has provided me with an excellent association during my research. This work was not possible without his valuable guidance and optimistic trust in me.

I want to thank P. Radhakrishna for allowing me to work on the SAR system and providing all the necessary support to continue my research work at LRDE.

I would like to thank T. Meghasyam, Gaurav Pooniwala, Jaivardhan Lal, Omkar Kothekar, S Teza Bhamidi, Izaz Ahamed Shaik Rasheed, Pranav Kulkarni, Anubhav Jain, Shubham Anand Jain, Ankita Bansal, Amarnath Kumar, Ameya Anjarlekar, and Ayush Agarwal for their invaluable support and uncountable hours of technical discussion to complete this work. I would like to also appreciate them for maintaining my motivation and reminding me about my ability. This thesis could not have been completed without their support. I am also thankful to Vasudev R., Shubham Kar, Shaan Ul Haque, Adway Girish, Parth Dodhia, and Titas Chakraborthy for improving the quality of this thesis.

I want to thank my research proposal committee for their constant support and guidance for improving the quality of the thesis.

Lastly, I am indebted to my lovely parents, parents-in-law, wife Gaurangi, son Pranay, nephew Pranjal, brother Anush and sister-in-law Deepti for their unconditional support, sacrifice, and love during my study.

Contents

List of Figures

List of Tables

List of Abbreviations

TFD	Time-frequency distribution
IF	Instantaneous frequency
LFM	Linear frequency modulation
QFM	Quadratic frequency modulation
CFM	Cubic frequency modulation
FT	Fourier transform
LCT	Linear canonical transform
CPF	Cubic phase function
CWT	Continuous wavelet transform
PSP	Principle of stationary phase
PPS	Polynomial phase signal
PFT	Polynomial Fourier transform
LPFT	Local polynomial Fourier transform
FrFT	Fractional Fourier transform
GTFT	Generalized time-frequency transform
ck-GTFT	Cubic kernel generalized time-frequency transform
STFT	Short-time Fourier transform
STFrFT	Short-time fractional Fourier transform
STGTFT	Short-time generalized time-frequency transform
AGFS	Adaptive Generalized fractional spectrogram
ck-AGFS	Cubic kernel based adaptive generalized fractional spectrogram
LO-AGFS	Locally optimized adaptive generalized fractional spectrogram
ECM	Energy concentration measure
TBP	Time-bandwidth product
AWGN	Additive white Gaussian noise

SNR	Signal to noise ratio
MSE	Mean square error
WVD	Wigner-Ville distribution based on Fourier tranform kernel
GFWVD	Generalized fractional Wigner-Ville distribution
AF	Ambiguity function based on Fourier tranform kernel
HAF	Higher order ambiguity function
GFAF	Generalized fractional Fourier ambiguity function
ck-GFAF	Cubic kernel based generalized fractional ambiguity function
CRLB	Cramer-Rao lower bound
SAR	Synthetic aperture radar
RCM	Range cell migration
RCMC	Range cell migration correction

Chapter 1

Introduction

1.1 Technical definitions

1.1.1 Classification of frequency modulated signals

Modulated signals whose frequency varies with respect to time, form a wide category of signal called LFM signals. The most common frequency modulated signals are chirp signals. A chirp can be classified into various kinds, depending on the frequency variation. Classifications of chirps are presented below in Table 1.1. Linear chirps are the most commonly found chirp signals. A general model of linear chirps is shown in Eq. (1.1):

$$\varphi(t) = 2\pi \left(\frac{\alpha}{2} t^2 + f_0 t + \phi_0 \right), \tag{1.1}$$

where $\alpha, \phi_0, f_0 \in R \;\; and \;\; \alpha \neq 0$,

$$f(t) = \frac{1}{2\pi} \frac{d\varphi(t)}{dt} = \alpha t + f_0, \tag{1.2}$$

where $\varphi(t)$ is instantaneous phase, α is the rate of change of frequency (chirp rate), f_0 is the start frequency or Doppler frequency, ϕ_0 is initial phase, and $f(t)$ is instantaneous frequency (IF) of signal. In Table 1.1, α_1 is Doppler frequency, α_2 is linear chirp rate, α_3 is quadratic rate, α_4 is cubic rate, ω_0 is fundamental frequency of sinusoidal frequency modulated signal, and a, c_1, c_2, c_3, c_4 are constants.

Table 1.1: Classification of chirp signals

Chirp signals	
Type	$\varphi(t)$
Linear frequency modulated	$\alpha_1 t + \alpha_2 t^2$
Quadratic frequency modulated	$\alpha_1 t + \alpha_2 t^2 + \alpha_3 t^3$
Cubic frequency modulated	$\alpha_1 t + \alpha_2 t^2 + \alpha_3 t^3 + \alpha_4 t^4$
Higher order Chirp	$\Sigma \alpha_j t^j$, where $j \geq 3$
Logarithmic chirp	$c_1 + c_2^t$
Hyperbolic chirp	$c_3 \cdot ln(1 + c_4 t)$
Sinusoidal frequency modulated signal	$a \cdot \sin(\omega_0 t)$

1.1.2 Need and classification of time-frequency distributions

Need of time-frequency distribution:

Non-stationary signals such as higher order polynomial chirps are extensively used in many practical systems like radar, sonar and bio-medical signal processing [6, 12, 32, 80, 84, 107]. Fourier transform is used to carry out spectral analysis of signals; however, a large variety of signals, including chirp signals, cannot be analyzed by Fourier transform. As Fourier transform doesn't provide information about the variation of frequency with respect to time and it is not suitable to localize a large variety of signals such as chirp signals. Many time-frequency distributions (TFDs) and transforms were proposed in literature to overcome these problems. Time-frequency distribution (TFD) is a visual representation of a signal in time and frequency domain. It gives information about the signal's instantaneous frequency with respect to time.

Classification of time-frequency distribution:

The broad categorization of TFDs and associated transforms are as follows:

1. Linear transform based TFD: Linear TFDs and transforms follow the superposition principle for the linear combination of signals and do not produce cross-terms during multicomponent analysis. If $P_{x_1}(t, f)$ is the TFD of the signals $x_1(t)$, $P_{x_2}(t, f)$ is TFD of signal $x_2(t)$ and

$P_{x_1+x_2}(t,f)$ is TFD of signal $x_1(t) + x_2(t)$ then

$$P_{x_1+x_2}(t,f) = P_{x_1}(t,f) + P_{x_2}(t,f). \tag{1.3}$$

Well-known examples of linear TFDs are short-time Fourier transform, short-time fractional Fourier transform, Gabor transform, and S-transform. All these TFDs are described in the subsequent sections.

2. Quadratic transform based TFD: Quadratic TFDs and transforms do not follow superposition principle for linear combination of signal .If $P_{x_1}(t,f)$ is TFD of signal $x_1(t)$, $P_{x_2}(t,f)$ is TFD of signal $x_2(t)$ and $P_{x_1+x_2}(t,f)$ is TFD of signal $ax_1 + bx_2$,(where a and b are real constants) then

$$P_{x_1+x_2}(t,f) = P_{x_1}(t,f) + P_{x_2}(t,f) + P_{x_1,x_2}(t,f) + P_{x_2,x_1}(t,f), \tag{1.4}$$

where $P_{x_1}(t,f)$ and $P_{x_2}(t,f)$ are called auto-terms and $P_{x_1,x_2}(t,f)$ and $P_{x_2,x_1}(t,f)$ are called cross-terms. Quadratic TFD produces unwanted cross-terms during multicomponent signal analysis.

Many Quadratic TFDs exist such as Wigner-Ville distribution, Pseudo-Wigner-Ville distribution, ambiguity function and Choi-Williams distribution. All these TFDs are described in the subsequent sections.

3. Higher order transform based TFD: Higher order TFDs and transforms are used mainly for time-frequency analysis of higher order chirp signals. Majority of higher order TFDs do not follow the superposition principle and produce cross-terms during multicomponent analysis. Cubic phase function, higher order ambiguity function, and polynomial Wigner-Ville distribution, etc. are the examples of such class of higher order TFDs.

Few higher order TFDs follow superposition principle and do not produce cross-terms during multicomponent analysis. Linear polynomial Fourier transform is an example of such a class of higher order distribution.

1.2 Preliminaries: Linear transform based TFDs

1.2.1 Short time Fourier transform and spectrogram

The Short time Fourier transform (STFT) is the most commonly used mathematical tool for the representation of the non-stationary signals. STFT represents the signal in a time-frequency plane and provides constant time and frequency resolution in a time-frequency plane. STFT uses a sliding window to analyze signal parameter variation over time and energy spectrum is calculated at each time instant. The evaluation of STFT of a signal $x(t)$ is given as

$$F_x(t,f) = \int_{-\infty}^{+\infty} x(\tau) \cdot g(\tau - t) \cdot e^{-i2\pi f\tau} d\tau, \tag{1.5}$$

where τ is the time delay and $g(\cdot)$ is a window-function. The spectrogram is defined as the measure of energy in STFT, the expression of spectrogram presented by Cohen [25] is

$$S_x(t,f) = |F_x(t,f)|^2 = \left| \int_{+\infty}^{+\infty} x(\tau) \cdot g^*(\tau - t) \cdot e^{-i2\pi f\tau} d\tau. \right|^2 \tag{1.6}$$

By multiplying the signal with a window function, the period of integration is reduced from $(-\infty, +\infty)$ to the period of the window function. The window function controls the relative weight imposed on different parts of the signal. Finer time resolution can be achieved by a compact window in the time domain. Similarly, high frequency resolution can be achieved by choosing a wider window in the time domain. Since the uncertainty principle holds true, a trade-off has to be made between fine frequency resolution and fine time resolution, and both can not be achieved simultaneously for any particular window.

1.2.2 Gabor Transform

A special case of STFT is Gabor Transform. Here Gaussian function is taken as a window function, and the signal $x(t)$ is multiplied with this Gaussian function; the obtained function is then transformed using the tool Fourier transform to analyze time-frequency distribution. Gabor transform of $x(t)$ is defined by Gabor [35] as

$$GABOR_x(t,f) = \frac{1}{\sqrt{2\pi}} \int_{-\infty}^{+\infty} e^{\frac{-\pi(\tau-t)^2}{2}} \; e^{-i2\pi f\tau} \; x(\tau) \; \mathrm{d}\tau. \tag{1.7}$$

Gaussian function has infinite time duration, so it is not implementable practically. As shown by S.C. Pei et al. [74], the practical implementation can be done, if level of significance (assume it to be 0.0001) is chosen within Gaussian function range. This level of significance turns out to be in the range (-4.2919, +4.2919) about the mid-point of the Gaussian function. Hence Gabor transform is approximated as follows:

$$GABOR_x(t,f) \approx \frac{1}{\sqrt{2\pi}} \int_{-4.2919+t}^{4.2919+t} e^{\frac{-\pi(\tau-t)^2}{2}}\ e^{-i2\pi f(\tau-t)}\ x(\tau)\ \mathrm{d}\tau. \tag{1.8}$$

This method of choosing a level of significance ensures the practical implementability of Gabor Transforms. Optimum time-frequency resolution, window width can be varied by replacing $-\pi(\tau-t)^2$ by $-\pi\alpha(\tau-t)^2$ where α is chosen depending upon application. Jones and Parks [49], have proposed a "data-adaptive" method to maximize the time-frequency concentration of the locally dominant component, by adaptively varying the parameters of Gaussian function.

Adaptive STFT:

S. Pai et al. [75], proposed low computation, high energy concentrated, adaptive STFT based TFD (ASTFT-TF). The author uses an adaptive Gaussian window, whose variance varies with respect to chirp rate and concentration measurement of signal. The variance of the Gaussian window is time and frequency-dependent. Adaptive STFT with Gaussian window as proposed by the author is:

$$ASTFT-TF(t,f) = \int_{-\infty}^{+\infty} x(\tau)\frac{1}{\sqrt{2\pi}\sigma(t,f)} e^{-\frac{(t-\tau)^2}{2[\sigma(t,f)]}} e^{-i2\pi f\tau} d\tau. \tag{1.9}$$

where $\sigma(t,f)$ is standard deviation of Gaussian window, and is a function of time and frequency. The author uses principal component analysis to estimate the chirp rate of the signal. The author demonstrates that time-frequency varying window-based TFD gives better performance as compared to time-varying or frequency-varying window based TFD in the case of non-linear monocomponent as well as a multicomponent chirp.

1.2.3 Continuous wavelet transform and scalogram

The continuous wavelet transform (CWT) is a translated-dilation distribution of signal $x(t)$, which is given as

$$CWT_x(t,a) = \frac{1}{\sqrt{a}} \int_{-\infty}^{+\infty} x(u)\ \Psi^* \left(\frac{u-t}{a}\right) \mathrm{d}u. \tag{1.10}$$

where a is the scale (dilation factor) for the analyzing wavelet, $\Psi(t)$. To create the wavelet transformation, the wavelet is shifted over the full signal with different dilation factors. The dot-product of shifted and time-scaled versions of $\Psi(t)$ are calculated with the signal $x(t)$. The dot-products are plotted over the time-scale plane. Different wavelet families have been proposed (e.g., Haar, Mexican-Hat, Meyer, Daubechies) with various mathematical properties by Mallat [68]. The squared amplitude of the CWT is the scalogram:

$$SCALOGRAM(t,a) = \frac{1}{a} \left[\int_{-\infty}^{+\infty} x(u)\ \Psi^* \left(\frac{u-t}{a}\right) \mathrm{d}u \right]^2. \tag{1.11}$$

Since the CWT is not plotted over the time-frequency plane, hence the CWT is not a TFD. The identification of frequency is only plausible as an approximation. Lower values of a represent a compressed wavelet with rapidly changing details, which corresponds to high frequencies. Similarly, high values of a represent slowly varying signals with low frequencies. The straightforward time-frequency version of the CWT is defined by Hlawatsch and Boudreaux-Bartels [37] as

$$CWT_x^{(\Gamma)}(t,f) = \int_{-\infty}^{+\infty} x(u)\ \sqrt{|f/f_0|}\quad \Gamma^* \left(\frac{f}{f_0}(u-t)\right) \mathrm{d}u, \tag{1.12}$$

where $\Gamma(t)$, the analyzing wavelet is a real or a complex bandpass function centered around $t = 0$ in the time domain. The parameter f_0 is the center frequency of $\Gamma(t)$. The CWT preserves time-shift and time-scaling but does not preserve frequency-shift.

$$\begin{aligned} \tilde{x}(t) = x(t-t_0) &\Rightarrow CWT_{\tilde{x}}^{(\Gamma)}(t,f) = CWT_x^{(\Gamma)}(t-t_0,f), \\ \tilde{x}(t) = \sqrt{|a|}\ x(at) &\Rightarrow CWT_{\tilde{x}}^{(\Gamma)}(t,f) = CWT_x^{(\Gamma)}(at,\frac{f}{a}). \end{aligned} \tag{1.13}$$

Similar to STFT, the CWT has time-frequency resolution limitation, because time-resolution and frequency-resolution can not be improved simultaneously due to the uncertainty principle. However, STFT provides constant time-resolution and frequency-resolution throughout the time-frequency plane, whereas the CWT analyzes higher frequency signals with better time-resolution and inferior frequency-resolution, while lower frequency signals with better frequency-resolution and inferior time-resolution as shown by Hlawatsch and Boudreaux-Bartels [37].

Sejdić et al. [95] presented a detailed quantitative analysis of scalogram and spectrogram of signals in the presence of additive white Gaussian noise. Mean square analysis of IF estimation of scalogram and spectrogram were performed to compare their performance. These results showed that the scalogram with the Morlet wavelet exhibited good performance for linear FM and hyperbolic FM signals in comparison to the spectrogram. However, these results can not be extended to all classes of signals.

1.2.4 S-Transform

Sejdić et al. [96] defined the S-transform of a signal $x(t)$ as follows:

$$S_c(t, \omega; w(\tau, \omega)) = e^{-i\omega t} \int_{-\infty}^{+\infty} x(t+\tau)\ w(\tau, \omega)\ e^{-i\omega\tau} \mathrm{d}\tau, \tag{1.14}$$

where the window function $w(\tau, \omega)$ is defined as:

$$w(\tau, \omega) = \frac{|\omega|}{(2\pi)^{1.5}}\ e^{\frac{-\tau^2\omega^2}{8\pi^2}}. \tag{1.15}$$

For lower frequencies, the window is wider in the time domain, while it is narrower in the time domain for higher frequencies. Here the window is a function of frequency as well as time. This means, good localization in the frequency domain for lower frequencies can be achieved by using a wider time-domain window, while good localization of IF signals in time-domain can be obtained by using narrow time-domain window.

Windows of different lengths are used in the S-transform for improving the result, whereas a fixed window is used in STFT. Instantaneous frequency estimation using STFT and pseudo-WVD are shown to be far inferior to estimation using adaptive S-transform TFD. However, the bias and the variance of the estimator remain signal-dependent, so this method is not suitable for all kinds of signals.

Thayaparan et al. [116] have shown that S-Transform provides better focusing of Inverse SAR image by compensating quadratic and higher even order phase term of moving targets. The authors demonstrated that S-transform performs better than Fourier transforms for highly maneuvering targets under low and high SNR conditions, and it provides higher SNR gain as compared to Fourier transform, and it is also computationally efficient.

1.2.5 Fractional Fourier transform

The fractional Fourier transform (FrFT) is a generalization of the Fourier transform (FT). It depends on the parameter α, which can be interpreted as an angle of rotation in the time-frequency (TF) plane [2, 18, 73, 98, 115, 123]. The FrFT of a signal $x(t)$ is defined as

$$X_\alpha(f) = \int_{-\infty}^{+\infty} x(t) \cdot K_\alpha(t, f) dt, \tag{1.16}$$

where the kernel $K_\alpha(t, f)$ of FrFT is given by [33]

$$K_\alpha(t, f) = \begin{cases} (\sqrt{1 - i\cot\alpha}) \cdot exp\left(i\pi t_0^2 f^2 \cot\alpha + i\pi f_0^2 t^2 \cot\alpha - i2\pi f t \operatorname{cosec}\alpha\right), & \text{if } \alpha \text{ is not a multiple of } \pi \\ \delta(f_0 t - t_0 f), & \text{if } \alpha \text{ is a multiple of } 2\pi \\ \delta(f_0 t + t_0 f), & \text{if } \alpha + \pi \text{ is a multiple of } 2\pi \end{cases}$$

where t_0, f_0 are dimensional normalization factors, $t_0^2 = \frac{T_{max}}{f_s}$, $f_0^2 = \frac{f_s}{T_{max}}$, $t_0^2 f_0^2 = 1$, T_{max} is the window length during FrFT and f_s is the sampling frequency. The unit of t_0 is second and f_0 is Hz.

It should be noted that at $\alpha = \frac{\pi}{2}$, K_α becomes the kernel of the Fourier transform, and hence the FrFT of the signal becomes the Fourier transform of the signal. The FrFT is a linear transform, so it does not produce cross-terms during multicomponent signal analysis.

FrFT follows the property of index additivity of angle. Hence it is computationally efficient.

1.2.6 Short time fractional Fourier transform

Ran Tao et al. [115] have defined short time version of FrFT called short time fractional Fourier transform (STFrFT) for generating TFD, and it is defined for signal $x(t)$ as follows:

$$STFrFT_{x,\alpha}(t, u) = \int_{-\infty}^{+\infty} x(\tau) g(\tau - t) K_\alpha(t, u) d\tau, \tag{1.17}$$

Where $g(\cdot)$ is type of window, $x(\tau)$ is the signal to be analyzed and $K_\alpha(t, u)$ is the kernel of FrFT.

The advantage of STFrFT over other TFDs is described in the following sections. The author demonstrates that STFrFT could be used for estimating the pulse width of a waveform. Due to dispersive support in the time-frequency plane, STFT does not have the ability to represent closely spaced chirp signals separately. However, due to compact support in the time-frequency plane, STFrFT has the ability to represent closely spaced signals separately.

STFrFT provides higher SNR gain as compared to FrFT due to compact support of linear chirp signal. As a result, STFrFT provides better estimation accuracy for low SNR targets in comparison to STFT and FrFT.

Ran Tao et al. [6] stated that a prominent point SAR processing algorithm requires a high signal-to-background ratio with respect to the prominent point. To achieve a high signal-to-background ratio, the author presented an improved prominent point pre-processing technique based on the short-time fractional Fourier transform (STFrFT). The performance of the proposed STFrFT based autofocus algorithm is better than prominent point SAR processing, and it is validated using real SAR data.

STFrFT follows the property of the index additivity of angle. Hence it is computationally efficient.

1.3 Preliminaries: Quadratic transform based TFDs

1.3.1 Wigner-Ville distribution

The mathematical form of WVD for a real-valued signal $x(t)$ is given by Mertins [69].

$$WVD_x(t,\omega) = \int_{-\infty}^{+\infty} x^*(t-\frac{\tau}{2})\; x(t+\frac{\tau}{2})\; e^{-i\omega\tau}\; \mathrm{d}\tau. \tag{1.18}$$

Rao and Taylor [87] showed that Wigner-Ville distribution (WVD) provides optimal IF estimation for linear FM signals with high to moderate SNR by locating the energy peaks on WVD surface. WVD provides better understanding of IF along with group delay of signal [26]. Wong and Jin [120] studied this estimator. At high SNR, WVD peak extraction method of IF estimation has worked very well for LFM, but at low SNR it fails to provide a reasonable estimation of IF. This is primarily due to appearance of the function $x(t)$ as $x^*(\cdot)$ and $x(\cdot)$ as shown in the definition of WVD, which makes this TFD quadratic in nature.

WVD is non-linear and quadratic transform based TFD and produces cross-terms during multicomponent signal analysis. In certain cases, the amplitude of cross-terms is higher than the auto-terms, as presented in [15]. In the case of WVD, sometimes it is observed that spurious peaks are present on WVD surface even though the signal is zero during the specified time duration, this happens because of the quadratic nature of WVD.

One problem associated with WVD is the "noisy" surface, as shown by Cohen [25]. If

noise is present for a small duration of a signal, then it spreads to other parts of WVD surface. If the signal time duration is infinite, then noise spreads over the entire WVD surface. Therefore WVD at any particular time reflects the properties that the signal has at other times. This is because of the bilinear or quadratic nature of WVD, which makes it highly non-local.

Moving towards improving the noise immunity of WVD, especially to reduce impulsive noise, Roenko et al. [90] presented the idea of clipping techniques. Clipping can be applied either at the input stage, so that chirp signal can be filtered, or it can be used to filter the output of the auto-correlation function. This method is promising, but the estimation of the clipping level involves a complicated procedure.

1.3.2 Pseudo Wigner-Ville distribution and smoothed Wigner-Ville distribution

Many good mathematical properties of WVD have been mentioned by Claasen and Mecklenbrauker [24], especially time marginal property, frequency marginal property, total energy property, invariance to translations, and dilation property. While calculating the Wigner-Ville distribution of any signal say $x(t)$, a practical problem, one encounters is that Eq. (1.18) can only be evaluated for a time-limited $x(t)$. Therefore the concept of windowing is introduced for any signal. In this concept, single-window $h(t)$ is not applied to $x(t)$, but window function $h(\cdot)$ is applied around the respective time of analysis.

$$WVD^{(P)}(t,\omega) = \int_{-\infty}^{+\infty} x^*(t-\frac{\tau}{2})\; x(t+\frac{\tau}{2})\; h(\tau)\; e^{-i\omega\tau}\; \mathrm{d}\tau. \tag{1.19}$$

According to Eq. (1.19), obtained TFD corresponds approximately to the WVD of the original signal. Therefore, Claasen and Mecklenbrauker [24] have proposed a new TFD named as Pseudo-WVD, ($\mathrm{WVD}^{(\mathrm{P})}$).

The calculation of Pseudo Wigner-Ville distribution ($\mathrm{WVD}^{(\mathrm{P})}$) from WVD can be done as shown below:

$$WVD^{(P)}(t,\omega) = \frac{1}{2\pi}\int_{-\infty}^{+\infty} WVD(t,\omega')\; H(\omega-\omega')\; \mathrm{d}\omega', \tag{1.20}$$

where $H(\omega)$ is the Fourier transform of $h(t)$.

Another drawback of WVD is that it produces cross-terms during multicomponent signal analysis. Consider a signal $z(t)$ expressed as a sum of two signals $z(t) = x(t) + y(t)$. By applying

WVD, we have:

$$W_h(t,\omega) = W_x(t,\omega) + W_y(t,\omega) + 2\Re\{W_{x,y}(t,\omega)\}, \tag{1.21}$$

where

$$W_{x,y}(t,\omega) = \int_{-\infty}^{+\infty} x(t+\frac{\tau}{2})\ y^*(t-\frac{\tau}{2})\ e^{-i\omega\tau}\ \mathrm{d}\tau, \tag{1.22}$$

where W_x and W_y are the WVD of single components $x(t)$ and $y(t)$, W_h is WVD of signal $[x(t)+y(t)]$, and $W_{x,y}$ represents the cross-term introduced by the quadratic nature of WVD and $\Re\{W_{x,y}(t,\omega)\}$ represents real part of $W_{x,y}(t,\omega)$.

Smoothening can be performed on WVD surface to reduce the cross-terms of WVD during the multicomponent signal analysis. Mertins [69] has introduced a general form of a smoothed distribution intended to reduce cross-terms in the WVD in the cost of reduced resolution. Expression of the SWVD$^{(\mathrm{P})}$ is given by

$$SWVD^{(P)}(t,\omega) = \frac{1}{2\pi}\int_{-\infty}^{+\infty}\int_{-\infty}^{+\infty} WVD(t',\omega')\ G(t,t',\omega,\omega')\ \mathrm{d}t'\ \mathrm{d}\omega'. \tag{1.23}$$

The time-frequency resolution of the smoothed Wigner-Ville distribution (SWVD$^{(\mathrm{P})}$) depends on the spread of the kernel $G(\cdot)$. If we impose the translational-invariance properties $G(t,t',\omega,\omega') = G(t-t',\omega-\omega')$, then expression of SWVD$^{(\mathrm{P})}$ is reduced to

$$SPWVD^{(\mathrm{P})}(t,\omega) = \frac{1}{2\pi}\int_{-\infty}^{+\infty}\int_{-\infty}^{+\infty} WVD(t',\omega')\ G(t-t',\omega-\omega')\ \mathrm{d}t'\ \mathrm{d}\omega'. \tag{1.24}$$

Nature of the kernel $G(\cdot)$ is responsible for the loss of some of the desired properties of WVD.

1.3.3 Ambiguity Function

Mertins [69] described the ambiguity function of a signal $x(t)$ as follows:

$$A_{xx}(\nu,\tau) = \int_{-\infty}^{+\infty} x^*(t-\frac{\tau}{2})\ x(t+\frac{\tau}{2})\ e^{-i\nu t}\mathrm{d}t. \tag{1.25}$$

The WVD is the two dimensional Fourier Transform of $A_{xx}(\nu,\tau)$, defined as follows:

$$W_{xx}(t,\omega) = \frac{1}{2\pi}\int_{-\infty}^{+\infty}\int_{-\infty}^{+\infty} A_{xx}(\nu,\tau)\ e^{i\nu t}\ e^{-i\omega\tau}\ \mathrm{d}\nu\ \mathrm{d}\tau, \tag{1.26}$$

where, ν is frequency and τ is time-delay.

Ristic and Boashash [88] have shown that in general, it is possible to express any bilinear TFD as the two-dimensional Fourier transform of the product of a kernel function $\varphi(\nu,\tau)$, and the ambiguity function of the signal,

$$TFD_{xx}(t,\omega) = \frac{1}{2\pi}\int_{-\infty}^{+\infty}\int_{-\infty}^{+\infty} A_{xx}(\nu,\tau)\ \varphi(\nu,\tau)\ e^{i\nu t}\ e^{-i\omega\tau}\ \mathrm{d}\nu\ \mathrm{d}\tau. \tag{1.27}$$

Simple constraints on the kernel reflect the properties of a particular distribution, and thus, it is possible to choose kernels having pre-defined and desirable properties.

1.3.4 Choi-Williams TFD

In the case of WVD, sometimes, it is observed that spurious peaks are present on the WVD surface even though the signal is zero during the specified time durations. These spurious values, sometimes called artifacts, are attributable to the quadratic nature of WVD. Choi and Williams [23] have presented a TFD, which addresses this drawback of the WVD. The authors have suggested that spurious peaks have to be minimized, instead of eliminating them completely.

$$CW_x(t,\omega) = \int_{-\infty}^{+\infty}\int_{-\infty}^{+\infty} \sqrt{\frac{\pi\sigma}{\tau^2}}\ e^{-\pi^2\sigma(u-t)^2/\tau^2}\ x^*\left(u-\frac{\tau}{2}\right)\ x\left(u+\frac{\tau}{2}\right)\ e^{-i\omega\tau}\ \mathrm{d}u\ \mathrm{d}\tau. \tag{1.28}$$

Cohen [25] has shown that Choi-Williams TFD is more suitable compared to the WVD while analyzing multicomponent linear chirp signals, multicomponent sinusoidal signals, and the sum of linear chirps and sinusoidal signals.

1.4 Preliminaries: Higher order transform based TFDs

1.4.1 Polynomial Wigner-Ville Distribution

Barkat and Boashash [10] proposed the Polynomial Wigner-Ville Distribution (PWVD), and it is further discussed by Boashash [12]. Given a signal $x(t) = a(t)\ e^{i\phi(t)}$, where $\phi(t)$ is the time varying phase and polynomial WVD of order p , where p can be assumed to be even, in such condition, the expression of PWVD of order p (assuming that $a(t) = 1$) is given by :

$$PWVD_x(t,f) = \int_{-\infty}^{+\infty} R_x^{(p)}(t,\tau)\ e^{-i2\pi f\tau}\ \mathrm{d}\tau, \tag{1.29}$$

where,

$$R_x^{(p)}(t,\tau) = \prod_{l=1}^{p/2} [x(t + c_l\tau)\ x^*(t - c_l\tau)]^{b_l}.$$

The general definition of PWVD is further elaborated by Boashash [12]. A Polynomial WVD of order p of the signal x(t) is a function given by Eq. (1.29), such that the coefficients b_l and c_l satisfy Eq. (1.30), when $\phi(t)$ is a polynomial of degree not exceeding p. For polynomial WVD of order p, where p is assumed to be even, phase differentiation $\phi'(t)$ can be defined as:

$$\phi'(t) = \frac{1}{\tau} \sum_{l=1}^{p/2} b_l[\phi(t + c_l\tau) - \phi(t - c_l\tau)]. \tag{1.30}$$

Boashash [12] has explained a detailed method for the calculation of coefficients of polynomial phase signals. In case the instantaneous phase is a polynomial having a degree less than or equal to p, then the unbiased estimate of that instantaneous frequency is described as PWVD of order p. For high SNR signals, polynomial IF estimation using PWVD is an efficient method. Ristic and Boashash [89] also suggested an iterative method for the analysis of low SNR signals.

1.4.2 Higher order ambiguity function and its variants

Simeunović et al. [103] presented an explicit discussion on these methods. Higher order ambiguity function (HAF) and its variants are the most commonly used methods for parameter estimation of polynomial phase signals, which are described by Peleg and Porat [78], Barbarossa and Petrone [8], Barbarossa et al. [9], Peleg and Porat [77], Peleg and Friedlander [76], Golden and Friedlander [36], and Porat and Friedlander [85].

HAF:

HAF iteratively reduces received signal phase order by one using conjugate multiplication of time-delayed version of the same signal, i.e., auto-correlation operation. Once the order of received signal becomes one (pure sinusoid), then the frequency of sinusoid becomes proportional to the highest phase order coefficient value. So iteratively, all the phase coefficients of the signal can be estimated. Porat and Friedlander [85], however, have shown that each auto-correlation operation increases the number of interference terms and increases the SNR threshold by approximately 6dB.

Multi-lag HAF and Product HAF:

Barbarossa et al. [9], have defined multi-lag HAF for estimating higher order polynomial phase signal. Let $x(n)$ be a polynomial phase signal, then multi-lag high order instantaneous moments or correlations of signal $x(n)$ are defined as :

$$x_1(n) = x_1(n), \tag{1.31}$$

$$x_2(n;\tau_1) = x_1(n+\tau_1)x_1^*(n-\tau_1), \tag{1.32}$$

$$x_3(n;\tau_2) = x_2(n+\tau_2)x_2^*(n-\tau_2), \tag{1.33}$$

$$\dots$$

$$x_p(n;\tau_{p-1}) = x_{p-1}(n+\tau_{p-1})x_{p-1}^*(n-\tau_{p-1}), \tag{1.34}$$

where τ_1, τ_2 etc. are different time delays for p^{th} order HAF. Multi lag higher order ambiguity function (Ml-HAF) is defined as a Fourier transform of multi-lag high order instantaneous moments:

$$X(f,\tau_{p-1}) = \sum_{n=0}^{N} x_p(n,\tau_{p-1})e^{-j2\pi fn}. \tag{1.35}$$

Multi-lag higher order ambiguity function is similar to HAF with different time delays. Multi-lag higher order ambiguity function has cross-terms in the case of multicomponent polynomial-phase signal analysis. Auto-terms can be differentiated from cross-terms based on the multiplication of different time delays.

Popović et al. [84] has proposed PHAF, which further reduces cross-terms and enhances auto-terms by multiplication of Ml-HAFs. PHAF method reduces computation as compared to the polynomial Fourier transform. The author proved using simulations that third order PHAF gives better focusing of SAR image for moving as well as stationary targets as compared to the adaptive S-transform based method.

1.4.3 Cubic phase function and its variants

Cubic phase function based transform:

The cubic-phase function (CPF) is introduced to enable a more accurate estimation of parameters of a cubic-phase signal with a lower SNR threshold than the HAF, O'Shea [72]. Only one auto-correlation of the original signal is performed instead of two required in the HAF. The CPF-based method requires one-dimensional maximization, whereas the maximum likelihood

(ML) method requires three-dimensional maximization. Moreover, the CPF parameter estimates are asymptotically optimal or near-optimal at high SNRs. Equation of CPF for signal $x(t)$ is defined as follows:

$$CPF(t,\Omega) = \int_{-\infty}^{+\infty} x(t+\tau)x(t-\tau)e^{-i\Omega\tau^2}d\tau. \tag{1.36}$$

Product CPF based transform:

Jianyu Yang et al. [48], claimed that the traditional algorithm for estimating the chirp rate parameters of multicomponent chirp signals based on cubic phase function (CPF) gives rise to multiple spurious signals or cross-terms. To overcome this problem, the author proposed an estimator based on product cubic phase function (PCPF).

$$PCPF(t,\Omega) = \prod_{t=t_1}^{t=t_N} CPF(t,\Omega). \tag{1.37}$$

In PCPF, the author presented a method to reduce or eliminate spurious terms by multiplying CPF of different time lags. The author demonstrated the better performance of PCPF as compared to CPF for the estimation of a multicomponent signal. He proved that PCPF has advantages over CPF for improving auto-term SNR, noise rejection, suppression of cross-terms, and spurious peak elimination.

CPF evaluation techniques:

I. Djurovic et al. [29], has proposed CPF evaluation techniques of multicomponent, non-overlapping, non-linear chirp signal for reducing cross-terms of CPF. The author demonstrated the validity of the proposed method on the SAR scene with three stationary scatters in the same range cell and obtained better performance than the CPF method in this multicomponent chirp scenario. The author considered three moving and two stationary targets in the SAR scene with additive white Gaussian noise conditions and demonstrated that the proposed method has the capability to focus all targets in the SAR scene.

Integrated CPF:

Wang et al. [118], introduced an integrated cubic phase function (ICPF) for the estimation and detection of linear frequency-modulated (LFM) signals. With the framework of CPF, The ICPF extended the standard cubic phase function (CPF), to take care of scenarios that involve low

SNR and multicomponent LFM signals. Auto-terms in the CPF are distributed along straight lines, which are parallel to the time axis in the time-"frequency-rate" domain. This property of auto-terms in CPF is exploited by the ICPF, and thus the enhancement of the auto-terms is carried out by integrating over these straight lines. Wang et al. [118] showed that on comparing ICPF to CPF, the ICPF provided lower MSE at low SNR while at the same time being better at the rejection of spurious peaks or cross-terms for the multicomponent LFM signals.

Hybrid CPF-HAF:

Simeunović and Djurović [102] proposed an extension of the CPF for higher order polynomial phase signals detection, referred to as the hybrid CPF-HAF (HCH). The HCH performs one auto-correlation less as compared to the HAF, and the error-propagation effect is reduced by two times. Simeunović and Djurović [102] showed that the SNR threshold becomes less by about 9dB and the estimation of the MSE is lowered by approximately 2dB. A coarse and fine search strategy is performed for parameter estimation. In the case of coarse search, peak location is performed on considered function (HAF, CPF, or HCH), where the function is evaluated over a pre-defined grid of values. In the case of fine search, peak maximization is performed through oversampling or an iterative procedure. CPF and HCH calculation cannot be performed by fast Fourier transform, unlike the HAF. Therefore the number of calculated samples have to be reduced.

1.4.4 High resolution time-frequency rate representation based transforms

L. Zuo, et al. [144], has proposed a transform to have higher frequency rate resolution than CPF. High-resolution time-frequency rate representation (HR-TFRR) for signal $x(t)$ is defined as follows:

$$HR-TFRR(t,\Omega) = \int_0^T x(t+\tau)x(t-\tau)e^{-i\Omega\tau^2}d\tau^2. \tag{1.38}$$

HR-TFRR is a bilinear or quadratic transform like CPF, so this transform suffers from the cross-terms during multicomponent signal analysis. These cross-terms are located near the origin of amplitude vs. chirp rate curve. The author proposed smoothed HR-TFRR (SHR-TFRR) method.

In this method, bandpass filter (BPF) is used to remove these cross-terms and pass auto terms when IF functions cross each other in the TF plane. Let $P(\omega)$ be BPF with $P(\omega)$=1 for $(\omega_1 \leq |\omega| \leq \omega_2)$ else 0. $U(t,\Omega)$ and $V(t,\Omega)$ are defined below:

$$U(t,\Omega) = \int_0^T x(t+\tau)e^{-i\Omega\tau^2}d\tau^2, \tag{1.39}$$

$$V(t,\Omega) = \int_0^T x(t-\tau)e^{-i\Omega\tau^2}d\tau^2. \tag{1.40}$$

Then equation of SHR-TFRR is defined below:

$$SHR-TFRR(t,\Omega) = \int_{-\infty}^{+\infty} P(\omega)U(t,\Omega/2+\omega)U(t,\Omega/2-\omega)d\omega. \tag{1.41}$$

By simulation, the author has proved that HR-TFRR is less sensitive as compared to time-chirp duration transform (TCD) and has demonstrated higher chirp rate resolution as compared to CPF.

1.4.5 Sinusoidal frequency modulation Fourier transform

The authors B. Peng et al. [81] have demonstrated that sinusoidal frequency modulation Fourier transform is a parametric transform and provides a better estimation of sinusoidal frequency modulated signal as compared to non-parametric transforms. Rotating and vibrating objects produce a sinusoidal frequency modulated signals or micro-Doppler signals as radar return signals. Detection of such sinusoidal frequency modulated signal gives information of rotating and vibrating targets classification for radar [20, 21].

Authors proposed that all practical vibrating and rotating targets produce sinusoidal frequency modulated signals and can be represented by using sinusoidal frequency modulated signal as a basis function, (it is also shown in this paper that these bases are orthogonal). The equation of sinusoidal frequency modulation for signal $x(t)$ and the weighting factor A_k are given as follows:

$$x(t) = exp\left[i\sum_{k=0}^{\infty} A_k exp(iexp(ik\omega_0 t))\right], \tag{1.42}$$

where $A_k \in \mathbf{C}$,

$$A_k = \lim_{T\to\infty}\frac{1}{T}\int_{-T/2}^{T/2} ln\left\{x(t)^{-iexp(-ik\omega_o t)}\right\}dt.$$

The author demonstrated that FrFT based method to estimate micro-Doppler provides worse frequency resolution, higher SNR requirement, higher computation time, etc. as compared to sinusoidal frequency modulated transform.

1.4.6 Polynomial Fourier transform

I. Djurovic et al. [32] proposed polynomial Fourier transform (PFT and its application in SAR moving target focusing. Discrete PFT $X(\omega, \alpha_2, \alpha_3, ..., \alpha_n)$ is an extension of Fourier transform and is defined for a discrete signal $x[n]$ as follows

$$X(\omega, \alpha_2, \alpha_3, ..., \alpha_n) = \sum_n x[n] exp(-i\omega n - i\alpha_2 n^2 - i\alpha_3 n^3 - ..... - i\alpha_k n^k), \tag{1.43}$$

Where ω is first-order derivatives of the IF of the signal and the superscript k indicates the order of the LPFT, and $\alpha_2, \alpha_3 \ldots \alpha_k$ are the parameters related to the 2^{nd} order, 3^{rd} order... k^{th} order derivatives of the IF of the signal.

PFT is a linear transform, so there are no cross-terms during multicomponent signal analysis. According to the author's experiments, estimation of the polynomial order up to three is sufficient for SAR imaging of stationary as well as moving targets. Estimation of a higher order could introduce higher computation. Simulation is performed over moving targets and stationary targets on SAR data. Performance of the proposed algorithm is better as compared to the standard S-method (S-method has cross-terms) for focusing SAR image.

It is to be noted that the FrFT is similar to the 2^{nd} order polynomial Fourier transform, but PFT does not follow the property of index additivity of angle.

1.4.7 Local polynomial Fourier transform

Local polynomial Fourier transform (LPFT) is a generalization of STFT. LPFT is useful for analyzing higher order chirp signals. LPFT is a linear transform, and it does not produce cross-terms during multicomponent signal analysis. Katkovnik [50] and Lia et al. [59] defined the M^{th}- order LPFT as:

$$LPFT_h^{\{M\}}(x; t, \omega, \omega_1 \cdots \omega_{(M-1)}) = \int_{-\infty}^{+\infty} x(t+\tau)\ h(\tau)\ exp\left\{-i\omega\tau - i\sum_{m=2}^{M} \frac{\omega_{(m-1)}\tau^m}{m!}\right\}\ \mathrm{d}\tau, \tag{1.44}$$

where $h(\tau)$ is the window function, the superscript M indicates the order of the LPFT, and $\omega_1, \omega_2 \ldots \omega_{(M-1)}$ are the parameters related to the derivatives of the IF of the signal i.e. $\omega_1 = \frac{\mathrm{d}\Omega(t)}{\mathrm{d}t}, \omega_2 = \frac{\mathrm{d}^2\Omega(t)}{\mathrm{d}t^2}, \ldots, \omega_{(M-1)} = \frac{\mathrm{d}^{M-1}\Omega(t)}{\mathrm{d}t^{M-1}}$, where $\Omega(t)$ is the IF of the signal.

The kernel of the LPFT uses polynomial phase signal. Therefore, it significantly improves the signal concentration in the time-frequency domain for higher order chirp compared to that obtained by the STFT. It is to be noted that the STFrFT is similar to the 2^{nd} order local polynomial Fourier transform (LPFT), but LPFT does not follow the property of index additivity of angle.

1.4.8 General parameterized time-frequency transform

The Author Yang et al. [130], proposed parametric TFD for analysis of large variety of frequency modulated signals. Equation of General parameterized time-frequency transform (GPTF for signal $x(t)$ is as follows:

$$GPTF(t_0, \omega; C) = \int_{-\infty}^{+\infty} x(\tau)\phi_C^R(\tau)\phi_{C,t_0}^S(\tau)w^*(\tau - t_0)e^{-i\omega\tau}d\tau, \tag{1.45}$$

where C denotes parameter set and w is window function. $\phi_C^R(\tau)$ and $\phi_{C,t_0}^S(\tau)$ denotes the kernel based rotational and shift operators respectively and it is defined as follows:

$$\phi_C^R(\tau) = e^{-i\int k_C(\tau)d\tau}, \tag{1.46}$$

$$\phi_{t_0,C}^S(\tau) = e^{-i\tau.k_C(t_0)}. \tag{1.47}$$

Polynomial chirplet transform:

Kernel $k_C(t)$ of Polynomial chirplet transform (PCT) for analysing higher order polynomial chirp and it is defined as follows:

$$k_C(t) = \sum_{i=2}^{i=n+1} C_{i-1}t^{i-1}, \tag{1.48}$$

$$\phi_{c1,c2\ldots cn}^R(\tau) = e^{-i\sum_{i=2}^{n+1}\frac{1}{i}c_{i-1}(\tau)^i}, \tag{1.49}$$

$$\phi_{c1,c2\ldots cn,t_0}^S(\tau) = e^{i\sum_{i=2}^{n+1}c_{i-1}t_0^{i-1}\tau}. \tag{1.50}$$

By simulation, the authors have proved that PCT performs better than STFT, wavelet, WVD, adaptive STFT, reassignment pseudo WVD, and chirplet transform for analyzing polynomial phase signal.

Spline chirplet transform :

Time and IF relationship of signal is complex in nature, which consists of sinusoidal and non-sinusoidal signal in T-F plane with discontinuities. Analysis of this complex IF over long time interval requires higher order polynomial approximation of phase and that approximation requires large computation and produces runge effect. To avoid these, spline function is used, so that it can be approximated using lower order polynomial and hence computation is reduced.

$\phi^R_C(\tau)$ and $\phi^S_{C,t_0}(\tau)$ of spline Chirplet transform are defined as follows:

$$\phi^R_C(\tau) = e^{-i\sum_{i=1}^{n}\frac{C_{l,i}}{i}(\tau-t_l)^i+o_l}, \tag{1.51}$$

$$\phi^S_{C,t_0}(\tau) = e^{i\tau\sum_{i=1}^{n}C_{l,i}(t_0-t_l)^{i-1}}, \tag{1.52}$$

where t_l is spline knot. Spline kernel considers discontinuous point as unconnected knot. o_l is integration constant and it is given by equation (1.53)

$$o_l - o_{l+1} = \sum_{i=1}^{n}\frac{C_{l+1,i}}{i}(t_l - t_{l+1})^i. \tag{1.53}$$

Generalized warblet transforms:

Generalized warblet transform is proposed for analyzing sinusoidal signals in T-F plane. Any continuous periodic phase signal in T-F plane is expressed in terms of Fourier series. Analysis of periodic phase signal using warblet transform requires fewer parameter searches and reduces computation complexity as compared to spline chirplet transform.

Rotational $\phi^R_P(\tau)$ and shift operator $\phi^S_P(\tau)$ of Generalized warblet transform are defined as follows:

$$\phi^R_{a,b,f_m}(\tau) = e^{-i\left[\sum_{i=1}^{n}\frac{a_i}{fm_i}\cos(2\pi.fm_i.\tau)+\sum_{i=1}^{n}\frac{b_i}{fm_i}\sin(2\pi fm_i.\tau)\right]}, \tag{1.54}$$

$$\phi^S_{a,b,f_m}(\tau) = e^{-i2\pi\tau\left[-\sum_{i=1}^{n}a_i\sin(2\pi fm_i.t_0)+\sum_{i=1}^{n}b_i\cos(2\pi.fm_i.t_0)\right]}. \tag{1.55}$$

Polynomial localized frequency delay transform:

Polynomial localized frequency delay transform is dual of polynomial chirplet transform. Polynomial localized frequency delay transform's kernel is represented in terms of polynomial order of frequency. This transform analyzes signal with any continuous localized frequency delay, but it suffers from runge effect in case of complex IF analysis.

Rotational $\Gamma^R_{q1,q2,\ldots qn}(\theta)$ and shift operator $\Gamma^S_{Q,\omega_0}(\theta)$ of Polynomial localized frequency delay transform are defined as follows:

$$\Gamma^R_{q1,q2,\ldots qn}(\theta) = e^{-i\sum_{i=2}^{n+1}\frac{1}{i}q_{i-1}\theta^{i-1}}, \tag{1.56}$$

$$\Gamma^S_{Q,\omega_0,q1,q2,\ldots qn}(\theta) = e^{i\theta.\sum_{i=2}^{n+1}q_{i-1}\omega_0^{i-1}}. \tag{1.57}$$

Fourier series localized frequency delay transform:

Fourier series localized frequency delay transform is dual of the warblet transform. Fourier series localized frequency delay transform's kernel is represented in terms of Fourier series of frequency. This transform has ability to analyze any periodic signal in frequency domain.

Rotational operator $\Gamma^{R}_{a,b,f_m}(\theta)$ and shift operator $\Gamma^{S}_{a,b,f_m,\omega_0}(\theta)$ of Fourier series localized frequency delay transform are defined as follows:

$$\Gamma^{R}_{\hat{a},\hat{b},f_{\hat{m}}}(\theta) = e^{-i\left[\sum_{i=1}^{n}\frac{\hat{a}_i}{f_{\hat{m}_i}}\cos(2\pi.f_{\hat{m}_i}.\theta)+\sum_{i=1}^{n}\frac{\hat{b}_i}{f_{\hat{m}_i}}\sin(2\pi f_{\hat{m}_i}.\theta)\right]}, \tag{1.58}$$

$$\Gamma^{S}_{\hat{a},\hat{b},f_{\hat{m}},\omega_0}(\theta) = e^{-i2\pi\tau\left[-\sum_{i=1}^{n}\hat{a}_i\sin(2\pi f_{\hat{m}_i}.\omega_0)+\sum_{i=1}^{n}\hat{b}_i\cos(2\pi.f_{\hat{m}_i}.\omega_0)\right]}. \tag{1.59}$$

Author proposed optimum kernel identification of GPTF transform. In kernel identification method, bias of IF estimation is reduced during each iteration and when error in IF estimation in i^{th} iteration and $i^{th}-1$ iteration is less than threshold value, then iteration process is terminated. Initial kernel can be assumed as Fourier transform kernel. During each iteration, mean IF error is calculated. The kernel, which gives least IF error is considered to be optimum kernel for that particular signal.

$$\text{Mean IF error} = mean\left(\int\left|\frac{IF^{i}_{est}(t)-IF^{i-1}_{est}(t)}{IF^{i}_{est}(t)}\right|dt\right). \tag{1.60}$$

Mean Error is calculated based on equation (1.60). Here IF^{i}_{est} is IF estimated at i^{th} iteration and $IF^{i-1}_{est}(t)$ is IF estimated at $(i-1)^{th}$ iteration.

1.4.9 Generalized time-frequency transform

If a signal $x(t)$ has finite absolute integral (finite L^1 norm), its Generalized time-frequency transform (GTFT) evaluated at parameters (α,λ) is given by

$$X_{\alpha,\lambda}(f) = \int_{-\infty}^{+\infty} x(t)\cdot K_{\alpha,\lambda}(t,f)dt, \tag{1.61}$$

where $K_{\alpha,\lambda}(t,f)$ is the kernel of GTFT and it is defined as [92–94]

$$K_{\alpha,\lambda}(t,f) = \begin{cases} \sqrt{1-i\cot\alpha}\cdot exp\Big(i\pi t_0^2 f^2\cot\alpha + i\pi f_0^2 t^2\cot\alpha \\ -i2\pi f t\,\mathrm{cosec}\alpha + i\cdot h(\lambda,t_0 f) - i\cdot h(\lambda,f_0 t)\Big), & \text{if } \alpha \text{ is not a multiple of } \pi \\ \delta(f_0 t - t_0 f), & \text{if } \alpha \text{ is a multiple of } 2\pi \\ \delta(f_0 t + t_0 f), & \text{if } \alpha+\pi \text{ is a multiple of } 2\pi \end{cases} \tag{1.62}$$

where $h(\cdot)$ is a real valued dimensionless function, and α and λ are the real valued GTFT parameters.

One specialty of the GTFT kernel is that it follows the property of index additivity of angle [2, 93], similar to FrFT i.e

$$\int_{-\infty}^{+\infty} K_{\alpha_1,\lambda}(t,f)K_{\alpha_2,\lambda}(f,u)df = K_{(\alpha_1+\alpha_2),\lambda}(t,u). \tag{1.63}$$

This property is used to reduce the computational complexity for parameter estimation.

The GTFT is a generalization of the FrFT, and hence a further generalization of the Fourier transform. It can be used to analyze a much wider variety of frequency modulated signals by varying $h(\cdot)$ in the GTFT kernel. While estimating the instantaneous frequency of an unknown chirp signal with a known model, we can use this extra freedom to handle non-linearity in the nature of instantaneous frequency. Thus, we are not limited, to estimating the instantaneous frequency of unknown chirps with linear frequency modulation, as in the case of FrFT. For example, if $h(\cdot)$ is defined as a polynomial function, then the resultant GTFT can be used to analyze polynomial phase signals. On the other hand, if $h(\cdot)$ is defined as a sinusoidal function, the resultant GTFT can be used to analyze sinusoidal frequency modulated signals, and so on. Some of the GTFT kernels are as shown below:

- Cubic-kernel-GTFT (ck-GTFT) may be defined by substituting the parametric function $h(\cdot)$ as $h(\lambda, z) = \pi\lambda z^3$. Ck-GTFT is a highly useful transform used to analyze quadratic chirp signals, and is explored in detail in the later parts of this thesis. It is to be noted that the ck-GTFT is similar to the 3^{rd} order polynomial Fourier transform (PFT) [32], with the added advantage of possessing the property of index additivity of angle.

- Sinusoidal-kernel-GTFT may be defined by substituting the multiparametric function $h(\cdot)$ as $h(A, \phi, \lambda, z) = A\sin(\pi\lambda z + \phi)$, where A, ϕ and λ are the variable parameters, which can be tuned to match the kernel with signal for estimating parameters. This transform can be used to analyze micro-Doppler effects in radar for the classification of rotating and vibrating targets.

Inverse GTFT is defined as [94]

$$x(t) = \int_{-\infty}^{\infty} X_{\alpha,\lambda}(f) \cdot K^*_{\alpha,\lambda}(t,f)df, \tag{1.64}$$

where $K^*_{\alpha,\lambda}(t, f)$ is the complex conjugate of $K_{\alpha,\lambda}(t, f)$. If $X_{\alpha,\lambda}(f)$ has a finite absolute sum (finite L^1 norm), the above inverse exists. GTFT is a linear transform. It does not produce cross-terms, which is beneficial during multicomponent signal analysis. GTFT is used for estimation of parameters of quadratic chirp and separation of individual chirp from a mixture of chirps under Gaussian noise using extensive simulation [92–94].

1.5 Preliminaries: Brief description of synthetic aperture radar fundamentals

1.5.1 Basic synthetic aperture radar principles

The synthetic aperture radar (SAR) is an all-weather imaging radar that achieves fine along-track resolution by taking advantage of platform motion to synthesize a large antenna aperture. SAR is designed for taking high-resolution images of static targets. SAR sends multiple pulses during one observation time to get the ground images, and the single pulse duration is known as pulse repetition time (PRT). Linear chirp is the most common waveform used as a radar waveform during pulse high time of PRT.

In a conventional SAR, antenna is oriented to look sideways, and it is mounted on a moving platform, generally an aircraft or satellite. The direction of orientation of the radar is usually called the "range" direction, and the direction of movement of the platform/aircraft is called the "azimuth" direction.

Fig.1.1 describes a typical imaging scenario using SAR. The aircraft/moving platform carrying the radar is assumed to be moving along direction parallel to the positive y (azimuth) direction with a constant velocity v_a. The ground range direction is taken along positive x direction. It flies at a constant altitude/platform height of H. The system is required to image a point target situated at slant range R_0 from the platform, at time $t_a = 0$, (which is the time of minimum distance between the point target and platform, if the target is assumed to be stationary), as shown. At any azimuth direction time t_a, the slant range of the point target is $R(t_a)$, which can be calculated as:

$$R(t_a) = \sqrt{R_0^2 + v_a^2.t_a^2} \approx R_0 + \frac{(v_a.t_a)^2}{2R_0}. \tag{1.65}$$

The approximation holds if $\frac{v_a.t_a}{R_0} \ll 1$.

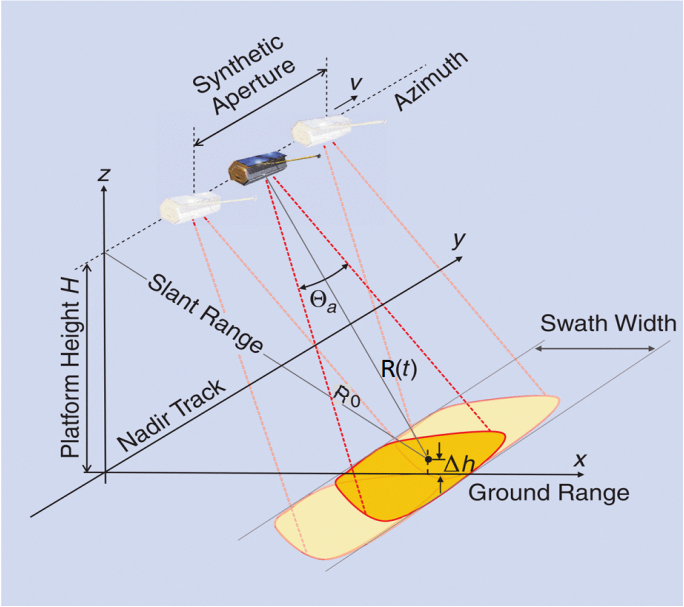

Figure 1.1: SAR Imaging Geometries (Image courtesy: Moreira et al. [70])

Here, the azimuth time variable is t_a. Phase difference ($\phi(t_a)$) of the received wave with respect to the transmitted wave is related to the instantaneous range $R(t_a)$ as:

$$\phi(t_a) = \frac{-4\pi R(t_a)}{\lambda} \approx \frac{-4\pi}{\lambda}(R_0 + \frac{(v_a.t_a)^2}{2R_0}), \tag{1.66}$$

where λ is wave length. Here, we note that $R(t_a)$, and hence $\phi(t_a)$ has a parabolic behavior. Also, approximation of Eq.(1.65) is an over simplifying approximation. In Eq.(1.66), quadratic phase $\phi(t_a)$ makes linear frequency modulated signal in the direction of azimuth. Azimuth direction phase can be approximately modeled as linear chirp waveform.

Azimuth direction chirp parameter is unknown, so to calculate azimuth direction chirp rate the following formula shown in Eq. (1.67) is used in conventional SAR signal processing [139]. Azimuth chirp rate K_a is derived for stationary targets assuming SAR azimuth squint angle is zero.

$$K_a = \frac{2}{\lambda}\frac{d^2R(t)}{dt^2}\,|_{t=0} = \frac{2v_a^2}{\lambda.R_0}, \tag{1.67}$$

Where v_a is the mean aircraft velocity and R_0 is minimum slant range of stationary target from aircraft/satellite.

So azimuth direction chirp parameters for static targets in SAR as shown in Eq. (1.67) are calculated based on aircraft velocity, wavelength and height of aircraft from ground.

1.5.2 Resolution

Slant range resolution (δ_r) is defined by system bandwidth as $\delta_r = c_0/2B_r$, where B_r is transmitted waveform bandwidth and c_0 is velocity of light. Azimuth resolution (δ_a) is defined by synthetic aperture length (L_{sa}), which is the path length when echo from the point target is received, and is depicted in Fig. 1.1. From the same figure, it can be seen that $L_{sa} = \Theta_a R_0 = \lambda R_0/d_a$, where d_a is azimuth true antenna length. Hence, a virtual beam-width Θ_{sa} maybe defined as $\Theta_{sa} = \lambda/2L_{sa}$, and hence the effective azimuth resolution is now:

$$\delta_a = R_0\Theta_{sa} = \frac{d_a}{2}. \tag{1.68}$$

As shown in Eq.(1.68), azimuth resolution depends on true azimuth length of antenna and it does not depend on radar wavelength, slant range etc. SAR has become popular for ground imaging due to this property.

1.5.3 Processing using the range-Doppler algorithm for stationary target

After receiving the signals, they are down-converted to baseband, digitized, and stored in the form of a 2D array/matrix of complex numbers representing amplitude and phase. One dimension of this array will correspond to the range direction (or fast time), and the other will correspond to the azimuth (or slow time).

We can not visualize SAR raw data like optical data, and pre-processing of the signal will be required, as illustrated by Fig.1.2:

There are two main matched filtering operations, First for range direction and the second one for azimuth direction. The matched filtering operation is achieved by a convolution with the reference function in the time domain or by multiplication of complex conjugate of the frequency transform of the same reference function in the frequency domain. Matched filtering in range direction gives us the "data compressed in range" or the "range compressed data" from which range information can be inferred.

Azimuth direction can be modeled as a chirp waveform for stationary/moving targets based upon two assumptions: every target is considered as a point target and size of the target should not increase more than one range cell; no target should move to the next range cell during observation time of image, this is called no range migration [139].

In general, SAR uses higher transmitted chirp bandwidth to get better range resolution. In

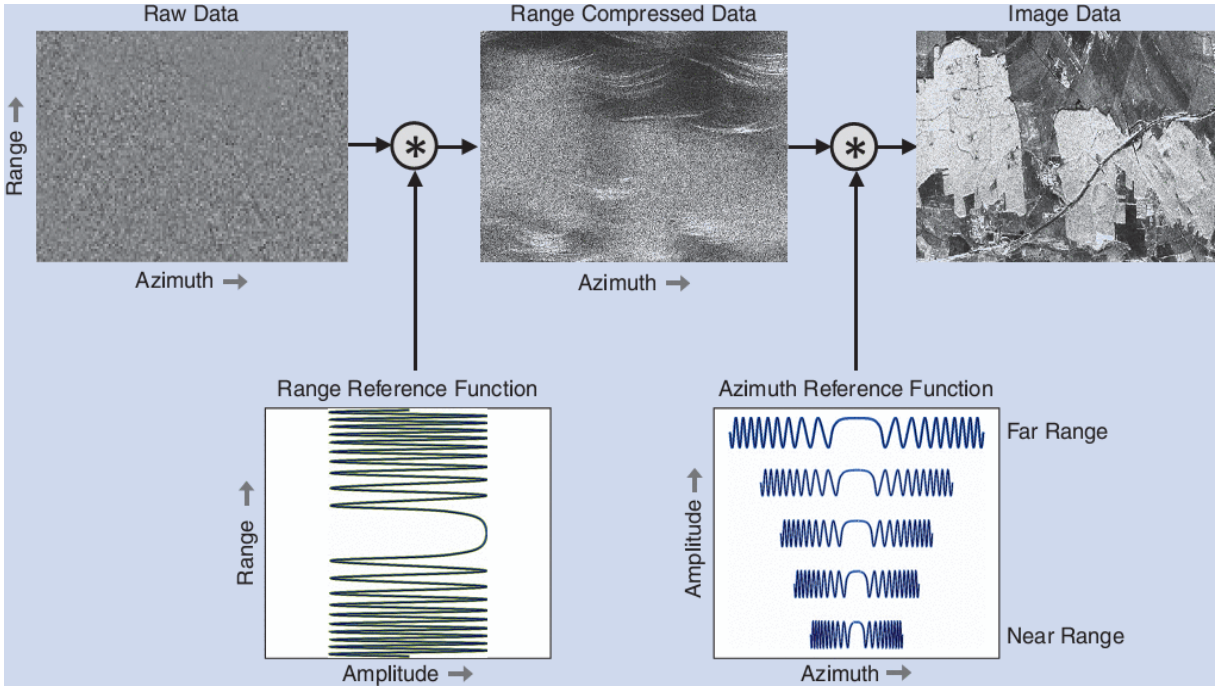

Figure 1.2: SAR Processing using Range Doppler Algorithm (Image courtesy: Moreira et al. [70])

order to ensure no range migration across multiple PRT during the observation time, range cell migration compensation (RCMC) has to be performed after range compression.

Currently, azimuth direction chirp parameters are calculated based on aircraft velocity, wavelength, and height of aircraft from the ground for static targets in SAR as shown in Eq. (1.67). These azimuth direction chirp parameters will be used in performing azimuth direction matched filtering. Inaccuracies in aircraft velocity and height lead to inaccurate target positions and blurred SAR images.

In short, range-Doppler algorithm (RDA) performs two dimensional (range and azimuth) radar matched filtering along with RCMC if required. The flowchart in Fig.1.3 describes the full flow of a conventional RDA to process SAR images [70].

1.6 Motivation and scope

Many real world applications associated with radar, sonar and bio-medical signal processing involve multicomponent higher order polynomial chirps [6,12,32,80,84,107]. Fourier transform (FT) is one of the simplest ways to analyze them in the frequency domain, but it is not suitable to localize a large variety of frequency modulated signals such as chirp signals. Similarly, STFT

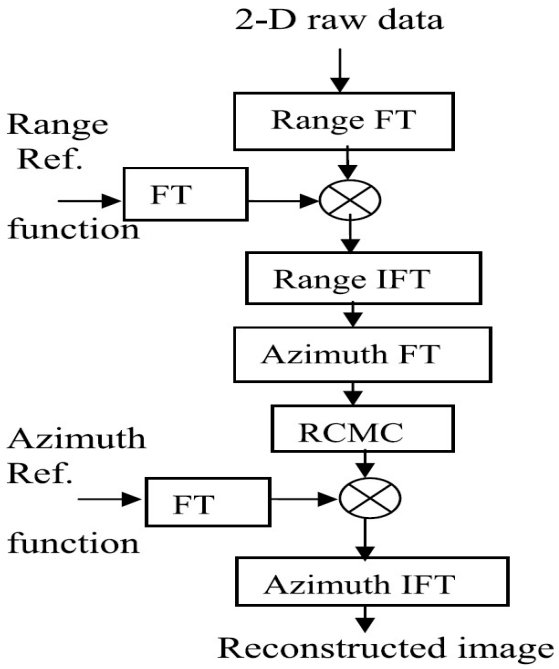

Figure 1.3: Flowchart of SAR Processing using RDA

is one of the simplest ways of representing them in the time-frequency plane, but it is not able to produce high concentration, high resolution, based TFD for multicomponent higher order polynomial chirps and a large variety of frequency modulated signals. Therefore, alternative time-frequency distributions and transforms are proposed in the literature and mentioned in the previous section [12, 15, 25, 37, 107]. Drawback and performance summary of the transforms and TFDs are as follows:

1.6.1 Drawbacks of linear transform based TFDs

Linear transforms and TFDs such as STFT, Gabor Transform, CWT, S-transform, and S-transform based spectrogram are linear in nature, and they do not produce cross-terms during multicomponent polynomial signal analysis. They are ineffective in localizing linear, quadratic, and higher order chirps.

Synchrosqueezed STFT and synchrosqueezed wavelet transform do not provide better time-frequency resolution and parameter estimation than STFT and wavelet transform; they only improve the readability of TFD [3, 47].

FrFT, STFrFT and adaptive fractional spectrogram [5,51] are linear transforms, and they are capable of localizing linear chirp signals, but fail to provide high concentration, high resolution TFD for quadratic and higher order chirps. STFrFT and FrFT follow the property of index

additivity of angle. Hence they are computationally efficient.

1.6.2 Drawbacks of quadratic transform based TFDs

To overcome the shortcomings of linear transforms, many quadratic transforms and TFDs are proposed in the literature and mentioned in the previous section, such as WVD, Pseudo WVD, Smooth WVD, ambiguity function, and Choi-Williams TFDs. All these TFDs can localize a linear chirp but produce cross-terms in multicomponent signal analysis. Similar to linear TFDs, quadratic TFDs are incapable of providing high concentration, high-resolution TFD for quadratic, and higher order chirps.

1.6.3 Drawbacks of higher order transform based TFDs

To overcome the shortcomings of linear and quadratic transforms, many higher order transforms, and TFDs have been proposed in the existing literature and mentioned in the previous section, such as CPF and its variants, and high resolution time-frequency rate representation. They are able to localize quadratic chirps, but both are non-linear transforms and produce cross-terms in multicomponent signal analysis.

Similarly, PWVD and HAF can estimate parameters of higher order polynomial chirp and are computationally efficient, but both TFDs are non-linear in nature and produce cross-terms in multicomponent polynomial signal analysis. Each iterative correlation or moment in HAF produces cross-terms and increases the 6 dB SNR threshold for parameter estimation for the multicomponent polynomial chirp. [12]

Sinusoidal frequency modulated transform can localize sinusoidal frequency modulated signals and is useful for rotating and vibrating target classification in radar application but is incapable of localizing higher order polynomial signals.

PFT and LPFT are linear transforms, and they are extensions of Fourier transform and STFT, respectively. PFT and LPFT can localize higher order polynomial chirps and do not produce cross-terms in multicomponent polynomial signal analysis. Neither of the transforms follow the property of index additivity of angle; therefore, they are not computationally efficient. PFT, LPFT are capable of localizing only higher order polynomial chirps and are incapable of producing high concentration, high-resolution TFD for a large variety of signals such as sinusoidal frequency modulated signals.

Generalized parametric time-frequency transform can localize a large variety of signals by selecting optimum kernel functions. GPTF is a linear transform, and it does not produce cross-terms in multicomponent signal analysis. GPTF does not follow the property of index additivity of angle; thereby, it is not computationally efficient. GPTF window does not change with signal length. Hence, the author does not claim to give high concentration, high-resolution TFD for a larger variety of signals.

Hence, there is a strong requirement to represent multicomponent higher order polynomial chirps on a high concentration, high-resolution cross-term free spectrogram using computationally efficient TFDs and transforms.

The generalized time-frequency transform (GTFT) has been shown to analyze many multicomponent higher order polynomial chirp signals [92–94]. GTFT is a parametric transform, and it can analyze a variety of signals by an appropriate selection of the parametric function in the GTFT kernel. GTFT is a linear transform, and it does not produce any cross term during the analysis of the multicomponent signal. GTFT follows the property of index additivity of angle (similar to FrFT), thereby it is computationally efficient. However, GTFT has the following fundamental limitations in analyzing multicomponent frequency modulated signals:

1. GTFT is not adequate to represent the variation of frequency over time for non-stationary signals.

2. The computational complexity of GTFT to analyze higher order polynomial chirps (order > 3) is high due to the parameter search operation.

3. Signal to noise ratio (SNR) gain of GTFT transform is less than time domain matched filtering. So it is difficult to analyze/detect low SNR targets.

4. The application of GTFT in practical systems is not yet explored.

Above mentioned shortcomings of linear, quadratic and higher order TFDs, is the motivation to work on TFDs and transforms of multicomponent higher order frequency modulated signals and their application in the field of radar.

1.7 Objectives and contributions

1.7.1 Objectives

The following are some of the fundamental problems explored in this thesis:

1. Are there effective methods to represent a wide variety of multicomponent higher order chirps and other frequency modulated signals, whose parameters (quadratic rate, chirp rate, Doppler frequency, etc.) change over time by generating a high concentration, high resolution, cross-term free time-frequency distribution for detection, extraction, analysis and representation purposes?

2. Are there ways to detect moving targets' parameters such as tangential acceleration, radial velocity, and tangential velocity over SAR data for better detection probability and less parameter estimation error and focusing of moving target on SAR image?

3. Are there methods to analyze higher order chirp waveform properties such as peak to side-lobe ratio, time delay resolution, Doppler resolution, and tolerance characteristic for radar applications? Are there ways to detect multicomponent frequency modulated signals with reduced computational complexity and better detectability in the presence of noise?

4. Are there ways to perform joint estimation of time delay, Doppler frequency, Doppler rate, and rate of change of Doppler rate simultaneously with maximum SNR gain (equivalent to time domain matched filtering) in the presence of AWGN? Are there ways to reduce SNR gain degradation due to the range-Doppler coupling effect of chirp waveforms?

1.7.2 Contributions

This thesis attempts to solve the above mentioned problems in the following ways:

1. Short-time GTFT (STGTFT) and STGTFT based adaptive generalized fractional spectrogram (AGFS) are proposed. The AGFS is capable of providing a high concentration, high resolution, cross-term free time-frequency distribution (TFD) for analyzing multicomponent frequency modulated signals. It is also a generalization of the short-time Fourier transform (STFT) based spectrogram and the short-time fractional Fourier transform (STFrFT) based spectrogram. The uncertainty principle is derived for STGTFT,

fractional ambiguity function, and fractional WVD, and TBP of the quadratic chirp of STGTFT is shown to be less than the TBP of STFrFT, STFT, and lower bound of TBP of fractional ambiguity function. The extraction algorithm is demonstrated for signals having two closely spaced amplitude modulated quadratic chirps whose parameters change during the length, and they indicate better performance of ck-AGFS as compared to the STFT based spectrogram. A mathematical derivation of the SNR gain of ck-AGFS for analyzing multicomponent quadratic chirps shows that it is higher than those of GTFT and STFT, and the same was corroborated in simulations. Ck-AGFS based parameter estimation is demonstrated to be better than GTFT, and fractional ambiguity function based parameter estimation by reporting mean error in parameter estimation. The superiority of locally optimized-cubic kernel AGFS is demonstrated as compared to locally optimized STFrFT based spectrogram for the representation of closely spaced long and short overlapping chirps. Locally optimized cubic kernel AGFS outperformed other well-known TFDs in representing a real multicomponent bat signal. Local optimum window and global optimum window based STGTFT follows the property of index additivity of angle (similar to FrFT); hence, AGFS is computationally efficient. An application of AGFS to estimate higher order polynomial phase components in SAR ground moving target imaging is presented.

2. An approach is proposed for estimating and imaging of accelerated target over SAR data using AGFS, Radon, and keystone transform. The proposed method for SAR imaging of a moving target gives a decent performance during the non-negligible third order phase of the SAR moving target. It successfully corrects the range migrations and generates a focused image of the point target and can estimate the velocity and acceleration parameters of the SAR moving target. The superiority of AGFS based approach as compared to GTFT based approach is demonstrated, in terms of point target impulse response, SNR gain, mean estimation error, and target detection probability.

3. Generalized time-frequency transform (GTFT) based generalized fractional ambiguity function (GFAF), and generalized fractional Wigner-Ville Distribution (GFWVD) are proposed to analyze higher order radar waveform properties. An application of GFAF is presented to detect higher order multicomponent chirp with reduced computation as compared to GTFT and better detectability as compared to HAF transform. The Com-

putational complexity of GFAF is lesser than generalized CPF, maximum likelihood, and QML estimator for estimating higher order chirp parameters. GFAF is computationally efficient as compared to the GTFT for estimating the same higher order chirp. SNR gain of ck-GFAF for multicomponent cubic frequency modulated signal is less than that of time domain matched filter but is more than that of FrFT based AF and classical AF. At lower SNR, the mean error of ck-GFAF for parameter estimation of multicomponent cubic frequency modulated signal is high due to the presence of cross-terms. GFAF can provide better SNR threshold as compared to HAF, and other multi-lag phase differentiation transforms due to the use of a single de-chirping operation. At higher SNR, GFAF estimated parameters follow CRLB estimated parameters. Ck-GFAF is capable of estimating fourth order parameters of all the four components of the real multicomponent bat signal, and it is comparable with estimated parameters of FrFT based AF.

4. GTFT based generalized fractional matched filtering (GFMF) is proposed to detect target's higher order target parameters with equivalent SNR gain of time domain matched filtering and reduced SNR gain degradation due to the range-Doppler coupling effect of chirp waveforms. The SNR gain and impulse response of GFMF is derived. Simulations of SNR gain comparison are demonstrated to show the superior noise performance of GFMF as compared to time domain matched filtering, FrFT, and GTFT in the case of quadratic chirps. Simulation results are also presented to show that GFMF gives lesser SNR degradation than time-domain matched filtering for high-speed targets. The double quadratic chirp waveform proposed provides a method for joint estimation of time delay, velocity, acceleration, and jerk with a reasonable accuracy using GFMF. Finally, the MSE of estimated parameters is presented, from which it can be inferred that the MSE of GFMF is lower compared to other existing methods for the same input SNR.

1.8 Linkage between different chapters

This section presents the linkage between different chapters of the thesis. Chapter 1 presents brief classification time-frequency approaches, SAR, problem definition, and contribution.

Chapter 2 presents short-time GTFT (STGTFT) and STGTFT based adaptive generalized fractional spectrogram for providing a high concentration, high resolution, cross-terms free time-frequency distribution (TFD) for analyzing multicomponent frequency modulated signals.

Computational complexity and SNR gain are also demonstrated for parameter estimation of multicomponent frequency modulated signal.

As an application of AGFS, chapter 3 presents a novel approach for estimation of SAR ground moving target's radial velocity, tangential velocity, and tangential acceleration parameters, and SAR ground moving target imaging. In this chapter, the third order azimuth phase of SAR is considered non-negligible. The superiority of the proposed approach with AGFS is compared with GTFT based parameter estimation approach in terms of MSE, SNR gain, impulse responses, and region of convergence (ROC). Finally, SAR multiple ground moving targets imaging is presented based on AGFS to strengthen the proposed approach.

To reduce the computational complexity for parameter estimation of multicomponent higher order polynomial phase signal, chapter 4 presents generalized time-frequency transform (GTFT) based generalized fractional AF (GFAF), and generalized fractional Wigner-Ville distribution (GFWVD) are proposed. As an application, GFAF is presented for analyzing higher order polynomial chirp waveforms and estimating parameters of multicomponent higher order polynomial chirp with reduced computation complexity and comparable noise performance.

Chapter 5 presents GTFT domain matched filtering for estimating the parameters of higher order chirp signals with higher SNR gain in radar application. In terms of SNR gain, the GTFT domain matched filtering outperforms the FrFT transformation gain and is equal to that of the time domain matched filter in the case of time domain additive white Gaussian noise. SNR gain of time domain is superior to GTFT, GFAF, and AGFS. As an application of GTFT domain matched filtering, SNR gain degradation due to the range-Doppler coupling effect of quadratic chirp for a high-speed target is presented. Finally, a new waveform named double quadratic chirp is proposed to detect time delay, velocity, acceleration, and jerk of the moving target simultaneously using GTFT based matched filtering.

1.9 Organization of thesis

Chapter 1 presents a thorough literature study of various linear, quadratic and, higher order time-frequency distributions and transforms. This chapter presents problem definitions, objectives and contributions of the thesis.

Chapter 2 presents the STGTFT, inverse STGTFT, and AGFS, along with its properties and computational complexity. This chapter also presents the uncertainty principle of STGTFT and

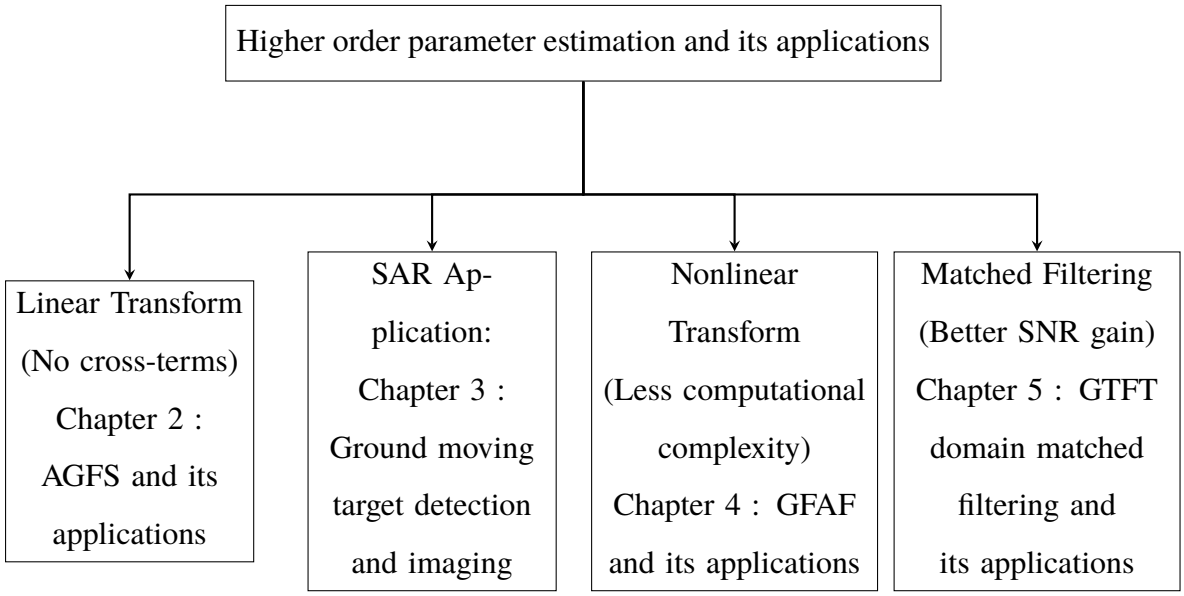

Figure 1.4: Broad organization of thesis

the comparison of AGFS with other TFDs. Extraction and estimation for the multicomponent quadratic signals are also presented along with real signals to validate results.

Chapter 3 presents an application of AGFS and GTFT for moving target detection and imaging over SAR data. This chapter presents an approach to estimate the moving target's tangential acceleration, radial velocity, and tangential velocity over SAR data.

Chapter 4 presents a generalized fractional ambiguity function (GFAF) and generalized fractional Wigner-Ville Distribution (GFWVD). This chapter presents GFAF for radar chirp waveform analysis and parameter estimation of higher order chirps with reduced computational complexity and less estimation error.

Chapter 5 presents a generalized fractional matched filtering for target detection with low SNR and reduces SNR gain degradation due to the range-Doppler coupling effect of chirp waveforms in radar. This chapter also presents a double quadratic chirp waveform for joint estimation of moving target's range, velocity, acceleration, and jerk simultaneously.

Chapter 6 contains a summary of the contributions of this thesis and some directions for further research on these topics. Fig (1.4) presents a broad organization of the thesis.

Chapter 2

Adaptive generalized fractional spectrogram

The generalised time-frequency transform (GTFT) is a powerful tool to analyse a large variety of frequency modulated signals. However, it is not adequate to represent the variation of frequency over time for non-stationary signals. To solve this problem, short-time GTFT and short-time GTFT based adaptive generalised fractional spectrogram (AGFS) are proposed. The AGFS is capable of providing a high concentration, high resolution, cross-term free time-frequency distribution for analysing multicomponent frequency modulated signals. It is also a generalisation of the short-time Fourier transform based spectrogram and the short-time fractional Fourier transform based spectrogram. The uncertainty principle for short-time GTFT is derived, and its time-bandwidth product is compared with other time-frequency distributions. With the help of simulated data examples, the effectiveness of AGFS is demonstrated in comparison to other time-frequency distributions for resolving and extracting individual components of multicomponent quadratic chirps. Robustness of AGFS is demonstrated under different input signal to noise ratio conditions. A local spectrogram optimisation technique is adopted for AGFS to represent simulated and real chirp signals. Finally, an application of the AGFS is presented to resolve multiple ground moving targets in synthetic aperture radar data and obtain its focused synthetic aperture radar image.

2.1 Introduction

Non-stationary signals such as higher order polynomial chirps are present in many practical systems like radar, sonar and bio-medical signal processing [6, 12, 32, 80, 84, 107]. Non-stationary signals can be analysed using time-frequency analysis for classification, detection and feature extraction purpose in many fields [13, 14, 97]. The short-time Fourier transform (STFT) based spectrogram is one of the simplest ways of representing them in the time-frequency plane, but it is not suitable to localise a large variety of signals such as chirp signals. Therefore, alternative time-frequency distributions (TFDs) are proposed in the literature, such as the Wigner-Ville distribution (WVD) [107], polynomial WVD [12, 107], chirplet transform based spectrogram [107], polynomial chirplet transform based spectrogram [130, 133], adaptive fractional spectrogram [5, 51], S-method based spectrogram [116], STFT adaptive window based spectrogram [75], high resolution time-frequency rate representation [144], cubic-phase function based distribution [29] and synchrosqueezing transform [3]. The WVD, the polynomial WVD, the high resolution time-frequency rate representation and cubic-phase function based distribution are all non-linear in nature and produce cross-terms when analysing multicomponent chirp signals. Similarly, a chirplet based spectrogram, adaptive fractional spectrogram, and STFT adaptive window based spectrogram are linear transforms but are unable to localise quadratic and higher order chirps. Similarly, synchrosqueezed STFT and synchrosqueezed wavelet transform do not provide better time-frequency resolution and parameter estimation than STFT and wavelet transform; it only improves the readability of time-frequency distribution (TFD) [47]. Hence, there is a strong requirement to represent multicomponent higher order polynomial chirps on a high concentration, high resolution cross-term free spectrogram.

The generalised time-frequency transform (GTFT) has been shown to analyse any higher order polynomial chirp signals [92–94]. In this chapter, the short-time GTFT (STGTFT) based adaptive generalised fractional spectrogram (AGFS) is proposed to analyse a large variety of multicomponent higher order polynomial and frequency modulated signals. The optimum window length of AGFS changes with signal length, hence it is adaptive in nature.

STGTFT follows the property of index additivity of angle (similar to FrFT); hence, AGFS is also computationally efficient. Non-parametric transforms such as FT, WVD, FrFT are unable to provide high concentration, high resolution TFDs for a variety of signals. AGFS overcomes this shortcoming and can provide a high concentration, high resolution TFD at its matched angle,

and optimum window. AGFS is capable of providing cross-term free TFD for multicomponent signal if the components have non-overlapping STGTFTs. AGFS can analyse a variety of signals by appropriate selection of the parametric function in the GTFT kernel. The short-time nature of AGFS allows it to represent and analyse the signals with changing parameters over the signal duration. These properties make AGFS superior to other TFDs.

This chapter is organized as follows:

- Section 2.2 reviews the basics of the fractional Fourier transform (FrFT), GTFT and inverse GTFT.

- Section 2.3 presents the STGTFT, inverse STGTFT, and AGFS and section 2.4 presents of AGFS properties and its computational complexity.

- Section 2.5 presents brief advantage of AGFS. Section 2.6 and section 2.7 present the derivation and simulation results for optimum window length in time and minimum variance in GTFT domain for the quadratic chirp signal, for different cases. The compactness of the quadratic chirp in the time-frequency plane at its matched angle and optimum window variance is demonstrated.

- Section 2.8 presents the derivation of the uncertainty principle for the STGTFT. Subsequently, as an example, the time-bandwidth product (TBP) of quadratic chirp analysed using the cubic kernel STGTFT (ck-STGTFT), fractional Fourier based ambiguity function (FrAF) and fractional Fourier based Wigner-Ville distribution(FrWVD) are derived. TBP of quadratic chirp obtained by ck-STGTFT is shown to be lower than the TBP obtained by short-time fractional Fourier transform (STFrFT), FrAF, and STFT.

- Section 2.9 presents the comparison of AGFS at its optimum order and optimum window length against well-known spectrograms for the representation of multicomponent quadratic chirp on the time-frequency plane.

- Section 2.10 presents the extraction of two closely spaced multicomponent quadratic chirps using AGFS for different cases in the presence of noise and results are compared with STFT based spectrogram.

- Section 2.11 shows the robustness of AGFS in terms of signal to noise ratio (SNR) gain and mean error in parameter estimation under different SNR conditions. Mathematical

derivation and simulation results of multicomponent quadratic chirps for SNR gain analysis of AGFS and its comparison with STFT, GTFT, FrAF, and time domain matched filtering SNR gain are also presented. Monte Carlo simulation results of mean error for estimation of quadratic frequency rate, chirp rate, and Doppler frequency parameters for multicomponent quadratic chirps using AGFS are presented, and it is compared with GTFT and FrAF based parameter estimation techniques.

- Section 2.12 presents a detailed description of locally optimized AGFS (LO-AGFS) method to analyze closely spaced long and short overlapping chirps. Furthermore, this section also shows a comparison of locally optimized ck-AGFS (LO-ck-AGFS) with locally optimized STFrFT based spectrogram for the representation of closely spaced long and short overlapping quadratic chirps in the time-frequency plane.

- Section 2.13 presents LO-ck-AGFS of real multicomponent bat echolocation signal and its comparison against well-known TFDs.

- Section 2.14 presents an application of AGFS to resolve two closely spaced synthetic aperture radar (SAR) ground moving targets. It compares the distinguishing capability of AGFS with STFT based spectrogram for the representation of two closely spaced SAR ground moving targets. A focused image of SAR ground moving targets after parameter estimation is presented.

2.2 Preliminaries

2.2.1 Fractional Fourier transform

The fractional Fourier transform (FrFT) is a generalization of the Fourier transform (FT). It depends on the parameter α, which can be interpreted as an angle of rotation in the time-frequency (TF) plane [2, 18, 73, 98, 115, 123]. The FrFT of a signal $x(t)$ is defined as

$$X_\alpha(f) = \int_{-\infty}^{+\infty} x(t) \cdot K_\alpha(t, f) dt, \tag{2.1}$$

where the kernel $K_\alpha(t, f)$ of FrFT is given by [33]

$$K_\alpha(t,f) = \begin{cases} (\sqrt{1 - i\cot\alpha}) \cdot exp\Big(i\pi t_0^2 f^2 \cot\alpha \\ \qquad + i\pi f_0^2 t^2 \cot\alpha - i2\pi f t \mathrm{cosec}\alpha\Big), & \text{if } \alpha \text{ is not a multiple of } \pi \\ \delta(f_0 t - t_0 f), & \text{if } \alpha \text{ is a multiple of } 2\pi \\ \delta(f_0 t + t_0 f), & \text{if } \alpha + \pi \text{ is a multiple of } 2\pi \end{cases} \tag{2.2}$$

where t_0, f_0 are dimensional normalization factors, $t_0^2 = \frac{T_{max}}{f_s}$, $f_0^2 = \frac{f_s}{T_{max}}$, $t_0^2 f_0^2 = 1$, T_{max} is the window length during FrFT and f_s is the sampling frequency. The unit of t_0 is seconds and f_0 is Hz.

It should be noted that at $\alpha = \frac{\pi}{2}$, K_α becomes the kernel of the Fourier transform, and hence the FrFT of the signal becomes the Fourier transform of the signal. The FrFT is a linear transform, so it does not produce cross-terms during multicomponent signal analysis.

2.2.2 Generalized time-frequency transform

If a signal $x(t)$ has finite absolute integral (finite L^1 norm), its GTFT evaluated at parameters (α, λ) is given by

$$X_{\alpha,\lambda}(f) = \int_{-\infty}^{+\infty} x(t) \cdot K_{\alpha,\lambda}(t,f) dt, \tag{2.3}$$

where $K_{\alpha,\lambda}(t, f)$ is the kernel of GTFT and it is defined as [92–94]

$$K_{\alpha,\lambda}(t,f) = \begin{cases} \sqrt{1 - i\cot\alpha} \cdot exp\Big(i\pi t_0^2 f^2 \cot\alpha + i\pi f_0^2 t^2 \cot\alpha \\ \qquad - i2\pi f t \mathrm{cosec}\alpha + i \cdot h(\lambda, t_0 f) - i \cdot h(\lambda, f_0 t)\Big), & \text{if } \alpha \text{ is not a multiple of } \pi \\ \delta(f_0 t - t_0 f), & \text{if } \alpha \text{ is a multiple of } 2\pi \\ \delta(f_0 t + t_0 f), & \text{if } \alpha + \pi \text{ is a multiple of } 2\pi \end{cases} \tag{2.4}$$

where $h(\cdot)$ is a real valued dimensionless function, and α and λ are the real valued GTFT parameters.

One speciality of the GTFT kernel is that it follows the property of index additivity of angle [2, 93], i.e

$$\int_{-\infty}^{+\infty} K_{\alpha_1,\lambda}(t,f) K_{\alpha_2,\lambda}(f,u) df = K_{(\alpha_1+\alpha_2),\lambda}(t,u). \tag{2.5}$$

The GTFT is a generalization of the FrFT, and hence a further generalization of the Fourier transform. It can be used to analyze a much wider variety of frequency modulated signals by varying $h(\cdot)$ in the GTFT kernel. For example, if $h(\cdot)$ is defined as a polynomial function, then

the resultant GTFT can be used to analyze polynomial phase signals. On the other hand, if $h(\cdot)$ is defined as a sinusoidal function, then the resultant GTFT can be used to analyze sinusoidal frequency modulated signals, and so on. Some of the GTFT kernels are as shown below:

- Cubic-kernel-GTFT (ck-GTFT) may be defined by substituting the parametric function $h(\cdot)$ as $h(\lambda, z) = \pi\lambda z^3$. Ck-GTFT is a highly useful transform used to analyze quadratic chirp signals, and is explored in detail in the later parts of this chapter. It is to be noted that the ck-GTFT is similar to the 3$^{\text{rd}}$ order polynomial Fourier transform (PFT) [32], with the added advantage of possessing the property of index additivity of angle.

- Sinusoidal-kernel-GTFT may be defined by substituting a multiparametric function $h(\cdot)$ as $h(A, \phi, \lambda, z) = A\sin(\pi\lambda z + \phi)$, where A, ϕ and λ are the variable parameters, which can be tuned to match the kernel with signal for estimating parameters. This can be a useful transform to analyze certain micro-Doppler effects in radar for the classification of rotating and vibrating targets [20, 21].

Inverse GTFT is defined as [94]

$$x(t) = \int_{-\infty}^{\infty} X_{\alpha,\lambda}(f) \cdot K^*_{\alpha,\lambda}(t, f)df, \tag{2.6}$$

where $K^*_{\alpha,\lambda}(t, f)$ is the complex conjugate of $K_{\alpha,\lambda}(t, f)$. If $X_{\alpha,\lambda}(f)$ has a finite absolute sum (finite L^1 norm), the above inverse exists. GTFT is a linear transform. It does not produce cross-terms, which is beneficial during multicomponent signal analysis.

2.2.3 Relationship of GTFT with other transforms

As shown in the Eq. (2.3), GTFT has the capability to analyze different type of signals by changing its function $h(\cdot)$. So GTFT can be related to multiple transforms by changing its $h(\cdot)$ function. A Table (2.1) is presented to show the relationship of GTFT with other transforms [2, 81, 130, 133].

2.2.4 Useful formulae

Gaussian integral:

$$\int_{-\infty}^{+\infty} e^{-At^2 \pm 2Bt + C} dt = \sqrt{\frac{\pi}{A}} e^{\frac{B^2}{A} + C}, \tag{2.7}$$

Table 2.1: Relationship of GTFT with other transforms

Sl No.	$h(\lambda, t)$	α	transform type
1	0	90°	Fourier transform
2	0	$\neq 90°$	Fractional Fourier transform
3	$\lambda_1 t^3 + \lambda_2 t^4 + .. + \lambda_{n-2} t^n$	$\neq 90°$	Polynomial Fourier Transform
4	$\sum_{-\infty}^{+\infty} \sin \lambda \omega t$	90°	Fourier sinusoidal transfrom
5	$\sum_{-\infty}^{+\infty} \sin \lambda_0 \omega t + \lambda_1 t^3 + \lambda_2 t^4 + .. + \lambda_{n-2} t^n$	$\neq 90°$	Polynomial spline transform

where A, B, $C \in \mathbb{C}$, $A \neq 0$, and $Re(A) \geq 0$ [115].

Principle of stationary phase:

The principle of stationary phase (PSP) is used to obtain an approximate closed-form expression for the integral of a function, whose amplitude $A(t)$ varies very slowly in comparison to the phase $\phi(t)$. Over the interval where the phase varies rapidly compared to amplitude, the contribution to the integral is negligible because positive and negative parts of the phase cancel each other. Hence, the non-zero contribution comes mainly from the stationary phase point 't_0' [107] which implies

$$\int_{-\infty}^{+\infty} A(t) \cdot e^{i\phi(t)} \cdot dt \approx \sqrt{\frac{2\pi}{\phi''(t_0)}} \cdot A(t_0) e^{i\phi(t_0)} \cdot e^{\frac{i\pi}{4}}, \tag{2.8}$$

where $\phi''(t)$ is second derivative of the phase function $\phi(t)$ and 't_0' is the point where derivative of the phase function becomes equal to 0 ($\phi'(t_0) = 0$). At this point phase of the signal $\phi(t)$ is considered to be 'stationary'. If t_0, $t_1 ... t_n$ are the solutions of $\phi'(t) = 0$, then the integral can be approximated as

$$\int_{-\infty}^{+\infty} A(t) \cdot e^{i\phi(t)} \cdot dt \approx \sum_{k=0}^{n} \sqrt{\frac{2\pi}{\phi''(t_k)}} \cdot A(t_k) e^{i\phi(t_k)} \cdot e^{\frac{i\pi}{4}}. \tag{2.9}$$

This stationary phase approximation is accurate for high time-bandwidth products [27]. If a_0 is the coefficient of t in the phase function $\phi(t)$, then PSP is valid for $|a_0| >> 0$.

2.3 Definition of proposed STGTFT and AGFS

2.3.1 Proposed short-time GTFT

The short-time GTFT (STGTFT) of a signal $x(t)$ evaluated using a window $g(t)$, at parameters (α, λ) can be defined as

$$X^{g}_{\alpha,\lambda}(t,f) = \int_{-\infty}^{+\infty} x(\tau) \cdot g(\tau - t) \cdot K_{\alpha,\lambda}(\tau, f) d\tau, \tag{2.10}$$

where $g(\cdot)$ is a window (typically Gaussian) and $K_{\alpha,\lambda}(\tau, f)$ is the GTFT kernel.

2.3.2 Property of index additivity of angle for STGTFT

The STGTFT follows the property of index additivity of angle as depicted by Eq. (2.11). It is to be noted that the ck-GTFT kernel based STGTFT is similar to the 3$^{\text{rd}}$ order localized polynomial Fourier transform (LPFT), with the added advantage of possessing the property of index additivity of angle. As a result, many different STGTFTs can be calculated easily using a single STGTFT; hence STGTFT is computationally efficient.

$$X^{g}_{\alpha_1+\alpha_2,\lambda}(t,u) = \int_{-\infty}^{+\infty} X^{g}_{\alpha_1,\lambda}(t,f) K_{\alpha_2,\lambda}(f,u) df. \tag{2.11}$$

Proof:

Using formula of $X^{g}_{\alpha_1+\alpha_2,\lambda}(t,u)$ from equation 2.10 and placing it at the LHS, we get the condition for index additivity to be true.

$$X^{g}_{\alpha_1+\alpha_2,\lambda}(t,f) = \int_{-\infty}^{+\infty} x(\tau) \cdot g(\tau - t) \cdot K_{\alpha_1+\alpha_2,\lambda}(\tau, f) d\tau,$$

$$\int_{-\infty}^{+\infty} x(\tau) \cdot g(\tau - t) \cdot K_{\alpha_1+\alpha_2,\lambda}(\tau, u) d\tau = \int_{-\infty}^{+\infty} X^{g}_{\alpha_1,\lambda}(t,f) K_{\alpha_2,\lambda}(f,u) df,$$

Here, Eq. (2.11) is valid iff

$$K_{\alpha+\beta,\lambda}(t,u) = \int_{-\infty}^{+\infty} K_{\alpha,\lambda}(t,f) K_{\beta,\lambda}(f,u) df. \tag{2.12}$$

$$
\begin{aligned}
K_{\alpha+\beta,\lambda}(t,u) &= \sqrt{1-i\cot(\alpha+\beta)}\cdot exp[i\pi(t^2f_0^2\cot(\alpha+\beta)+u^2t_0^2\cot(\alpha+\beta)\\
&\quad -2tu\text{cosec}(\alpha+\beta))-ih(\lambda,tf_0)+ih(\lambda,ft_0)],\\
&= \sqrt{1-i\cot(\alpha+\beta)}\cdot exp\left(i\pi(t^2f_0^2\cot\alpha+u^2t_0^2\cot\beta)\right)\\
&\quad \cdot exp\left[i\pi\left(\frac{t^2f_0^2\cos(\alpha+\beta)+u^2t_0^2\cos(\alpha+\beta)-2tu}{\sin(\alpha+\beta)}\right)\right.\\
&\quad \left.-i\pi t^2f_0^2\cot\alpha-i\pi u^2t_0^2\cot\beta-ih(\lambda,tf_0)+ih(\lambda,ft_0)\right],\\
&= \sqrt{1-i\cot(\alpha+\beta)}\cdot exp(i\pi(t^2f_0^2\cot\alpha+u^2t_0^2\cot\beta))\\
&\quad \cdot exp\left[i\pi\left(\frac{t^2f_0^2(\cos(\alpha+\beta)\sin\alpha-\cos\alpha\sin(\alpha+\beta))}{\sin(\alpha+\beta)\sin\alpha}\right.\right.\\
&\quad +\frac{u^2t_0^2(\cos(\alpha+\beta)\sin\beta-\cos\beta\sin(\alpha+\beta))}{\sin(\alpha+\beta)\sin\beta}\\
&\quad \left.\left.-\frac{2tu}{\sin(\alpha+\beta)}\right)-ih(\lambda,tf_0)+ih(\lambda,ft_0)\right],
\end{aligned}
\tag{2.13}
$$

$$
\begin{aligned}
K_{\alpha+\beta,\lambda}(t,u) &= \sqrt{1-i\cot(\alpha+\beta)}\cdot exp(i\pi(t^2f_0^2\cot\alpha+u^2t_0^2\cot\beta))\\
&\quad exp\left[i\pi\left(\frac{-t^2f_0^2sin\beta}{\sin(\alpha+\beta)\sin\alpha}-\frac{u^2t_0^2sin\alpha}{\sin(\alpha+\beta)\sin\beta}-\frac{2tu}{\sin(\alpha+\beta)}\right)\right.\\
&\quad \left.-ih(\lambda,tf_0)+ih(\lambda,ft_0)\right],\\
&= \sqrt{1-i\cot(\alpha+\beta)}\cdot exp(i\pi(t^2f_0^2\cot\alpha+u^2t_0^2\cot\beta))\\
&\quad \cdot exp\left[i\pi\left(\frac{-t^2f_0^2sin^2\beta-u^2t_0^2sin^2\alpha-2tusin\alpha\sin\beta}{\sin(\alpha+\beta)\sin\alpha\sin\beta}\right)\right.\\
&\quad \left.-ih(\lambda,tf_0)+ih(\lambda,ft_0)\right],
\end{aligned}
$$

$$
\begin{aligned}
K_{\alpha+\beta,\lambda}(t,u) &= \sqrt{1-i\cot(\alpha+\beta)}exp(i\pi(t^2f_0^2\cot\alpha+u^2t_0^2\cot\beta))\\
&\quad \cdot exp\left[i\pi\left(\frac{-(tf_0sin\beta+ut_0sin\alpha)^2}{\sin(\alpha+\beta)\sin\alpha\sin\beta}\right)-ih(\lambda,tf_0)+ih(\lambda,ft_0)\right],
\end{aligned}
\tag{2.14}
$$

$$\int_{-\infty}^{+\infty} K_{\alpha,\lambda}(t,f)K_{\beta,\lambda}(f,u)df = \sqrt{1-i\cot\alpha}\times\sqrt{1-i\cot\beta}\int_{-\infty}^{\infty} exp[i\pi t^2 f_0^2\cot\alpha + i\pi f^2 t_0^2\cot\alpha$$
$$- i2\pi t f\text{cosec}\alpha - ih(\lambda,tf_0) + ih(\lambda,ft_0) + i\pi f^2 t_0^2\cot\beta$$
$$+ i\pi u^2 t_0^2\cot\beta - 2i\pi f u t_0^2\text{cosec}\beta - ih(\lambda,ft_0) + ih(\lambda,ut_0)]df,$$
$$= \sqrt{(1-i\cot\alpha)(1-i\cot\beta)}\cdot exp[i\pi(t^2 f_0^2\cot\alpha + u^2 t_0^2\cot\beta)$$
$$- ih(\lambda,tf_0) + ih(\lambda,ut_0)]\int_{-\infty}^{\infty} exp[i\pi(f^2 t_0^2(\cot\alpha+\cot\beta)$$
$$- 2ft_0(tf_0\text{cosec}\alpha + ut_0\text{cosec}\beta))]df.$$

Using Gaussian integral formula (eq. 2.7) with $A = -i\pi(\cot\alpha+\cot\beta)$, $B = \pi i(tf_0\text{cosec}\alpha$ $+ ut_0\text{cosec}\beta)$ and $C = 0$,

$$\int_{-\infty}^{+\infty} K_{\alpha,\lambda}(t,f)K_{\beta,\lambda}(f,u)df = \frac{\sqrt{(1-i\cot\alpha)(1-i\cot\beta)}}{\sqrt{-i(\cot\alpha+\cot\beta)}}\cdot exp\Big[i\pi(t^2 f_0^2\cot\alpha + u^2 t_0^2\cot\beta)$$
$$- ih(\lambda,tf_0) + ih(\lambda,ut_0)\Big]exp\left[i\pi\left(\frac{-(tf_0\text{cosec}\alpha + ut_0\text{cosec}\beta)^2}{\cot\alpha+\cot\beta}\right)\right],$$
$$= \sqrt{1-i\cot(\alpha+\beta)}\cdot exp(i\pi(t^2 f_0^2\cot\alpha + u^2 t_0^2\cot\beta))$$
$$\cdot exp\left[i\pi\left(\frac{-(tf_0 sin\beta + ut_0 sin\alpha)^2}{\sin(\alpha+\beta)\sin\alpha\sin\beta}\right) - ih(\lambda,tf_0) + ih(\lambda,ft_0)\right],$$

$$\int_{-\infty}^{+\infty} K_{\alpha,\lambda}(t,f)K_{\beta,\lambda}(f,u)df = \sqrt{1-i\cot(\alpha+\beta)}\cdot exp(i\pi(t^2 f_0^2\cot\alpha + u^2 t_0^2 cot\beta))$$
$$\cdot exp\left[i\pi\left(\frac{-(tf_0 sin\beta + ut_0 sin\alpha)^2}{\sin(\alpha+\beta)\sin\alpha\sin\beta}\right) - ih(\lambda,tf_0) + ih(\lambda,ft_0)\right]. \tag{2.15}$$

From Eqns. (2.14) & (2.15),

$$K_{\alpha+\beta,\lambda}(t,u) = \int_{-\infty}^{+\infty} K_{\alpha,\lambda}(t,f)K_{\beta,\lambda}(f,u)df.$$

2.3.3 Proposed inverse short-time GTFT

For a unit L^2 norm window $g(t)$, the inverse short-time GTFT (I-STGTFT) of $X^g_{\alpha,\lambda}(t,f)$ having a finite L^1 norm is defined as

$$x(\tau) = \iint_{-\infty}^{+\infty} X^g_{\alpha,\lambda}(t,f)g^*(\tau-t)K^*_{\alpha,\lambda}(\tau,f)dtdf, \tag{2.16}$$

where $K^*_{\alpha,\lambda}(\tau, f)$ is a complex conjugate of $K_{\alpha,\lambda}(\tau, f)$. This inverse is unique.

Proof:

To prove this, we assume the retrieval formula as

$$\tilde{x}(\rho) = C \iint_{-\infty}^{+\infty} X^g_{\alpha,\lambda}(t, f)\hat{g}(\rho - t)K^*_{\alpha,\lambda}(\rho, f)dtdf, \tag{2.17}$$

where 'C' is a real constant and $\hat{g}(\cdot)$ is a window. Substituting Eq. (2.10) in Eq. (2.17), we get

$$\begin{aligned}
\tilde{x}(\rho) &= C \iiint_{-\infty}^{+\infty} x(\tau)g(\tau - t)K_{\alpha,\lambda}(\tau, f)\hat{g}(\rho - t)K^*_{\alpha,\lambda}(\rho, f)dtdfd\tau, \\
&= C \iint_{-\infty}^{+\infty} x(\tau)g(\tau - t)\hat{g}(\rho - t)\left(\int_{-\infty}^{+\infty} K_{\alpha,\lambda}(\tau, f)K^*_{\alpha,\lambda}(\rho, f)df\right)dtd\tau, \\
&= C \iint_{-\infty}^{+\infty} x(\tau)g(\tau - t)\hat{g}(\rho - t) \cdot \Big(exp[i\pi \cot\alpha(f_0^2(\tau^2 - \rho^2)) \\
&\qquad - i(h(\lambda, f_0\tau) - h(\lambda, f_0\rho))]\delta(\rho - \tau)\Big)dtd\tau.
\end{aligned} \tag{2.18}$$

Collapsing the integral in τ, we obtain:

$$\tilde{x}(\rho) = C \cdot x(\rho) \int_{-\infty}^{+\infty} g(\rho - t)\hat{g}(\rho - t)dt = C \cdot x(\rho) \int_{-\infty}^{+\infty} g(t)\hat{g}(t)dt. \tag{2.19}$$

To guarantee $\tilde{x}(\rho) = x(\rho)$, we require

$$\int_{-\infty}^{+\infty} g(t)\hat{g}(t)dt = \frac{1}{C}. \tag{2.20}$$

We choose $\hat{g}(t) = g^*(t)$, i.e, the complex conjugate of $g(t)$. Hence, it is required that $g(t)$ have a finite L^2 norm for the inverse to exist. Under these conditions, inverse STGTFT is

$$\begin{aligned}
x(\rho) &= C \iint_{-\infty}^{+\infty} X^g_{\alpha,\lambda}(t, f)g^*(\rho - t)K^*_{\alpha,\lambda}(\rho, f)dtdf, \\
&= \frac{1}{\int_{-\infty}^{+\infty} |g(t)|^2 dt} \iint_{-\infty}^{+\infty} X^g_{\alpha,\lambda}(t, f)g^*(\rho - t)K^*_{\alpha,\lambda}(\rho, f)dtdf.
\end{aligned} \tag{2.21}$$

Hence, for a unit L^2 norm window $g(t)$, Eq. (2.21) becomes Eq. (2.16). It is also easy to see that the inverse is unique.

2.3.4 Proposed AGFS

AGFS, denoted by $\rho^{x,g}_{\alpha,\lambda}(t,f)$ of a signal $x(t)$, evaluated using a window $g(t)$, at parameters (α,λ) is defined as

$$\rho^{x,g}_{\alpha,\lambda}(t,f) = \left| \int_{-\infty}^{+\infty} x(\tau) g(\tau - t) K_{\alpha,\lambda}(\tau, f) d\tau \right|^2 = |X^g_{\alpha,\lambda}(t,f)|^2, \tag{2.22}$$

where $K_{\alpha,\lambda}(\tau,f)$ is the GTFT kernel and window function $g(\cdot)$ is typically Gaussian.

AGFS can provide a high concentration, high resolution TFD for a variety of signals (polynomial, sinusoidal frequency modulated etc.) by appropriate selection of the parametric function $h(\cdot)$ in the GTFT kernel. For example, AGFS can use polynomial phase GTFT kernel to analyze multicomponent polynomial phase signals. Cubic-kernel-AGFS (ck-AGFS) may be defined by using cubic-kernel GTFT to analyze multicomponent quadratic frequency modulated signals with changing parameters over its duration. On the other hand, AGFS can use sinusoidal-kernel GTFT to analyze multicomponent sinusoidal frequency modulated phase signals with changing parameters over its duration. Furthermore, AGFS with the appropriately selected kernel can be used to analyse hybrid sinusoidal frequency modulated-polynomial phase signals with changing parameters over its duration. Similarly, parametric function $h(\cdot)$ of GTFT kernel can be appropriately selected for other types of frequency modulated signals.

2.4 Properties of AGFS

Summary of properties of AGFS are presented in Table 2.2 and properties of ck-AGFS are presneted in Table 2.3 .

Table 2.2: Summary of AGFS properties

Sl No.	Property name	Mathematical description
1	Relationship with other spectrograms	1. $\alpha = 90^\circ$ and $h(.) = 0$,$\rho^{x,g}_{\alpha,\lambda}(t,f)$ becomes STFT based spectrogram. 2. At $\alpha \neq 90^\circ$ and $h(.) = 0$, $\rho^{x,g}_{\alpha,\lambda}(t,f)$ becomes Fractional spectrogram 3. At $\alpha \neq 90^\circ$ and $h(.) \neq 0$ becomes Generalized Fractional Spectrogram
2	GTFT form of AGFS	$\rho^{x,g}_{\alpha,\lambda}(t,f) = \lvert\mathrm{cosec}\alpha\rvert \left\lvert \int_{-\infty}^{+\infty} X_{\alpha,\lambda}(f_1) G_{\frac{\pi}{2}}[(f-f_1)\mathrm{cosec}\alpha] K^*_{\alpha,\lambda}(t,f_1) df_1 \right\rvert^2$, where $X_{\alpha,\lambda}(f_1)$ is the GTFT of $x(\tau)$ and $G_{\frac{\pi}{2}}[(f-f_1)\mathrm{cosec}\alpha]$ is the Fourier transform of window $g(\cdot)$ at frequency $(f-f_1)\mathrm{cosec}\alpha$.
3	Reality	$\rho^{x,g*}_{\alpha,\lambda}(t,f) = \rho^{x,g}_{\alpha,\lambda}(t,f)$ AGFS is always real for any signal
4	Time marginality	$\int_{-\infty}^{+\infty} \rho^{x,g}_{\alpha,\lambda}(t,f)df = \lvert x(t)\rvert^2 *_t \lvert g(t)\rvert^2$, where $*_t$ is convolution over time variable t, $g(\cdot)$ is even window.
5	Frequency marginality	$\int_{-\infty}^{+\infty} \rho^{x,g}_{\alpha,\lambda}(t,f)dt = \lvert X_{\alpha,\lambda}(f)\rvert^2 *_f \lvert G_{\frac{\pi}{2}}(f)\rvert^2$; where $*_f$ is convolution over GTFT domain variable f and $G_{\frac{\pi}{2}}(f)$ is the symmetric Fourier transform of the window function $g(t)$.
6	Moyal property	$\iint_{-\infty}^{+\infty} \rho^{x,g}_{\alpha,\lambda}(t,f)dtdf = \iint_{-\infty}^{+\infty} \lvert x(\tau)\rvert^2 \lvert g(\tau-t)\rvert^2 d\tau dt = E_x \cdot E_g$, where E_x is the energy of the signal, and E_g is the energy of the window.
7	Time moments	$\iint_{-\infty}^{+\infty} t^n \rho^{x,g}_{\alpha,\lambda}(t,f)df\,dt = \int_{-\infty}^{+\infty} t^n \left[\lvert x(t)\rvert^2 *_t \lvert g(t)\rvert^2\right] dt$, for even window $g(\cdot)$.
8	Frequency moments	$\iint_{-\infty}^{+\infty} f^n \rho^{x,g}_{\alpha,\lambda}(t,f)df\,dt = \int_{-\infty}^{+\infty} f^n \left[\lvert X_{\alpha,\lambda}(f)\rvert^2 *_f \lvert G_{\frac{\pi}{2}}(f)\rvert^2\right] df$, for symmetric window Fourier transform $G_{\frac{\pi}{2}}(f)$
9	Time domain multiplication	$\rho^{z,g}_{\alpha,\lambda}(t,f) = \left\lvert \int_{-\infty}^{+\infty} X_{\alpha,\lambda}(f_1) K_{\alpha,\lambda}(t,f) K^*_{\alpha,\lambda}(t,f_1) G_{\frac{\pi}{2}}(f') *_{f'} [Y_{\frac{\pi}{2}}(f') e^{i2\pi t f'}] df_1 \right\rvert^2$ where $z(t) = x(t)y(t)$, $*_{f'}$ is convolution over variable $f' = (f-f_1)\mathrm{cosec}\alpha$ and $Y_{\frac{\pi}{2}}(f')$ is Fourier transform of $y(t)$ at frequency f'
10	Discretization in time	$\rho^{z,g}_{\alpha,\lambda}(t,f) = \sum_{n=-\infty}^{\infty} \rho^{x,g}_{\alpha,\lambda}(t, f - nf_s \sin\alpha)$, where $z(t)$ is sampled version of $x(t)$, f_s is Nyquist sampling frequency.

Table 2.3: Summary of ck-AGFS properties

Sl No.	Property name	Mathematical description
11	Time scaling	$\rho^{y,g}_{\alpha,\lambda}(t,f) = \|Y^{g}_{\alpha,\lambda}(t,f)\|^2 = \left\|\frac{\text{cosec}\alpha}{p\text{cosec}\beta}\right\| \rho^{x,g_1}_{\beta,\gamma}\left(pt, \frac{f\text{cosec}\alpha}{p\text{cosec}\beta}\right)$, where, $y(t) = \sqrt{p}\cdot x(pt)$, $\cot\beta = \cot\alpha/p^2$, $\gamma = \lambda/p^3$ and $g_1(t) = g(t/p)$
12	Time delay	$\rho^{y,g}_{\alpha,\lambda}(t,f) = \left\|\frac{\text{cosec}\alpha}{\text{cosec}\beta}\right\| \rho^{x,g}_{\beta,\lambda}\left(t-t_d, \frac{\text{cosec}\alpha}{\text{cosec}\beta}\left[f+\frac{3}{2}f_0^3\lambda t_d^2\sin\alpha - f_0^2 t_d\cos\alpha\right]\right)$, where, $\cot\beta = \cot\alpha - 3f_0\lambda t_d$, $\cot\beta = \cot\alpha - 3f_0\lambda t_d$, $y(t) = x(t-t_d)$
13	Frequency shift	$\rho^{y,g}_{\alpha,\lambda}(t,f) = \rho^{x,g}_{\alpha,\lambda}(t, f - f_d\sin\alpha)$, where $y(t) = x(t)\exp(2\pi f_d t)$
14	Convolution	AGFS of $h(\cdot)$ is given as $\|H^{g_1}_{\alpha,\lambda}(t,f)\|^2$, and $H^{g_1}_{\alpha,\lambda}(t,f) = [(g(t)K_{\alpha,\lambda}(t,f)) *_t F^{g_1}_{\alpha,\lambda}(t,f)]\cdot e^{-i\pi t_0^3\lambda f^3 - i\pi t_0^2 f^2\cot\alpha}$, where $h(\cdot) = f(\cdot) * g(\cdot)$ and $F^{g_1}_{\alpha,\lambda}(t,f)$ is the STGTFT of $f(\cdot)$ with window $g_1(\cdot)$
15	Linearity	$\rho^{x_1+x_2,g}_{\alpha,\lambda}(t,f) = \rho^{x_1,g}_{\alpha,\lambda}(t,f) + \rho^{x_2,g}_{\alpha,\lambda}(t,f)$, if $x_1(t)$ and $x_2(t)$ have non-overlapping STGTFTs.

2.4.1 Relationship with other spectrograms

It can be seen that, if:

Case 1: $\alpha = 90^\circ$ and $h(\cdot) = 0$ $\rho^{x,g}_{\alpha,\lambda}(t,f)$ becomes the short-time FT based spectrogram.

Case 2: $\alpha \neq 90^\circ$ and $h(\cdot) = 0$ $\rho^{x,g}_{\alpha,\lambda}(t,f)$ becomes the short-time FrFT based spectrogram. [115] [6] [79]

Case 3: $\alpha \neq 90^\circ$ and $h(\cdot) \neq 0$ $\rho^{x,g}_{\alpha,\lambda}(t,f)$ becomes the short-time GTFT based spectrogram.

2.4.2 GTFT form of AGFS

Inverse GTFT is defined as

$$x(\tau) = \int_{-\infty}^{+\infty} X_{\alpha,\lambda}(f_1)\cdot K^*_{\alpha,\lambda}(\tau, f_1)\mathrm{d}f_1. \tag{2.23}$$

Substitute inverse GTFT form of $x(\tau)$ in AGFS expression. Then

$$\rho^{x,g}_{\alpha,\lambda}(t,f) = \left|\iint_{-\infty}^{+\infty} X_{\alpha,\lambda}(f_1)K^*_{\alpha,\lambda}(\tau,f_1)g(\tau-t)K_{\alpha,\lambda}(\tau,f)df_1 d\tau\right|^2,$$

$$= |1 - i\cot\alpha|^2 \left| \iint_{-\infty}^{+\infty} X_{\alpha,\lambda}(f_1) g(\tau - t) exp[i\pi t_0^2 \cot\alpha(f^2 - f_1^2) + i\pi f_0^2 \cot\alpha(\tau^2 - \tau^2) + ih(\lambda, t_0 f) - ih(\lambda, t_0 f_1) + i2\pi\tau \mathrm{cosec}\alpha(f_1 - f)] d\tau df_1 \right|^2.$$

Substitute $\tau - t = \tau^{'}, \quad d\tau = d\tau^{'}$ and $\tau = \tau^{'} + t$. Then

$$\rho_{\alpha,\lambda}^{x,g}(t,f) = \left| \int_{-\infty}^{+\infty} X_{\alpha,\lambda}(f_1) G_{\frac{\pi}{2}}[(f - f_1)\mathrm{cosec}\alpha] K_{\alpha,\lambda}(t,f) K_{\alpha,\lambda}^*(t,f_1) df_1 \right|^2, \tag{2.24}$$

where,

$$\int_{-\infty}^{+\infty} g(\tau^{'}) e^{-i2\pi\tau^{'}\mathrm{cosec}\alpha(f-f_1)} d\tau^{'} = G_{\frac{\pi}{2}}[(f - f_1)\mathrm{cosec}\alpha],$$

i.e, $G_{\frac{\pi}{2}}[(f - f_1)\mathrm{cosec}\alpha]$ is Fourier transform of $g(\cdot)$ at $f = (f - f_1)\mathrm{cosec}\alpha$.

Eq.(2.24) can be simplified as

$$\rho_{\alpha,\lambda}^{x,g}(t,f) = |\mathrm{cosec}\alpha| \left| \int_{-\infty}^{+\infty} X_{\alpha,\lambda}(f_1) G_{\frac{\pi}{2}}[(f - f_1)\mathrm{cosec}\alpha] K_{\alpha,\lambda}^*(t,f_1) df_1 \right|^2. \tag{2.25}$$

The GTFT form of AGFS is given by

$$\rho_{\alpha,\lambda}^{x,g}(t,f) = |\mathrm{cosec}\alpha| \left| \int_{-\infty}^{+\infty} X_{\alpha,\lambda}(f_1) G_{\frac{\pi}{2}}[(f - f_1)\mathrm{cosec}\alpha] K_{\alpha,\lambda}^*(t,f_1) df_1 \right|^2, \tag{2.26}$$

where $X_{\alpha,\lambda}(f_1)$ is the GTFT of $x(\tau)$ and $G_{\frac{\pi}{2}}[(f - f_1)\mathrm{cosec}\alpha]$ is the Fourier transform of window $g(\cdot)$ at frequency $(f - f_1)\mathrm{cosec}\alpha$.

2.4.3 Reality

AGFS is always real for any signal, even if signal is complex.

$$\begin{aligned}
\rho_{\alpha,\lambda}^{x,g^*}(t,f) &= \left[|X_{\alpha,\lambda}^g(t,f)|^2 \right]^* = \left[X_{\alpha,\lambda}^g(t,f) X_{\alpha,\lambda}^{g^*}(t,f) \right]^*, \\
&= X_{\alpha,\lambda}^{*g}(t,f) \left[X_{\alpha,\lambda}^{*g}(t,f) \right]^*, \\
&= X_{\alpha,\lambda}^{*g}(t,f) \left[\int_{-\infty}^{+\infty} x^*(\tau) g^*(\tau - t) K_{\alpha,\lambda}^*(\tau,f) d\tau \right]^*, \\
&= X_{\alpha,\lambda}^{*g}(t,f) \int_{-\infty}^{+\infty} x(\tau) g(\tau - t) \left[K_{\alpha,\lambda}^*(\tau,f) \right]^* d\tau.
\end{aligned} \tag{2.27}$$

GTFT kernel follows index additivity and unitary property so,

$$\begin{aligned} \left[K^*_{\alpha,\lambda}(\tau,f)\right]^* &= K_{\alpha,\lambda}(\tau,f), \\ \Rightarrow X^{*g}_{\alpha,\lambda}(t,f)X^{g}_{\alpha,\lambda}(t,f) &= \rho^{x,g}_{\alpha,\lambda}(t,f), \\ \Rightarrow \rho^{x,g*}_{\alpha,\lambda}(t,f) &= \rho^{x,g}_{\alpha,\lambda}(t,f). \end{aligned} \tag{2.28}$$

2.4.4 Time marginality

AGFS follows the time marginal property of the spectrogram similar to the STFT based spectrogram. It is obtained by integrating AGFS over frequency i.e.

$$\begin{aligned} \int_{-\infty}^{+\infty} \rho^{x,g}_{\alpha,\lambda}(t,f)df &= \int_{-\infty}^{+\infty} \left| \int_{-\infty}^{+\infty} x(\tau)g(\tau-t)K_{\alpha,\lambda}(\tau,f)d\tau \right|^2 df, \\ &= \iiint_{-\infty}^{+\infty} x(\tau_1)x^*(\tau_2)g(\tau_1-t)g^*(\tau_2-t)K_{\alpha,\lambda}(\tau_1,f)K^*_{\alpha,\lambda}(\tau_2,f)d\tau_1 d\tau_2 df, \\ &= \iiint_{-\infty}^{+\infty} x(\tau_1)x^*(\tau_2)g(\tau_1-t)g^*(\tau_2-t)|\text{cosec}\alpha| \cdot exp\left[i\pi\cot\alpha \cdot f_0^2(\tau_1^2-\tau_2^2)\right. \\ &\qquad \left. +i2\pi f\,\text{cosec}\alpha(\tau_2-\tau_1) + i\cdot h(\lambda,f_0\tau_2) - i\cdot h(\lambda,f_0\tau_1)\right] d\tau_1 d\tau_2 df, \\ &= |\text{cosec}\alpha| \iint_{-\infty}^{+\infty} x(\tau_1)x^*(\tau_2)g(\tau_1-t)g^*(\tau_2-t)exp\left[i\pi\cot\alpha \cdot f_0^2(\tau_1^2-\tau_2^2)\right. \\ &\qquad \left. +i\cdot h(\lambda,f_0\tau_2) - i\cdot h(\lambda,f_0\tau_1)\right] \left[\int_{-\infty}^{+\infty} exp[i2\pi f\,\text{cosec}\alpha(\tau_2-\tau_1)]df\right] d\tau_1 d\tau_2, \\ &= |\text{cosec}\alpha| \iint_{-\infty}^{+\infty} x(\tau_1)x^*(\tau_2)g(\tau_1-t)g^*(\tau_2-t)exp[i\pi\cot\alpha f_0^2(\tau_1^2-\tau_2^2) \\ &\qquad + i\cdot h(\lambda,f_0\tau_2) - i\cdot h(\lambda,f_0\tau_1)\left[\frac{\delta(\tau_2-\tau_1)}{\text{cosec}\alpha}\right] d\tau_1 d\tau_2, \end{aligned} \tag{2.29}$$

$$\int_{-\infty}^{+\infty} \rho^{x,g}_{\alpha,\lambda}(t,f)df = \int_{-\infty}^{+\infty} |x(\tau)|^2|g(\tau-t)|^2 d\tau, \tag{2.30}$$

$$\int_{-\infty}^{+\infty} \rho^{x,g}_{\alpha,\lambda}(t,f)df = |x(t)|^2 *_t |g(t)|^2, \tag{2.31}$$

where $*_t$ is convolution over time 't' and $g(\cdot)$ is even window. So time marginal property of AGFS is not satisfied with correct marginal $|x(t)|^2$ due to presence of window.

2.4.5 Frequency marginality

AGFS follows the frequency marginal property of the spectrogram similar to the STFT based spectrogram and it is obtained by integrating AGFS over time i.e. Frequency Marginal Property can be easily derived from GTFT form AGFS as shown in equation(2.26)

$$\begin{aligned}\int_{-\infty}^{+\infty} \rho_{\alpha,\lambda}^{x,g}(t,f)dt &= \int_{-\infty}^{+\infty} \left| \int_{-\infty}^{+\infty} X_{\alpha,\lambda}(f_1) G[(f-f_1)\mathrm{cosec}\alpha] \cdot K_{\alpha,\lambda}(t,f) \cdot K_{\alpha,\lambda}^*(t,f_1) df_1 \right|^2 dt, \\ &= \iiint_{-\infty}^{+\infty} X_{\alpha,\lambda}(f_{11}) X_{\alpha,\lambda}^*(f_{22}) G[(f-f_{11})\mathrm{cosec}\alpha] G^*[(f-f_{22})\mathrm{cosec}\alpha] \\ &\quad \cdot K_{\alpha,\lambda}(t,f) \cdot K_{\alpha,\lambda}^*(t,f_{11}) \cdot K_{\alpha,\lambda}^*(t,f) K_{\alpha,\lambda}(t,f_{22}) df_{11} df_{22} dt.\end{aligned} \tag{2.32}$$

Similarly $f_{11} = f_{22} = f_1$,

$$\int_{-\infty}^{+\infty} \rho_{\alpha,\lambda}^{x,g}(t,f)dt = \int_{-\infty}^{+\infty} |X_{\alpha,\lambda}(f_1)|^2 \cdot |G[(f-f_1)\mathrm{cosec}\alpha]|^2 df_1, \tag{2.33}$$

$$\int_{-\infty}^{+\infty} \rho_{\alpha,\lambda}^{x,g}(t,f)dt = |X_{\alpha,\lambda}(f)|^2 *_f |G_{\frac{\pi}{2}}(f)|^2, \tag{2.34}$$

where $*_f$ is convolution over GTFT domain variable f and $G_{\frac{\pi}{2}}(f)$ is the symmetric Fourier transform of the window function $g(t)$.

2.4.6 Total energy or Moyal property

Total energy property of AGFS can be easily derived using time marginal property of AGFS as shown in equation(2.31) .

$$\iint_{-\infty}^{+\infty} \rho_{\alpha,\lambda}^{x,g}(t,f)dtdf = \iint_{-\infty}^{+\infty} |x(\tau)|^2 |g(\tau-t)|^2 d\tau dt = E_x \cdot E_w, \tag{2.35}$$

where E_x is the energy of the signal, and E_w is the energy of the window.

2.4.7 Time moments

Time moments property of AGFS can be easily derived using time marginal property of AGFS as shown in Eq. (2.31). For even window function $g(\cdot)$,

$$\iint_{-\infty}^{+\infty} t^n \rho_{\alpha,\lambda}^{x,g}(t,f)df\,dt = \iint_{-\infty}^{+\infty} t^n |x(\tau)|^2 |g(\tau-t)|^2 d\tau dt = \int_{-\infty}^{+\infty} t^n [|x(t)|^2 *_t |g(t)|^2] dt. \tag{2.36}$$

2.4.8 Frequency moments

Frequency moments property of AGFS can be easily derived using frequency marginal property of AGFS as shown in Eq. (2.34). For symmetric Fourier transform window

$$\iint_{-\infty}^{+\infty} f^n \rho_{\alpha,\lambda}^{x,g}(t,f)\,df\,dt = \iint_{-\infty}^{+\infty} f^n \left[|X_{\alpha,\lambda}(f_1)|^2 \cdot |G[(f-f_1)\mathrm{cosec}\alpha]|^2\right] \cdot df_1 df, \tag{2.37}$$

$$= \int_{-\infty}^{+\infty} f^n \left[|X_{\alpha,\lambda}(f)|^2 *_f |G(f)|^2\right] df. \tag{2.38}$$

2.4.9 Time scaling

Let $y(t) = \sqrt{p}x(pt)$. Then the ck-STGTFT of $y(t)$ is given by

$$Y_{\alpha,\lambda}^{g}(t,f) = \int_{-\infty}^{\infty} \sqrt{p}x(p\tau)\, g(\tau - t)\, K_{\alpha,\lambda}(\tau, f)\, d\tau. \tag{2.39}$$

Applying the transformation $\tau = \tau'/p$,

$$\begin{aligned}
Y_{\alpha,\lambda}^{g}(t,f) &= \frac{1}{\sqrt{p}} \int_{-\infty}^{\infty} x(\tau')\, g\left(\frac{\tau'}{p} - t\right) K_{\alpha,\lambda}\left(\frac{\tau'}{p}, f\right) d\tau', \\
&= \frac{\sqrt{1 - i\cot\alpha}}{\sqrt{p}} \int_{-\infty}^{\infty} x(\tau')\, g\left(\frac{\tau'}{p} - t\right) \exp\left(i\pi\cot\alpha\left(f_0^2\frac{\tau'^2}{p^2} + t_0^2 f^2\right)\right. \\
&\quad \left. - i2\pi\frac{\tau'}{p} f\mathrm{cosec}\alpha - i\pi f_0^3\lambda\frac{\tau'^3}{p^3} + i\pi t_0^3\lambda f^3\right) d\tau', \\
&= +\frac{\sqrt{1 - i\cot\alpha}}{\sqrt{p}} \exp\left(-i\pi t_0^2 f'^2\cot\beta + i\pi t_0^2 f^2\cot\alpha + i\pi t_0^3\lambda f^3\right. \\
&\quad \left. - i\pi t_0^3\gamma f'^3\right) \cdot \int_{-\infty}^{\infty} x(\tau')\, g\left(\frac{\tau'}{p} - t\right) \exp\left(i\pi\cot\beta\left(f_0^2\tau'^2 + t_0^2 f'^2\right)\right. \\
&\quad \left. - i2\pi f'\tau'\mathrm{cosec}\beta - i\pi f_0^3\gamma\tau'^3 + i\pi t_0^3\gamma f'^3\right) d\tau', \\
&= \frac{\sqrt{1 - i\cot\alpha}}{\sqrt{p(1 - i\cot\beta)}} \exp\left(-i\pi t_0^2 f'^2\cot\beta + i\pi t_0^2 f^2\cot\alpha + i\pi t_0^3\lambda f^3\right. \\
&\quad \left. - i\pi t_0^3\gamma f'^3\right) \cdot \int_{-\infty}^{\infty} x(\tau')\, g_1(\tau' - pt)\, K_{\beta,\gamma}(\tau', f')\, d\tau',
\end{aligned} \tag{2.40}$$

where $\cot\beta = \cot\alpha/p^2$, $f'\mathrm{cosec}\beta = f\mathrm{cosec}\alpha/p$, $\gamma = \lambda/p^3$ and $g_1(t) = g(t/p)$. Hence, if the ck-AGFS of $x(t)$ is analyzed using window function $g(t)$ is $\rho_{\alpha,\lambda}^{x,g}(t,f)$, then the AGFS of $y(t) = \sqrt{p}x(pt)$ is given by

$$\rho_{\alpha,\lambda}^{y,g}(t,f) = |Y_{\alpha,\lambda}^{g}(t,f)|^2 = \left|\frac{\mathrm{cosec}\alpha}{p\mathrm{cosec}\beta}\right| \rho_{\beta,\gamma}^{x,g_1}\left(pt, \frac{f\mathrm{cosec}\alpha}{p\mathrm{cosec}\beta}\right), \tag{2.41}$$

where $\cot\beta = \cot\alpha/p^2$, $\gamma = \lambda/p^3$ and $g_1(t) = g(t/p)$.

If the ck-AGFS of $x(t)$ is analyzed using window function $g(t)$ is $\rho^{x,g}_{\alpha,\lambda}(t,f)$, then the ck-AGFS of $y(t) = \sqrt{p}\cdot x(pt)$ is given by

$$\rho^{y,g}_{\alpha,\lambda}(t,f) = |Y^{g}_{\alpha,\lambda}(t,f)|^2 = \left|\frac{\mathrm{cosec}\alpha}{p\mathrm{cosec}\beta}\right| \rho^{x,g_1}_{\beta,\gamma}\left(pt, \frac{f\mathrm{cosec}\alpha}{p\mathrm{cosec}\beta}\right), \tag{2.42}$$

where, $\cot\beta = \cot\alpha/p^2$, $\gamma = \lambda/p^3$ and $g_1(t) = g(t/p)$

2.4.10 Time delay property

Let $y(t) = x(t-t_d)$ where t_d is the time delay. Then the ck-STGTFT of $y(t)$ is given by

$$\begin{aligned} Y^{g}_{\alpha,\lambda}(t,f) &= \int_{-\infty}^{\infty} x(\tau - t_d) g(\tau - t) K_{\alpha,\lambda}(\tau, f)\, d\tau, \\ &= \int_{-\infty}^{\infty} x(\tau') g(\tau' - (t - t_d)) K_{\alpha,\lambda}(\tau' + t_d, f)\, d\tau', \end{aligned} \tag{2.43}$$

where $\tau' = \tau - t_d$. Therefore,

$$\begin{aligned} Y^{g}_{\alpha,\lambda}(t,f) &= \int_{-\infty}^{\infty} x(\tau') g(\tau' - (t-t_d)) . \sqrt{1 - i\cot\alpha} . \exp[i\pi\cot\alpha(f_0^2(\tau' + t_d)^2 + t_0^2 f^2) \\ &\quad - i2\pi(\tau' + t_d) f\mathrm{cosec}\alpha - i\pi f_0^3 \lambda(\tau' + t_d)^3 + i\pi t_0^3 \lambda f^3] d\tau', \\ &= \sqrt{1 - i\cot\alpha} . \exp[i\pi f_0^2 t_d^2 \cot\alpha + i\pi t_0^2 f^2 \cot\alpha - i2\pi t_d f\mathrm{cosec}\alpha - i\pi f_0^3 \lambda t_d^3 \\ &\quad + i\pi t_0^3 \lambda f^3) . \int_{-\infty}^{\infty} x(\tau') g(\tau' - (t - t_d)) . \exp\left[i\pi(f_0^2\cot\alpha - 3f_0^3\lambda t_d)\tau'^2\right. \\ &\quad \left. - i2\pi\left(f\mathrm{cosec}\alpha - f_0^2 t_d\cot\alpha + \frac{3}{2} f_0^3 \lambda t_d^2\right)\tau' - i\pi f_0^3 \lambda \tau'^3\right] d\tau', \\ &= \frac{\sqrt{1 - i\cot\alpha}}{\sqrt{1 - i\cot\beta}} \exp(i\pi f_0^2 t_d^2 \cot\alpha + i\pi t_0^2 f^2 \cot\alpha - i2\pi t_d f\mathrm{cosec}\alpha - i\pi f_0^3 \lambda t_d^3 \\ &\quad + i\pi t_0^3 \lambda f^3 - i\pi t_0^2 f'^2 \cot\beta - i\pi t_0^3 \lambda f'^3) . \int_{-\infty}^{\infty} x(\tau') g(\tau' - (t - t_d)) \\ &\quad \cdot K_{\beta,\lambda}(\tau', f') d\tau', \end{aligned} \tag{2.44}$$

where $f'\mathrm{cosec}\beta = f\mathrm{cosec}\alpha - f_0^2 t_d\cot\alpha + \frac{3}{2} f_0^3 \lambda t_d^2$. Hence, AGFS of $y(t)$ is given by

$$\rho^{y,g}_{\alpha,\lambda}(t,f) = \left|\frac{\mathrm{cosec}\alpha}{\mathrm{cosec}\beta}\right| \rho^{x,g}_{\beta,\lambda}\left(t - t_d, \frac{\mathrm{cosec}\alpha}{\mathrm{cosec}\beta}\left[f + \frac{3}{2} f_0^3 \lambda t_d^2 \sin\alpha - f_0^2 t_d \cos\alpha\right]\right), \tag{2.45}$$

where $\cot\beta = \cot\alpha - \frac{3 f_0^3 \lambda t_d}{f_0^2}$. If the ck-AGFS of $x(t)$ is analyzed using window function $g(t)$ is $\rho^{x,g}_{\beta,\lambda}(t,f)$, then the ck-AGFS of $y(t) = x(t-t_d)$ is given by

$$\rho^{y,g}_{\alpha,\lambda}(t,f) = \left|\frac{\mathrm{cosec}\alpha}{\mathrm{cosec}\beta}\right| \rho^{x,g}_{\beta,\lambda}\left(t - t_d, \frac{\mathrm{cosec}\alpha}{\mathrm{cosec}\beta}\left[f + \frac{3}{2} f_0^3 \lambda t_d^2 \sin\alpha - f_0^2 t_d \cos\alpha\right]\right), \tag{2.46}$$

where $\cot\beta = \cot\alpha - 3 f_0 \lambda t_d$ So by shifting a signal in time by t_d amounts corresponds to shifting a AGFS by same amount t_d .

2.4.11 Frequency shift

Let $y(t) = x(t)\exp(i2\pi f_d t)$, where f_d is the frequency shift. Then ck-STGTFT of $y(t)$ is given by

$$\begin{aligned}
Y^g_{\alpha,\lambda}(t,f) &= \int_{-\infty}^{\infty} x(\tau)\exp(i2\pi f_d\tau)g(\tau-t)K_{\alpha,\lambda}(\tau,f)d\tau,\\
&= \int_{-\infty}^{\infty} x(\tau)g(\tau-t).\sqrt{1-i\cot\alpha}.\exp[i\pi\cot\alpha(f_0^2\tau^2+t_0^2f^2)\\
&\quad - i2\pi(f-f_d\sin\alpha)\tau\mathrm{cosec}\alpha - i\pi f_0^3\lambda\tau^3 + i\pi t_0^3\lambda f^3]d\tau,\\
&= \int_{-\infty}^{\infty} x(\tau)g(\tau-t).\sqrt{1-i\cot\alpha}.\exp[i\pi\cot\alpha(f_0^2\tau^2\\
&\quad + t_0^2(f-f_d\sin\alpha)^2) - i2\pi(f-f_d\sin\alpha)\tau\mathrm{cosec}\alpha - i\pi f_0^3\lambda\tau^3\\
&\quad + i\pi t_0^3\lambda(f-f_d\sin\alpha)^3]d\tau\cdot\exp(it_0^2\pi\cot\alpha(-f_d^2\sin^2\alpha\\
&\quad + 2f_d f\sin\alpha) + i\pi t_0^3\lambda(f_d^3\sin^3\alpha + 3f^2 f_d\sin\alpha - 3f f_d^2\sin^2\alpha)).
\end{aligned} \tag{2.47}$$

Hence, the ck-AGFS of $y(t)$ is

$$\rho^{y,g}_{\alpha,\lambda}(t,f) = |Y^g_{\alpha,\lambda}(t,f)|^2 = \rho^{x,g}_{\alpha,\lambda}(t,f-f_d\sin\alpha). \tag{2.48}$$

If the ck-AGFS of $x(t)$ is analyzed using window function $g(t)$ is $\rho^{x,g}_{\alpha,\lambda}(t,f)$, then the ck-AGFS of $y(t) = x(t)\exp(2\pi f_d t)$ is given by

$$\rho^{y,g}_{\alpha,\lambda}(t,f) = \rho^{x,g}_{\alpha,\lambda}(t,f-f_d\sin\alpha). \tag{2.49}$$

2.4.12 Time domain multiplication

Consider $z(t) = x(t)\cdot y(t)$. AGFS of $z(t)$,$\rho^{z,g}_{\alpha,\lambda}(t,f)$ is given by

$$\begin{aligned}
\rho^{z,g}_{\alpha,\lambda}(t,f) &= \left|\int_{-\infty}^{+\infty} x(\tau)y(\tau)g(\tau-t)K_{\alpha,\lambda}(\tau,f)d\tau\right|^2,\\
&= \left|\iint_{-\infty}^{+\infty} X_{\alpha,\lambda}(f_1)K^*_{\alpha,\lambda}(\tau,f_1)df_1\, y(\tau)g(\tau-t)K_{\alpha,\lambda}(\tau,f)d\tau\right|^2,\\
&= \left|\iiint_{-\infty}^{+\infty} X_{\alpha,\lambda}(f_1)K_{\alpha,\lambda}(\tau,f)K^*_{\alpha,\lambda}(\tau,f_1)Y_{\frac{\pi}{2}}(f_2)e^{i2\pi f_2\tau}g(\tau-t)d\tau df_1 df_2\right|^2.
\end{aligned} \tag{2.50}$$

Substitute $\tau - t = \tau^{'} \implies \tau = \tau^{'} + t$,$d\tau = d\tau^{'}$. Then

$$\rho^{z,g}_{\alpha,\lambda}(t,f) = |\text{cosec}\alpha| \Bigg| \iint_{-\infty}^{+\infty} X_{\alpha,\lambda}(f_1) Y_{\frac{\pi}{2}}(f_2) exp[i2\pi f_2 t + i\pi t_0^2 (f^2 - f_1^2.cot\alpha) \\ - i2\pi t(f - f_1)\text{cosec}\alpha + ih(\lambda, t_0 f) - ih(\lambda, t_0 f_1))] df_1 df_2 \\ \cdot \int_{-\infty}^{+\infty} g(\tau^{'}) exp[-i2\pi\tau^{'}[(f - f_1)\text{cosec}\alpha - f_2] d\tau^{'} \Bigg|^2 .$$

$g(\cdot) \leftrightarrow G_{\frac{\pi}{2}}(\cdot)$ is a Fourier Transform pair. Hence,

$$\rho^{z,g}_{\alpha,\lambda}(t,f) = |\text{cosec}\alpha| \Bigg| \int_{-\infty}^{+\infty} X_{\alpha,\lambda}(f_1) exp[i\pi t_0^2 (f^2 - f_1^2) cot\alpha \\ - i2\pi t \cdot \text{cosec}\alpha(f - f_1) + ih(\lambda, t_0 f) - ih(\lambda, t_0 f_1)] df_1 \\ \cdot \int_{-\infty}^{+\infty} G_{\frac{\pi}{2}}[(f - f_1)\text{cosec}\alpha - f_2] Y_{\frac{\pi}{2}}(f_2) e^{i2\pi f_2 t} df_2 \Bigg|^2 . \tag{2.51}$$

Eq.(2.51) can be written in other form as

$$\rho^{z,g}_{\alpha,\lambda}(t,f) = \left| \int_{-\infty}^{+\infty} X_{\alpha,\lambda}(f_1) K_{\alpha,\lambda}(t,f) K^{*}_{\alpha,\lambda}(t,f_1) [G_{\frac{\pi}{2}}(f^{'}) *_{f'} Y_{\frac{\pi}{2}}(f^{'}) e^{i2\pi t f^{'}}] df_1 \right|^2 , \tag{2.52}$$

where $*_{f'}$ is convolution over $f^{'} = (f - f_1)\text{cosec}\alpha$. If signals $x(t)$ and $y(t)$ have respective GTFTs $X_{\alpha,\lambda}(f)$ and $Y_{\alpha,\lambda}(f)$, then a signal $z(t) = x(t)y(t)$ has an AGFS given by

$$\rho^{z,g}_{\alpha,\lambda}(t,f) = \left| \int_{-\infty}^{+\infty} X_{\alpha,\lambda}(f_1) K_{\alpha,\lambda}(t,f) K^{*}_{\alpha,\lambda}(t,f_1) \left[G_{\frac{\pi}{2}}(f^{'}) *_{f'} Y_{\frac{\pi}{2}}(f^{'}) e^{i2\pi t f^{'}} \right] df_1 \right|^2 , \tag{2.53}$$

where $*_{f'}$ is convolution over variable $f^{'} = (f - f_1)\text{cosec}\alpha$ and $Y_{\frac{\pi}{2}}(f^{'})$ is Fourier transform of $y(\cdot)$ at frequency $f^{'}$

2.4.13 Discretization in time of AGFS

Consider $y(t) = \sum_{n=-\infty}^{\infty} \delta(t - n.T_s)$ in Eq. (2.53), so $Y_{\frac{\pi}{2}}(f) = \frac{\sqrt{2\pi}}{Ts} \sum_{n=-\infty}^{\infty} \delta(f - nf_s)$ where T_s =Time period and $f_s = 1/T_s$ =Frequency period

$$Y_{\frac{\pi}{2}}[(f - f_1)\text{cosec}\alpha].exp(i2\pi t(f - f_1)\text{cosec}\alpha) = \frac{\sqrt{2\pi}}{T_s} \sum_{n=-\infty}^{\infty} \delta[(f - f_1)\text{cosec}\alpha - n.f_s] \\ \cdot exp(i.2\pi.n.f_s t). \tag{2.54}$$

$$\rho^{z,g}_{\alpha,\lambda}(t,f) = |\text{cosec}\alpha| \Bigg| \int_{-\infty}^{+\infty} X_{\alpha,\lambda}(f_1) exp[i\pi t_0^2(f^2 - f_1^2)cot\alpha - i2\pi t \text{cosec}(f - f_1) + i.h(\lambda, t_0 f) - i.h(\lambda, t_0 f_1)][G_{\frac{\pi}{2}}[(f - f_1)\text{cosec}\alpha] * \frac{\sqrt{2\pi}}{Ts} \cdot \sum_{n=-\infty}^{\infty} \delta[(f - f_1)\text{cosec}\alpha - n.f_s] exp(i2\pi t.n.f_s)] df_1 \Bigg|^2, \tag{2.55}$$

$$= |\text{cosec}\alpha| \Bigg| \sum_{n=-\infty}^{\infty} \int_{-\infty}^{+\infty} X_{\alpha,\lambda}(f_1) exp[i\pi t_0^2(f^2 - f_1^2)cot\alpha - i2\pi t \text{cosec}(f - f_1) + i.h(\lambda, t_0 f) - i.h(\lambda, t_0 f_1)][G_{\frac{\pi}{2}}[(f - f_1)\text{cosec}\alpha - n.f_s] df_1 \Bigg|^2,$$

$$= |\text{cosec}\alpha| \Bigg| \sum_{n=-\infty}^{\infty} \int_{-\infty}^{+\infty} X_{\alpha,\lambda}(f_1) exp[i\pi[t_0^2((f - n.f_s.\sin\alpha)^2 - f_1^2)]cot\alpha - i2\pi t.\text{cosec}\alpha .(f - nf_s \sin\alpha - f_1) + i.h(\lambda, t_0(f - n.f_s.\sin\alpha)) - i.h(\lambda, t_0 f_1) + i.2\pi.t_0^2.f.n.f_s.\sin\alpha - i\pi.n^2.t_0^2.f_s^2.\sin^2\alpha - i.h(\lambda, t_0(f - n.f_s.\sin\alpha)) + i.h(\lambda, t_0 f)].G_{\frac{\pi}{2}}[(f - n.f_s.\sin\alpha - f_1)\text{cosec}\alpha] df_1 \Bigg|^2$$

$$= \Bigg| \sum_{n=-\infty}^{\infty} \int_{-\infty}^{+\infty} X_{\alpha,\lambda}(f_1) K_{\alpha,\lambda}(t, f - n.f_s.\sin\alpha) K^*(t, f_1).G_{\frac{\pi}{2}}(f - nf_s \sin\alpha - f_1).\text{cosec}\alpha df_1 .exp[i2\pi n.t_0^2.f_s.f.\sin\alpha + i2\pi n.t_0.f_s \sin\alpha + i.h(\lambda, t_0 f) - i.h(\lambda, t_0(f - n.f_s.\sin\alpha))] \Bigg|^2, \tag{2.56}$$

$$\Rightarrow \rho^{z,g}_{\alpha,\lambda}(t,f) = \Bigg| \sum_{n=-\infty}^{\infty} X^{*g}_{\alpha,\lambda}(t, f - nf_s \sin\alpha) \Bigg|^2. \tag{2.57}$$

If $z(t)$ is sampled version of $x(t)$ with Nyquist sampling frequency f_s (no aliasing condition), then AGFS of $z(t)$ is periodic with period $f_s \sin\alpha$ in the GTFT domain. AGFS of $z(t)$ with window $g(\cdot)$ is given as

$$\rho^{z,g}_{\alpha,\lambda}(t,f) = \sum_{n=-\infty}^{\infty} \rho^{x,g}_{\alpha,\lambda}(t, f - nf_s \sin\alpha), \tag{2.58}$$

where n is an integer. Periodicity property of AGFS is similar to the periodicity property of FrFT [113]. This property can be proved using the time domain multiplication property of AGFS with one of the signals being an impulse train.

2.4.14 Convolution

Here we define the convolution operation in a different sense to preserve the multiplication property of convolution [134]. Let $h(\cdot)$ be the convolution of $f(\cdot)$ and $g(\cdot)$. For the cubic phase kernel of GTFT, we define

$$h(t) = \tilde{h}(t)e^{-i\pi f_0^2 t^2 \cot\alpha + i\pi f_0^3 \lambda t^3},$$

where $\tilde{h}(t) = \tilde{f}(t) * \tilde{g}(t)$ is the standard convolution with $\tilde{f}$ and $\tilde{g}$ defined as

$$\tilde{f}(t) = f(t)e^{i\pi f_0^2 t^2 \cot\alpha - i\pi f_0^3 \lambda t^3},$$

$$\tilde{g}(t) = g(t)e^{i\pi f_0^2 t^2 \cot\alpha - i\pi f_0^3 \lambda t^3}.$$

Taking the cubic phase GTFT kernel to be $\pi\lambda z^3$ and window function to be $g_1(\cdot)$, the expression for AGFS of $h(\cdot)$ is given as $|H^{g_1}_{\alpha,\lambda}(t,f)|^2$, where

$$H^{g_1}_{\alpha,\lambda}(t,f) = [(g(t)K_{\alpha,\lambda}(t,f)) *_t F^{g_1}_{\alpha,\lambda}(t,f)] \cdot e^{-i\pi t_0^3 \lambda f^3 - i\pi t_0^2 f^2 \cot\alpha}, \tag{2.59}$$

where $F^{g_1}_{\alpha,\lambda}(t,f)$ is the STGTFT of $f(\cdot)$ with window $g_1(\cdot)$

$$\begin{aligned}
H^{g_1}_{\alpha,\lambda}(t,f) &= \int_{-\infty}^{\infty} h(\tau)g_1(\tau - t)K_{\alpha,\lambda}(\tau,f)d\tau, \\
&= \int_{-\infty}^{\infty} \tilde{h}(\tau)e^{-i\pi f_0^2 \tau^2 \cot\alpha + i\pi f_0^3 \lambda \tau^3} g_1(\tau - t)K_{\alpha,\lambda}(\tau,f)d\tau, \\
&= \iint_{-\infty}^{\infty} \tilde{f}(x)\tilde{g}(\tau - x)e^{-i\pi f_0^2 \tau^2 \cot\alpha + i\pi f_0^3 \lambda \tau^3} g_1(\tau - t)K_{\alpha,\lambda}(\tau,f)dxd\tau, \\
&= \iint_{-\infty}^{\infty} f(x)e^{i\pi f_0^2 x^2 \cot\alpha - i\pi f_0^3 \lambda x^3} g(\tau - x)e^{i\pi f_0^2 (\tau - x)^2 \cot\alpha - i\pi f_0^3 \lambda (\tau - x)^3} \\
&\qquad \cdot e^{-i\pi f_0^2 \tau^2 \cot\alpha + i\pi f_0^3 \lambda \tau^3} g_1(\tau - t)K_{\alpha,\lambda}(\tau,f)dxd\tau.
\end{aligned} \tag{2.60}$$

Substituting $K_{\alpha,\lambda}(\tau,f)$ and simplifying, we get

$$\begin{aligned}
H^{g_1}_{\alpha,\lambda}(t,f) = \iint_{-\infty}^{\infty} f(x)g(\tau - x)g_1(\tau - t)exp[i\pi(2f_0^2 x^2 \cot\alpha - 2\tau f_0^2 x \cot\alpha + 3f_0^3 \lambda \tau^2 x \\
- 3f_0^3 \lambda \tau x^2 + f_0^2 \tau^2 \cot\alpha + t_0^2 f^2 \cot\alpha - 2f\tau \mathrm{cosec}\alpha - f_0^3 \lambda \tau^3 + t_0^3 \lambda f^3)]dxd\tau.
\end{aligned}$$

Substituting $\tau - x = v$ and simplifying we have,

$$H^{g_1}_{\alpha,\lambda}(t,f) = \iint_{-\infty}^{\infty} f(x)g(v)g_1(x+v-t)exp[i\pi(f_0^2x^2\cot\alpha + t_0^2f^2\cot\alpha - 2fx\mathrm{cosec}\alpha$$
$$- f_0^3\lambda x^3 + t_0^3\lambda f^3)]exp[i\pi(f_0^2v^2\cot\alpha + t_0^2f^2\cot\alpha - 2fv\mathrm{cosec}\alpha$$
$$- f_0^3\lambda v^3 + t_0^3\lambda f^3)]exp[i\pi(-t_0^2f^2\cot\alpha\ - t_0^3\lambda f^3)]dxdv,$$

$$H^{g_1}_{\alpha,\lambda}(t,f) = \iint_{-\infty}^{\infty} f(x)g(v)g_1(x+v-t)K_{\alpha,\lambda}(x,f)K_{\alpha,\lambda}(v,f)$$
$$\cdot exp[i\pi(-t_0^2f^2\cot\alpha\ - t_0^3\lambda f^3)]dxdv,$$

$$H^{g_1}_{\alpha,\lambda}(t,f) = \int_{-\infty}^{\infty} g(v)K_{\alpha,\lambda}(v,f)\left[\int_{-\infty}^{\infty} f(x)g_1(x+v-t)K_{\alpha,\lambda}(x,f)dx\right]dv \tag{2.61}$$
$$\cdot e^{i\pi(-t_0^2f^2\cot\alpha\ -t_0^3\lambda f^3)},$$

$$H^{g_1}_{\alpha,\lambda}(t,f) = \left[\int_{-\infty}^{\infty} g(v)K_{\alpha,\lambda}(v,f)F^{g_1}_{\alpha,\lambda}(t-v,f)dv\right]\cdot e^{i\pi(-t_0^2f^2\cot\alpha\ -t_0^3\lambda f^3)}, \tag{2.62}$$

where $F^{g_1}_{\alpha,\lambda}(t,f)$ is STGTFT of $f(t)$.

$$H^{g_1}_{\alpha,\lambda}(t,f) = [(g(t)K_{\alpha,\lambda}(t,f)) *_t F^{g_1}_{\alpha,\lambda}(t,f)]\cdot e^{i\pi(-t_0^2f^2\cot\alpha\ -t_0^3\lambda f^3)}, \tag{2.63}$$

where $*_t$ is standard convolution over time.

Now we consider special cases.

For $\lambda = 0$ we get expression for convolution property of STFrFT as

$$H^{g_1}_{\alpha}(t,f) = [(g(t)K_{\alpha}(t,f)) *_t F^{g_1}_{\alpha}(t,f)]\cdot e^{-i\pi t_0^2f^2\cot\alpha},$$

where $H^{g_1}_{\alpha}(t,f)$ and $F^{g_1}_{\alpha}(t,f)$ is the STFrFT of $h(t)$ and $f(t)$ with window $g_1(\cdot)$ receptively.

At $\lambda = 0$ and $\alpha = \pi/2$ we get expression for convolution property of STFT as

$$H^{g_1}_{\pi/2}(t,f) = (g(t)e^{-i\omega t}) *_t F^{g_1}_{\pi/2}(t,f),$$

where $H^{g_1}_{\pi/2}(t,f)$ and $F^{g_1}_{\pi/2}(t,f)$ is the STFT of $h(t)$ and $f(t)$ with window $g_1(\cdot)$ and $\omega = 2\pi f$.

Now for $g_1(\cdot) = 1$ we get expression for convolution property of Fourier transform as

$$H_{\pi/2}(\omega) = G_{\pi/2}(\omega)\cdot F_{\pi/2}(\omega),$$

where $H_{\pi/2}(\omega)$, $G_{\pi/2}(\omega)$ and $F_{\pi/2}(\omega)$ are the Fourier transforms of $h(t)$, $f(t)$ and $g(t)$ receptively.

2.4.15 Finite support

If $x(t) = 0$ for all $t \notin [t_1, t_2]$, then $\rho^{x,g}_{\alpha,\lambda}(t, f)$ is not strictly zero for all $t \notin [t_1, t_2]$. This is due to the fact that there exists $t \notin [t_1, t_2]$ such that $g(\tau - t)$ may still overlap with some portion of signal $x(t)$, making the spectrogram non-zero at t (see Eq.(2.22)). If a window function $g(\cdot)$ is of finite width T, then for all $t \notin [t_1 - \frac{T}{2}, t_2 + \frac{T}{2}]$, $\rho^{x,g}_{\alpha,\lambda}(t, f) = 0$. This is finite support in a weak sense. For an infinite window, finite support does not hold. By similar arguments, if $X_{\alpha,\lambda}(f) = 0$ for all $f \notin [f_1, f_2]$, then $\rho^{x,g}_{\alpha,\lambda}(t, f)$ is not necessarily zero for all $f \notin [f_1, f_2]$ (see Eq.(2.26)). Hence AGFS does not follow the finite support property in a strict sense, similar to the STFT based spectrogram [26].

2.4.16 Linearity and cross-term free condition

Let $\rho^{x_1,g}_{\alpha,\lambda}(t, f)$, $\rho^{x_2,g}_{\alpha,\lambda}(t, f)$ be AGFS of the signals $x_1(t)$ and $x_2(t)$ respectively. Then AGFS of the signal $x_1(t) + x_2(t)$ is given by

$$\rho^{x_1+x_2,g}_{\alpha,\lambda}(t, f) = \rho^{x_1,g}_{\alpha,\lambda}(t, f) + \rho^{x_2,g}_{\alpha,\lambda}(t, f) + X^{g}_{1_{\alpha,\lambda}}(t, f) \cdot X^{*g}_{2_{\alpha,\lambda}}(t, f) + X^{*g}_{1_{\alpha,\lambda}}(t, f) \cdot X^{g}_{2_{\alpha,\lambda}}(t, f), \quad (2.64)$$

where $X^{g}_{1_{\alpha,\lambda}}(t, f)$ and $X^{g}_{2_{\alpha,\lambda}}(t, f)$ are respective STGTFTs of $x_1(t)$ and $x_2(t)$.

The linearity property $\rho^{x_1+x_2,g}_{\alpha,\lambda}(t, f) = \rho^{x_1,g}_{\alpha,\lambda}(t, f) + \rho^{x_2,g}_{\alpha,\lambda}(t, f)$ holds iff

$$X^{g}_{1_{\alpha,\lambda}}(t, f) \cdot X^{*g}_{2_{\alpha,\lambda}}(t, f) + X^{*g}_{1_{\alpha,\lambda}}(t, f) \cdot X^{g}_{2_{\alpha,\lambda}}(t, f) = 0. \quad (2.65)$$

A sufficient (but not necessary) condition for this to hold is that $x_1(t)$ and $x_2(t)$ have non-overlapping STGTFTs. This condition is also equivalent for the AGFS to be a cross-term free TFD.

2.4.17 Computation complexity of digital AGFS

AGFS is formed by a short-time GTFT. Computational requirement of the GTFT for an N length quadratic chirp signal is $O(Nlog_2N)$. If N/ϵ is the step size during the sliding window, then the digital computational complexity of AGFS will be $O(\epsilon Nlog_2N)$. For step size 1, i.e. $\epsilon = N$, complexity is $O(N^2log_2N)$ [73] [115].

2.5 Advantages of AGFS

Simulations are presented in subsequent sections to show below mentioned advantages of AGFS over STFT based Spectrogram

1. AGFS is the generalization of STFT based spectrogram, so it gives similar performance to the STFT based spectrogram for sinusoidal signal analysis and similar performance to the STFrFT spectrogram for linear chirp signal analysis.

2. AGFS gives higher resolution TFD at the optimum angle and optimum window for any higher order single component chirp, Whereas STFT and STFrFT based spectrogram at their optimum window fails to gives such higher resolution TFD for higher order chirps.

3. Multicomponent quadratic chirp with equal quadratic rates and chirp rates but different (very close) Doppler frequencies can be visible separately in AGFS, whereas in STFT based spectrogram, multicomponent quadratic chirp get mixed with each other, and it is not possible to extract a single component from multicomponent STFT based spectrogram.

4. In case of multicomponent quadratic chirp with equal quadratic rates and Doppler frequencies, but different (nearby) chirp rates, single component quadratic chirp can be extracted from multicomponent quadratic chirp using AGFS algorithm, whereas in STFT based spectrogram, each component of multicomponent quadratic chirp get mixed with each other, and it is not possible to extract single component quadratic chirp from multicomponent quadratic chirp using STFT based spectrogram.

5. In case of multicomponent quadratic chirp with equal quadratic rates but different (nearby) Doppler frequencies and different (nearby) chirp rates, single component quadratic chirp can be extracted from multicomponent quadratic chirp using AGFS algorithm.

2.6 Ck-AGFS of quadratic chirps

Consider a quadratic chirp signal $x(\tau)$ and a unit energy Gaussian window function $g(\tau)$ as

$$x(\tau) = A \exp\left(i\pi c\tau^3 + i\pi a\tau^2 + i2\pi f_d \tau\right), \tag{2.66}$$

$$g(\tau) = (\pi\sigma_{t_0}^2)^{-\frac{1}{4}} \exp\left(-\frac{\tau^2}{2\sigma_{t_0}^2}\right), \tag{2.67}$$

where c is the quadratic rate, a is the chirp rate, f_d is the Doppler frequency, A is the amplitude and σ_{t_0} is time variance of Gaussian window. The STGTFT of $x(t)$ is calculated using cubic phase GTFT kernel $h(\lambda, t_0 f) = \pi\lambda(t_0 f)^3$ and $h(\lambda, f_0 t) = \pi\lambda(f_0 t)^3$.

2.6.1 Analytical expression of ck-AGFS for unmatched cubic phase

The STGTFT of $x(t)$ for unmatched cubic phase is

$$\begin{aligned} X^{g}_{\alpha,\lambda}(t,f) &= \int_{-\infty}^{+\infty} x(\tau) g(t-\tau) K_{\alpha,\lambda}(\tau, f) d\tau \\ &= A_0 \cdot e^{i\phi_0(f)} \int_{-\infty}^{+\infty} exp\left(-\frac{(t-\tau)^2}{2\sigma_{t_0}^2}\right) \\ &\quad \cdot exp(i\pi c^{'}\tau^3 + i\pi a^{'}\tau^2 + i2\pi f^{'}\tau) d\tau, \end{aligned} \tag{2.68}$$

where,

$$A_0 = A(\pi\sigma_{t_0}^2)^{\frac{-1}{4}}\sqrt{1 - i\cot\alpha},\ \phi_0(f) = \lambda\pi t_0^3 f^3 + i\pi t_0^2 f^2 \cot\alpha,$$
$$c' = c - f_0^3\lambda,\ f' = f_d - f\mathrm{cosec}\alpha, a' = a + f^2\cot\alpha.$$

Hence, STGTFT magnitude:

$$\left|X_{\alpha,\lambda}(t,f)\right| = |A_0||exp(i\phi_0(f))|\left|\int_{-\infty}^{\infty} exp\left(-\frac{(t-\tau)^2}{2\sigma_{t_0}^2}\right).exp(i\pi c^{'}\tau^3 + i\pi a^{'}\tau^2 + i2\pi f^{'}\tau)d\tau\right|. \tag{2.69}$$

Consider the integral:

$$\begin{aligned} I_0 &= \int_{-\infty}^{\infty} exp\left(-\frac{(t-\tau)^2}{2\sigma_{t_0}^2}\right).exp(i\pi c^{'}\tau^3 + i\pi a^{'}\tau^2 + i2\pi f^{'}\tau)d\tau, \\ &= \int_{-\infty}^{\infty} f(\tau)e^{i\cdot\phi_1(\tau)}d\tau, \end{aligned} \tag{2.70}$$

where,

$$f(\tau) = exp\left(-\frac{(t-\tau)^2}{2\sigma_{t_0}^2}\right), \tag{2.71}$$

$$\phi_1(\tau) = (\pi c^{'}\tau^3 + \pi a^{'}\tau^2 + 2\pi f^{'}\tau). \tag{2.72}$$

Since $f(\tau)$ is localized (around 't'), and $\phi_1(t)$ is oscillating, we can use the principle of stationary phase (PSP) to approximate this integral. The "Stationary" points ($\tau_{1,2}$) are obtained from:

$$\phi_1^{'}(\tau) = 3\pi c^{'}\tau^2 + 2\pi a^{'}\tau + 2\pi f^{'} = 0.$$
$$\implies \tau_{1,2} = \underbrace{\frac{-a^{'}}{3c^{'}}}_{\alpha_0} \pm \underbrace{\frac{\sqrt{a^{'2} - 6c^{'}f^{'}}}{3c^{'}}}_{\beta_0}, \tag{2.73}$$

At these points, rate of change of frequency:

$$\begin{aligned} \phi_1^{''}(\tau) &= 6\pi c^{'}\tau + 2\pi a^{'}, \\ \implies \phi_1^{''}(\tau_1) &= 6\pi c^{'}\beta_0, \\ \phi_1^{''}(\tau_2) &= -6\pi c^{'}\beta_0. \end{aligned} \tag{2.74}$$

Therefore stationary approximation of I_0:

$$\begin{aligned} I_0 &\approx \sqrt{\frac{\pi}{3\pi c^{'}\beta_0}} e^{\frac{\pi}{4}} e^{i\phi_1(\tau_1)} f(\tau_1) + \sqrt{\frac{-\pi}{3\pi c^{'}\beta_0}} e^{\frac{i\pi}{4}} e^{i\phi_1(\tau_2)} f(\tau_2), \\ &= \sqrt{\frac{1}{3c^{'}\beta_0}} e^{\frac{i\pi}{4}} \left[e^{i\phi_1(\tau_1)} f(\tau_1) + i e^{i\phi_1(\tau_2)} f(\tau_2) \right], \\ &= \sqrt{\frac{1}{3c^{'}\beta_0}} e^{i\phi_{10}} e^{\frac{i\pi}{4}} \left[e^{i\phi_{20}} f(\tau_1) + i e^{-i\phi_{20}} f(\tau_2) \right], \end{aligned} \tag{2.75}$$

where

$$\begin{aligned} \phi_{10} &= \pi \left[c^{'}(\alpha_0^3 + 3\alpha_0\beta_0^2) + a^{'}(\alpha_0^2 + \beta_0^2) + f^{'}\alpha_0 \right], \\ \phi_{20} &= \pi \left[c^{'}(\beta_0^3 + 3\beta_0\alpha_0^2) + 2a^{'}\alpha_0\beta_0 + f^{'}\beta_0 \right]. \end{aligned} \tag{2.76}$$

Hence,

$$\begin{aligned} |I_0| &\approx \left| \sqrt{\frac{1}{3c^{'}\beta_0}} e^{i\phi_{10}} \left[e^{i\phi_{20}} f(\tau_1) + i e^{-i\phi_{20}} f(\tau_2) \right] \right|, \\ &= \frac{1}{\sqrt{3c^{'}\beta_0}} \left[f(\tau_1)^2 + f(\tau_2)^2 + 2f(\tau_1)f(\tau_2)\sin 2\phi_{20} \right]^{1/2}, \\ &= \frac{\sqrt{2}}{\sqrt{3c^{'}\beta_0}} exp\left[\frac{-\left[(\alpha_0 - t)^2 + \beta_0^2\right]}{2\sigma_{t0}^2} \right]^{1/2} \left[cosh\left(\frac{2\beta_0(\alpha_0 - t)}{\sigma_{t0}^2} \right) + \sin 2\phi_{20} \right]^{1/2}. \end{aligned} \tag{2.77}$$

Therefore, from Eqns. (2.77) and (2.69), we have:

$$\begin{aligned} \left| X_{\alpha,\lambda}(t,f) \right|^2 = \frac{2|A|^2(\pi\sigma_{t0}^2)^{-1/2}|\text{cosec}\alpha|}{3c^{'}\beta_0} exp\left[\frac{-\left[(\alpha_0 - t)^2 + \beta_0^2\right]}{\sigma_{t_0}^2} \right], \\ \left[cosh\left(\frac{2\beta_0(\alpha_0 - t)}{\sigma_{t_0}^2} \right) + \sin 2\phi_{20} \right]. \end{aligned} \tag{2.78}$$

Alternatively, we can write the above equation in the following form, ignoring $\sin 2\phi_{20}$:

$$\begin{aligned}\left|X_{\alpha,\lambda}(t,f)\right|^2 &= \frac{|A|^2(\pi\sigma_{t0}^2)^{-1/2}|\mathrm{cosec}\alpha|}{3c'\beta_0}\left[exp\left(-\frac{(\alpha_0-t+\beta_0)^2}{\sigma_{t_0}^2}\right)+exp\left(-\frac{(\alpha_0-t-\beta_0)^2}{\sigma_{t_0}^2}\right)\right],\\ &= \frac{|A|^2|\mathrm{cosec}\alpha|}{\sqrt{\pi\sigma_{t_0}^2(a'^2-6c'f')}}\left[exp\left(-\frac{\left(\sqrt{a'^2-6c'f'}-(a'+3c't)\right)^2}{(3c'\sigma_{t_0})^2}\right)\right.\\ &\quad\left.+exp\left(-\frac{\left(\sqrt{a'^2-6c'f'}+(a'+3c't)\right)^2}{(3c'\sigma_{t_0})^2}\right)\right].\end{aligned} \tag{2.79}$$

Therefore, final expression for AGFS of cubic chirp:

$$\begin{aligned}\left|X_{\alpha,\lambda}(t,f)\right|^2 &= \frac{|A|^2|\mathrm{cosec}\alpha|}{\sqrt{\pi\sigma_{t_0}^2(a'^2-6c'f')}}\left[exp\left(-\frac{\left(\sqrt{a'^2-6c'f'}-(a'+3c't)\right)^2}{(3c'\sigma_{t_0})^2}\right)\right.\\ &\quad\left.+exp\left(-\frac{\left(\sqrt{a'^2-6c'f'}+(a'+3c't)\right)^2}{(3c'\sigma_{t_0})^2}\right)\right].\end{aligned} \tag{2.80}$$

2.6.2 Cubic matching condition

For matching Cubic phase, c' approaches zero. In this limit, Eqn. (2.80) becomes:

$$\left|X_{\alpha,\lambda}(t,f)\right|^2 = \frac{|A|^2|\mathrm{cosec}\alpha|}{\sqrt{\pi\sigma_{t_0}^2a'^2}}\left[\underbrace{exp\left(-\frac{\left(\sqrt{a'^2}-a'\right)^2}{(3(0)\sigma_{t_0})^2}\right)}_{0/0\,form}+\underbrace{exp\left(-\frac{\left(\sqrt{a'^2}+a'\right)^2}{(3(0)\sigma_{t_0})^2}\right)}_{e^{-\infty}=0}\right]. \tag{2.81}$$

As we can see, in this limit, the second exponential maybe ignored. Also, the argument of the first exponential takes a 0/0 form. To find the limit we apply L'Hospital's rule to the argument, as follows:

$$\lim_{c'\to 0}\frac{\left(\sqrt{a'^2-6c'f'}-(a'+3c't)\right)}{3c'\sigma_{t_0}} = \lim_{c'\to 0}\frac{\frac{d\left(\sqrt{a'^2-6c'f'}-(a'+3c't)\right)}{dc'}}{\frac{d3c'\sigma_{t_0}}{dc'}} = -\left(\frac{f'+a't}{a'\sigma_{t0}}\right). \tag{2.82}$$

Substituting and rearranging this result, we get the AGFS of cubic chirp in matched condition:

$$\lim_{c'\to 0}\left|X_{\alpha,\lambda}(t,f)\right| \approx \frac{|A|}{(\pi\sigma_{t_0}^2)^{\frac{1}{4}}\cdot(a\sin\alpha+f_0^2\cos\alpha)^{\frac{1}{4}}} \cdot exp\left[-\frac{1}{2}\left(\frac{f-(f_d sin\alpha+at\sin\alpha+f_0^2 t\cos\alpha)}{\sigma_{t_0}(a\sin\alpha+f_0^2 cos\alpha)}\right)^2\right]. \tag{2.83}$$

This is the approximate STGTFT expression for the limiting case $c^{'} \to 0$ (matched cubic phase) derived from unmatched cubic phase condition when $|f_d - f\text{cosec}\alpha| >> 0$. An exact expression of ck-AGFS for matched cubic phase condition is derived using the Gaussian integral formula of Eq. (2.7) in Section 2.7.

2.7 Expression for optimum window size of quadratic chirp ck-AGFS for matched cubic phase

2.7.1 Mathematical derivation for variance of cubic chirp signal based AGFS

For the signal $x(\tau)$ and unit energy Gaussian window function $g(\tau)$ given by Eqns.(2.66) & (2.67), mathematical derivation for variance of quadratic chirp signal is presented for Gaussian window based AGFS.

$$\rho_{\alpha,\lambda}^{x,g}(t,f) = \left|\int_{-\infty}^{+\infty} x(\tau)g(\tau-t)K_{\alpha,\lambda}(\tau,f)d\tau\right|^2 = \left|X_{\alpha,\lambda}^{g}(t,f)\right|^2. \tag{2.84}$$

To get optimum window, we concentrate on STGTFT part

$$\left|X_{\alpha,\lambda}^{g}(t,f)\right| = \left|\int_{-\infty}^{+\infty} x(\tau)g(\tau-t)K_{\alpha,\lambda}(\tau,f)d\tau\right|, \tag{2.85}$$

$$\left|X_{\alpha,\lambda}^{g}(t,f)\right| = \left|(A\sqrt{1-icot\alpha})(\pi\sigma_{t0}^2)^{-\frac{1}{4}}\int_{-\infty}^{+\infty} e^{i\pi c\tau^3+i\pi a\tau^2+i2\pi f_d\tau}.exp\left[i\pi t_0^2 f^2 cot\alpha\right.\right.$$
$$\left.\left.+i\pi^2 f_0^2\tau^2 cot\alpha - i2\pi f\tau\text{cosec}\alpha - i\cdot h(\lambda,f_0\tau)+i\cdot h(\lambda,t_0 f)\right] exp(-\frac{(\tau-t)^2}{2\sigma_{t0}^2})d\tau\right|. \tag{2.86}$$

At matched GTFT of cubic phase,

$$\lambda f_0^3 = c,\ h(\lambda, f_0\tau) = \pi\lambda(f_0\tau)^3,\ h(\lambda, t_0 f) = \pi\lambda(t_0 f)^3, \tag{2.87}$$

$$\left|X^g_{\alpha,\lambda}(t,f)\right| = \left|(A\sqrt{1-icot\alpha})(\pi\sigma_{t0}^2)^{-\frac{1}{4}} \int_{-\infty}^{+\infty} exp\left[\cancel{i\pi c\tau^3} + i\pi a\tau^2 + i2\pi f_d\tau + i\pi\tau^2 f_0^2\cot\alpha \right.\right.$$
$$\left.\left. + i\pi f^2\cot\alpha t_0^2 - i2\pi f\tau\mathrm{cosec}\alpha - \cancel{i\pi c\tau^3} + i\pi c t_0^6 f^3 - \frac{(\tau-t)^2}{2\sigma_{t0}^2}\right] d\tau\right|, \tag{2.88}$$

$$\left|X^g_{\alpha,\lambda}(t,f)\right| = |A|\underbrace{\left|(\sqrt{1-icot\alpha})\right|}_{\sqrt{|\mathrm{cosec}\alpha|}}(\pi\sigma_{t0}^2)^{-\frac{1}{4}}\left|\int_{-\infty}^{+\infty} exp\left[i\pi c t_0^6 f^3 + i\pi a\tau^2 + i2\pi f_d\tau \right.\right.$$
$$\left.\left. + i\pi\tau^2 f_0^2\cot\alpha + i\pi f^2\cot\alpha t_0^2 - i2\pi f\tau\mathrm{cosec}\alpha - \frac{(\tau-t)^2}{2\sigma_{t0}^2}\right] d\tau\right|,$$

$$\phi = i\pi c t_0^6 f^3 + i\pi a\tau^2 + i2\pi f_d\tau + i\pi\tau^2 f_0^2\cot\alpha + i\pi f^2 cot\alpha t_0^2 - i2\pi f\tau\mathrm{cosec}\alpha - \frac{(\tau-t)^2}{2\sigma_{t0}^2},$$
$$= \tau^2\underbrace{\left[-\frac{1}{2\sigma_{t0}^2} + i\pi(a + f_0^2\cot\alpha)\right]}_{-\mu^2} + \tau\underbrace{\left[\frac{t}{\sigma_{t0}^2} + i2\pi(f_d - f\csc\alpha))\right]}_{v}$$
$$+ \underbrace{\left[\frac{-t^2}{2\sigma_{t0}^2} + i\pi t_0^2 f^2\cot\alpha + i\pi c t_0^6 f^3\right]}_{\gamma + i\phi_0}.$$

Final term is independent of τ and hence can be brought out of the integral:

$$\left|X^g_{\alpha,\lambda}(t,f)\right| = |A|\sqrt{|\mathrm{cosec}\alpha|}(\pi\sigma_{t0}^2)^{-\frac{1}{4}} e^{\frac{-t^2}{2\sigma_{t0}^2}}\left|\int_{-\infty}^{\infty} exp(-\mu^2\tau^2 + v\tau)d\tau\right|.$$

Here we observe that since $Re(\mu^2) > 0$, the definite integral converges. Solving this integral at matched GTFT of cubic phase condition, $f_0^3\lambda = c$ using Gaussian integral formula of Eq. (2.7) gives as:

$$\left|X^g_{\alpha,\lambda}(t,f)\right| = |A|\sqrt{|\mathrm{cosec}\alpha|}(\pi\sigma_{t0}^2)^{-\frac{1}{4}} e^{\frac{-t^2}{2\sigma_{t0}^2}} \left|\frac{\sqrt{\pi}}{\mu} e^{v^2/4\mu^2}\right|,$$

$$= |A|\sqrt{|\mathrm{cosec}\alpha|}(\pi\sigma_{t0}^2)^{-\frac{1}{4}} e^{\frac{-t^2}{2\sigma_{t0}^2}} \frac{\sqrt{\pi}}{|\mu|} \left| exp\left(\frac{\left[\overbrace{\frac{t}{\sigma_{t0}^2}}^{\alpha_1} + i \overbrace{2\pi(f_d - f\csc\alpha)}^{\beta_1} \right]^2}{4\left[\underbrace{\frac{1}{2\sigma_{t0}^2}}_{\alpha_2} - i \underbrace{\pi(a + f_0^2\cot\alpha)}_{\beta_2} \right]} \right) \right|,$$

$$\therefore \left|X^g_{\alpha,\lambda}(t,f)\right| = |A| e^{\frac{-t^2}{2\sigma_{t0}^2}} \frac{\sqrt{\pi|\mathrm{cosec}\alpha|}}{|\mu|} (\pi\sigma_{t0}^2)^{-\frac{1}{4}} \left| exp\left[\frac{(\alpha_1 + i\beta_1)^2}{4(\alpha_2 - i\beta_2)} \right] \right|, \tag{2.89}$$

where,

$$|\mu| = \left[\left(\frac{1}{2\sigma_{t0}^2} \right)^2 + \pi^2(a + f_0^2 cot\alpha)^2 \right]^{\frac{1}{4}},$$
$$\alpha_1 = \frac{t}{\sigma_{t0}^2}, \qquad \beta_1 = 2\pi(f_d - f\csc\alpha),$$
$$\alpha_2 = \frac{1}{2\sigma_{t0}^2}, \qquad \beta_2 = \pi(a + f_0^2\cot\alpha),$$

$$\left|X^g_{\alpha,\lambda}(t,f)\right| = |A| e^{\frac{-t^2}{2\sigma_{t_0}^2}} \frac{\sqrt{\pi|\mathrm{cosec}\alpha|}}{|\mu|} (\pi\sigma_{t_0}^2)^{-\frac{1}{4}} \left| exp\left[-\frac{\alpha_2\beta_1^2 + 2\alpha_1\beta_2\beta_1 - \alpha_1^2\alpha_2}{4(\alpha_2^2 + \beta_2^2)} \right] \right|,$$

$$= |A| e^{\frac{-t^2}{2\sigma_{t_0}^2}} \frac{\sqrt{\pi|\mathrm{cosec}\alpha|}}{|\mu|} (\pi\sigma_{t_0}^2)^{-\frac{1}{4}} \left| exp\left[-\frac{\left(\beta_1 + \frac{\alpha_1\beta_2}{\alpha_2}\right)^2 - \left(\alpha_1^2 + \frac{\alpha_1^2\beta_2^2}{\alpha_2^2}\right)}{4\left(\alpha_2 + \frac{\beta_2^2}{\alpha_2}\right)} \right] \right|, \tag{2.90}$$

$$= |A| e^{\frac{-t^2}{2\sigma_{t_0}^2}} \frac{\sqrt{\pi|\mathrm{cosec}\alpha|}}{|\mu|} (\pi\sigma_{t_0}^2)^{-\frac{1}{4}} exp\left[\frac{\left(\alpha_1^2 + \frac{\alpha_1^2\beta_2^2}{\alpha_2^2}\right)}{4\left(\alpha_2 + \frac{\beta_2^2}{\alpha_2}\right)} \right] exp\left[-\frac{\left(2\pi(f_d - f\csc\alpha) + \frac{\alpha_1\beta_2}{\alpha_2}\right)^2}{4\left(\alpha_2 + \frac{\beta_2^2}{\alpha_2}\right)} \right],$$

$$= |A| \frac{\sqrt{\pi|\mathrm{cosec}\alpha|}}{|\mu|} (\pi\sigma_{t_0}^2)^{-\frac{1}{4}} exp\left(\frac{\alpha_1^2}{4\alpha_2} \right) exp\left(\frac{-t^2}{2\sigma_{t_0}^2} \right) exp\left[-\frac{\left(2\pi(f_d - f\csc\alpha) + \frac{\alpha_1\beta_2}{\alpha_2}\right)^2}{4\left(\alpha_2 + \frac{\beta_2^2}{\alpha_2}\right)} \right], \tag{2.91}$$

$$= |A|\frac{\sqrt{\pi|\text{cosec}\alpha|}}{|\mu|}(\pi\sigma_{t_0}^2)^{-\frac{1}{4}}exp\left[-\frac{\left(2\pi(f_d - f\csc\alpha) + \frac{\alpha_1\beta_2}{\alpha_2}\right)^2}{4\left(\alpha_2 + \frac{\beta_2^2}{\alpha_2}\right)}\right]. \tag{2.92}$$

Substituting for μ, α_1, α_2, β_1 and β_2, we get:

$$\left|X_{\alpha,\lambda}^g(t,f)\right| = |A|\frac{\sqrt{\pi|\text{cosec}\alpha|}(\pi\sigma_{t_0}^2)^{-\frac{1}{4}}}{\left[\left(\frac{1}{2\sigma_{t_0}^2}\right)^2 + \pi^2(a + f_0^2 cot\alpha)^2\right]^{\frac{1}{4}}}exp\left[-\frac{\left[(f - f_d\sin\alpha) - \frac{\alpha_1\beta_2\sin\alpha}{2\pi\alpha_2}\right]^2}{\frac{4\sin^2\alpha}{4\pi^2}\left(\alpha_2 + \frac{\beta_2^2}{\alpha_2}\right)}\right],$$

$$= |A|\frac{\sqrt{\pi|\text{cosec}\alpha|}(\pi\sigma_{t_0}^2)^{-\frac{1}{4}}}{\left[\left(\frac{1}{2\sigma_{t_0}^2}\right)^2 + \pi^2(a + f_0^2 cot\alpha)^2\right]^{\frac{1}{4}}}exp\left[-\frac{[f - f_d\sin\alpha - t(a + f_0^2\cot\alpha)\sin\alpha]^2}{\frac{\sin^2\alpha}{\pi^2}\left(\frac{1}{2\sigma_{t0}^2} + \pi^2(a + f_0^2 cot\alpha)^2(2\sigma_{t0}^2)\right)}\right]. \tag{2.93}$$

Rearranging Eq. (2.93), we get

$$\begin{aligned}\left|X_{\alpha,\lambda}^g(t,f)\right| = \frac{|A|}{(\pi\sigma_{t_0}^2)^{\frac{1}{4}}}&\frac{\sqrt{\pi|\text{cosec}\alpha|}}{\left[\left(\frac{1}{2\sigma_{t_0}^2}\right)^2 + \pi^2(a + f_0^2 cot\alpha)^2\right]^{\frac{1}{4}}} \\ &\cdot exp\left[-\frac{1}{2}\frac{\left(f - (at\sin\alpha + f_d\sin\alpha + f_0^2 tcos\alpha)\right)^2}{\frac{\sin^2\alpha}{\sigma_{t_0}^2 4\pi^2} + \sigma_{t_0}^2(f_0^2\cos\alpha + a\sin\alpha)^2}\right].\end{aligned} \tag{2.94}$$

Hence, the exact form of cubic kernel STGTFT of a quadratic chirp in Eq.(2.94) almost (but not exactly) matches with approximate form of cubic kernel STGTFT of unmatched cubic phase at limiting condition as shown in Eq.(2.83).This is a Gaussian expression in f, and its variance can be extracted by comparison with the standard Gaussian form as

$$\sigma_{\alpha_0}^2 = \frac{\sin^2\alpha}{\sigma_{t_0}^2 4\pi^2} + \sigma_{t_0}^2(f_0^2\cos\alpha + a\sin\alpha)^2. \tag{2.95}$$

Here, $\sigma_{t_0}^2$ is the variance of the Gaussian window in time and its unit is sec^2. $\sigma_{\alpha_0}^2$ is the variance of the Gaussian window in GTFT domain, and its unit is Hz^2. Variance should be dimensionless in the GTFT domain, so dimension normalisation of $\sigma_{\alpha_0}^2$ is required, and it is done as shown below:

$$\sigma_{t_0}^2 = \frac{\sigma_t^2}{f_s^2},$$

where σ_t^2 is the variance in time domain in terms of samples (dimensionless).

$$\therefore \sigma_{\alpha_0}^2 = \frac{f_s^2\sin^2\alpha}{\sigma_t^2 4\pi^2} + \frac{\sigma_t^2}{f_s^2}(f_0^2\cos\alpha + a\sin\alpha)^2. \tag{2.96}$$

Similarly, if σ_α^2 is the variance of Gaussian window in GTFT domain, then

$$\therefore \sigma_\alpha^2 = f_s^2 \sigma_{\alpha_0}^2 = \frac{f_s^4 \sin^2 \alpha}{\sigma_t^2 4\pi^2} + \sigma_t^2 (f_0^2 \cos \alpha + a \sin \alpha)^2. \tag{2.97}$$

σ_α^2 has the unit Hz^4 in the GTFT domain. Hence, dimension normalisation in the GTFT domain is required. It is done by defining

$$\sigma_{\alpha'}^2 = t_0^4 \sigma_\alpha^2 = \frac{t_0^4 f_s^4 \sin^2 \alpha}{\sigma_t^2 4\pi^2} + \sigma_t^2 (\cos \alpha + t_0^2 a \sin \alpha)^2, \tag{2.98}$$

where $\sigma_{\alpha'}^2$ is the variance in the GTFT domain in terms of samples (dimensionless). Considering $N = f_s \tau$ and half-length sliding window of STGTFT ($T_{max} = \frac{\tau}{2}$), with τ as the signal duration leads to $t_0^2 = \frac{\tau}{2 f_s}$.

$$\therefore \sigma_{\alpha'}^2 = \left(\frac{N}{4\pi}\right)^2 \frac{\sin^2 \alpha}{\sigma_t^2} + \sigma_t^2 (\cos \alpha + \frac{a\tau}{2 f_s} \sin \alpha)^2. \tag{2.99}$$

Hence, for a quadratic chirp signal, it can be observed that:

1. If cubic kernel STGTFT (ck-STGTFT) is 'cubic matched', then the cubic portion of the phase function of the signal will be cancelled using the ck-GTFT kernel. If cubic kernel STGTFT (ck-STGTFT) is 'matched ck-STGTFT', then the cubic *and* quadratic portions of the phase functions of the signal will be cancelled using the ck-GTFT kernel.

2. Any Gaussian window function in the time domain has a Gaussian cubic-matched ck-STGTFT response.

3. Shift parameter t, quadratic rate c, and Doppler frequency f_d do not affect the variance of the Gaussian window in the cubic-matched ck-STGTFT domain.

2.7.2 Optimum time window for minimum variance in cubic-matched ck-STGTFT domain

For an optimum σ_t^2, which gives a minimum $\sigma_{\alpha'}^2$,

$$\frac{d\sigma_{\alpha'}^2}{d\sigma_t^2} = -\left(\frac{N}{4\pi}\right)^2 \frac{\sin^2 \alpha}{\sigma_t^4} + \left(\cos \alpha + \frac{a\tau}{2 f_s} \sin \alpha\right)^2 = 0, \tag{2.100}$$

$$\sigma_{t_{opt}}^2 = \left| \frac{\frac{N}{4\pi} \sin \alpha}{\cos \alpha + \frac{a\tau \sin \alpha}{2 f_s}} \right|. \tag{2.101}$$

The minimum $\sigma^2_{\alpha'}$ at $\sigma^2_{t_{opt}}$ is given by

$$\sigma^2_{\alpha'_{min}} = \left| \frac{N}{2\pi} \sin\alpha \left(\cos\alpha + \frac{a\tau \sin\alpha}{2f_s} \right) \right|. \tag{2.102}$$

Consider the following cases:

1. When $a = 0$ and $\alpha \neq \alpha_{opt}$, from Eq. (2.101) and Eq. (2.102)

$$\sigma^2_{t_{opt}} = \left| \frac{N}{4\pi} tan\alpha \right|, \tag{2.103}$$

$$\sigma^2_{\alpha'_{min}} = \left| \frac{N}{4\pi} \sin 2\alpha \right|. \tag{2.104}$$

   A similar result was obtained in [17] for a Gaussian window in FrFT domain.

2. When $a \neq 0$ and $\alpha = 90^\circ \neq \alpha_{opt}$ (STFT case), from Eq. (2.101) and Eq. (2.102)

$$\sigma^2_{t_{opt}}\big|_{\alpha=90^\circ} = \left| \frac{f_s^2}{2\pi a} \right|, \tag{2.105}$$

$$\sigma^2_{\alpha'}\big|_{\alpha=90^\circ} = \left| \frac{a\tau^2}{4\pi} \right|. \tag{2.106}$$

   A similar result was obtained in [75] [26] for Gaussian window in STFT domain.

3. When $a \neq 0$ and $\alpha \neq \alpha_{opt}$, $\sigma^2_{t_{opt}}$ and $\sigma^2_{\alpha'}$ are given by the generic formulae Eq. (2.101) and Eq. (2.102) respectively.

4. When $a\epsilon(-\infty, \infty)$ and $\alpha = \alpha_{opt}$, where α_{opt} is optimum matched angle, Eq. (2.102) becomes

$$\sigma^2_{\alpha'_{min}} = \left(\frac{N}{4\pi} \right)^2 \frac{\sin^2\alpha}{\sigma^2_{t_{opt}}}. \tag{2.107}$$

   This means that a minimum variance in the GTFT domain is obtained at infinite time windowing. It is similar to the uncertainty principle, which is derived in subsequent section 2.8. Infinite time windowing is not practical, and a compromise is needed. Hence $5\sigma_t$ window can be considered, which contains 98.75% energy in $\frac{N}{2}$ Gaussian window.

$$\therefore 5\sigma_{t_{opt}} = \frac{N}{2}, \implies \sigma_{t_{opt}} = \frac{N}{10} \quad \text{for 98.75\% energy.} \tag{2.108}$$

$$\therefore (\sigma_{\alpha'})_{min} = \left[\left(\frac{N}{4\pi} \right)^2 \frac{\sin^2(\alpha)}{\left(\frac{N}{10}\right)^2} \right]^{\frac{1}{2}} = \frac{10}{4\pi} \sin\alpha. \tag{2.109}$$

   This $(\sigma_{\alpha'})_{min}$ is always less than unity. Hence, Case 4 ($f_0^3\lambda = c$ and $\alpha = \alpha_{opt}$) gives the least standard deviation in GTFT domain out of all cases.

2.7.3 Results: Optimum time window and minimum variance in ck-STGTFT domain for different cases of single-component quadratic chirp

The simulation results are listed in Table 2.4 for different cases of Gaussian window based cubic-matched ck-STGTFT domain analysis of single component quadratic chirps. Table 2.4 is constructed using the following procedure:

1. Mean $(\sigma_{\alpha'})_{min}$ is the average standard deviation of the Gaussian response in GTFT domain across different window positions. Variance in GTFT domain is calculated based on the three sigma rule of the Gaussian for each window position, meaning that 99.7% energy of the Gaussian distribution lies within first three standard deviations on each side of the mean.

2. Mean $\sigma_{t_{opt}}$ is optimum time window length, which gives least mean $(\sigma_{\alpha'})_{min}$.

3. Estimated optimum standard deviation in time domain $(Est.\ \sigma_{t_{opt}})$ and estimated optimum standard deviation in cubic-matched ck-STGTFT domain $(Est.(\sigma_{\alpha'})_{min})$ are calculated based on the formula derived for $\sigma_{t_{opt}}$ and $(\sigma_{\alpha'})_{min}$ for different cases in subsection 2.7.2.

4. Energy concentration measure (ECM) [12, pp. 401-408] is used as a measure for comparing the best TFD concentration.

$$M = \frac{\left(\sum_t \sum_f \left|(\rho^{x,g}_{\alpha,\lambda}(t,f))\right|^{\frac{1}{2}}\right)^2}{\sum_t \sum_f \left|\rho^{x,g}_{\alpha,\lambda}(t,f)\right|}. \tag{2.110}$$

   ECM is a standard criterion for measuring concentration for any type of window function. The window type and length which produces minimum M is the optimum window according to this criterion.

5. M_{min} is the best energy concentration measure obtained for the optimum window and $(\sigma_{t_{opt}})_M$ is the optimum standard deviation of window in time for minimum M.

Based on Table 2.4, we can observe that case 4 has the least mean $(\sigma_{\alpha'})_{min}$ standard deviation in the cubic-matched ck-STGTFT domain and it is less than unity as derived in Eq.

Table 2.4: Simulation results for different cases in STGTFT domain for single-component quadratic chirp

Parameters	Case 1 $a = 0$ and $\alpha \neq 90° \neq \alpha_{opt}$		Case2 $a \neq 0$ and $\alpha = 90° \neq \alpha_{opt}$		Case 3 $a \neq 0$ and $\alpha \neq \alpha_{opt}$		Case 4 $a \in (-\infty, \infty)$ and $\alpha = \alpha_{opt}$	
τ (sec)	1	1	1	2	1	2	1	2
a (Hz^2)	0	0	100	150	-100	100	100	50
$f_s\ (Hz)$	400	800	400	800	400	800	400	600
N	400	800	400	1600	400	1600	400	1200
$f_d\ (Hz)$	20	30	0	20	30	20	10	10
c (Hz^3)	10	10	10	10	10	20	10	5
α	72°	27°	90°	90°	−72°	−72°	82.37°	85.23°
α_{opt}	90°	90°	82.87°	79.38°	−82.87°	82.87°	82.87°	85.23°
$Mean\ \sigma_{t_{opt}}$	10	6	17	27	14	17	44	125
$Est.\sigma_{t_{opt}}$	9.89	5.7	15.96	26.06	12.61	16.82	40	120
$Mean\ (\sigma_{\alpha'})_{min}$	3.79	6.9	2.41	6.52	2.99	9.79	0.55	0.56
$Est.\ (\sigma_{\alpha'})_{min}$	4.32	7.18	2.82	6.90	3.40	10.18	0.789	0.793
M_{min}	$6.66 * 10^3$	$2.08 * 10^4$	$4.67 * 10^3$	$4.22 * 10^4$	$5.39 * 10^3$	$6.03 * 10^4$	$2.16 * 10^3$	$7.48 * 10^3$
$(\sigma_{t_{opt}})_M$	10	6	16	26	12	17	42	115

(2.109). This condition is equivalent to matched ck-STGTFT. Hence, AGFS produces least variance and high concentrated spectrogram at matched ck-STGTFT ($f_0^3\lambda = c\ and\ \alpha = \alpha_{opt}$) and optimum window length. We also note that $(\sigma_{t_{opt}})_M$ and $Mean\ \sigma_{t_{opt}}$ match significantly in Table 2.4, implying that the optimum window length found by 3 sigma rule for Gaussian window is also close to optimum window length according to the ECM criterion.

2.8 Uncertainty of the STGTFT

The uncertainty of the STGTFT can be derived in a manner similar to the STFT [26] and the STFrFT [115]. It yields the same result as the STFrFT, as shown in the next section. Subsequently, the TBP for the special case of quadratic chirp analyzed by cubic kernel STGTFT is presented as an example.

2.8.1 2-D resolution of STGTFT

The 2-Dimensional resolution of STGTFT is similar to the 2-Dimensional resolution of GTFT at any particular instant of time 't'. When a window is sliding, multiple 2-Dimensional GTFT resolution cells can be obtained at different instants of time 't'. The GTFT TBP is greater than or equal to $|\sin\alpha|/2$ as obtained in [93]. Therefore, the 2-Dimensional resolution of GTFT, which is always less than or equal to $2/|\sin\alpha|$. So the 2-Dimensional resolution of STGTFT at any particular instant of time 't' is always less than or equal to $2/|\sin\alpha|$.

2.8.2 TBP of STGTFT

The STGTFT is defined over the domain of two variables. We would like to know the spread of this function over both of these variables. For any given input signal, most of the energy of the STGTFT lies within a rectangle on the time-GTFT frequency plane. A measure of the support of the input can be the product of the two sides of this rectangle (also known as the time-GTFT bandwidth product (TGBP)) [83].

We define the mean time ($\bar{t_S}$), mean GTFT frequency ($\bar{f_S}$), time width (T_S^2) and GTFT-bandwidth ($B_{S,\alpha,\lambda}^2$) of the STGTFT as follows:

$$\bar{t_S} = \frac{1}{||X_{\alpha,\lambda}^g(t,f)||^2}\int_{-\infty}^{\infty}\int_{-\infty}^{\infty} t|X_{\alpha,\lambda}^g(t,f)|^2 \mathrm{d}t\mathrm{d}f, \tag{2.111}$$

$$\bar{f_S} = \frac{1}{||X_{\alpha,\lambda}^g(t,f)||^2}\int_{-\infty}^{\infty}\int_{-\infty}^{\infty} f|X_{\alpha,\lambda}^g(t,f)|^2 \mathrm{d}t\mathrm{d}f, \tag{2.112}$$

$$T_S^2 = \frac{1}{||X_{\alpha,\lambda}^g(t,f)||^2}\int_{-\infty}^{\infty}\int_{-\infty}^{\infty} (t-\bar{t_S})^2|X_{\alpha,\lambda}^g(t,f)|^2 \mathrm{d}t\mathrm{d}f, \tag{2.113}$$

$$B_{S,\alpha,\lambda}^2 = \frac{1}{||X_{\alpha,\lambda}^g(t,f)||^2}\int_{-\infty}^{\infty}\int_{-\infty}^{\infty} (f-\bar{f_S})^2|X_{\alpha,\lambda}^g(t,f)|^2 \mathrm{d}t\mathrm{d}f. \tag{2.114}$$

For the original signal $x(t)$, the mean time ($\bar{t_x}$), mean GTFT frequency ($\bar{f_x}$), time width (T_x^2) and GTFT bandwidth ($B_{x,\alpha,\lambda}^2$) are considered as per standard definition.

Also for the window function $g(t)$, mean time ($\bar{t_g}$), mean frequency ($\bar{f_g}$), time width (T_g^2) and bandwidth (B_g^2) are similarly considered as per standard definition.

It can be proved that

$$\bar{t_S} = \bar{t_x} - \bar{t_g}, \tag{2.115}$$

$$\bar{f_S} = \bar{f_x} - \bar{f_g}, \tag{2.116}$$

$$T_S^2 = T_x^2 + T_g^2 - \bar{t_S}^2 - 2\bar{t_x}\bar{t_g}, \tag{2.117}$$

$$B_{S,\alpha,\lambda}^2 = B_{x,\alpha,\lambda}^2 + B_g^2 \sin^2\alpha - \bar{f_x}^2 - \bar{f_g}^2. \tag{2.118}$$

It can be shown that a Gaussian window leads to the maximum 2D resolution. We consider a unit energy Gaussian window as

$$g(\tau) = (\pi\sigma^2)^{-1/4} e^{-\tau^2/2\sigma^2}. \tag{2.119}$$

Its squared time width and bandwidth are

$$T_g^2 = \frac{\sigma^2}{2}, \tag{2.120}$$

$$B_g^2 = \frac{1}{2\sigma^2}. \tag{2.121}$$

If $x(t)$ and $g(t)$ are real and zero mean, then the time- GTFT bandwidth product is given by

$$\mathrm{TGBP}_{S,\alpha,\lambda}^2 = T_S^2 B_{S,\alpha,\lambda}^2 = T_x^2 B_{x,\alpha,\lambda}^2 + \frac{1}{2\sigma^2} T_x^2 \sin^2\alpha + \frac{\sigma^2}{2} B_{x,\alpha,\lambda}^2 + \frac{1}{4}\sin^2\alpha. \tag{2.122}$$

We can easily show that

$$\begin{aligned} \mathrm{TGBP}_{S,\alpha,\lambda}^2 \geq & T_x^2 B_{x,\alpha,\lambda}^2 + \frac{1}{4}\sin^2\alpha + 2\sqrt{\frac{1}{2\sigma^2} T_x^2 \sin^2\alpha . \frac{\sigma^2}{2} B_{x,\alpha,\lambda}^2} \\ = & \left(T_x B_{x,\alpha,\lambda} + \frac{1}{2}|\sin\alpha| \right)^2 . \end{aligned} \tag{2.123}$$

This equality is attained if and only if

$$\sigma^2 = \frac{T_x |\sin\alpha|}{B_{x,\alpha,\lambda}}. \tag{2.124}$$

Therefore, for minimum GTFT domain support, the optimal STGTFT is obtained by using the Gaussian window

$$g(\tau) = \left(\pi \frac{T_x |\sin\alpha|}{B_{x,\alpha,\lambda}} \right)^{-1/4} exp\left(-\frac{B_{x,\alpha,\lambda}\tau^2}{2T_x|\sin\alpha|} \right), \tag{2.125}$$

where $\alpha \neq k\pi, k \in \mathbb{Z}$. This will also ensure maximum 2D resolution.

2.8.3 Uncertainty in the case of a cubic signal analyzed by ck-STGTFT

For the signal $x(\tau)$ and unit energy Gaussian window function $g(\tau)$ given by Eqns.(2.66) & (2.67), we can construct the windowed signal and its L^2 normalized version as

$$h_t(\tau) = x(\tau) g(\tau - t), \tag{2.126}$$

$$\eta_t(\tau) = \frac{h_t(\tau)}{||h_t(\tau)||_2} = (\pi\sigma_{t_0}^2)^{-\frac{1}{4}} \exp\left[-\frac{(\tau-t)^2}{2\sigma_{t_0}^2}\right] \exp\left(i\pi c\tau^3 + i\pi a\tau^2 + i2\pi f_d\tau\right). \tag{2.127}$$

Then, the time mean (t_s) and variance (T_s^2) of this signal can be calculated as:

$$t_s = \int_{-\infty}^{\infty} \tau|\eta_t(\tau)|^2 d\tau = t, \tag{2.128}$$

$$T_s^2 = \int_{-\infty}^{\infty} (\tau - t_s)^2|\eta_t(\tau)|^2 d\tau = \frac{\sigma_t^2}{2}. \tag{2.129}$$

Similarly, the frequency centre (Ω_s) and frequency variance (B_s^2) can also be calculated as ($N_{t,\alpha,\lambda}(\Omega)$ is GTFT of $\eta_t(\tau)$ using a cubic polynomial kernel(ck-GTFT))as follows:

Derivation of formulas required for uncertainty:

$$\begin{aligned}
\Omega_s &= \int_{-\infty}^{\infty} \Omega|N_{t,\alpha,\lambda}(\Omega)|^2 d\Omega, \\
&= \int_{-\infty}^{\infty} \Omega \iint_{-\infty}^{\infty} \eta_t(\tau_1)\eta_t^*(\tau_2)K_{\alpha,\lambda}(\tau_1,\Omega)K_{\alpha,\lambda}^*(\tau_2,\Omega)d\tau_1 d\tau_2 d\Omega, \\
&= \int_{-\infty}^{\infty} \Omega\cdot\mathrm{cosec}\alpha \iint_{-\infty}^{\infty} \eta_t(\tau_1)\eta_t^*(\tau_2)\exp\left[i\pi f_0^2\cot\alpha(\tau_1^2-\tau_2^2)\right. \\
&\qquad \left. - i\pi f_0^3\lambda(\tau_1^3-\tau_2^3) - i\Omega\mathrm{cosec}\alpha(\tau_1-\tau_2)\right] d\tau_1 d\tau_2 d\Omega,
\end{aligned} \tag{2.130}$$

substitute $\Omega\cdot\mathrm{cosec}\alpha = \Omega'$ in Eq. (2.130), we get

$$\begin{aligned}
&= \sin\alpha \iint_{-\infty}^{\infty} \eta_t(\tau_1)\eta_t^*(\tau_2)\exp\left[i\pi f_0^2\cot\alpha(\tau_1^2-\tau_2^2) - i\pi f_0^3\lambda(\tau_1^3-\tau_2^3)\right] \\
&\quad \cdot\left(\int_{-\infty}^{\infty} \Omega'\exp(-i\Omega'(\tau_1-\tau_2))\,d\Omega'\right) d\tau_1 d\tau_2, \\
&= -i\sin\alpha \iint_{-\infty}^{\infty} \eta_t(\tau_1)\eta_t^*(\tau_2)\exp\left[i\pi f_0^2\cot\alpha(\tau_1^2-\tau_2^2) - i\pi f_0^3\lambda(\tau_1^3-\tau_2^3)\right] \\
&\quad \cdot\frac{\partial}{\partial\tau_2}(\delta(\tau_1-\tau_2))\,d\tau_1 d\tau_2, \\
&= -i\sin\alpha \iint_{-\infty}^{\infty} \eta_t^*(\tau_2)\exp\left[-i\pi f_0^2\tau_2^2\cot\alpha + i\pi f_0^3\lambda\tau_2^3\right] \\
&\quad \cdot\frac{\partial}{\partial\tau_2}\left(\eta_t(\tau_1)\exp\left[i\pi f_0^2\tau_1^2\cot\alpha - i\pi f_0^3\lambda\tau_1^3\right]\delta(\tau_1-\tau_2)\right) d\tau_1 d\tau_2, \\
&= -i\sin\alpha \int_{-\infty}^{\infty} \eta_t^*(\tau_2)\exp\left[-i\pi f_0^2\tau_2^2\cot\alpha + i\pi f_0^3\lambda\tau_2^3\right] \\
&\quad \cdot\frac{\partial}{\partial\tau_2}\left(\int_{-\infty}^{\infty} \eta_t(\tau_1)\exp\left[i\pi f_0^2\tau_1^2\cot\alpha - i\pi f_0^3\lambda\tau_1^3\right]\delta(\tau_1-\tau_2)d\tau_1\right) d\tau_2,
\end{aligned} \tag{2.131, 2.132}$$

$$\begin{aligned}
&= -i\sin\alpha \int_{-\infty}^{\infty} \eta_t^*(\tau_2)\exp\left[-i\pi f_0^2\tau_2^2\cot\alpha + i\pi f_0^3\lambda\tau_2^3\right] \\
&\quad \cdot\frac{\partial}{\partial\tau_2}\left(\eta_t(\tau_2)\exp\left[i\pi f_0^2\tau_2^2\cot\alpha - i\pi f_0^3\lambda\tau_2^3\right]\right) d\tau_2.
\end{aligned}$$

Substituting $\eta_t(\tau)$ from Eq.(2.127) in the above expression and evaluating the integral, we obtain

$$\Omega_s = \sin\alpha \left[2\pi \left(f_d + \left(a + f_0^2 \cot\alpha \right) t \right) + 3\pi (c - f_0^3 \lambda) \left(t^2 + \frac{\sigma_t^2}{2} \right) \right]. \tag{2.133}$$

For frequency variance,

$$\begin{aligned} B_s^2 &= \int_{-\infty}^{\infty} \Omega^2 |N_{t,\alpha,\lambda}(\Omega)|^2 d\Omega - \Omega_s^2, \\ &= \int_{-\infty}^{\infty} \Omega^2 \iint_{-\infty}^{\infty} \eta_t(\tau_1) \eta_t^*(\tau_2) K_{\alpha,\lambda}(\tau_1, \Omega) K_{\alpha,\lambda}^*(\tau_2, \Omega) d\tau_1 d\tau_2 d\Omega - \Omega_s^2, \\ &= \int_{-\infty}^{\infty} \Omega^2 \mathrm{cosec}\alpha \iint_{-\infty}^{\infty} \eta_t(\tau_1) \eta_t^*(\tau_2) \exp\left[i\pi f_0^2 \cot\alpha (\tau_1^2 - \tau_2^2) \right. \\ &\qquad \left. - i\, f_0^3 \lambda (\tau_1^3 - \tau_2^3) - i\Omega \cdot \mathrm{cosec}\alpha (\tau_1 - \tau_2) \right] d\tau_1 d\tau_2 d\Omega - \Omega_s^2, \end{aligned} \tag{2.134}$$

substitute $\Omega \cdot \mathrm{cosec}\alpha = \Omega'$ in Eq. (2.134), we get

$$\begin{aligned} &= \sin^2\alpha \iint_{-\infty}^{\infty} \eta_t(\tau_1) \eta_t^*(\tau_2) \exp\left[i\pi f_0^2 \cot\alpha (\tau_1^2 - \tau_2^2) - i\pi f_0^3 \lambda (\tau_1^3 - \tau_2^3) \right] \\ &\quad \cdot \left(\int_{-\infty}^{\infty} \Omega'^2 \exp(-i\Omega' (\tau_1 - \tau_2))\, d\Omega' \right) d\tau_1 d\tau_2 - \Omega_s^2, \\ &= -\sin^2\alpha \iint_{-\infty}^{\infty} \eta_t(\tau_1) \eta_t^*(\tau_2) \exp\left[i\pi f_0^2 \cot\alpha (\tau_1^2 - \tau_2^2) - i\pi f_0^3 \lambda (\tau_1^3 - \tau_2^3) \right] \\ &\quad \cdot \frac{\partial^2}{\partial \tau_2^2} (\delta(\tau_1 - \tau_2))\, d\tau_1 d\tau_2 - \Omega_s^2, \\ &= -\sin^2\alpha \iint_{-\infty}^{\infty} \eta_t^*(\tau_2) \exp\left[-i\pi f_0^2 \tau_2^2 \cot\alpha + i\pi f_0^3 \lambda \tau_2^3 \right] \\ &\quad \cdot \frac{\partial^2}{\partial \tau_2^2} \left(\eta_t(\tau_1) \exp\left[i\pi f_0^2 \tau_1^2 \cot\alpha - i\pi f_0^3 \lambda \tau_1^3 \right] \delta(\tau_1 - \tau_2) \right) d\tau_1 d\tau_2 - \Omega_s^2, \\ &= -\sin^2\alpha \int_{-\infty}^{\infty} \eta_t^*(\tau_2) \exp\left[-i\pi f_0^2 \tau_2^2 \cot\alpha + i\pi f_0^3 \lambda \tau_2^3 \right] \\ &\quad \cdot \frac{\partial^2}{\partial \tau_2^2} \left(\int_{-\infty}^{\infty} \eta_t(\tau_1) \exp\left[i\pi f_0^2 \tau_1^2 \cot\alpha - i\pi f_0^3 \lambda \tau_1^3 \right] \delta(\tau_1 - \tau_2) d\tau_1 \right) d\tau_2 - \Omega_s^2, \\ &= -\sin^2\alpha \int_{-\infty}^{\infty} \eta_t^*(\tau_2) \exp\left[-i\pi f_0^2 \tau_2^2 \cot\alpha + i\pi f_0^3 \lambda \tau_2^3 \right] \\ &\quad \cdot \frac{\partial^2}{\partial \tau_2^2} \left(\eta_t(\tau_2) \exp\left[i\pi f_0^2 \tau_2^2 \cot\alpha - i\pi f_0^3 \lambda \tau_2^3 \right] \right) d\tau_2 - \Omega_s^2. \end{aligned} \tag{2.135}$$

Substituting $\eta_t(\tau)$ from Eq.(2.127) in the above expression and evaluating the integral, we obtain

$$B_s^2 = \frac{sin^2\alpha}{2\sigma_t^2} \left[4\pi^2 \sigma_t^4 \left(\left(a + f_0^2 \cot\alpha \right) + 3t \left(c - f_0^3 \lambda \right) \right)^2 + 9\pi^2 \sigma_t^6 \left(c - f_0^3 \lambda \right)^2 + 1 \right]. \tag{2.136}$$

2.8.4 TBP of signal using ck-STGTFT vs using STFrFT or STFT

From Eq.(2.129) and Eq.(2.136), the TBP in STGTFT domain can be stated as follows:

$$\begin{aligned} TBP^2_{STGTFT} &= T_s^2 B_s^2 \\ &= \frac{\sin^2\alpha}{4}\left[4\pi^2\sigma_t^4\left(\left(a + f_0^2\cot\alpha\right) + 3t\left(c - f_0^3\lambda\right)\right)^2\right. \\ &\quad \left. + 9\pi^2\sigma_t^6\left(c - f_0^3\lambda\right)^2 + 1\right]. \end{aligned} \tag{2.137}$$

The following cases can be inferred from Eq. (2.137):

- Case 1: Quadratic chirp analysed using STFT ($\alpha = 90°$, $\lambda = 0$):

$$TBP^2_{STFT} = \frac{1}{4}\left[4\pi^2\sigma_t^4\left(a + 3ct\right)^2 + 9\pi^2\sigma_t^6 c^2 + 1\right]. \tag{2.138}$$

- Case 2: Quadratic chirp analysed using matched STFrFT ($\cot\alpha_{opt} = -a/f_0^2$, $\lambda = 0$):

$$\begin{aligned} TBP^2_{STFrFT} &= \frac{f_0^4}{4(f_0^4 + a^2)}\left[36\pi^2\sigma_t^4 t^2 c^2 + 9\pi^2\sigma_t^6 c^2 + 1\right] \\ &= \frac{\sin^2\alpha}{4}\left[36\pi^2\sigma_t^4 t^2 c^2 + 9\pi^2\sigma_t^6 c^2 + 1\right]. \end{aligned} \tag{2.139}$$

- Case 3: Quadratic chirp analysed using matched ck-STGTFT ($\cot\alpha = -a/f_0^2$, $f_0^3\lambda = c$):

$$TBP^2_{ck-STGTFT} = \frac{f_0^4}{4(f_0^4 + a^2)} = \frac{\sin^2\alpha}{4}. \tag{2.140}$$

Hence, it can be clearly seen that the following inequality holds as

$$TBP^2_{STFT} \geq TBP^2_{STFrFT} \geq TBP^2_{ck-STGTFT}. \tag{2.141}$$

In the case of quadratic chirp (non-zero 'a' and 'c'), these inequalities are strict. Hence, it is evident that for a quadratic chirp, the matched cubic kernel STGTFT has the most compact support.

As shown in Eq. (2.140) and Eq. (2.141), TBP of ck-STGTFT is always greater than or equal to $|\sin\alpha|/2$. So TBP of ck-STGTFT for a quadratic chirp at matched condition is almost equal to TBP of fractional Fourier transform for a linear chirp, which is equal to $|\sin\alpha|/2$ [100].

2.8.5 TBP comparison of ck-STGTFT with TBP of fractional Fourier ambiguity function, and fractional Fourier Wigner-Ville distribution

R. Tao et al. [111] and Tian-Wen Che et al. [19] proposed an ambiguity function (AF) based on the linear canonical transform (LCT) to estimate parameters of the quadratic signal. Similarly, WVD based on LCT has been proposed and used for the estimation of quadratic signal parameters [91, 106]. LCT kernel is a generalization of FrFT, and it is a quadratic transform.

- Fractional Fourier based AF (FrAF) associated with FrFT or LCT is defined as

$$FrAF_{x(t),\alpha}(\tau, f) = \int_{-\infty}^{\infty} x(t+\tau/2)x^*(t-\tau/2)K_\alpha(t, f)dt. \tag{2.142}$$

- Fractional Fourier based WVD (FrWVD) associated with FrFT or LCT (FrWVD) is defined as

$$FrWDF_{x(t),\alpha}(t, f) = \int_{-\infty}^{\infty} x(t+\tau/2)x^*(t-\tau/2)K_\alpha(\tau, f)d\tau. \tag{2.143}$$

Uncertainty principle for FrAF:

Consider a unit energy signal $x(t)$ and its FrFT $X_\alpha(\cdot)$. Let τ_{mean} be mean time and f_{mean} be mean frequency of $x(t)$.

$$\int_{-\infty}^{\infty} |x(\tau)|^2 d\tau = 1, \text{ and } \int_{-\infty}^{\infty} |X_\alpha(f)|^2 df = 1,$$
$$\int_{-\infty}^{\infty} \tau|x(\tau)|^2 d\tau = \tau_{mean}, \text{ and } \int_{-\infty}^{\infty} f|X_\alpha(f)|^2 df = f_{mean}.$$

Now consider time variance of FrAF is $\sigma^2_{t_{FrAF}}$

$$\begin{aligned}
\sigma^2_{t_{FrAF}} &= \iint_{-\infty}^{\infty} (\tau - \tau_{mean})^2 |AF^G_{x(t),\alpha}(\tau, f)|^2 d\tau df, \\
&= \int_{-\infty}^{\infty} (\tau - \tau_{mean})^2 \int_{-\infty}^{\infty}\int_{-\infty}^{\infty} x(t+\tau/2)x^*(t-\tau/2) \\
&\qquad x^*(t'+\tau/2)x(t'-\tau/2).\left[\int_{-\infty}^{\infty} K_\alpha(t, f)^* K_\alpha(t', f)df\right] dtdt'd\tau, \\
&= \iint_{-\infty}^{\infty} (\tau - \tau_{mean})^2 |x(t+\tau/2)|^2 |x(t-\tau/2)|^2 d\tau dt.
\end{aligned}$$

Put $t + \tau/2 = m$, $t - \tau/2 = n$, If $x(t)$ is real and zero mean, then $\tau_{mean} = 0$. Hence, the time-variance is given

$$\sigma^2_{t_{FrAF}} = \iint_{-\infty}^{\infty} (m-n)^2 |x(m)|^2 |x(n)|^2 dmdn = 2\int_{-\infty}^{\infty} m^2 |x(m)|^2 dm. \tag{2.144}$$

Now consider frequency variance of FrAF is $\sigma^2_{f_{FrAF}}$

$$\begin{aligned}
\sigma^2_{f_{FrAF}} &= \iint_{-\infty}^{\infty} (f - f_{mean})^2 |AF^G_{X_\alpha(u),\alpha}(f,\tau)|^2 d\tau df, \\
&= \int_{-\infty}^{\infty} (f - f_{mean})^2 \int_{-\infty}^{\infty} X_\alpha(u + f/2) X^*_\alpha(u - f/2) \\
&\qquad \int_{-\infty}^{\infty} X^*_\alpha(u' + f/2) X_\alpha(u' - f/2). \left[\int_{-\infty}^{\infty} K_\alpha(u,\tau)^* K_\alpha(u',\tau) d\tau \right] du du' df, \\
&= \iint_{-\infty}^{\infty} (f - f_{mean})^2 |X_\alpha(u + f/2)|^2 |X_\alpha(u - f/2)|^2 du df.
\end{aligned}$$

Put $u + f/2 = w$, $u - f/2 = v$, If $x(t)$ is real and zero mean, then $f_{mean} = 0$. Hence, the frequency-variance is given

$$\sigma^2_{f_{FrAF}} = \iint_{-\infty}^{\infty} (w-v)^2 |X_\alpha(w)|^2 |X_\alpha(v)|^2 dw dv = 2\int_{-\infty}^{\infty} w^2 |X_\alpha(w)|^2 dw. \tag{2.145}$$

From Eq. (2.144) and Eq. (2.145), square of time bandwidth product can be written

$$\sigma^2_{t_{FrAF}} \sigma^2_{f_{FrAF}} = 4\int_{-\infty}^{\infty} m^2 |x(m)|^2 dm \int_{-\infty}^{\infty} w^2 |X_\alpha(w)|^2 dw = 4 \cdot \sigma^2_{t_{GTFT}} \sigma^2_{f_{GTFT}},$$

where $\sigma^2_{t_{FrFT}}$ is time variance and $\sigma^2_{f_{FrFT}}$ is frequency variance of FrAF and their product is always greater than or equal to $\sin^2 \alpha/4$ [100].

$$\sigma^2_{t_{FrAF}} \cdot \sigma^2_{f_{FrAF}} \geq 4 \cdot \frac{\sin^2 \alpha}{4}.$$

$$\therefore \sigma_{t_{FrAF}} \cdot \sigma_{f_{FrAF}} \geq |\sin \alpha|. \tag{2.146}$$

Uncertainty principle for FrWVD:

we can also derive the uncertainty principle or TBP for FrWVD.

$$\sigma_{t_{FrWVD}} \cdot \sigma_{f_{FrWVD}} \geq \frac{|\sin \alpha|}{4}. \tag{2.147}$$

where $\sigma^2_{t_{FrWVD}}$ and is time variance and $\sigma^2_{f_{FrWVD}}$ is frequency variance of FrWVD.

As shown in Eq. (2.147), TBP of FrWVD for quadratic chirp is always greater than or equal to $|\sin\alpha|/4$. So FrWVD gives the least TBP for a quadratic chirp. However, it produces cross-term in the presence of a multicomponent signal, and it can not be possible to remove cross-terms without compromising the resolution of signal representation [26]. Similarly, as shown in Eq. (2.146), TBP of FrAF is always greater than or equal to $|\sin\alpha|$. So FrAF gives higher TBP as compared to ck-STGTFT for the representation of quadratic chirp and produces cross-terms in multicomponent signal analysis. Hence, it can be concluded that the following inequality holds in case of monocomponent quadratic chirp as

$$TBP^2_{FrAF} \geq TBP^2_{ck-STGTFT} \geq TBP^2_{FrWVD}. \tag{2.148}$$

2.9 ck-AGFS performance compared to existing TFDs

To demonstrate the effectiveness of ck-AGFS, two close amplitude modulated quadratic chirps are considered.

$$\begin{aligned} x_1(t) &= \begin{cases} e^{i\pi c_1 t^3 + i\pi a_1 t^2 + 2i\pi f_{d1}} & 0 \leq t < 2\text{sec} \\ e^{i\pi c_2 t^3 + i\pi a_2 t^2 + 2i\pi f_{d2}} & 2 \leq t < 4\text{sec} \end{cases}, \\ x_2(t) &= \begin{cases} e^{i\pi c_3 t^3 + i\pi a_3 t^2 + 2i\pi f_{d3}} & 0 \leq t < 2\text{sec} \\ e^{i\pi c_4 t^3 + i\pi a_4 t^2 + 2i\pi f_{d4}} & 2 \leq t < 4\text{sec} \end{cases}, \end{aligned} \tag{2.149}$$

$$x(t) = 2e^{-0.08t} \cdot x_1(t) + 1.5e^{-0.04t} \cdot x_2(t). \tag{2.150}$$

Here we consider $c_1 = c_3$, $c_2 = c_4$, $a_1 = a_3$ and $a_2 = a_4$. Signal parameters (quadratic rate, chirp rate and Doppler frequency) of both components change in between the signal duration. Parameters of simulated quadratic chirps are mentioned in Table 2.5.

Table 2.5: Simulation parameter of $x(t)$ for amplitude modulated quadratic chirps

Amplitude modulated quadratic chirps parameters									
τ (sec)	f_s (Hz)	$c_1(Hz^3)$	$a_1(Hz^2)$	f_{d1} (Hz)	f_{d2} (Hz)	$c_2(Hz^3)$	$a_2(Hz^2)$	f_{d3} (Hz)	f_{d4}(Hz)
4	1200	5	50	20	15	10	25	80	75

Fig. 2.1(a) shows ck-AGFS of quadratic chirp with approximate confined Gaussian window (ACGW) used. ACGW produces least frequency domain variance among all the windows with

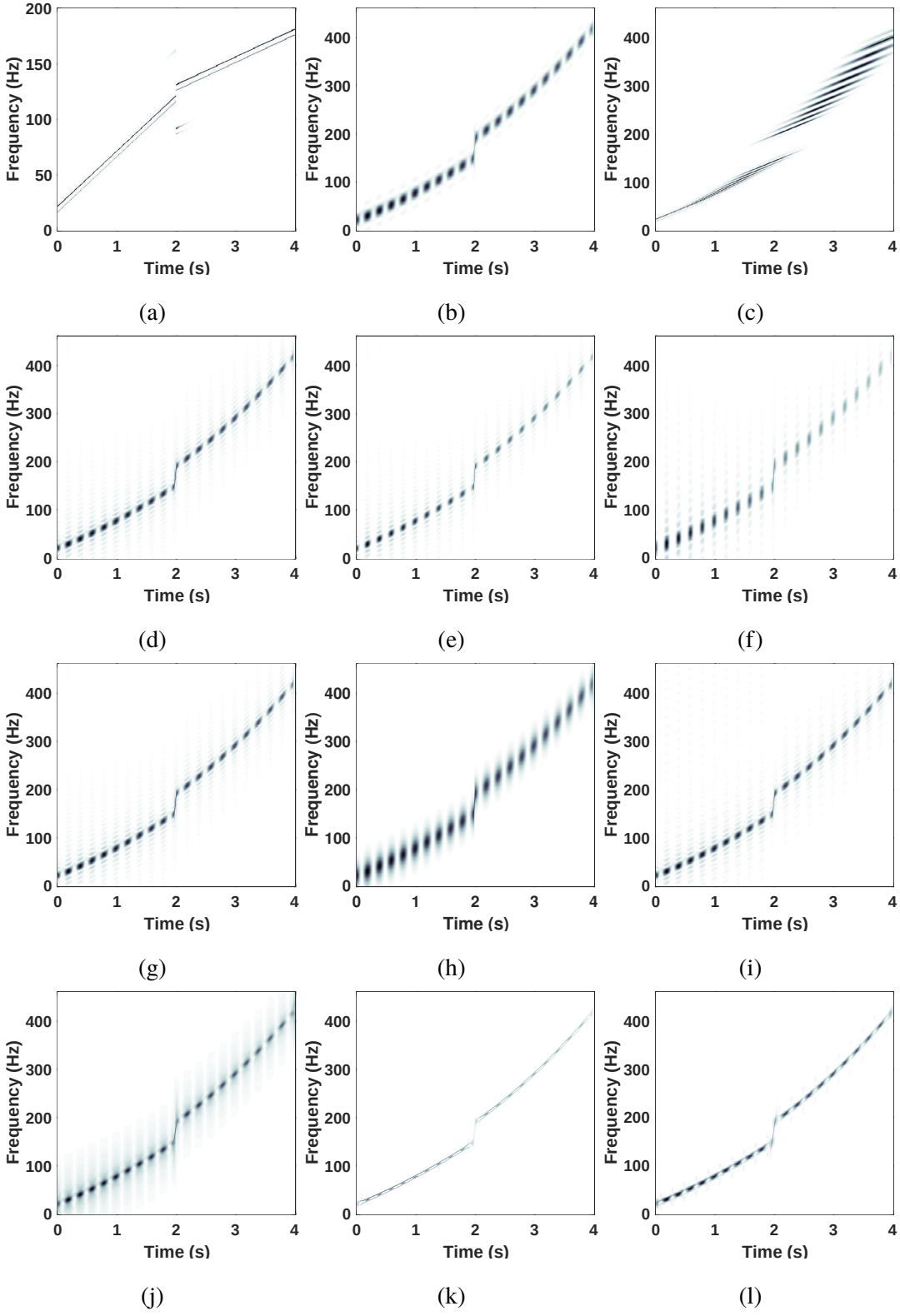

Figure 2.1: Comparison of different TFDs with ck-AGFS for multicomponent quadratic chirp (a) ck-AGFS (b) STFT (c) STFrFT (d) QWVD (e) PWVD4 (f) PWVD6 (g) MBD (h) EMBD (i) CW (j) AFS (k) CKD (l) AOK

given time domain variance [108]. Optimum Gaussian window length of AGFS is 480 samples as per Eq. (2.108), and estimated matched angle is 85.23° for $0 \leq t < 2$ seconds and 87.61° for $2 \leq t < 4$ seconds. It is observed that analysis with ACGW window produces marginally less spread in the frequency domain than using a Gaussian window. Fig. 2.1(b) shows the STFT based spectrogram of quadratic chirp, and its optimum window length of 64 samples. Fig. 2.1(c-l) show the STFrFT based TFD, the quadratic WVD (QWVD) based TFD, the 4^{th} order polynomial WVD (PWVD4) based TFD, the 6^{th} order polynomial WVD (PWVD6) based TFD, modified B distribution (MBD), extended modified B distribution (EMBD), Choi Williams (CW) distribution, adaptive fractional spectrogram (AFS), compact kernel distribution (CKD), and adaptive orthogonal kernel (AOK) respectively.

We can see from Fig. 2.1 that all other TFDs except AGFS are unable to represent two different nearby chirp signals distinguishably in the TF plane. Similarly Fig. 2.2 shows time slices of AGFS and other TFDs at time instant of 1 second and it shows that none of TFD except AGFS is capable to represent two peaks separately. This shows the superiority of ck-AGFS over other TFDs to resolve two nearby amplitude modulated quadratic chirps. Hence, AGFS has higher resolution than the existing TFDs. Mathematical results of uncertainty principle in Eq. (2.141) was also evident in simulation results shown in Fig. 2.1(a) of AGFS, Fig. 2.1(b) of STFT based TFD and Fig. 2.1(c) of STFrFT based TFD for representation of multicomponent quadratic chirp.

Similar to the adaptive fractional spectrogram (AFS), AGFS also suffers from energy leakage if the signal is absent in certain region [12, pp. 304].

ECM values as per Eq. (2.110) are also computed for all TFDs for multicomponent signal given by Eq. (2.149) and are reported in the Table 2.6. The least M value is obtained for ck-AGFS, indicating that it is the highest concentration TFD among all the TFDs. To quantitatively

Table 2.6: Comparison of energy concentration measurement (ECM) of different TFDs

TFD	**ck-AGFS**	STFrFT	STFT	QWVD	PWVD4	PWVD6
M	$\mathbf{1.29 * 10^5}$	$5.74 * 10^5$	$4.51 * 10^5$	$1.16 * 10^6$	$1.81 * 10^6$	$3.51 * 10^5$
TFD	MBD	EMBD	CW	CK TFD	AFS	AOK-TFD
M	$1.16 * 10^6$	$4.22 * 10^5$	$1.15 * 10^6$	$7.32 * 10^5$	$6.74 * 10^6$	$2.96 * 10^5$

measure the resolution of AGFS, Boashash-Sucic resolution measure [12, pp. 412-418] is used.

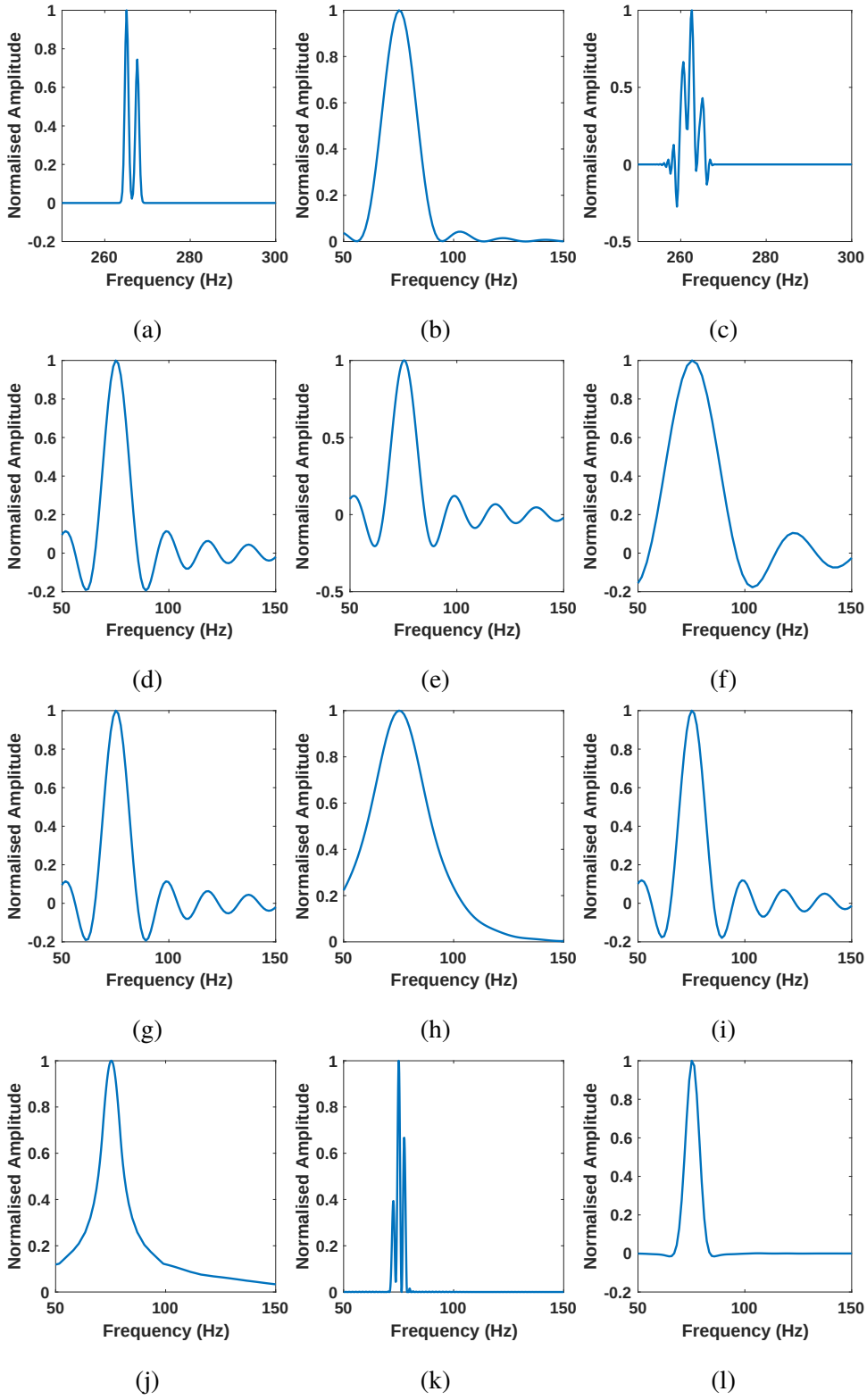

Figure 2.2: Comparison of time slice of different TFDs for multicomponent quadratic chirp (a) ck-AGFS (b) STFT (c) STFrFT (d) QWVD (e) PWVD4 (f) PWVD6 (g) MBD (h) EMBD (i) CW (j) AFS (k) CKD (l) AOK

For a time slice of the multicomponent signal at a time instant t, it is given as

$$P(t) = 1 - \frac{1}{3}\left[\left|\frac{A_s(t)}{A_m(t)}\right| + \frac{1}{2}\left|\frac{A_x(t)}{A_m(t)}\right| + \left(1 - \frac{S(t)}{D(t)}\right)\right], \tag{2.151}$$

where, for a pair of signal components, $A_m(t)$ is average amplitudes of the component's mainlobes; $A_s(t)$ is the average amplitudes of the component's sidelobes; $A_x(t)$ is the cross-term amplitude; $S(t)$ is the separation measure; and $D(t)$ is frequency separation of components' mainlobes. A high resolution TFD has a P value closer to 1, whereas a low resolution TFD has a P value closer to 0. The Boashash-Sucic resolution measure (P) is calculated for ck-AGFS of signal given by Eq. (2.149) at different time instants t and it is reported in Table 2.7 Least

Table 2.7: Boashash-Sucic resolution measure (P) at different time instants of ck-AGFS

t (s)	A_m	A_s	A_x	S	D	**P**
1	0.68	0.019	0.012	9	10	**0.9577**
3	0.78	0.018	0.011	9	10	**0.9565**

M value of AGFS from Table 2.6 indicates that AGFS is a highly concentrated TFD. From Table 2.7, we can see that AGFS is a high resolution TFD since P values are very close to 1. Fig. 2.1 and Fig. 2.2 illustrate the distinguishing capability of AGFS compared to other TFDs. From section 2.4.16, we can see that AGFS is also capable of providing cross term free TFD if individual components of a multicomponent signal have non-overlapping STGTFTs. These criteria combined together prove that AGFS can provide high resolution, high concentration, cross term free TFD for multicomponent frequency modulated signal.

2.10 Extraction of quadratic chirp of interest from multicomponent quadratic chirp using ck-AGFS

The FrFT can be used to extract different components of a noisy mixture of linear frequency modulated signals [124]. Since ck-AGFS has a third order kernel, it can be used to extract components of a noisy mixture of quadratic chirps. To illustrate this, we consider a noisy version of the bi-component amplitude modulated quadratic chirp signal $x(t)$ defined by Eq. (2.150). Hence, we have $y(t) = x(t) + n(t)$ with SNR = 0 dB, where $n(t)$ is additive white Gaussian noise. For extraction, multiple ck-AGFS (here, two) are used. Only one chirp is

focused in respective ck-AGFS at matched condition ($c_k = f_0^3 \lambda_k$ and $a_k = -f_0^2 \cot \alpha_k$, where k is the index of the chirp component). When ck-AGFS is matched, the time window variance is optimum only for the chirp component that is being matched. Four cases of variation of component chirp parameters are considered.

2.10.1 Case A: chirps differing only in their Doppler frequency

In this case, $x(t)$ has $c_1 = c_2 = c_3 = c_4 = c$ and $a_1 = a_2 = a_3 = a_4 = a$ and different Doppler frequencies f_{d1}, f_{d2}, f_{d3}, and f_{d4}. Doppler frequencies of both components change in between the signal duration. Simulation parameters are shown in Table 2.8. Once the ck-AGFS is computed on the received composite noisy signal, as shown in Fig. 2.1, the extraction of an individual component can be performed using the component extraction procedure described in [11]. The algorithmic steps are as follows:

1. Initialize $k = 1$.

2. Find out (t_{00}, f_{00}), the location of maximum energy in the TFD. The IF of the k$^{\text{th}}$ component at the time instant t_{00} is computed to be $IF_k(t_{00}) = f_{00}$. All points from $(t_{00}, f_{00} - l)$ to $(t_{00}, f_{00} + l)$ are assigned zero value. l is a predetermined value

3. Assign $t_r = t_{00} + (1/f_s)$, $t_l = t_{00} - (1/f_s)$,$f_l = f_{00}$ and $f_r = f_{00}$, where f_s is sampling frequency. The IF of signal component for the sub region $t < t_{00}$ and $t > t_{00}$ is calculated by the following procedure

   (a) Find out the frequency $\tilde{f}_0$ having the maximum energy in the range $(t_r, f_r - l)$ to $(t_r , f_r + l)$ and $\tilde{f}_1$ in the range $(t_l, f_l - l)$ to $(t_l , f_l + l)$. IF at instances t_l and t_r are calculated to be as $IF_k(t_l) = \tilde{f}_1$ and $IF_k(t_r) = \tilde{f}_0$.

   (b) Assign zeros in the range $(t_r, f_r - l)$ to $(t_r , f_r + l)$ and $(t_l, f_l - l)$ to $(t_l , f_l + l)$.

   (c) Assign $t_r = t_r + (1/f_s)$ and $t_l = t_l - (1/f_s)$.

   (d) Repeat from step (a) to step (d) till the boundary of the TFD is reached

4. Increment 'k' and repeat from step 2 to step 4 till all the components have been extracted.

Fig. 2.3(a) shows the STFT of the noisy signal with a window length of 64 samples, which clearly shows that the STFT is unable to resolve the two close components. Fig. 2.3(b) and Fig. 2.3(c) show the two ck-AGFS focused on each quadratic chirp component contained

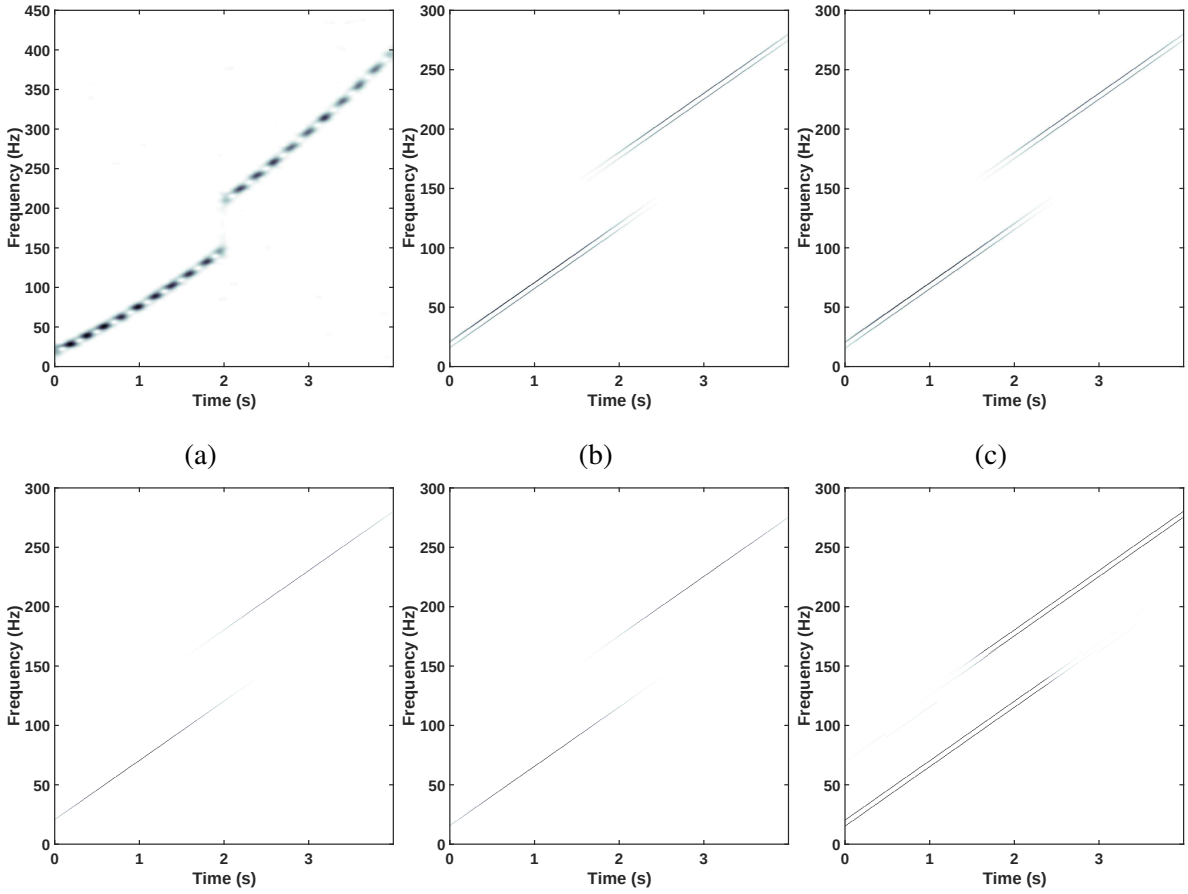

Figure 2.3: Spectrogram view of extraction of mono-component quadratic chirp from multicomponent quadratic chirp (quadratic chirp differs in terms of Doppler frequency) using ck-AGFS algorithm (a) STFT spectrogram (b) AGFS focused on first component (c) AGFS focused on second component (d) Extracted first component (e) Extracted second component (f) AGFS fusion

Table 2.8: Simulation parameters of two amplitude modulated quadratic chirps (different in terms of Doppler frequency) for extraction using ck-AGFS at its optimum window length and matched angle

Case A: Amplitude modulated chirps are separated only in Doppler							
τ (sec)	f_s (Hz)	$c(Hz^3)$	$a(Hz^2)$	f_{d1}(Hz)	f_{d2}(Hz)	f_{d3}(Hz)	f_{d4}(Hz)
4	1200	5	50	20	15	80	75

in the noisy received signal. The individual chirp components extracted using the algorithm described in [11] are shown in Fig. 2.3(d,e). The respective insignificant component (unfocused component) is zero padded to highlight the extracted component of interest. Fig. 2.3(f) shows the

combined AGFS spectrogram obtained by combining the spectrograms of individual extracted components.

2.10.2 Case B: chirps differing only in their chirp rate

In this case, $x(t)$ has $c_1 = c_2 = c_3 = c_4 = c$ and $f_{d1} = f_{d2} = f_{d3} = f_{d4} = f_d$ and different chirp rates a_1, a_2, a_3, and a_4. Chirp rates of both components change in between the signal duration. Simulation parameters are shown in Table 2.9 for two quadratic chirps with different chirp rates.

The subfigures of Fig. 2.4 respectively show the STFT spectrogram, AGFS focussed and

Table 2.9: Simulation parameters of two amplitude modulated quadratic chirps (which differ in terms of chirp rate) for extraction using ck-AGFS at its optimum window length and matched angle

Case B: Amplitude modulated chirps are separated only in Chirp Rates							
$\tau\ (s)$	$f_s\ (Hz)$	$c\ (Hz^3)$	$a_1\ (Hz^2)$	$a_2\ (Hz^2)$	$a_3\ (Hz^2)$	$a_4\ (Hz^2)$	$f_d\ (Hz)$
4	2500	5	200	190	180	170	20

extracted components and combined AGFS for this case using same procedure as in the previous case.

2.10.3 Case C: chirps differing only in their quadratic rate

In this case, $x(t)$ has $a_1 = a_2 = a_3 = a_4 = a$ and $f_{d1} = f_{d2} = f_{d3} = f_{d4} = f_d$ and different quadratic rates c_1, c_2, c_3, and c_4. Quadratic rates of both components change in between the signal duration. Simulation parameters are shown in Table 2.10.

Table 2.10: Simulation parameters of two amplitude modulated quadratic chirps (differ in terms of quadratic rates) for extraction using ck-AGFS at its optimum window length and matched angle

Case C: Amplitude modulated chirps are separated only in their Quadratic Rate								
$\tau\ (s)$	$f_s\ (Hz)$	$c_1\ (Hz^3)$	$c_2\ (Hz^3)$	$c_3\ (Hz^3)$	$c_4\ (Hz^3)$	$a\ (Hz^2)$	$f_{d1}\ (Hz)$	$f_{d2}\ (Hz)$
4	3000	5	15	25	35	25	30	10

The subfigures of Fig. 2.5 respectively show the STFT spectrogram, AGFS focussed and extracted components and combined AGFS for this case using same procedure as in the previous case.

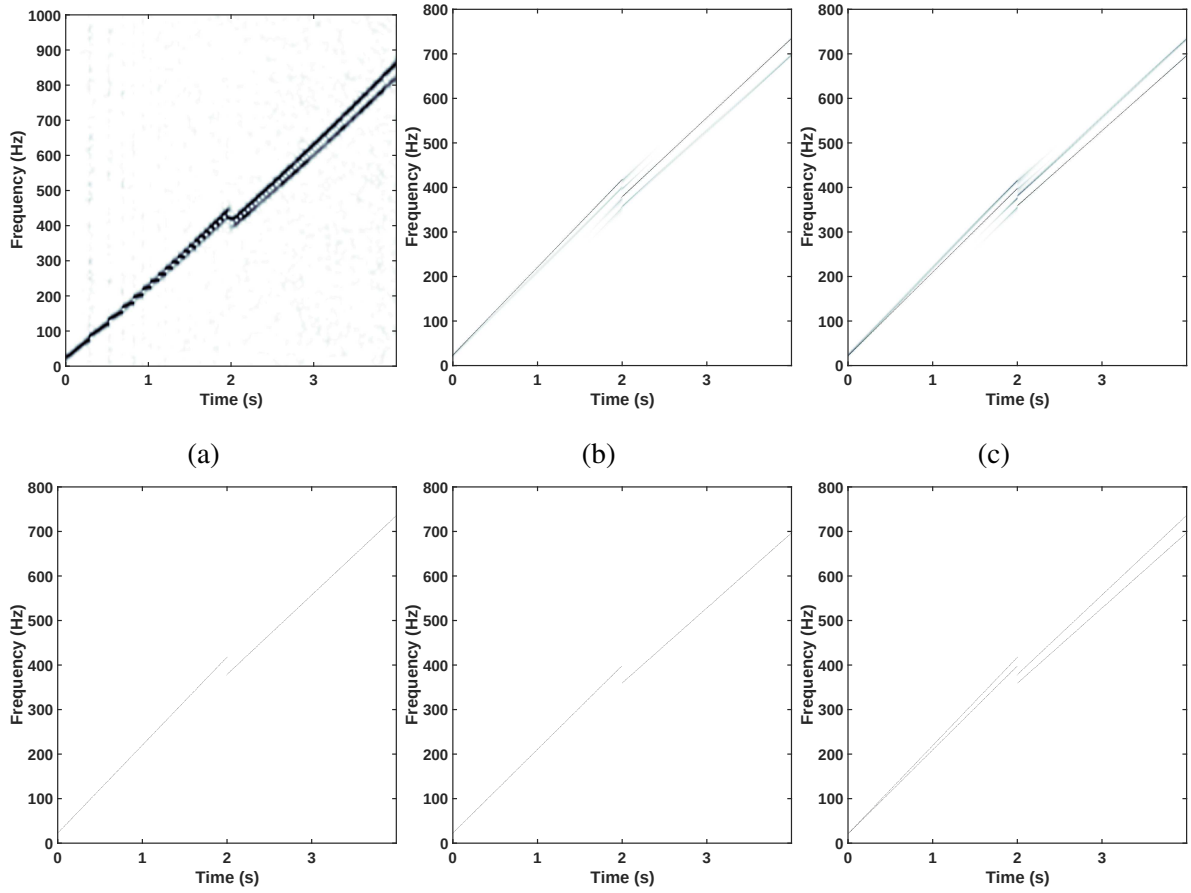

Figure 2.4: Spectrogram view of extraction of mono-component quadratic chirp from multicomponent quadratic chirp (which differ in terms of chirp rate) using ck-AGFS algorithm (a) STFT spectrogram (b) AGFS focused on first component (c) AGFS focused on second component (d) Extracted first component (e) Extracted second component (f) AGFS fusion

2.10.4 Case D: crossed chirps in time-frequency domain

Here we demonstrate effectiveness of ck-AGFS in the special application of component extraction from a mixture of two quadratic chirps with different orientations crossing in their TFDs. Simulation parameters are shown in Table 2.11 for two different quadratic chirps at their matched GTFT of quadratic and cubic phase.

The subfigures of Fig. 2.6 respectively show the STFT spectrogram, AGFS focussed and extracted components and combined AGFS for this case using same procedure as in the previous case.

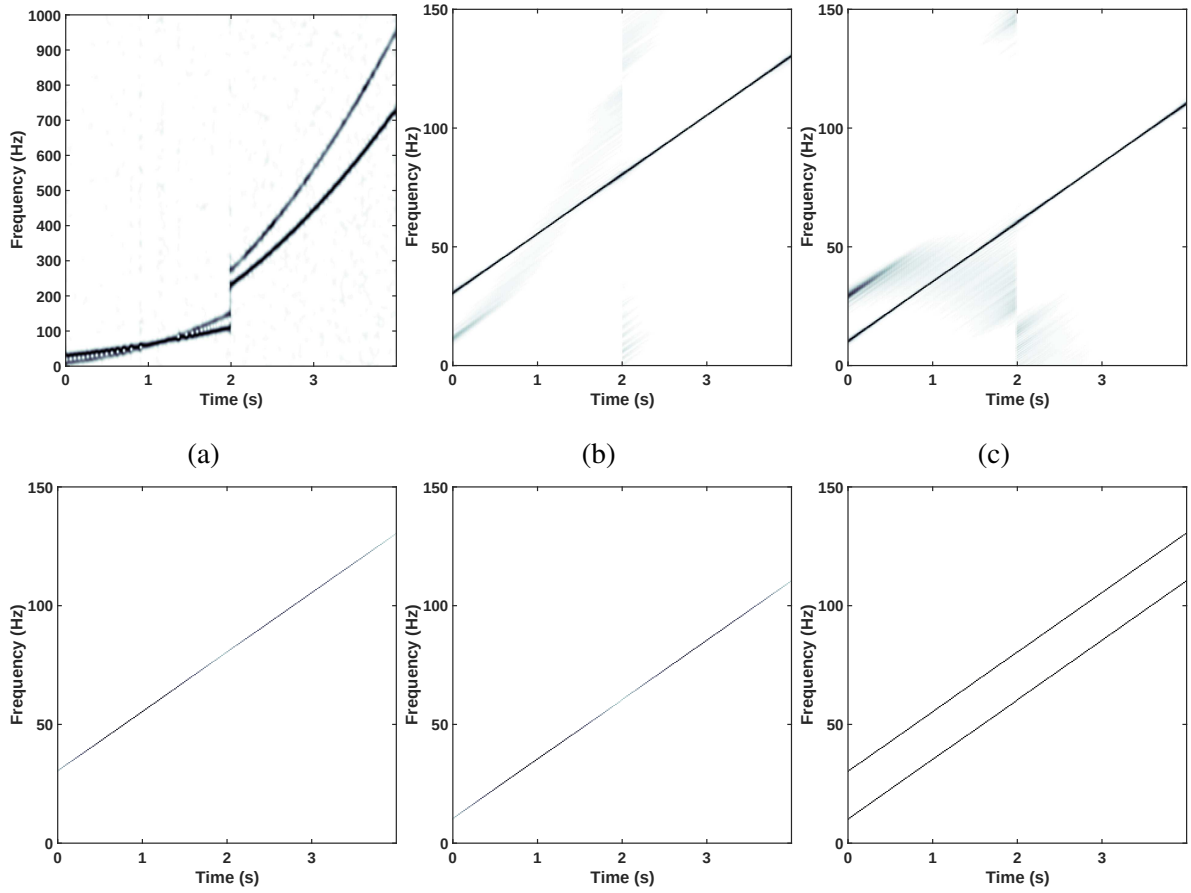

Figure 2.5: Spectrogram view of extraction of mono-component quadratic chirp from multi-component quadratic chirp (differ in terms of quadratic chirp rate) using ck-AGFS algorithm (a) STFT spectrogram (b) AGFS focused on first component (c) AGFS focused on second component (d) Extracted first component (e) Extracted second component (f) AGFS fusion

Table 2.11: Simulation parameters of two amplitude modulated quadratic chirps (crossed in time-frequency domain) for extraction using ck-AGFS at its optimum window length and matched angle

Case D. Amplitude modulated chirps are crossed in time-frequency domain						
$\tau\ (s)$	$f_s\ (Hz)$	$c_1\ (Hz^3)$	$c_2\ (Hz^3)$	$c_3\ (Hz^3)$	$c_4\ (Hz^3)$	$a_1\ (Hz^2)$
4	3000	5	8	9	12	100
$a_2\ (Hz^2)$	$a_3\ (Hz^2)$	$a_4\ (Hz^2)$	$f_{d1}\ (Hz)$	$f_{d2}\ (Hz)$	$f_{d3}\ (Hz)$	$f_{d4}\ (Hz)$
-200	50	-250	500	800	300	1180

2.11 SNR gain and mean squre error analysis of AGFS

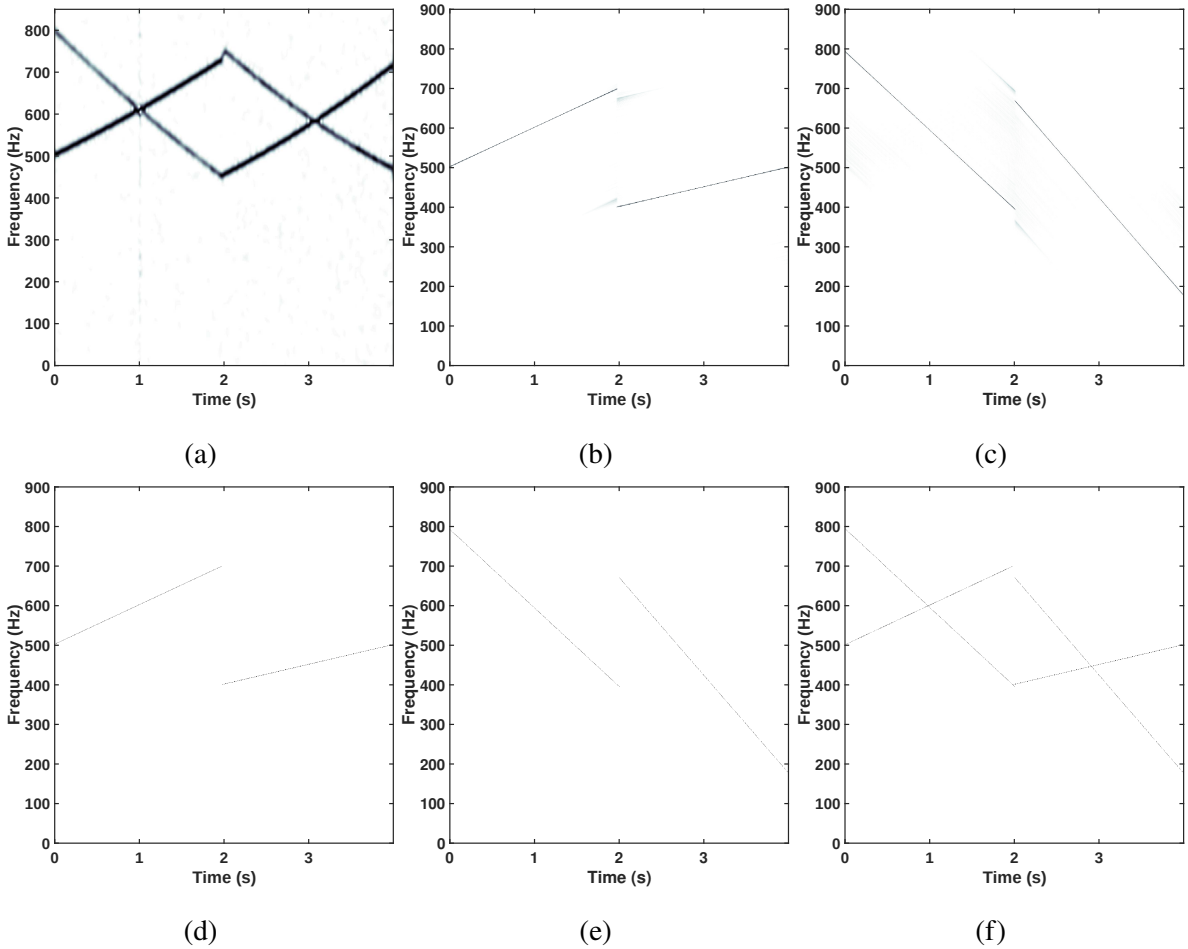

Figure 2.6: Spectrogram view of extraction of mono-component quadratic chirp from multicomponent quadratic chirp (components cross in time-frequency domain) using ck-AGFS algorithm (a) STFT spectrogram (b) AGFS focused on first component (c) AGFS focused on second component (d) Extracted first component (e) Extracted second component (f) AGFS fusion

2.11.1 SNR Gain of AGFS

In [58, 122] a new definition for SNR was introduced, which is transform dependent and relates directly to the bandwidth of the signal:

$$SNR_{3dB}(s(t)) = \frac{\frac{1}{B}\int_B |s(t)|^2 dt}{\sigma_n^2}, \tag{2.152}$$

where $s(t)$ is signal of interest and σ_n^2 is noise corrupting it. B is 3dB bandwidth of signal $s(t)$.

Based on this, an SNR in STGTFT domain can be defined as follows:

$$SNR_{3dB}^{STGTFT}(s(t)) = \frac{\frac{1}{B}\int_B |STGTFT(s(t))|^2 dt}{\sigma_{n,STGTFT}^2}, \tag{2.153}$$

where B is now the 3dB bandwidth of $s(t)$ in the STGTFT domain.

Mean ($3dB$) signal power in STGTFT domain:

Eq. (2.94) was derived for the $|STGTFT|$ for a quadratic signal $x(t)$ given by Eq. (2.66):

$$\left|X^g_{\alpha,\lambda}(t,f)\right| = |A|\frac{\sqrt{\pi|\text{cosec}\alpha|}(\pi\sigma_{t0}^2)^{-\frac{1}{4}}}{\left[\left(\frac{1}{2\sigma_{t0}^2}\right)^2 + \pi^2(a+f_0^2\cot\alpha)^2\right]^{\frac{1}{4}}} exp\left[-\frac{1}{2}\frac{\left(f-(at\sin\alpha + f_d\sin\alpha + f_0^2 tcos\alpha)\right)^2}{\frac{\sin^2\alpha}{\sigma_{t0}^2 4\pi^2} + \sigma_{t0}^2(f_0^2\cos\alpha + a\sin\alpha)^2}\right]. \tag{2.154}$$

$$\therefore \left|X^g_{\alpha,\lambda}(t,f)\right|^2 = \frac{|A|^2\pi|\text{cosec}\alpha|(\pi\sigma_{t0}^2)^{-\frac{1}{2}}}{\left[\left(\frac{1}{2\sigma_{t0}^2}\right)^2 + \pi^2(a+f_0^2\cot\alpha)^2\right]^{\frac{1}{2}}} exp\left[-\frac{\left(f-(at\sin\alpha + f_d\sin\alpha + f_0^2 tcos\alpha)\right)^2}{\frac{\sin^2\alpha}{\sigma_{t0}^2 4\pi^2} + \sigma_{t0}^2(f_0^2\cos\alpha + a\sin\alpha)^2}\right]. \tag{2.155}$$

Therefore, the maximum value of $|ck-STGTFT|^2$ of a signal $x(t)$ is given by:

$$\left|X^g_{\alpha,\lambda}(t,f)\right|^2_{max} = \frac{|A|^2}{\sqrt{\pi}\sqrt{\frac{\sin^2\alpha}{\sigma_{t0}^2 4\pi^2} + \sigma_{t0}^2(f_0^2\cos\alpha + a\sin\alpha)^2}} = \frac{|A|^2}{\sqrt{\pi\sigma_{\alpha 0}^2}}, \tag{2.156}$$

which occurs when $f = f' = at\sin\alpha + f_d\sin\alpha + f_0^2 t\cos\alpha$. Therefore, the $3dB$ $|ck-STGTFT|$ value is half the maximum value which is given by

$$\left|X^g_{\alpha,\lambda}(t,f)\right|^2_{3dB} = \frac{0.5|A|^2}{\sqrt{\pi}\sqrt{\frac{\sin^2\alpha}{\sigma_{t0}^2 4\pi^2} + \sigma_{t0}^2(f_0^2\cos\alpha + a\sin\alpha)^2}} = \frac{0.5|A|^2}{\sqrt{\pi\sigma_{\alpha 0}^2}}. \tag{2.157}$$

The upper and lower bounds of the frequency variable for this $3dB$ $|ck-STGTFT|$ value is given by

$$\underbrace{f' - \sigma_{\alpha 0}\sqrt{ln2}}_{f_1} < f < \underbrace{f' + \sigma_{\alpha 0}\sqrt{ln2}}_{f_2}. \tag{2.158}$$

Hence the mean value of the $|ck-STGTFT|^2$ over this interval is given by

$$\begin{aligned}\left\langle\left|X^g_{\alpha,\lambda}(t,f)\right|^2_{3dB}\right\rangle &= \frac{1}{f_2-f_1}\int_{f_1}^{f_2}\left|X^g_{\alpha,\lambda}(t,f)\right|^2 df,\\ &= \frac{B^2}{2\sigma_{\alpha 0}\sqrt{ln2}}\int_{f_1}^{f_2} exp\left(-\frac{(f-f')^2}{\sigma_{\alpha 0^2}}\right)df,\\ &= \frac{|A|^2}{\sqrt{\pi\sigma_{\alpha 0}^2}}\underbrace{\left(\frac{1}{\sqrt{ln2}}\int_0^{\sqrt{ln2}} e^{-u^2}du\right)}_{\gamma\approx 0.8}.\end{aligned} \tag{2.159}$$

Noise Variance:

STGTFT of Noise, at matched $\lambda = c$:

$$N_{\alpha,\lambda}(t,f) = \int_{-\infty}^{\infty} n(\tau)g(\tau - t)K_{\alpha,\lambda=c}(\tau,f)d\tau. \tag{2.160}$$

Hence Noise Variance in STGTFT:

$$\begin{aligned}
\sigma^2_{n,STGTFT} &= E\left[|N_{\alpha,\lambda}(t,f)|^2\right] = E\left[N_{\alpha,\lambda}(t,f)N^*_{\alpha,\lambda}(t,f)\right], \\
&= E\left[\iint n(\tau_1)g(\tau_1 - t)K_{\alpha,\lambda}(\tau_1,f)n^*(\tau_2)g^*(\tau_2 - t)K^*_{\alpha,\lambda}(\tau_2,f)d\tau_1 d\tau_2\right], \\
&= \iint \underbrace{E\left[n(\tau_1)n^*(\tau_2)\right]}_{R_{nn}(\tau_1,\tau_2)} g(\tau_1 - t)g^*(\tau_2 - t)K_{\alpha,\lambda}(\tau_1,f)K^*_{\alpha,\lambda}(\tau_2,f)d\tau_1 d\tau_2.
\end{aligned}$$

The autocorrelation function $R_{nn}(\tau_1,\tau_2) = \sigma_n^2\delta(\tau_1 - \tau_2)$ in case of white noise:

$$\begin{aligned}
\sigma^2_{n,STGTFT} &= \iint \sigma_n^2\delta(\tau_1 - \tau_2)g(\tau_1 - t)g^*(\tau_2 - t)K_{\alpha,\lambda}(\tau_1,f)K^*_{\alpha,\lambda}(\tau_2,f)d\tau_1 d\tau_2, \\
&= \int_{-\infty}^{\infty} \sigma_n^2\left|g(\tau 1 - t)\right|^2 \underbrace{\left|K_{\alpha,\lambda}(\tau_1,f)\right|^2}_{|\text{cosec}\alpha|} d\tau_1, \\
&= \sigma_n^2|\text{cosec}\alpha| \int_{-\infty}^{\infty} |g(\tau_1 - t)|^2 d\tau_1 = \sigma_n^2 E_w|\text{cosec}\alpha|,
\end{aligned}$$

here, the window energy $E_w = 1$ by design (Eq. (2.67)). Hence, the noise variance in STGTFT domain:

$$\therefore \sigma^2_{n,STGTFT} = \sigma_n^2|\text{cosec}\alpha|. \tag{2.161}$$

SNR gain over cubic-matched ck-STGTFT domain:

Hence, the SNR in cubic matched ck-STGTFT domain is given by

$$\begin{aligned}
SNR^{ck-STGTFT}_{3dB} &= \frac{\left\langle \left|X^g_{\alpha,\lambda}(t,f)\right|^2_{3dB} \right\rangle}{\sigma^2_{n,ck-STGTFT}}. \\
&= \frac{|A|^2\gamma\sin\alpha}{\sqrt{\pi}\sigma_{\alpha 0}\sigma_n^2} = \frac{\gamma\sin\alpha}{\sqrt{\pi}\sigma_{\alpha 0}} \cdot SNR_t,
\end{aligned} \tag{2.162}$$

where $SNR_t = |A|^2/\sigma_n^2$ is the time domain SNR of the signal. Hence, the SNR gain is given by

$$\frac{SNR^{ck-STGTFT}_{3dB}}{SNR_t} = \frac{\gamma\sin\alpha}{\sqrt{\pi}\sigma_{\alpha 0}}. \tag{2.163}$$

This will be maximum for cubic phase matched STFT ($\alpha = 90°$). In case of cubic phase matched STFT, minimum Fourier domain variance $\sigma_{\alpha 0} = \sqrt{\frac{a}{\pi}}$ at optimum time variance $\sigma_{t_0} = \frac{1}{\sqrt{2\pi a}}$ is obtained using Eq. (2.95) , i.e [58] [122]. In this case,

$$max\left(\frac{SNR_{3dB}^{STFT}}{SNR_t}\right) = \frac{\gamma}{\sqrt{a}}. \tag{2.164}$$

Similarly, maximum SNR gain is obtained using Eq. (2.95) for ck-STGTFT/ck-AGFS at $\alpha = \alpha_{opt}$ (Optimal matched angle). In this case,

$$max\left(\frac{SNR_{3dB}^{ck-STGTFT}}{SNR_t}\right) = 2\sqrt{\pi}\sigma_{t_0}\gamma. \tag{2.165}$$

If we consider a half-length ($N/2$) sliding Gaussian window, then we obtain SNR gain of the discrete ck-STGTFT $\approx 0.57 \cdot N_1$, where N_1 is the sampling frequency multiplied by signal duration (T). In general, for a discrete multicomponent case, SNR gain of ck-STGTFT is given by

$$\frac{SNR^{ck-STGTFTdiscrete}}{SNR_t} \approx D_1\frac{N_0}{K}, \tag{2.166}$$

where D_1 is a constant, K is the number of components and N_0 is the number of samples within a window length [58] [122].

2.11.2 GTFT SNR gain analysis

GTFT for a quadratic chirp in unmatched case ($c \neq \lambda$):

Consider GTFT of the quadratic chirp $x(\tau)$ specified in Eqn(2.167) and analyzed using ck-GTFT kernel: $h(\lambda, u) = \pi\lambda u^3$:

$$x(\tau) = Ae^{i\pi c t^3 + i\pi a t^2 + i2\pi f_d t} \tag{2.167}$$

The GTFT of signal $x(t)$ is $X_{\alpha,\lambda}(f)$ and it is defined as follows:

$$\begin{aligned} X_{\alpha,\lambda}(f) &= \int_{-\infty}^{\infty} x(\tau)K_{\alpha,\lambda}(\tau, f)d\tau, \\ &= A\sqrt{1 - i\cot\alpha}\int_{-\infty}^{\infty} exp(i\pi c\tau^3 + i\pi a\tau^2 \\ &+ i2\pi f_d\tau).exp[i\pi t_0^2 f^2\cot\alpha + i\pi f_0^2\tau^2\cot\alpha - i\cdot 2\pi f\tau\mathrm{cosec}\alpha \\ &+ i\pi\lambda t_0^3 f^3 - i\pi\lambda f_0^3\tau^3]d\tau, \\ &= A_0 exp(i\phi_0(f))\int_{-\infty}^{\infty} exp(i\pi c^{'}\tau^3 + i\pi a^{'}\tau^2 + i2\pi f^{'}\tau)d\tau, \end{aligned} \tag{2.168}$$

where,

$$A_0 = A\sqrt{1 - i\cot\alpha},\ \phi_0(f) = \lambda\pi f^3 + \pi t_0^2 f^2 \cot\alpha,$$
$$c' = c - \lambda f_0^3, a' = a + f_0^2 \cot\alpha,\ f' = f_d - f\text{cosec}\alpha.$$

Hence, GTFT magnitude:

$$\left|X_{\alpha,\lambda}(f)\right| = |A_0||e^{i.\phi_0(f)}|\left|\int_{-\infty}^{\infty} exp(i\pi c^{'}\tau^3 + i\pi a^{'}\tau^2 + i2\pi f^{'}\tau)d\tau\right|. \tag{2.169}$$

Consider the integral:

$$\begin{aligned} I_0 &= \int_{-\infty}^{\infty} exp(i\pi c^{'}\tau^3 + i\pi a^{'}\tau^2 + i2\pi f^{'}\tau)d\tau \\ &= \int_{-\infty}^{\infty} f(\tau)e^{i\phi_1(\tau)}d\tau, \end{aligned} \tag{2.170}$$

where,

$$f(\tau) = 1,\ \phi_1(\tau) = \pi c^{'}\tau^3 + \pi a^{'}\tau^2 + 2\pi f^{'}\tau.$$

Since $f(\tau)$ is localized (around 't'), and $\phi_1(t)$ is oscillating, we can use the principle of stationary phase (PSP) to approximate this integral. The "Stationary" points ($\tau_{1,2}$) are obtained from:

$$\begin{aligned} \phi_1^{'}(\tau) &= 3\pi c^{'}\tau^2 + 2\pi a^{'}\tau + 2\pi f^{'} = 0, \\ \implies \tau_{1,2} &= \underbrace{\frac{-a^{'}}{3c^{'}}}_{\alpha_0} \pm \underbrace{\frac{\sqrt{a^{'2} - 6c^{'}f^{'}}}{3c^{'}}}_{\beta_0}. \end{aligned} \tag{2.171}$$

At these points, rate of change of frequency:

$$\begin{aligned} \phi_1^{''}(\tau) &= 6\pi c^{'}\tau + 2\pi a^{'}. \\ \implies \phi_1^{''}(\tau_1) &= 6\pi c^{'}\beta_0, \\ \phi_1^{''}(\tau_2) &= -6\pi c^{'}\beta_0. \end{aligned} \tag{2.172}$$

Therefore stationary approximation of I_0:

$$\begin{aligned} I_0 &\approx \sqrt{\frac{\pi}{3\pi c^{'}\beta_0}}e^{i\phi_1 e^{i\pi/4}(\tau_1)}f(\tau_1) + \sqrt{\frac{-\pi}{3\pi c^{'}\beta_0}}e^{i\phi_1(\tau_2)}e^{i\pi/4}f(\tau_2), \\ &= \sqrt{\frac{1}{3c^{'}\beta_0}}e^{i\pi/4}\left[e^{i\phi_1(\tau_1)}f(\tau_1) + ie^{i\phi_1(\tau_2)}f(\tau_2)\right], \\ &= \sqrt{\frac{1}{3c^{'}\beta_0}}e^{i\pi/4}e^{i\phi_{10}}\left[e^{i\phi_{20}}f(\tau_1) + ie^{-i\phi_{20}}f(\tau_2)\right], \end{aligned} \tag{2.173}$$

where,

$$\begin{aligned}\phi_{10} &= \pi\left[c^{'}(\alpha_0^3 + 3\alpha_0\beta_0^2) + a^{'}(\alpha_0^2 + \beta_0^2) + f^{'}\alpha_0\right],\\ \phi_{20} &= \pi\left[c^{'}(\beta_0^3 + 3\beta_0\alpha_0^2) + 2a^{'}\alpha_0\beta_0 + f^{'}\beta_0\right].\end{aligned} \tag{2.174}$$

Hence,

$$\begin{aligned}|I_0| &\approx \left|\sqrt{\frac{1}{3c^{'}\beta_0}}e^{i\phi_{10}}\left[e^{i\phi_{20}}f(\tau_1) + ie^{-i\phi_{20}}f(\tau_2)\right]\right|,\\ &= \left|\sqrt{\frac{1}{3c^{'}\beta_0}}\left[\cos\phi_{20} + i\sin\phi_{20} + i\cos\phi_{20} + \sin\phi_{20}\right]\right|,\\ &= \left|\sqrt{\frac{2}{3c^{'}\beta_0}}\cos\left(\phi_{20} - \pi/4\right)[i+1]\right|,\\ &= 2\sqrt{\frac{1}{3c^{'}\beta_0}}\cos\left(\phi_{20} - \pi/4\right).\end{aligned} \tag{2.175}$$

Therefore, from Eqns. (2.175) and (2.169), we have:

$$\left|X_{\alpha,\lambda}(f)\right|^2 = 4\frac{|A|^2|\text{cosec}\alpha|}{3c^{'}\beta_0}\cos^2\left(\phi_{20} - \pi/4\right), \tag{2.176}$$

$$\left|X_{\alpha,\lambda}(f)\right|^2 = 4\frac{|A|^2|\text{cosec}\alpha|}{3c^{'}\beta_0}\cos^2\left(\pi\left[c^{'}(\beta_0^3 + 3\beta_0\alpha_0^2) + 2a^{'}\alpha_0\beta_0 + f^{'}\beta_0\right] - \pi/4\right), \tag{2.177}$$

$$\begin{aligned}\left|X_{\alpha,\lambda}(f)\right|^2 \approx\ & \frac{4|A|^2|\text{cosec}\alpha|}{\sqrt{\left(a + f_0^2\cot\alpha\right)^2 - 6\left(c - f_0^3\lambda\right)\left(f_d - f\text{cosec}\alpha\right)}}\\ & \cdot\cos^2\left(\frac{\pi\sqrt{\left(a + f_0^2\cot\alpha\right)^2 - 6\left(c - f_0^3\lambda\right)\left(f_d - f\text{cosec}\alpha\right)}}{27\left(c - f_0^3\lambda\right)^2}\right.\\ & \left.\cdot\left[3\left(c - f_0^3\lambda\right)\left(f_d - f\text{cosec}\alpha\right) - 2\left(a + f_0^2\cot\alpha\right)^2\right] - \frac{\pi}{4}\right).\end{aligned}$$

GTFT SNR gain analysis, matched condition ($c = \lambda$):

Consider a quadratic chirp signal $x(t)$ to be

$$x(\tau) = Ae^{i\pi ct^3 + i\pi at^2 + i2\pi f_d t}.$$

The GTFT of the signal x(t) is denoted by $X_{\alpha,\lambda}(f)$ and is defined as

$$X_{\alpha,\lambda}(f) = \int_{-\infty}^{+\infty} A \cdot exp\big[i\pi(c - f_0^3\lambda)t^3 + i\pi(a + f_0^2.\cot(\alpha))t^2 + i2\pi(f_d - f\mathrm{cosec}(\alpha))t + i\pi t_0^2\cot(\alpha)f^2 + i\pi t_0^3\lambda f^3\big]dt. \tag{2.178}$$

The approximate analytical expression of GTFT magnitude spectrum $|X_{\alpha,\lambda}(f)|^2$ of $x(t)$ using the stationary phase approximation for ($|f_d - f\mathrm{cosec}(\alpha)| >> 0$) for unmatched cubic phase condition is given by

$$\left|X_{\alpha,\lambda}(f)\right|^2 \approx \frac{|A|^2|\mathrm{cosec}\alpha|}{\sqrt{\left(a + f_0^2\cot\alpha\right)^2 - 6\left(c - f_0^3\lambda\right)(f_d - f\mathrm{cosec}\alpha)}} \cdot \cos^2\left(\frac{\pi\sqrt{\left(a + f_0^2\cot\alpha\right)^2 - 6\left(c - f_0^3\lambda\right)(f_d - f\mathrm{cosec}\alpha)}}{27\left(c - f_0^3\lambda\right)^2} \cdot \left[12\left(c - f_0^3\lambda\right)(f_d - f\mathrm{cosec}\alpha) - 2\left(a + f_0^2\cot\alpha\right)^2\right] - \frac{\pi}{4}\right). \tag{2.179}$$

At GTFT matched condition, ($c = f_0^3\lambda$ and $a = -f_0^2\cot(\alpha)$) response is an impulse at $f = f_d\sin(\alpha)$ with area $|A||A_\alpha|$, where $|A_\alpha|$ is the amplitude of GTFT kernel.

SNR gain analysis at GTFT matched condition is derived, considering $x(t)$ corrupted by AWGN $n(t)$ of variance σ_n^2. SNR of the signal $y(t) = x(t) + n(t)$ is given by [114] [61] [142]

$$SNR^{GTFT} = \frac{|\text{Peak signal Power in GTFT domain}|_{\tau=\tau'}}{\text{Variance of Output signal in GTFT domain}_{\tau=\tau'}},$$

where τ' is the instant where the maximum of numerator occurs. In general, GTFT uses the square modulus test, and test statistic can thus be taken as $|GTFT|^2$.

Hence, the GTFT SNR is given by

$$SNR^{GTFT} = \frac{|GTFT_x|^4}{Var[|GTFT_y|^2]}, \tag{2.180}$$

where $|GTFT_x|$ is peak modulus of the signal $x(t)$ in GTFT domain and $|GTFT_y|$ is peak modulus of the signal $y(t)$ in GTFT domain. $Var|GTFT_y|^2$ can be written as

$$Var[|GTFT_y|^2] = E\left[\left|GTFT_y\right|^4\right] - E^2\left[\left|GTFT_y\right|^2\right]. \tag{2.181}$$

Since the signal and noise are uncorrelated and noise is having zero mean,

$$\begin{aligned} E\left[\left|GTFT_y\right|^2\right] &= \iint_{-\infty}^{+\infty} E\left(\left[x(\tau_1)+n(\tau_1)\right]\left[x^*(\tau_2)+n^*(\tau_2)\right]\right) \\ &\qquad \cdot K_{\alpha,\lambda}(\tau_1,f)K^*_{\alpha,\lambda}(\tau_2,f)d\tau_1 d\tau_2. \\ \therefore E\left[\left|GTFT_y\right|^2\right] &= |A|^2|A_\alpha|^2T^2+\sigma_n^2|A_\alpha|^2T. \end{aligned} \tag{2.182}$$

where T is the time duration of $x(t)$. Similarly,

$$\begin{aligned} E\left[\left|GTFT_y\right|^4\right] &= \iiiint_{-\infty}^{+\infty} E\big(\left[x(\tau_1)+n(\tau_1)\right]\left[x(\tau_2)+n(\tau_2)\right]\left[x^*(\tau_3)+n^*(\tau_3)\right] \\ &\qquad \left[x^*(\tau_4)+n^*(\tau_4)\right]\big)K_{\alpha,\lambda}(\tau_1,f)K_{\alpha,\lambda}(\tau_2,f) \\ &\qquad K^*_{\alpha,\lambda}(\tau_3,f)K^*_{\alpha,\lambda}(\tau_4,f)d\tau_1 d\tau_2 d\tau_3 d\tau_4. \\ \therefore E\left[\left|GTFT_y\right|^4\right] &= |A_\alpha|^4\left[|A|^4T^4+2T^2\sigma_n^4+4T^3|A|^2\sigma_n^2\right]. \end{aligned} \tag{2.183}$$

Hence variance is given by

$$Var|GTFT_y|^2 = |A_\alpha|^4\left[\sigma_n^4T^2+2T^3|A|^2\sigma_n^2\right]. \tag{2.184}$$

Therefore GTFT SNR and SNR gain are given by

$$\begin{aligned} SNR^{GTFT} &= \frac{|A_\alpha|^4|A|^4T^4}{|A_\alpha|^4\left[\sigma_n^4T^2+2T^3|A|^2\sigma_n^2\right]} = \frac{T^2SNR_t^2}{2TSNR_t+1}, \\ \therefore \frac{SNR^{GTFT}}{SNR_t} &\approx \frac{T}{2}. \end{aligned} \tag{2.185}$$

where SNR_t is input SNR, defined as A^2/σ_n^2. In discrete case, SNR gain is given by

$$\frac{SNR^{GTFTdiscrete}}{SNR_t} \approx D\frac{N}{K}, \tag{2.186}$$

where D is a constant, K is the number of components and N is the number of samples during signal pulse time T.

2.11.3 SNR gain and mean error analysis simulations

Here a signal $s(t)$ is considered for SNR gain and mean error in parameter estimation under different SNR conditions (Monte Carlo simulation) as

$$s(t) = x_1(t)+x_2(t)+n(t), \tag{2.187}$$

where $n(t)$ is AWGN. $x_1(t)$ and $x_2(t)$ are quadratic chirp signals defined by

$$x_1(t) = e^{i\pi 80t^3+i\pi 40t^2+i\pi 25t}, x_2(t) = e^{i\pi 60t^3+i\pi 100t^2+i\pi 21t}, \text{where } 0 \le t < 1\text{sec}. \tag{2.188}$$

SNR gain simulation:

Monte Carlo simulation for 200 iterations has been performed to compare the SNR gain of ck-AGFS, ck-GTFT, time domain matched filtering, FrAF, and STFT for individual quadratic chirp components $x_1(t)$ and $x_2(t)$. The search range for the quadratic rate is considered to be (79: 0.1: 81) and (59 : 0.1: 61) for the first and second components, respectively. Similarly, the search range of the ck-AGFS angle is considered to be $(-88.1820° : 0.009° : -88.002°)$ and $(-85.329° : 0.009° : -85.149°)$ for the first and second component, respectively. Similarly, the search range of GTFT angle is considered $(-86.2759° : 0.009° : -86.0959°)$ and $(-80.6277° : 0.009° : -80.4477°)$ for first and second component respectively.Similarly, the search range of FrAF angle is considered $(-85.4543° : 0.09° : -83.6543°)$ and $(86.2376° : 0.09° : 88.0376°)$ for first and second component respectively.

As shown in the Fig. 2.7, time domain matched filtering gives the highest SNR in the case of AWGN, and it is equivalent to N_1, where N_1 is the product of the bandwidth and the pulse width. SNR gain of ck-STGTFT is observed to be lower than time domain matched filtering, close to the mathematically derived value ($\approx 0.57N_1$). We observe that ck-STGTFT also has a higher SNR gain compared to the ck-GTFT SNR gain ($\approx 0.5N_1$). STFT can not localize higher order chirp signals, so the SNR gain of STFT is found to be least among all, as shown in both graphs in Fig. 2.7 [122]. A nonlinear time-frequency distribution such as FrAF produces cross-terms during multicomponent signal analysis, so the SNR gain of FrAF is found to be less as compared to SNR gain of ck-GTFT, ck-AGFS in both graphs in Fig. 2.7. Hence, ck-AGFS SNR gain is higher than those of STFT, GTFT, and FrAF for multicomponent quadratic chirp signals.

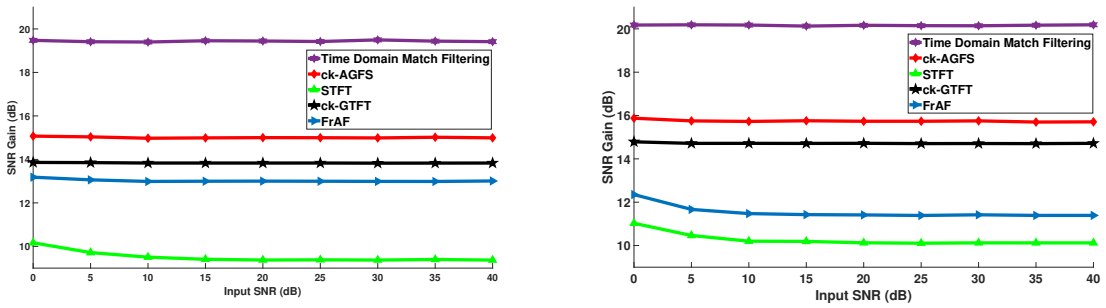

(a) (b)

Figure 2.7: (a) SNR gain comparison of first component (b) SNR gain comparison of second component

Mean error analysis for parameter estimation:

Monte Carlo simulation for 200 iterations has been performed to compare mean errors in estimating quadratic chirp parameters using ck-AGFS, ck-GTFT and FrAF of individual quadratic chirp components $x_1(t)$ and $x_2(t)$ of signal $s(t)$. The search range of quadratic rate, ck-AGFS matched angle, and FrAF matched angle are considered similar to the search range for SNR gain analysis for the first and second components. The GTFT based parameter estimation algorithm is used as given in [93]. Fig. 2.8 shows the mean error in the estimation of first quadratic chirp component $x_1(t)$ parameters, in presence of second quadratic chirp component $x_2(t)$ and AWGN noise $n(t)$. Similarly, Fig. 2.9 shows the mean error in the estimation of second quadratic chirp component $x_2(t)$ parameters in presence of first quadratic chirp component $x_1(t)$ and AWGN noise $n(t)$. GTFT was calculated on the full signal length N, whereas ck-AGFS used an $N/2$ size sliding window over which the estimated parameters were averaged. FrAF produces cross-terms during multicomponent signal analysis, so it gives higher MSE as compared to GTFT and AGFS for estimating parameters of multicomponent chirp. As shown in Fig. 2.8 and Fig. 2.9, ck-AGFS based parameter estimation techniques give less mean error than ck-GTFT and FrAF based parameter estimation techniques for estimating parameters of multicomponent quadratic chirp.

Furthermore, the signal given by Eq. (2.149) is considered to analyze the effect of amplitude modulation in parameter estimation in the presence of noise. It is observed that parameter estimation fails below SNR of 0 dB, and the TFD spreads away from the true instantaneous frequency. Similar claims have also been reported in [131].

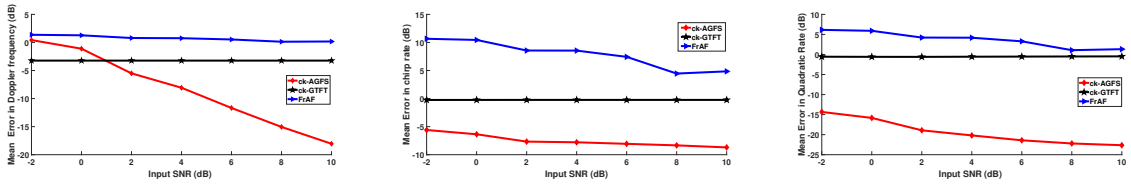

(a) (b) (c)

Figure 2.8: Mean error comparisons for parameters of first component (a) Doppler frequency (b) chirp rate (c) quadratic rate

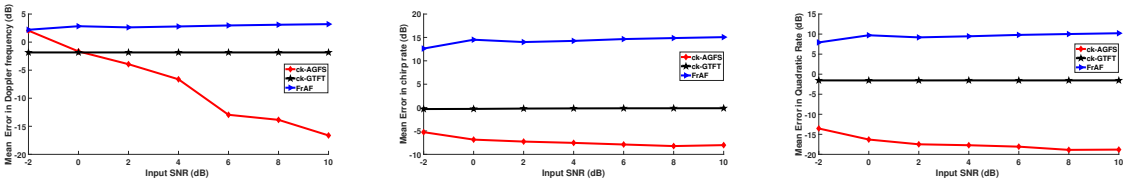

(a) (b) (c)

Figure 2.9: Mean error comparisons for parameters of second component (a) Doppler frequency (b) chirp rate (c) quadratic rate

2.12 TFD of long and short overlapping chirps: locally optimized AGFS

The extraction method in section 2.10 works fine when multiple components of the signal have the same duration, and each component is present at each time instant. If one of the overlapping components is of shorter duration than the other, the optimal parameter search with a single fixed optimal sliding window gives unsatisfactory results in the regions where only one component is present. Similar to the adaptive fractional spectrogram (AFS), the above method also suffers from energy leakage if the signal is absent in certain region [12, pp. 304]. This problem was noted, and a solution was proposed using locally optimized STFrFT [4, 5]. In a similar way, we use locally optimized AGFS to overcome these problems.

In the proposed approach, R numbers of AGFS spectrograms of the signal are constructed with a different choice of parameters (α, λ) and window variance (σ). Let the spectrograms be labelled as $j = 0, 1, 2, ..., R-1$. All these R spectrograms are equally divided into P smaller blocks of the same dimension and let these small blocks in each spectrogram be labeled as $i = 0, 1, 2, ..., P-1$. Energy concentration measure (ECM) is calculated for each block of every spectrogram. Now, ECM of every i^{th} block of R spectrograms is compared, and least ECM valued block's i, and j value is stored, and these least ECM blocks are called optimum blocks. Finally, all optimum blocks are concatenated to make a P blocked locally optimized AGFS (LO-AGFS). In this approach, dividing R spectrograms plays a key role, and it mainly depends on the number and orientation of signal components in the time-frequency plane. LO-AGFS method gives the flexibility to analyze any frequency modulated signals by choosing optimum parameter (α, σ) and $h(\cdot)$ parameter of GTFT kernel in blocked locally optimized AGFS for constructing final AGFS. In the future, a robust way to divide LO-AGFS can be explored.

Here four nearby amplitude quadratic chirp components that are present in different but partially overlapping regions along time are considered. Parameters of different components and mathematical equation of the combined signal are mentioned in Table 2.12 and Eq.(2.190) respectively.

$$x_1(t) = \begin{cases} e^{i\pi c_1 t^3 + i\pi a_1 t^2 + 2i\pi f_{d1}} & 0 \le t < 0.5\text{sec} \\ e^{i\pi c_2 t^3 + i\pi a_2 t^2 + 2i\pi f_{d2}} & 0.5 \le t < 0.75\text{sec} \end{cases},$$
$$x_2(t) = \begin{cases} e^{i\pi c_3 t^3 + i\pi a_3 t^2 + 2i\pi f_{d3}} & 0.5 \le t < 1\text{sec} \\ e^{i\pi c_4 t^3 + i\pi a_4 t^2 + 2i\pi f_{d4}} & 0 \le t < 1\text{sec} \end{cases}, \tag{2.189}$$

$$x(t) = 1.5e^{-0.08t} \cdot x_1(t) + 2e^{-0.04t} \cdot x_2(t). \tag{2.190}$$

Table 2.12: Simulation parameters of four amplitude modulated closely space long and short quadratic chirps

multicomponent long and short chirps parameter						
$\tau\ (s)$	$f_s\ (Hz)$	$c_1\ (Hz^3)$	$c_2\ (Hz^3)$	$c_3\ (Hz^3)$	$c_4\ (Hz^3)$	$a_1\ (Hz^2)$
1	600	140	130	100	80	30
$a_2\ (Hz^2)$	$a_3\ (Hz^2)$	$a_4\ (Hz^2)$	$f_{d1}\ (Hz)$	$f_{d2}\ (Hz)$	$f_{d3}\ (Hz)$	$f_{d4}\ (Hz)$
40	50	60	90	70	66	60

Fig. 2.10 (a-b) shows the locally optimised ck-AGFS and locally optimised STFrFT based spectrogram (considering $\lambda = 0$ or $h(\cdot) = 0$ in GTFT kernel) respectively, obtained as per the above method.Fig. 2.10 (c-d) the time slices of these at 0.61 seconds, and these indicate that locally optimized ck-AGFS can separate the components more distinctly as compared to locally optimized STFrFT based spectrogram, due to the presence of the cubic term in the kernel of ck-GTFT.

2.13 Real multicomponent bat echolocation signal analysis

A real multicomponent bat echolocation signal is analyzed using locally optimized ck-AGFS to demonstrate the effectiveness of AGFS. As shown in Fig. 2.11(a-e), TFDs such as STFT, WVD, EMBD, CKD, and AFS are unable to provide a high concentration TFD of the signal. Similar to [18], four components of the signal are detected with LO-ck-AGFS. Multiple locally

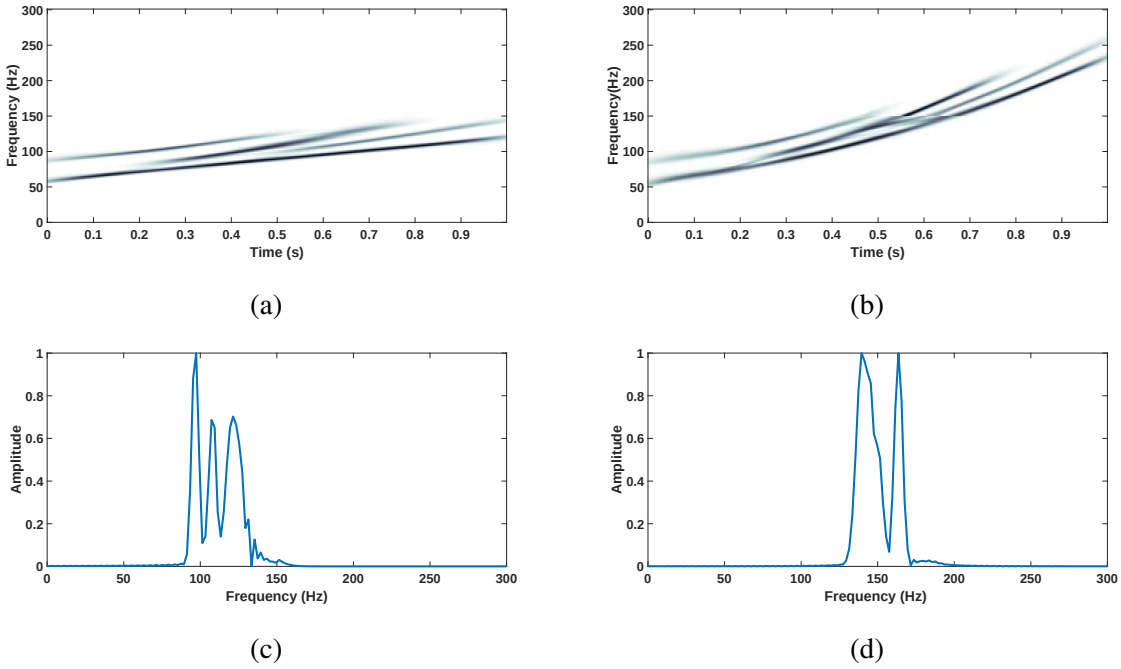

Figure 2.10: Spectrogram view of closely spaced multicomponent long and short chirps (a) Locally optimized ck-AGFS (b) Locally optimized STFrFT (c) time slice of locally optimized ck-AGFS at 0.61 sec. (d) time slice of locally optimized STFrFT at 0.61 sec.

optimized ck-AGFS blocks with locally optimum α,λ, and window variance are concatenated to make final LO-ck-AGFS and detailed method described in section 9. LO-ck-AGFS of bat signal is shown in Fig. 11(f). From the figure, it can be inferred that LO-ck-AGFS is comparatively better than other TFDs to represent multicomponent bat signal.

2.14 AGFS application: AGFS of SAR data

SAR is an imaging radar, which provides high resolution two-dimensional images from the reflectivity of a scene. In conventional SAR signal processing algorithms like range-Doppler algorithm (RDA), 2D matched filtering is performed for focusing SAR image in range and azimuth directions. Range cell migration compensation is performed after range compression to avoid range cell migration over SAR integration time. In case of stationary targets, SAR forms a linear chirp in the azimuth direction due to constant azimuth velocity motion of SAR carrying flight [27]. But in the case of moving targets, SAR forms a quadratic chirp in azimuth direction [45, 82, 128, 129]. The ck-AGFS can be used for the representation of these multicomponent quadratic chirps.

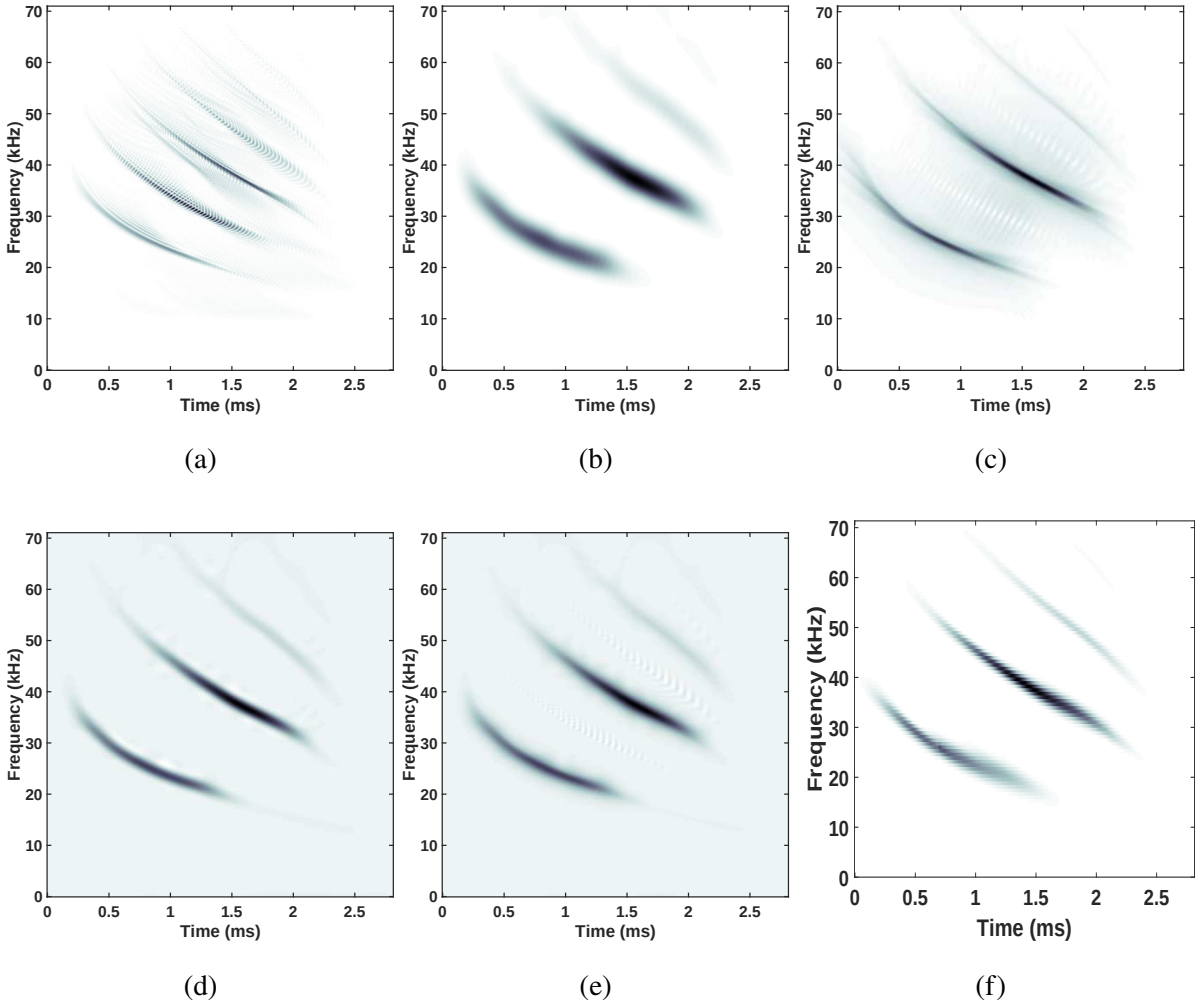

Figure 2.11: Spectrogram view of real bat echolocation signal using different TFDs (a) WVD (b) STFT (c) AFS (d) CKD (e) EMBD (f) LOS ck-AGFS

2.14.1 Comparison of spectrograms of simulated SAR data

SAR data in azimuth direction is represented in the TF plane after range compression and range cell migration compensation. SAR data of 1m resolution cell has been simulated to demonstrate the advantages of using ck-AGFS over conventional STFT based spectrogram. Two nearby ground moving point targets are simulated, which have the same position along range direction but different positions in the azimuth direction. Hence their impulse response in range direction overlap. Both ground moving target have the same centre slant range of 2000 cells, SNR of -10dB, a tangential velocity of 10 m/s, a radial velocity of 20 m/s, a tangential acceleration of 10 m/s^2, and a zero radial acceleration, but are separated in azimuth by 130 azimuth cells. For the simulation, SAR transmitting frequency of 1 GHz, radar waveform bandwidth of 160 MHz, and a SAR platform velocity of 200 m/s was considered.

As shown in Fig. 2.12(a), the STFT based spectrogram at its optimum window is unable to resolve two nearby ground moving targets. Whereas, as shown in Fig. 2.12(b), ck-AGFS at its optimum window, and matched ck-STGTFT can represent each ground moving target separately. Finally, Fig. 2.12(c) shows the focused SAR image of two ground moving point targets after phase correction.

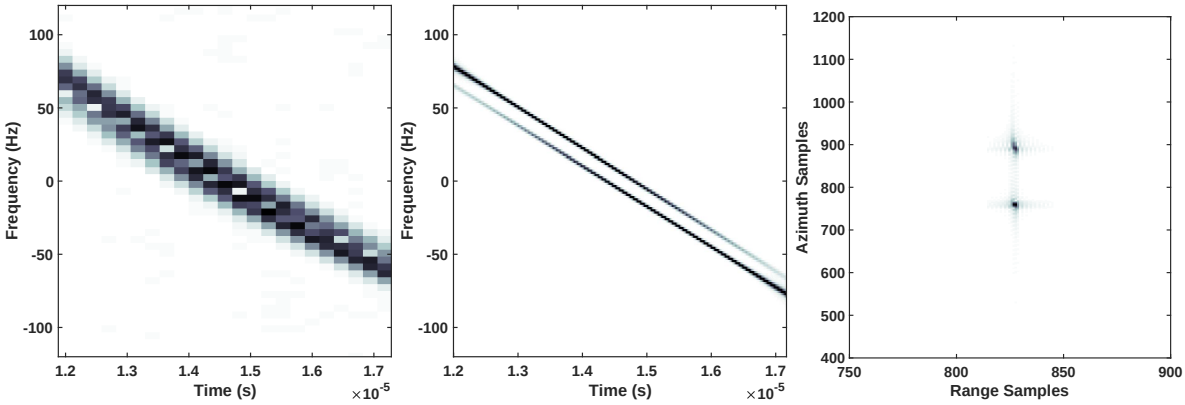

(a) (b) (c)

Figure 2.12: Comparison of spectrogram for simulated ground moving point targets of SAR (a) STFT based spectrogram (b) ck-AGFS (c) Focused SAR image

2.15 Conclusion

In this chapter, novel AGFS based on STGTFT is proposed, which can provide a high concentration, high resolution, cross-term free TFD. This is illustrated by considering two nearby amplitude modulated quadratic chirps whose parameters change in between signal duration. Matched ck-AGFS at optimum window length resolves the components more precisely than STFT and other TFDs. The optimum window length of ck-AGFS can be easily estimated from the signal length at matched ck-STGTFT of ck-AGFS. The uncertainty principle is derived for STGTFT, FrAF, and FrWVD, and TBP of STGTFT for quadratic chirp is shown to be less than the TBP of STFrFT, STFT, and lower bound of TBP of FrAF. The extraction algorithm is demonstrated for signals having two nearby amplitude modulated quadratic chirps whose parameters change during the length, and they indicate better performance of ck-AGFS as compared to the STFT based spectrogram. AGFS can be used to analyze a large variety of multicomponent frequency modulated signals by choosing the appropriate $h(\cdot)$ parameter in GTFT kernel. A mathematical derivation of the SNR gain of ck-AGFS for analyzing multicomponent quadratic

chirps shows that it is higher than those of GTFT,FrAF, and STFT, and the same was corroborated in simulations. ck-AGFS based parameter estimation is demonstrated to be better than GTFT and FrAF based parameter estimation by reporting mean errors in parameter estimation. The superiority of LO-ck-AGFS is demonstrated as compared to locally optimized STFrFT based spectrogram for the representation of closely spaced long and short overlapping chirps. LO-ck-AGFS outperformed other well-known TFDs in representing a real multicomponent bat signal. Local optimum window and global optimum window based STGTFT follows the property of index additivity of angle (similar to FrFT); hence, AGFS is computationally efficient. An application of AGFS to estimate higher polynomial phase components in SAR ground moving target imaging is presented, and it can be applied to similar applications, such as radar, sonar, and biomedical signal processing for representation, extraction, and parameter estimation of multicomponent frequency modulated signals.

In the future, the application of AGFS for SAR ground moving target detection and imaging will be explored further and compared with existing methods. AGFS can be used for the representation of a different variety of signals by appropriate selection of the parametric function $h(\cdot)$ in the GTFT kernel.

Chapter 3

AGFS application: SAR ground moving target detection and imaging

This chapter presents a novel approach for estimation of SAR ground moving target's radial velocity, tangential velocity, and tangential acceleration parameters, and SAR ground moving target imaging (GMTI) using AGFS based method. In this chapter, the third order azimuth phase of SAR is considered non-negligible. In the proposed algorithm, keystone transform, Radon transforms are used for range cell migration corrections(RCMCs), and ck-AGFS is used for parameters estimation of ground moving targets. The superiority of the proposed approach with ck-AGFS is compared with ck-GTFT based parameter estimation approach in terms of MSE, SNR gain, impulse responses, and region of convergence (ROC). Finally, SAR multiple ground moving targets imaging is presented based on ck-AGFS to strengthen the proposed approach.

3.1 Introduction

Conventional SAR is used for taking high-resolution images of static targets. Since it works in the radio frequency range of the electromagnetic spectrum, it can work well despite lack of daylight, cloud coverage, and weather conditions. These properties make it an attractive technology for remote sensing and defense applications.

Traditionally, moving targets have not been imaged using SAR. Separate ground moving target detection mode is present to detect ground moving targets from SAR. Detection of the ground moving targets over SAR images is one of the desirable features for futuristic radar. The presence of ground moving target on the SAR scene produces phase distortion, and it causes

defocusing of SAR image. The blurriness of the image due to the ground moving target can be removed after the detection of the proper moving target phase.

Moving targets have not been imaged using SAR due to the generation of higher polynomial phase components, which in turn cause blurring in the final formed SAR image. Since the late 90's and early 2000s, work has been initiated to extend SAR to moving target imagery, fueled by the availability of better computational resources and the need to image moving objects in defense applications. Perry et al. [82] were among the first authors to propose a method to deal with SAR imaging of moving targets. They used keystone transform for lower order range cell migration compensation and then used a curve fitting method to compensate higher order phase components, which results in deblurring of moving target SAR image. Thereafter many other authors attempted to use higher order Keystone transformations to correct range cell migration, various higher transforms such as Fractional Fourier Transform [38, 121], short time fractional Fourier transform [79, 139], Hough transform [45, 127], Radon transform [129], polynomial Fourier transform [32] , etc. to estimate moving target motion parameters.

Quadratic transform such as Wigner-Ville distribution produces unwanted cross-terms in the presence of multiple moving targets, and these cross-terms corrupt the detection performance and, detection of weak targets near to strong targets become difficult due to these the cross-terms. [101]. Linear transforms such as FrFT and PFT are better than WVD for the detection of multiple moving targets in SAR. In order to detect weak targets near a strong target successive filtering approach ("CLEAN technique") in the FrFT domain can be performed. [38]

Some of the literature considered second-order azimuth phase for SAR ground moving target detection and imaging and focused moving target and estimated its velocity parameters [41, 42, 79, 128, 143].

Some researchers have considered third order phase and third order range migration in ground based detection radar for estimating velocity, acceleration and jerk parameters of maneuvering targets [39, 40, 52, 57, 138].

Some of the literature considered third order phase for SAR ground moving target detection and imaging, but all these sources considered the negligible effect of third order range migration phase. [43–45, 126, 127, 129]. All of the literature considered third order range migration to be negligible in the case of SAR.

3.1.1 Need for the third order range migration

In the previous section, we have seen that many researchers have used imaging algorithms for targets moving with constant velocity and successfully obtained SAR images of the moving target. But what if the target under consideration shows higher order motions? There may be cases when the target, apart from velocity, also has tangential acceleration. Both radial, as well as the tangential acceleration of moving targets, have a serious effect on the estimation of moving target's tangential velocity, and as validated by experimental data and simulation [99]. In that case, apart from the usual first order and second order range migrations, a target begins to show third order range migration also. Similarly, in some of the applications, higher integration time or synthetic aperture time (SAT) and fine resolution are required to obtain a better quality image [143], after which third order range migration becomes dominant. as shown in Eq.(3.8). also, for non-zero squint angle, the third order range migration increases as the squint angle increases. So, compensation of third-order range cell migration (RCM) is necessary before the estimation of moving target parameters can be performed. We propose a new method based on third-order keystone transform for correcting third order and lower order range migrations.

So there is a strong need to detect ground moving targets using SAR data and obtain clean images in SAR in the presence of dominant third order phase. This chapter presents an approach for the detection of radial as well as tangential velocity and acceleration for ground moving targets using time-frequency methods and for obtaining clean images in SAR.

3.2 Preliminaries

3.2.1 Preliminaries: Basic SAR Principles

The SAR is an all-weather imaging radar that achieves fine along-track resolution by taking advantage of platform motion to synthesize a large antenna aperture. SAR is designed for taking high-resolution images of static targets. SAR sends multiple pulses during one observation time to get the ground images, and the single pulse duration is known as pulse repetition time (PRT). Linear chirp is the most common waveform used as a radar waveform during pulse high time of PRT.

In a conventional SAR, an antenna is oriented to look sideways, and it is mounted on a moving platform, generally an aircraft or satellite. The direction of orientation of the radar is

usually called the "range" direction, and the direction of movement of the platform/aircraft is called the "azimuth" direction. Fig.3.1 describes a typical imaging scenario using SAR. The

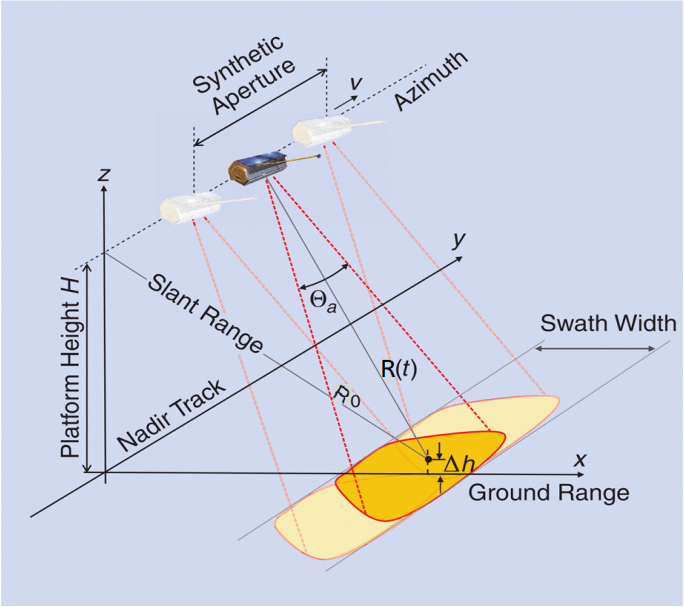

Figure 3.1: SAR Imaging Geometries (Image courtesy: Moreira et al. [70])

aircraft/moving platform carrying the radar is assumed to be moving along direction parallel to the positive y (azimuth) direction with a constant velocity v_a. The ground range direction is taken along positive x direction. It flies at a constant altitude/platform height of H. The system is required to image a point target situated at slant range R_0 from the platform, at time $t_a = 0$, (which is the time of minimum distance between the point target and platform, if the target is assumed to be stationary), as shown. At any azimuth direction time t_a, the slant range of the point target is $R(t_a)$, which can be calculated as:

$$R(t_a) = \sqrt{R_0^2 + v_a^2.t_a^2} \approx R_0 + \frac{(v_a.t_a)^2}{2R_0}. \tag{3.1}$$

The approximation holds if $\frac{v_a.t_a}{R_0} \ll 1$. Here, the azimuth time variable is t_a.

Phase difference $\phi(t_a)$ of the received wave with respect to the transmitted wave is related to the instantaneous range $R(t_a)$ as:

$$\phi(t_a) = \frac{-4\pi R(t_a)}{\lambda} \approx \frac{-4\pi}{\lambda}(R_0 + \frac{(v_a.t_a)^2}{2R_0}), \tag{3.2}$$

where λ is wave length. Here, we note that $R(t_a)$, and hence $\phi(t_a)$ have a parabolic behavior. Also, approximation of Eq.(3.1) is an over simplifying approximation. In Eq.(3.2), quadratic phase $\phi(t_a)$ makes linear frequency modulated signal in the direction of azimuth. Azimuth direction phase can be approximately modeled as linear chirp waveform.

Azimuth direction chirp parameter is unknown, so to calculate azimuth direction chirp rate the following formula shown in Eq. (3.3) is used in conventional SAR signal processing [139]. Azimuth chirp rate K_a is derived for stationary targets assuming SAR azimuth squint angle is zero.

$$K_a = \frac{2}{\lambda}\frac{d^2R(t)}{dt^2}\ |_{t=0} = \frac{2v_a^2}{\lambda.R_0}, \tag{3.3}$$

Where v_a is the mean aircraft velocity and R_0 is minimum slant range of stationary target from aircraft/satellite.

So azimuth direction chirp parameters for static targets in SAR as shown in Eq. (3.3) are calculated based on aircraft velocity, wavelength and height of aircraft from ground.

3.2.2 Preliminaries: Received echo signal model of SAR

After receiving the signals, they are down converted to baseband. SAR received echo signal model can be represented for static target is as follows [27]

$$s(t_r,t_a) = A_0.w_r\left(t_r - \frac{2R(t_a)}{c}\right).w_a(t_a - t_c).rect\left(\frac{t_r - \frac{2R(t_a)}{c}}{\tau}\right).exp\left[j\pi.K_r\left(t_r - \frac{2R(t_a)}{c}\right)^2\right] .exp\left(\frac{-j4\pi.R(t_a)}{\lambda}\right). \tag{3.4}$$

Substituting Eq.(3.1) and Eq.(3.3) in Eq.(3.4)

$$s(t_r,t_a) = A_0.w_r\left(t_r - \frac{2R(t_a)}{c}\right).w_a(t_a - t_c).rect\left(\frac{t_r - \frac{2R(t_a)}{c}}{\tau}\right).exp\left[j\pi.K_r\left(t_r - \frac{2R(t_a)}{c}\right)^2\right] .exp\left(\frac{-j4\pi.R_0}{\lambda}\right).exp\left(-j\pi.K_a.t_a^2)\right), \tag{3.5}$$

where A_0 is complex constant and its depends on radar cross section, attenuation and scattering phase, t_a and t_r are azimuth and range time respectively, τ is pulse width of radar, K_a is azimuth chirp rate, K_r is chirp rate of transmitted LFM waveform, w_r and w_a are range and azimuth beam envelope respectively, t_c is referred as time of zero Doppler (or beam center crossing time) and t_c is defined as follows:

$$t_c = -\frac{R(t_c).\sin(\theta_{r,c})}{v_a}, \tag{3.6}$$

where R(t_c) is slant range at $t_a = t_c$ and $\theta_{r,c}$ is squint angle of beam at beam center crossing time. Squint angle $\theta_{r,c}$ is zero for bore sight operation of SAR and it is non-zero for squint mode of SAR .

3.2.3 Preliminaries: Removal of stationary clutter for moving target detection

In order to detect SAR ground moving target, signal to stationary clutter ratio (SCR) needs to be increased by suppressing stationary clutter. In the case of multi-received channel SAR following techniques are used to suppress stationary clutter.

Multichannel SAR uses displaced phase centered antenna (DPCA) to detect ground moving targets. In DPCA, relative Doppler is zero for static target and non-zero for moving targets, but in a noisy or low SNR environment, DPCA techniques become ineffective to detect moving target parameters in SAR raw as well as processed data. Fractional Fourier transform along with DPCA has been used to detect moving target chirp parameters during a noisy environment as well. Three channel DPCA processing subtracts range compression received echoes from one sub-aperture (channel) to another sub-aperture (channel). Moving target parameters will remain same, and the stationary clutter is removed after DPCA processing. [60]

Along Track Interferometry (ATI) uses two antennae to detect the azimuth phase shift to obtain the position of moving target; both antennae get the same picture at two different times. ATI detected interferometry phase of moving targets is corrupted due to unavoidable stationary clutter, so the image of moving targets gets displaced due to the wrong estimation of ATI phase. To avoid such a problem, DPCA is used for clutter cancellation before ATI processing in three channel receiver. ATI works well when clutter is less. [119]

Space-time adaptive processing uses multiple sets of the signal received from the antenna array and uses joint space and time processing for removing clutter. This approach has the best performance for SAR ground moving target imaging, but it is heavily suffered by computational burden. [127]

In the case of single-received channel SAR, the following techniques are used to suppress stationary clutter.

If a target is unambiguous and present in a clutter-free zone, then a high pass filter can be used to remove stationary clutter. If a target is ambiguous (high-speed target) or if a target

is merged under stationary clutter (very slow-moving target), then a sub-aperture algorithm can be used to detect the moving target. One of the methods of the sub-aperture approach is to divide the whole synthetic aperture into two sub-apertures in the range-Doppler domain and then perform azimuth compression to form two separate sub-aperture images. Then, the clutter can be removed by conjugate multiplication of two sub-aperture images because clutter has the same Doppler history, but moving targets have different Doppler history [128], [127].

3.3 Effect on SAR image due to ground moving targets

Stationary point target SAR image and raw video are simulated in Fig. (3.2) for analyzing the effect of ground moving target on SAR image. Stationary point target is near the perfect formation of the image, with maximum energy concentrated at about one pixel. Simulation parameters are mentioned in Table 3.1.

Table 3.1: SAR system parameters

Pulse Repetition Frequency (PRF)	2301
Carrier frequency(f_c)	8 GHz
Platform Velocity(V_a)	150 m/s
Antenna length(La)	2m
Chirp pulse duration(T_p)	2.5 μs
Signal Bandwidth(B_0)	160MHz

For simulation purpose, a point target with different configurations are considered, as shown in Table 3.2.

The performance of the algorithm is compared with the conventional range-Doppler algorithm. SAR system parameters are shown in Table (3.1). First, a stationary target is compressed with conventional RDA (as mentioned in Section 1.5.3), and then its impulse response in azimuth and range direction is plotted. SAR image of stationary target and its impulse response are shown in Fig. (3.2) and Fig. (3.3) respectively. Three cases are considered to analyze effect of moving target's parameters on SAR image and its impulse reponses. these three cases are mentioned in Table (3.2.)

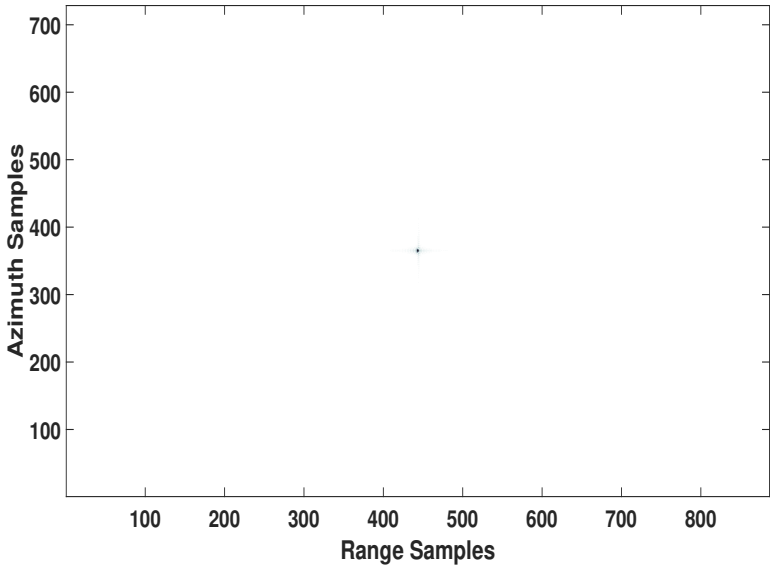

Figure 3.2: Final image in the Range Doppler algorithm for a stationary target in the center of the target space

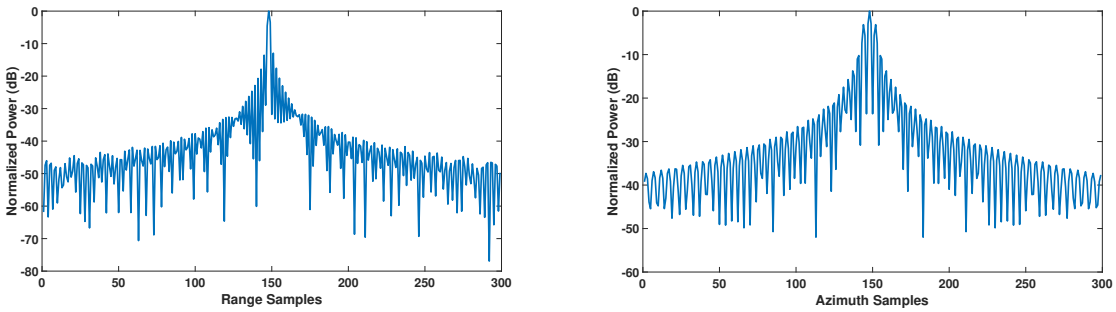

(a) Range impulse response

(b) Azimuth impulse response

Figure 3.3: Range and azimuth impulse response of stationary point target

Table 3.2: Different cases considered for simulation of moving target v_r

Cases	Radial velocity (m/s)	Tangential velocity (m/s)	Tangential acceleration (m/s^2)
case 1	10	0	0
case 2	10	20	0
case 3	10	20	40

The Fig.3.4 is the SAR image of a point target, which is moving with a constant radial velocity of $10m/s$. It is visible that a point target is spread to many cells due to the radial velocity

of the point target. The Fig.3.5(a) is range impulse response of point target with radial velocity $10m/s$. The Fig. 3.5(b) is azimuth impulse response of point target with radial velocity $10m/s$.

As we can see, the point target is not properly focused, and it has spread to many cells. Similarly, the point target spreads after the addition of tangential velocity and radial acceleration, as shown in Fig.3.6 and Fig.3.8. This point target spreads are visible in their corresponding range and azimuth impulse response, as shown in Fig.3.7 and Fig.3.9.

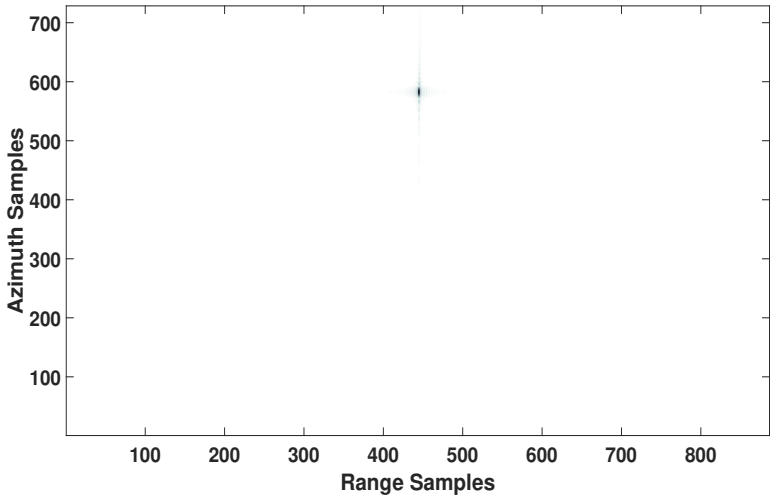

Figure 3.4: Conventional RDA output for point target with radial velocity $10m/s$

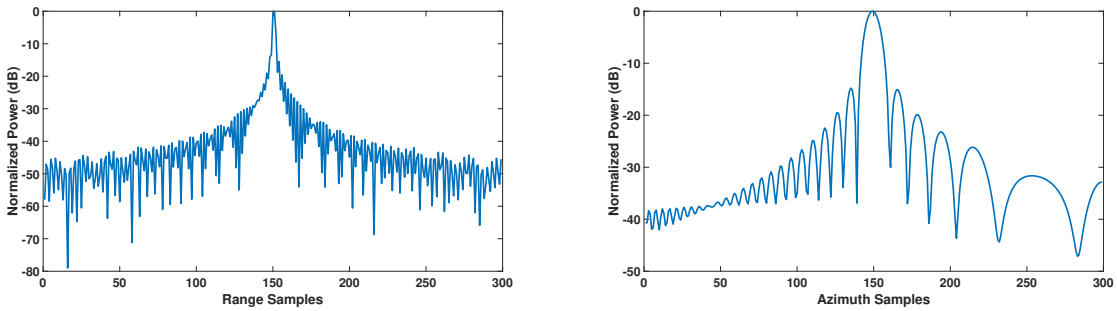

(a) Range Impulse response

(b) Azimuth Impulse response

Figure 3.5: Output of Conventional RDA: Impulse response of point target with radial velocity $10m/s$

Hence, the main questions asked are:

1. How do we form sharp images even in the presence of target velocity and acceleration, given SAR raw data?

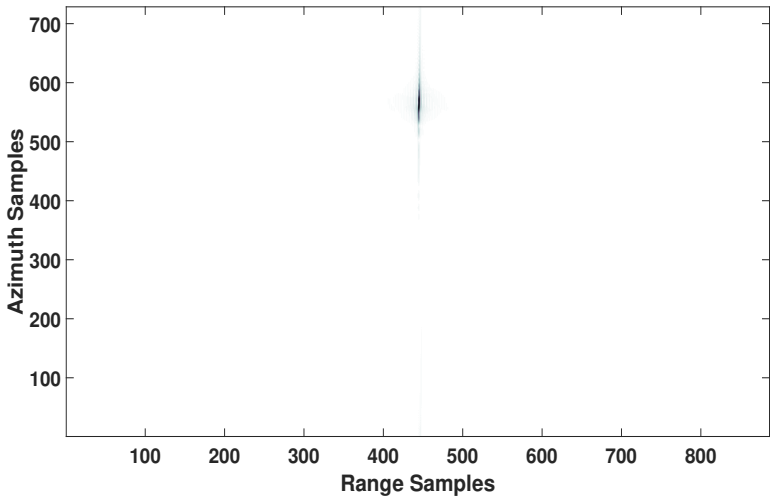

Figure 3.6: Conventional RDA output for point target with radial velocity $10m/s$, and tangential velocity $20m/s$

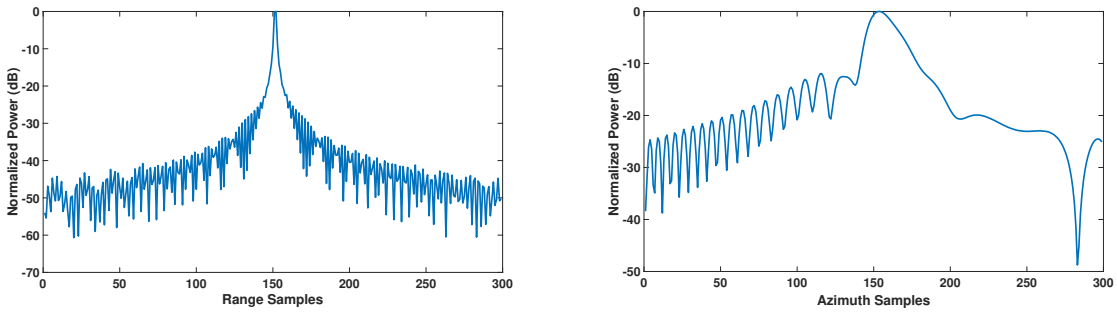

(a) Range Impulse Response

(b) Azimuth Impulse Response

Figure 3.7: Output of conventional RDA: Impulse response of point target with radial velocity $10m/s$, and tangential velocity $20m/s$

2. Can we estimate velocity and acceleration of the moving target given SAR raw data in the process?

3.4 Mathematical derivation of single moving target detection and imaging in SAR

3.4.1 Instantaneous slant range derivation for moving targets in SAR

The echo from the moving target should be analyzed first to detect and estimate the parameters of moving target. The Fig. (3.10), shows the 2D geometry of the moving target in the slant

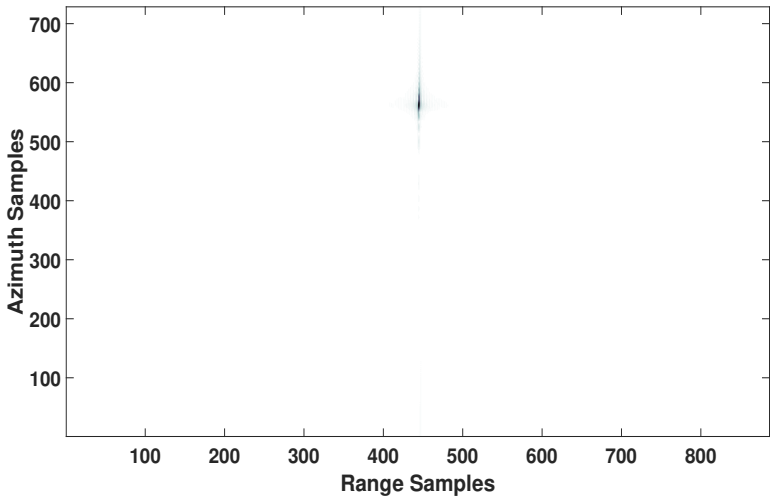

Figure 3.8: Conventional RDA output for point target with radial velocity $10m/s$, tangential velocity $20m/s$, and tangential acceleration $40m/s^2$

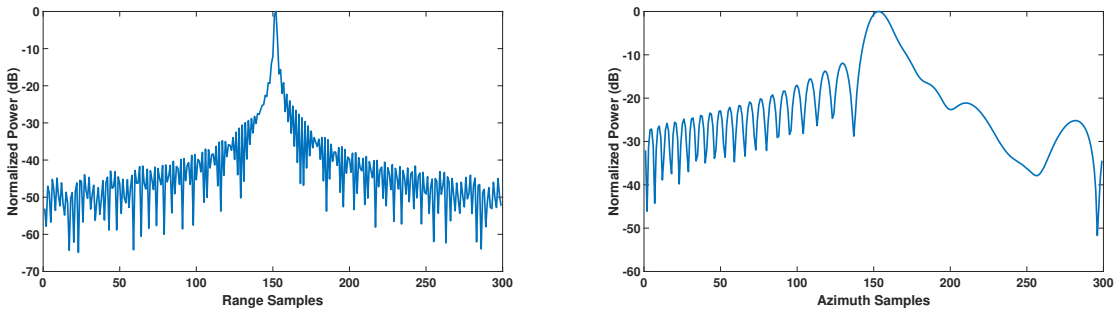

(a) Range Impulse Response

(b) Azimuth Impulse Response

Figure 3.9: Output of conventional RDA: Impulse response of point target with radial velocity $10m/s$, tangential velocity $20m/s$ and tangential acceleration $40m/s^2$

range. R_0 is the reference range at $t_a = 0$ and V_a is the flight velocity, V_r is initial radial velocity, a_r is initial radial acceleration and V_c, a_c are initial tangential velocity and initial tangential acceleration of the target respectively.

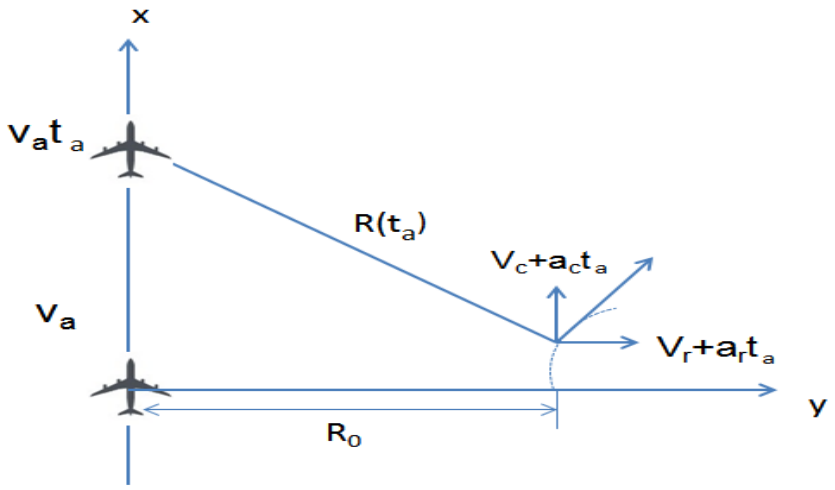

Figure 3.10: The geometric model between target and radar in slant range plane

For side-looking SAR, consider higher order terms in the slant Range $R(t_a)$ as

$$\begin{aligned}
R(t_a) &= \left[(v_a t_a - (v_c t_a + a_c t_a^2/2))^2 + (R_0 + v_r t_a + a_r t_a^2/2)^2\right]^{1/2}, \\
R(t_a) &\approx R(t_a)\big|_{t_a=0} + \frac{dR(t_a)}{dt_a}\big|_{t_a=0} t_a + \frac{d^2R(t_a)}{dt_a^2}\big|_{t_a=0} t_a^2/2! + \frac{d^3R(t_a)}{dt^3}\big|_{t_a=0} t_a^3/3! \\
&\quad + \frac{d^4R(t_a)}{dt_a^4}\big|_{t_a=0} t_a^4/4!, \\
&= R_0 + v_r t_a + \left[\frac{v_a^2 + v_c^2 + R_0 a_r - 2v_a v_c}{2R_0}\right] t_a^2 + \frac{(v_c - v_a)}{2R_0}\left[a_c - \frac{v_r(v_c - v_a)}{R_0}\right] t_a^3 \\
&\quad + \frac{1}{8R_0^3}\left[(v_c - v_a)^2(4v_r^2 - 2R_0 a_r) - 4R_0 a_c(v_c - v_a)v_r - (v_c - v_a)^4 + R_0^2 a_c^2\right] t_a^4.
\end{aligned} \tag{3.7}$$

3.4.2 Mathematical equation for range migration

Using Eq.(3.7), we can find the expression for total range migration of a moving target. Total range migration can be calculated as difference between target range at the end of aperture time and the target closest range. The total range migration can be determined as follows:

θ_r denotes the squint angle and $\theta_{r,c}$ is the value of squint angle at the beam center crossing time t_c, $R(t_c)$ denotes the instantaneous slant range from aircraft to beam center .

$$\begin{aligned}
R(t_a) &= \left[(v_a t_a - (v_c t_a + a_c t_a^2/2))^2 + (R_0 + v_r t_a + a_r t_a^2/2)^2\right]^{1/2}, \\
R(t_a) &\approx R(t_a)\big|_{t_a=t_c} + \frac{dR(t_a)}{dt_a}\big|_{t_a=t_c} \cdot (t_a - t_c) + \frac{d^2R(t_a)}{dt_a^2}\big|_{t_a=t_c} \cdot (t_a - t_c)^2/2! \\
&\quad + \frac{d^3R(t_a)}{dt^3}\big|_{t_a=t_c} \cdot (t_a - t_c)^3/3!,
\end{aligned}$$

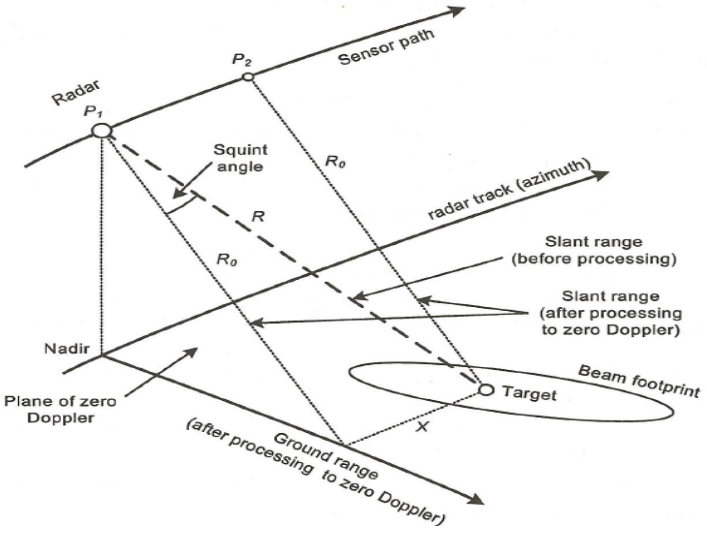

Figure 3.11: The geometric model between target and radar (Image courtesy: Cumming et al. [27])

$$\begin{aligned}\implies R(t_a) \approx R(t_c) + \left[\cos\theta_{r,c}(v_r + a_r t_c) + \sin\theta_{r,c}(v_a - v_c - a_c t_c)\right].(t_a - t_c) + \Big[\big[\sin\theta_{r,c} \\ \cdot(v_r + a_r t_c) - \cos\theta_{r,c}(v_a - v_c - a_c t_c)\big]^2 + R(t_c)(\cos\theta_{r,c}.a_r - \sin\theta_{r,c}a_c)\Big] \\ \cdot\frac{(t_a - t_c)^2}{2R(t_c)} + \Bigg[\frac{-3}{R^2(t_c)}\Big[\big[\sin\theta_{r,c}(v_r + a_r t_c) - \cos\theta_{r,c}(v_a - v_c - a_c t_c)\big]^2 \\ \cdot\big[\cos\theta_{r,c}(v_r + a_r t_c) + \sin\theta_{r,c}(v_a - v_c - a_c t_c)\big]\Big] + \frac{3(a_r.\sin\theta_{r,c} + a_c.\cos\theta_{r,c})}{R(t_c)} \\ \cdot\left[\sin\theta_{r,c}(v_r + a_r t_c) - \cos\theta_{r,c}(v_a - v_c - a_c t_c)\right]\Bigg]\frac{(t_a - t_c)^3}{6}.\end{aligned}$$

where $\cos\theta_{r,c} = \frac{R_0 + v_r t_c + a_r t_c^2/2}{R(t_c)}$, $\sin\theta_{r,c} = \frac{(v_a t_c - (v_c t_c + a_c t_c^2/2))}{R(t_c)}$ and t_c is the "beam center crossing time" of SAR referenced to the time of zero Doppler frequency and $t_c = \frac{-R(t_c)\cdot\sin\theta_{r,c}}{v_a}$.

Then the total range migration δR is given by

$$\delta R = R\left(\frac{T_a}{2} + t_c\right) - R(t_c),$$

where T_a is the total aperture time which varies inversely as $\cos\theta_{r,c}$ and is given by

$$T_a = \frac{0.886\lambda R(t_c)}{L_a v_a \cos\theta_{r,c}},$$

where $\frac{0.886\lambda}{L_a}$ is the azimuth beam-width, so therefore $\frac{0.886\lambda R(t_c)}{L_a}$ represents the projection of this beam-width on the ground.

The total range migration for a non-zero squint angle is given by the expression

$$\begin{aligned}\delta R = &\left[\cos\theta_{r,c}(v_r + a_r t_c) + \sin\theta_{r,c}(v_a - v_c - a_c t_c)\right].\frac{0.443\lambda R(t_c)}{L_a v_a cos\theta_{r,c}} + \left[[\sin\theta_{r,c}(v_r + a_r t_c)\right.\\ &\left.-\cos\theta_{r,c}(v_a - v_c - a_c t_c)]^2 + R(t_c)(\cos\theta_{r,c}.a_r - \sin\theta_{r,c}.a_c)\right].\frac{0.443^2\lambda^2 R(t_c)}{2L_a^2 v_a^2\cdot\cos^2\theta_{r,c}}\\ &+\left[\frac{-1}{R^2(t_c)}\left([\sin\theta_{r,c}(v_r + a_r t_c) - \cos\theta_{r,c}(v_a - v_c - a_c t_c)]^2.[\cos\theta_{r,c}(v_r + a_r t_c)\right.\right.\\ &\left.\left.+\sin\theta_{r,c}(v_a - v_c - a_c t_c)]\right) + \frac{(a_r.\sin\theta_{r,c} + a_c.\cos\theta_{r,c})}{R(t_c)}\left(\sin\theta_{r,c}(v_r + a_r t_c)\right.\right.\\ &\left.\left.-\cos\theta_{r,c}(v_a - v_c - a_c t_c)\right)\right].\frac{0.443^3\lambda^3 R^3(t_c)}{2L_a^3 v_a^3\cdot\cos^3\theta_{r,c}}.\end{aligned} \tag{3.8}$$

If squint angle $\theta_{r,c}$ is zero, then $t_c = 0 \implies \sin\theta_{r,c} = 0, \cos\theta_{r,c} = 1$ and $R(t_c) = R_0$. Therefore, range migration given in Eq. (3.8) is reduces to

$$\implies \delta R = v_r\frac{T_a}{2} + \left[\frac{a_r}{2} + \frac{(v_c - v_a)^2}{2R_0}\right]\frac{T_a^2}{4} + \frac{(v_c - v_a)}{2R_0}\left[a_c - v_r\frac{(v_c - v_a)}{R_0}\right]\frac{T_a^3}{8}. \tag{3.9}$$

As shown in Eq. (3.8) and Eq. (3.9), the third order range migration increases with an increase in squint angle and increase in synthetic aperture time.

3.4.3 Received signal model for single moving target

As shown in Eq. (3.4), received signal can be modeled as

$$\begin{aligned}s(t_r, t_a) = A_0.w_a(t_a - t_c).w_r\left(t_r - \frac{2R(t_a)}{c}\right).exp\left[i\pi.K_r\left(t_r - \frac{2R(t_a)}{c}\right)^2\right]\\ .exp\left(\frac{-i4\pi.R(t_a)}{\lambda}\right),\end{aligned} \tag{3.10}$$

where $w_r(t_r) = rect\left[\frac{\tau}{PRT}\right]$, τ is pulse on time of PRT, $w_a(t_a)$ is azimuth aperture. [27]

Substituting $R(t_a)$ from Eq. (3.7) in Eq. (3.10), we limit our derivation till third order of slant range $R(t_a)$ of Eq. (3.7). So after substitution, we obtain SAR received signal modeled for

moving target

$$s(t_r,t_a) = A_0.\overbrace{w_a(t_a - t_c)}^{\text{Delayed azimuth envelope}} \overbrace{.w_r\left(t_r - \frac{2R(t_a)}{c}\right).exp\left[i\pi.K_r\left(t_r - \frac{2R(t_a)}{c}\right)^2\right]}^{\text{Delayed transmitted chirp}}$$
$$.exp\left(\frac{-i4\pi.}{\lambda}\left[R_0 + \underbrace{v_r t_a}_{\text{Doppler shift}} + \underbrace{\frac{v_a^2 + v_c^2 + R_0 a_r - 2v_a v_c}{2R_0}t_a^2}_{\text{Azimuth chirp rate}} + \underbrace{\frac{(v_c - v_a)}{2R_0}[a_c - \frac{v_r(v_c - v_a)}{R_0}]t_a^3}_{\text{Azimuth quadratic rate}}\right]\right). \tag{3.11}$$

After conjugate multiplication with transmitted radar waveform or range reference function in the range frequency-azimuth time domain, received signal in Eq. (3.11) in range, frequency-azimuth time domain can be written as:

$$\begin{aligned} S(f_r,t_a) = A_0.w_a(t_a - t_c).P(f_r)exp[-i\frac{4\pi}{c}(f_r + f_c)R_0] \cdot \overbrace{exp[-i\frac{4\pi}{c}(f_r + f_c)v_r t_a]}^{\text{Range walk migration}} \\ \underbrace{\cdot exp\left[-i\frac{4\pi}{c}(f_r + f_c)\left[\frac{v_a^2 + v_c^2 + R_0 a_r - 2v_a v_c}{2R_0}\right]t_a^2\right]}_{\text{Range Cell Migration}} \\ \underbrace{\cdot exp\left[-i\frac{4\pi}{c}(f_r + f_c)\frac{(v_c - v_a)}{2R_0}\left(a_c - \frac{v_r(v_c - v_a)}{R_0}\right)t_a^3\right]}_{\text{Third order range cell migration}}, \end{aligned} \tag{3.12}$$

where f_r is range frequency, and $P(t_r) = w_r(t_r).exp\left[i\pi.K_r.t_r^2\right]$.

From the above Eq. (3.12), we see that there is coupling between range frequency and azimuth time in second, third, and fourth exponential terms. Coupling between range frequency and first-order azimuth time leads to range walk migration (RWM). Coupling between range frequency and second-order azimuth time leads to range curve migration (RCM). Similarly, the coupling between range frequency and third order azimuth time leads to third order range migration.

3.5 SAR imaging of single moving targets: Phase errors

So far, the ideal scenario has been discussed, where:

1. aircraft travels at a constant velocity along a single direction.

2. Aircraft velocity, wavelength, and height are used to calculate azimuth direction chirp parameters, and we assume that these are available to us with zero error.

3. We assume SAR carrying aircraft is stable during radar operation.

However, in a real scenario, one or more of these assumptions will not hold. These will manifest as adverse effects on the final processed SAR image, in the form of blurring, noise, etc.

Any moving target will have velocity and acceleration, which have the along-track (tangential) component and across-track (radial) component. Effects of these will result in higher order terms in the expansion of Eq.(3.7) and hence the polynomial phase components in Eq.(3.7). In Eq.(3.7), coefficient of t is related to Doppler shift and range walk, which dislocate ground moving target from its true position, whereas the coefficient of t^2 is related to RCM, the latter of which is responsible for broadening of main lobe or reduction of azimuth resolution. Third order azimuth phase is responsible for asymmetric side lobes, and fourth order azimuth phase is responsible for raising side lobes [127]. Fig. 3.4, Fig. 3.6, and Fig. 3.8, show the effects of various velocities, accelerations, and higher components in SAR image formation. To get a

Source of Error		Image Misregistration	Image Shift	Azimuth Defocus	Range Defocus	Range Walk	Azimuth Walk	Image Main Lobe loss	Image Sidelobe Increase
Platform									
Along-track	x	×							
	$\dot{x}$			×				×	×
	$\ddot{x}$			×			×	×	×
	higher derivatives			×			×	×	×
Altitude	H	×							
	$\dot{H}$		×			×			
	$\ddot{H}$			×	×			×	×
	higher derivatives			×	×			×	×
Cross-track	y	×							
	$\dot{y}$		×			×			
	$\ddot{y}$			×	×			×	×
	higher derivatives			×	×			×	×
Target									
Range	R	×							
	$\dot{R}$		×			×			
	$\ddot{R}$			×	×			×	×
	higher derivatives			×	×			×	×
Along track	x	×							
	$\dot{x}$			×				×	×
	$\ddot{x}$			×			×	×	×
	higher derivatives			×			×	×	×
Propagation Path									
	phase jitter			×	×			×	×
Electronic Stability									
	phase jitter			×	×			×	×

Figure 3.12: Table showing effects of various phase errors (Image courtesy: K. Tomiyasu [117])

"clean" SAR image, it is imperative to estimate velocity and acceleration components accurately first and then incorporate the information into the matched filtering processes.

3.6 Target exhibits large constant velocities

If the velocity v_r is large, such that:

$$\frac{2v_r}{\lambda_c} \geq \frac{PRF}{2}. \tag{3.13}$$

that is the Doppler frequency shift, which is more than half the PRF of the radar, then the phenomenon of "Doppler Ambiguity" occurs, which results in fold over of the frequency response due to aliasing. Such a velocity that induces this Doppler ambiguity can be modeled as [45]:

$$v_r = v_{r0,est} + \frac{M_{amb}\lambda_c PRF}{2}, \tag{3.14}$$

where, v_{r0} is the base velocity observed using the limited PRF system, M_{amb} defined as the ambiguity number is the number of times the fold-over happens. The fold over factor can be defined as:

$$M_{amb} = \frac{f_{h,actual} - f_{h,obs}}{F_s}, \tag{3.15}$$

where $f_{h,actual}$ and $f_{h,obs}$ are the actual highest frequency and the highest frequency observed in the limited sampling frequency region and F_s is the rate of sampling required as per band-pass theorem.

3.7 Radon transform

Radon transform is widely used for detection of the straight line of arbitrary orientation in any image. Application of Radon transform for the estimation of target velocity is given as follows [129],

$$v_{r0,est} = -\frac{\tan\theta * PRF * c}{2F_s}, \tag{3.16}$$

where $v_{r0,est}$ is the estimated base velocity observed using the limited PRF system, c is velocity of light and F_s is range sampling frequency of SAR.

3.8 Proposed algorithm for imaging ground moving targets with accelerated motion

A moving target with non-zero tangential acceleration a_c(considering $a_r = 0$) is considered. The range compressed received base-band signal in range frequency-azimuth time domain in

Eq. (3.11) can be written as

$$\begin{aligned} S(f_r,t_a) =& A_0.w_a(t_a-t_c).P(f_r).exp[-i\frac{4\pi}{c}(f_r+f_c)R_0]\cdot exp[-i\frac{4\pi}{c}(f_r+f_c)v_r t_a] \\ &\cdot exp\left[-i\frac{4\pi}{c}(f_r+f_c)\left[\frac{v_a^2+v_c^2-2v_a v_c}{2R_0}\right]t_a^2\right] \\ &\cdot exp\left[-i\frac{4\pi}{c}(f_r+f_c)\frac{(v_c-v_a)}{2R_0}\left(a_c-\frac{v_r(v_c-v_a)}{R_0}\right)t_a^3\right]. \end{aligned} \tag{3.17}$$

If ambiguity is present then, $v_r = v_{r0,est} + \frac{M_{amb}PRF\lambda_c}{2}$ [45].

So the received signal in Eq.(3.12) in range frequency-azimuth time domain can be modified as

$$\begin{aligned} S(f_r,t_a) =& A_0.w_a(t_a-t_c).P(f_r).exp[-i\frac{4\pi}{c}(f_r+f_c)R_0]\cdot exp[-i\frac{4\pi}{c}(f_r+f_c)v_{r0,est}t_a] \\ &\cdot exp[-i\frac{4\pi}{c}(f_r+f_c)\frac{M_{amb}\cdot PRF\lambda_c}{2}t_a]exp\left[-i\frac{4\pi}{c}(f_r+f_c)\left[\frac{v_a^2+v_c^2-2v_a v_c}{2R_0}\right]t_a^2\right]\cdot \\ &\cdot exp\left[-i\frac{4\pi}{c}(f_r+f_c)\frac{(v_c-v_a)}{2R_0}\left(a_c-\frac{v_{r0,est}(v_c-v_a)}{R_0}\right)t_a^3\right]\cdot \\ &\cdot exp\left[-i\frac{4\pi}{c}(f_r+f_c)\frac{(v_c-v_a)^2}{2R_0}\frac{M_{amb}\cdot PRF\lambda_c}{2}t_a^3\right]. \end{aligned} \tag{3.18}$$

Coefficient of t^3 in Eq.(3.18) causes third order range migration, which is significant and must be compensated in order to get a focused image. The third order Keystone transform is defined by:

$$t_a = \left(\frac{f_c}{f_r+f_c}\right)^{\frac{1}{3}}t_n. \tag{3.19}$$

After application of third order Keystone transform, Eq.(3.18) can be expressed as,

$$\begin{aligned} S(f_r,t_n) =& A_0.W_a(t_n-t_c').P(f_r)exp\left[-i\frac{4\pi}{c}(f_r+f_c)R_0\right] \\ &\cdot exp\left[-i\frac{4\pi}{c}(f_r+f_c)^{\frac{2}{3}}f_c^{\frac{1}{3}}v_{r0,est}t_n\right]\cdot exp[-i\frac{4\pi}{c}(f_r+f_c)^{\frac{2}{3}}f_c^{\frac{1}{3}}\frac{M_{amb}\cdot PRF\lambda_c}{2}t_n] \\ &\cdot exp\left[-i\frac{4\pi}{c}(f_r+f_c)^{\frac{1}{3}}f_c^{\frac{2}{3}}\frac{(v_a-v_c)^2}{2R_0}t_n^2\right]\cdot exp\left[-i\frac{4\pi}{c}f_c\frac{(v_c-v_a)^2}{2R_0}\frac{M_{amb}\cdot PRF\lambda_c}{2}t_n^3\right] \\ &\cdot exp\left[-i\frac{4\pi}{c}f_c\frac{(v_a-v_c)}{R_0}\left(a_c-\frac{v_{r0,est}(v_c-v_a)}{R_0}\right)t_n^3\right], \end{aligned} \tag{3.20}$$

where $N = \left(\frac{f_r+f_c}{f_c}\right)^{\frac{1}{3}}$ and $t_c' = N.t_c$.

The third order coupling in the fourth exponential term has been removed, range migration of first order has become $\frac{2}{3}$ of previous coupling and range migration of second order has become

$\frac{1}{3}$ of the previous coupling. Now, multiplying with the correction term H_c in order to remove second order coupling/range migration.

$$H_c(f_r, t_n) = exp\left[i\frac{4\pi}{c}\frac{f_r}{3}\frac{v_a^2}{2R_0}t_n^2\right]. \tag{3.21}$$

After multiplication of Eq.(3.20) and Eq.(3.21), assuming $\frac{f_r}{f_c} << 1$, the third exponential term ϕ_n of Eq.(3.20) can be rewritten as:

$$\begin{aligned} \phi_n &= exp\left[-i\frac{4\pi}{c}\frac{f_c}{2R_0}t_n^2\left((v_a - v_c)^2\left(1 + \frac{f_r}{3f_c}\right) - \frac{f_r v_{a^2}}{3f_c}\right)\right], \\ \implies \phi_n &= exp\left[-i\frac{4\pi}{c}\frac{f_c}{2R_0}(v_a - v_c)^2 t_n^2\right].exp\left[-i\frac{4\pi}{c}\frac{f_c}{2R_0}\left(v_c^2 - 2v_a v_c\right)\frac{f_r}{3f_c}t_n^2\right]. \end{aligned} \tag{3.22}$$

For typical values of SAR carrying aircraft ($v_a = 200m/s, v_c = 20m/s, f_c = 3GHz$), the second exponential term in the above Eq.(3.22) become negligible and can be neglected in comparison to the first exponential term.

$$\phi_n \approx exp\left[-i\frac{4\pi}{c}\frac{f_c}{2R_0}(v_a - v_c)^2 t_n^2\right]. \tag{3.23}$$

Substituting the approximated value of ϕ_n in Eq.(3.20),

$$\begin{aligned} S_1(f_r, t_n) = A_0 \cdot W_a(t_n - t_c') \cdot P(f_r) \cdot exp\left[-i\frac{4\pi}{c}(f_r + f_c)R_0\right] \\ \cdot exp\left[-i\frac{4\pi}{c}\frac{f_c}{2R_0}(v_a - v_c)^2 t_n^2\right] \cdot exp\left[-i\frac{4\pi}{c}(f_r + f_c)^{\frac{2}{3}} f_c^{\frac{1}{3}}\frac{M_{amb} \cdot PRF\lambda_c}{2}t_n\right] \\ \cdot exp\left[-i\frac{4\pi}{c}(f_r + f_c)^{\frac{2}{3}} f_c^{\frac{1}{3}} v_{r0,est} t_n\right] exp\left[-i\frac{4\pi}{c}f_c\frac{(v_a - v_c)}{2R_0}\left(a_c - \frac{v_{r0,est}(v_c - v_a)}{R_0}\right)t_n^3\right] \\ \cdot exp\left[-i\frac{4\pi}{c}f_c\frac{(v_c - v_a)^2}{2R_0}\frac{M_{amb} \cdot PRF\lambda_c}{2}t_n^3\right]. \end{aligned} \tag{3.24}$$

$$\begin{aligned} S_2(f_r, t_n) = A_0.W_a(t_n - t_c').P(f_r).exp[-i\frac{4\pi}{c}(f_r + f_c)R_0] \\ \overbrace{exp[-i\frac{4\pi}{c}(f_r + f_c)^{\frac{2}{3}} f_c^{\frac{1}{3}}\frac{M_{amb} \cdot PRF\lambda_c}{2}t_n]}^{\text{Compensated ambiguity using iteration}} \cdot \overbrace{exp[-i\frac{4\pi}{c}(f_r + f_c)^{\frac{2}{3}} f_c^{\frac{1}{3}} v_{r0,est} t_n]}^{\text{Compensated using Radon estimated velocity}} \\ \underbrace{exp[-i\frac{4\pi}{c}\frac{f_c}{2R_0}(v_a - v_c)^2 t_n^2]}_{\text{Compensated using ck-AGFS estimated chirprate}} . \underbrace{exp[-i\frac{4\pi}{c}f_c\frac{(v_a - v_c)}{2R_0}\left[a_c - \frac{v_r(v_c - v_a)}{R_0}\right]t_n^3]}_{\text{Compensated using ck-AGFS estimated quadratic-rate}}. \end{aligned} \tag{3.25}$$

From the above Eq. (3.25), it is observed that the second and third order migration have been corrected. Subsequently, the first order range migration can be corrected by using Radon transform.

A correction function (H_c) is constructed based on the estimated value of $v_{r0,est}$. Similarly, ambiguity can be corrected using an iterative method.

$$H_c(f_r,t_n) = exp\left[i\frac{4\pi}{c}(f_r+f_c)^{\frac{2}{3}}f_c^{\frac{1}{3}}v_{r0,est}t_n\right].exp\left[i\frac{4\pi}{c}(f_r+f_c)^{\frac{2}{3}}f_c^{\frac{1}{3}}\frac{M_{amb}\cdot PRF\lambda_c}{2}t_n\right]. \quad (3.26)$$

After multiplication of Eq.(3.26) with Eq.(3.25),

$$S_3(f_r,t_n) = A_0.W_a(t_n-t_c').P(f_r).exp\left[-i\frac{4\pi}{c}(f_r+f_c)R_0\right].exp\left[-i\frac{4\pi}{c}\frac{f_c}{2R_0}(v_a-v_c)^2t_n^2\right]$$
$$exp\left[-i\frac{4\pi}{c}f_c\frac{(v_a-v_c)}{2R_0}\left(a_c-\frac{v_r(v_c-v_a)}{R_0}\right)t_n^3\right].$$

Signal in azimuth - range time domain

$$S_3(t_r,t_n) = A_0.W_a(t_n-t_c').sinc\left[K_rT_r(t_r-\frac{2R_0}{c})\right].exp\left[-i\frac{4\pi}{c}\frac{f_c}{2R_0}(v_a-v_c)^2t_n^2\right]$$
$$.exp\left[-i\frac{4\pi}{c}f_c\frac{(v_a-v_c)}{2R_0}\left(a_c-\frac{v_r(v_c-v_a)}{R_0}\right)t_n^3\right]. \quad (3.27)$$

From the above Eq. (3.27), it is evident that the range migration has been corrected, and after azimuth compression, the target can be imaged successfully.

After performing azimuth match filtering, focus point target response in range time and azimuth time can be given as:

$$S_3(t_r,t_n) = A_0.W_a(t_n-t_c')\cdot sinc\left[K_rT_r(t_r-\frac{2R_0}{c})\right]. \quad (3.28)$$

The processing steps can be summarized as shown in Fig.3.13

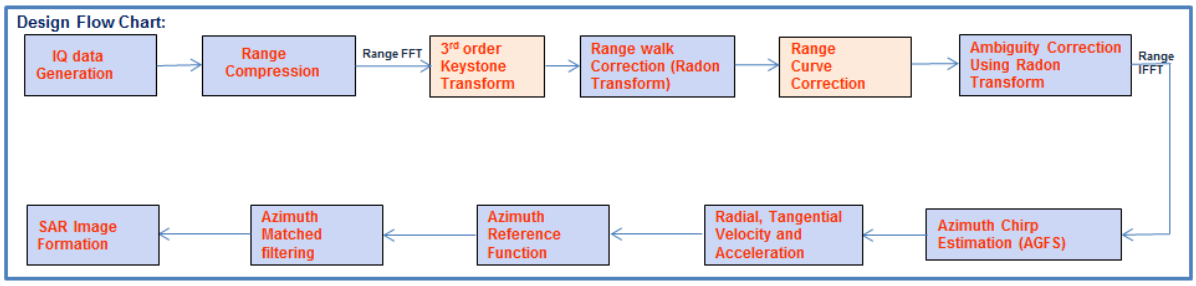

Figure 3.13: The flow of steps for proposed SAR moving target imaging algorithm

3.9 Computational complexity analysis

For analysis of computational complexity, a single moving target without any Doppler ambiguity within a square SAR scene is considered. Assume that N denotes the number of range

cells/azimuth cells. The computational complexity of the proposed algorithm mainly includes a third order keystone transform operation, a Radon transform operation, azimuth chirp estimation using ck-AGFS, range compression, and azimuth compression. The Radon transform is used to detect the line in time-frequency domain with a computational complexity of $O(N^2.logN)$. If the interpolation operation is used to realize the third order Keystone transform, then its computational complexity is about $O[N^3 + N^2.(N-1)]$ [39]. If a sliding window of step size 1 is considered while computing the AGFS for an N length quadratic chirp signal in the azimuth-range time domain, then its computational complexity is $O(N^2.log_2N)$. The computational complexity caused by the range compression and azimuth compression is $O(N^2.logN)$. Hence the overall computational complexity is equal to the sum of individual computational complexity, i.e., $O(N^2.logN) + O[N^3 + N^2.(N-1)] + O(N^2.log_2N)$

3.10 Simulation Results

Various simulations have been performed to establish the validity of the algorithm for imaging moving targets. This section is divided into three subsections. The first part contains the simulation results for multi-target parameter estimation. There are three cases which arise while imaging multiple targets, firstly, when the target spectrum lies entirely in the first PRF band, and two other cases when Doppler ambiguity occurs. The two cases are when the spectrum lies completely in one PRF band and when the target spectrum spans over the $(M_{amb}-1)^{th}$ and M_{amb}^{th} bands. The second section contains results for mean square error, and the third section contains the probability of detection vs. input SNR plot of the target in the fixed probability of false alarm, i.e., 10^{-6}.

3.10.1 Simulations for three targets with constant acceleration

For the simulation, three targets are considered with SNR of 0 dB, where the first target lies in the first PRF band, the second target contains Doppler ambiguity, and the third target lies between two PRF bands. Similar SAR system parameter are considered as shown in Table (3.1). Simulation parameters and estimated parameters of three moving targets are shown in Table (3.3), Table (3.4), and Table (3.5) respectively. Fig. 3.14 shows the trajectory of the moving targets in the range-time and azimuth-time domain. The spectrum is divided into n non-overlapping parts, where n is the number of moving targets that need to be imaged. The

spectrum of each target is individually processed, and the radial velocity is calculated. If the target contains Doppler ambiguity, the fold over factor is calculated and compensated. In the case of three targets, the spectrum spans over the $(M_{amb} - 1)^{th}$ and M_{amb}^{th} PRF bands, then the spectrum is shifted by $PRF/2$ in Doppler domain such that it lies completely within one band. Doppler ambiguity is corrected by finding the fold-over factor for the new spectrum using Eq.(3.15). When the target spectrum lies in the first PRF band, Doppler ambiguity correction is not required. In such a case, keystone transform can be applied directly. After range migration correction using third order keystone transform, the spectrum of the three targets are combined back, as shown in Fig. 3.15. Radon transform is used to calculate the radial velocity of the objects. The spectrum is further processed by ck-AGFS. The results are shown in Fig. 3.16 respectively. Three-point targets can be clearly viewed in the images for proposed algorithms.

Table 3.3: Target Parameters for target 1

Parameters	Defined	Estimated
tangential velocity(v_c)	20	19.5725
tangential acceleration(a_c)	20	19.9655
radial velocity(v_r)	10	9.8833
radial acceleration(a_r)	0	-

Table 3.4: Target Parameters for target 2

Parameters	Defined	Estimated
tangential velocity(v_c)	20	19.5570
tangential acceleration(a_c)	20	19.9646
radial velocity(v_r)	40	39.5404
radial acceleration(a_r)	0	-

3.10.2 Simulation Performance Analysis

Monte Carlo simulation for 50 iterations has been performed to compare mean errors in moving target parameters estimation and detection probability using ck-AGFS and ck-GTFT. The ck-AGFS based algorithm was compared with ck-GTFT, based on its performance in the mean error

Table 3.5: Target Parameters for target 3

Parameters	Defined	Estimated
tangential velocity(v_c)	-20	-20.3804
tangential acceleration(a_c)	40	39.8387
radial velocity(v_r)	60	60.7392
radial acceleration(a_r)	0	-

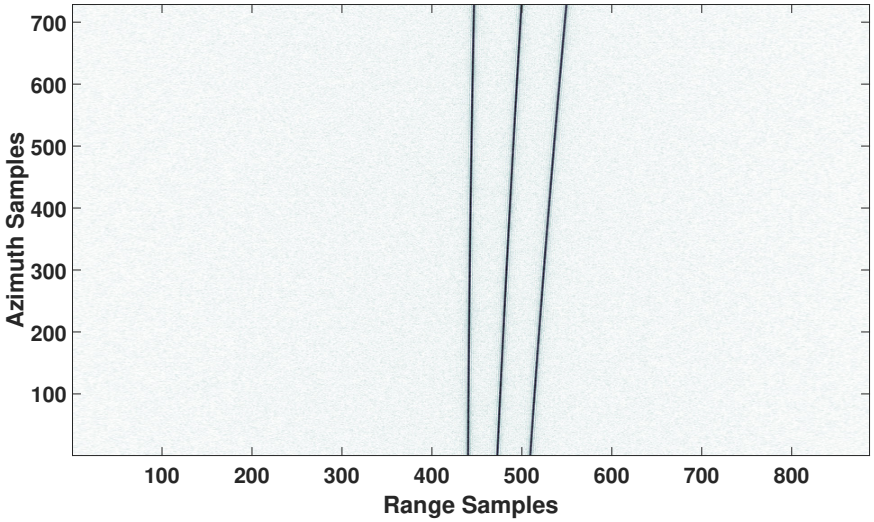

Figure 3.14: After range compression and before range walk and range migration correction.

of the moving target parameters estimation and the probability of distribution (P_d)-probability of false alarm (P_{FA}) curves. Fig. 3.18(a) shows the MSE while estimating the tangential acceleration observed while varying the signal to noise ratio in the input. Similarly Fig. 3.18(b) and 3.18(c) show the MSE plots for estimating tangential acceleration and radial velocity. Fig. 3.19 shows the probability of detection versus input SNR plot comparing the results when using ck-AGFS and ck-GTFT. Fig 3.20 shows the comparison of output SNR versus input SNR plot using ck-AGFS and ck-GTFT approaches. In probability of detection and output SNR plots, assume the probability of false alarm to be 10^{-6}. All the simulations are done for a single moving target without ambiguity and assuming a zero swerling model. It is evident from the plots that ck-AGFS performs better and is a more reliable algorithm for detection and compression of moving targets as compared to GTFT based parameter estimation approach.

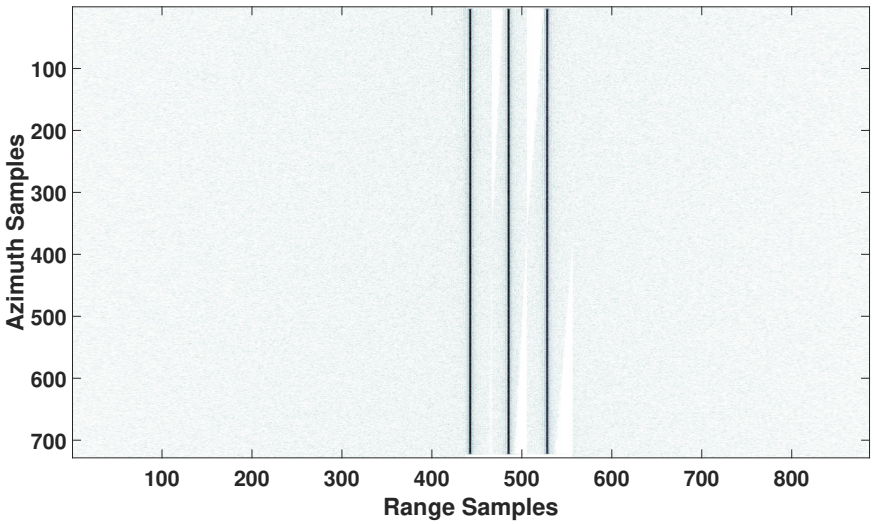

Figure 3.15: After range walk, range migration and Doppler ambiguity correction.

3.11 Conclusion

The proposed method for SAR imaging of moving target gives a decent performance during the non-negligible third order azimuth phase of SAR moving target. It successfully corrects the range migrations and generates a focused image of the point target and is able to estimate velocity and tangential acceleration parameters of SAR moving target. The superiority of ck-AGFS based approach as compared to ck-AGFS based approach is demonstrated, in terms of point target impulse response, SNR Gain, mean estimation error, and target detection probability. In the future, this approach will be validated using real SAR data. Extension of this approach can be explored to correct fourth order range cell migration and estimate higher order parameters of SAR moving target.

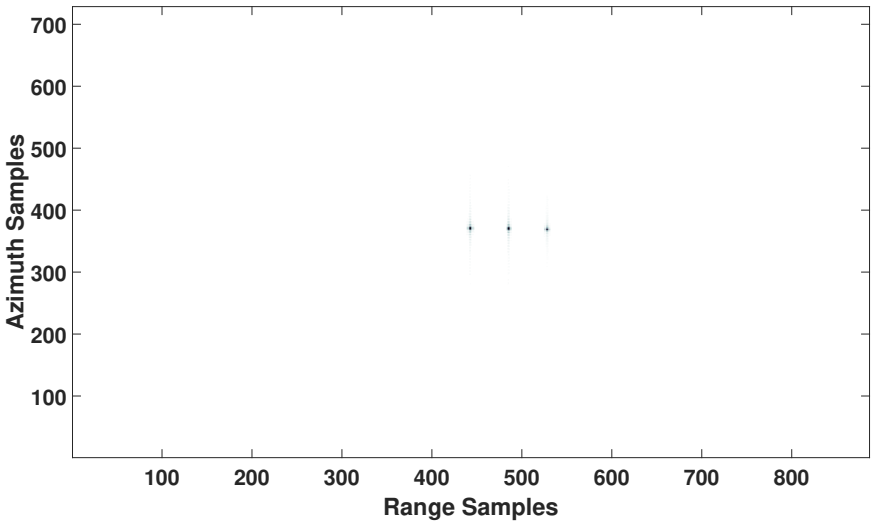

Figure 3.16: Compressed SAR image of three point targets using ck-AGFS method

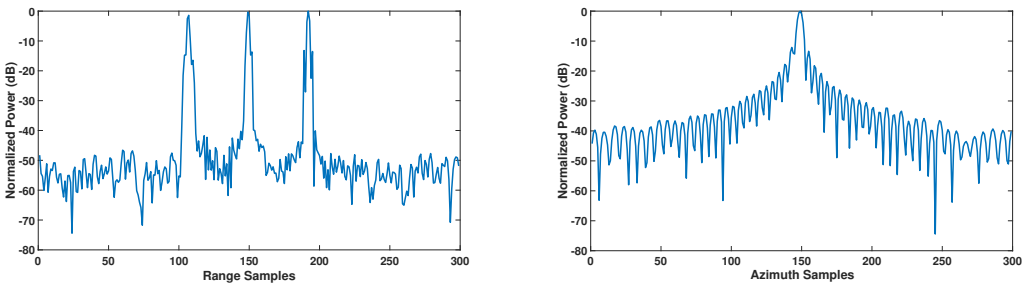

(a) Impulse response in range using ck-AGFS method

(b) Impulse response in azimuth using ck-AGFS method

Figure 3.17: Impulse response of three point targets using ck-AGFS method

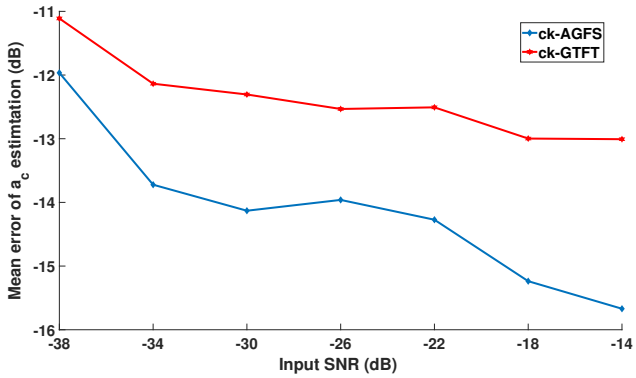

(a) Comparison of mean error estimation in tangential acceleration of target using ck-GTFT and ck-AGFS

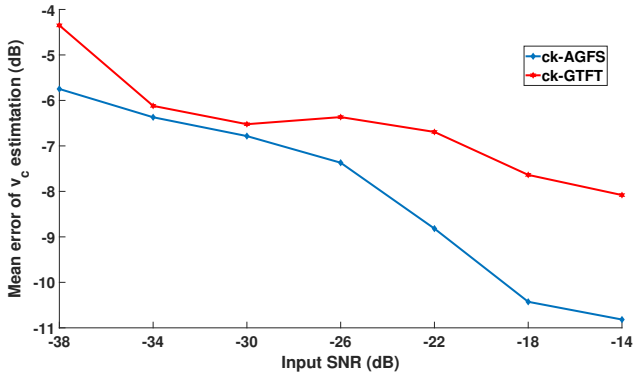

(b) Comparison of mean error estimation in tangential velocity of target using ck-GTFT and ck-AGFS

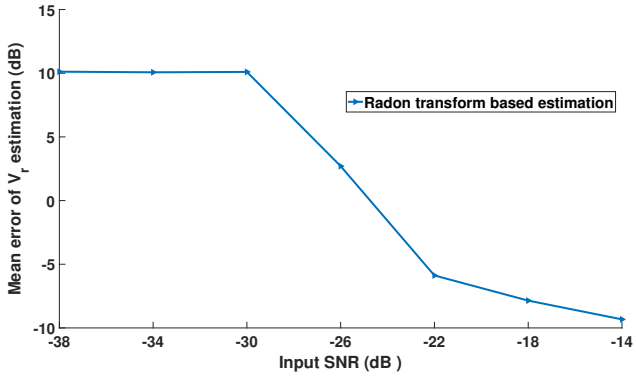

(c) Comparison of mean error estimation in radial velocity of target using ck-GTFT and ck-AGFS

Figure 3.18: Mean Square Error in estimating parameters.

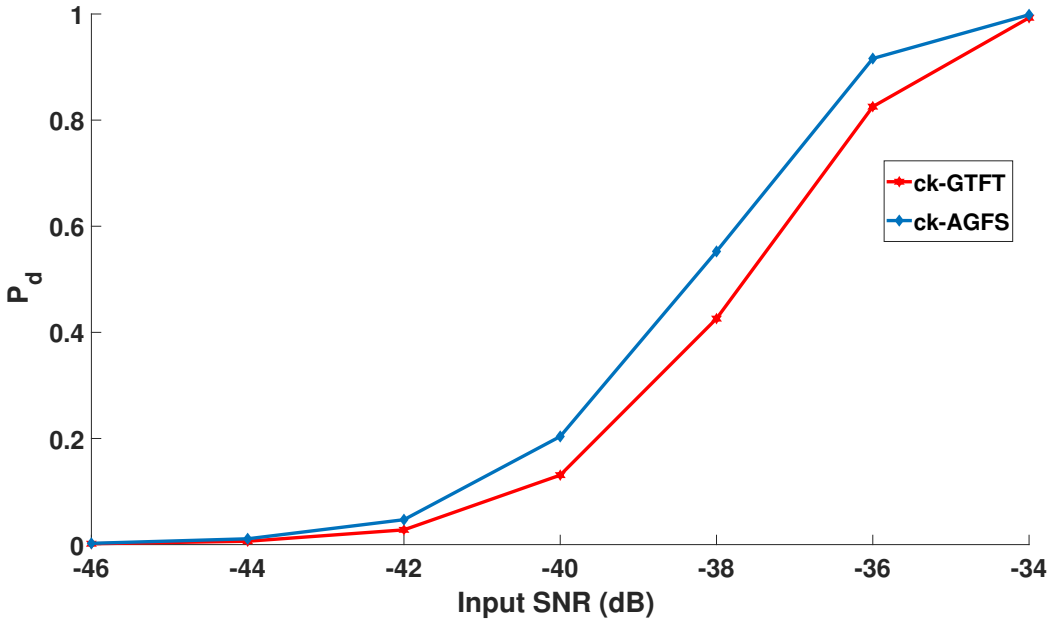

Figure 3.19: Comparison of probability of detection of target vs input SNR plot (when probability of false alarm is 10^{-6}) for ck-GTFT and ck-AGFS

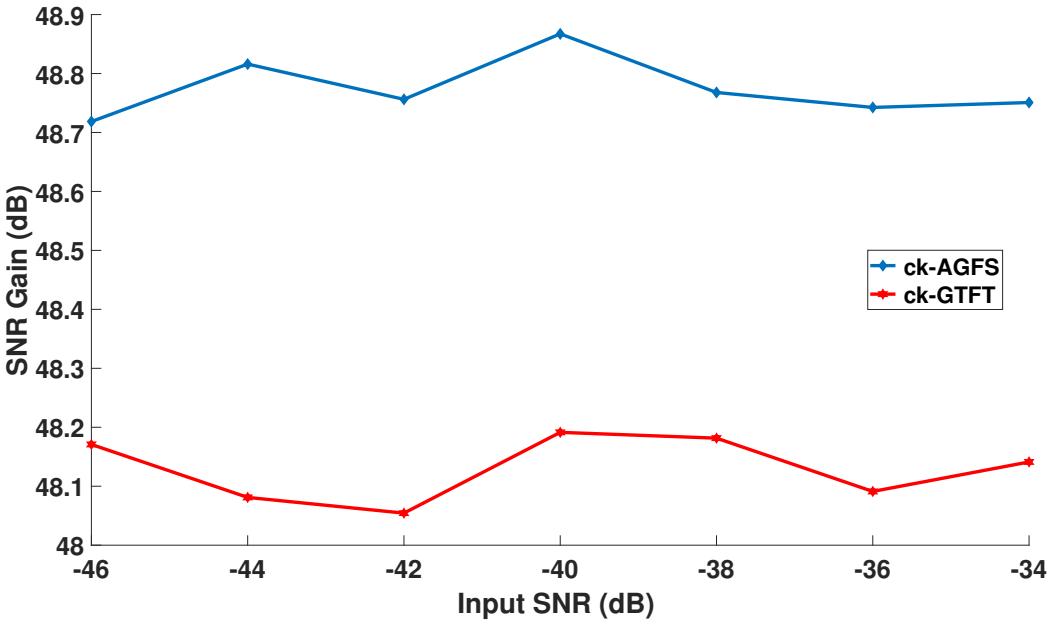

Figure 3.20: Comparison of output SNR Gain vs Input SNR of ck-GTFT and ck-AGFS

Chapter 4

Generalized fractional ambiguity function and its application

The ambiguity function (AF) is an essential time-frequency analysis tool to analyze the radar waveform properties in radar applications. It can be used effectively and reliably to analyze properties like the peak to side-lobe ratio, time delay resolution, Doppler resolution, and tolerance characteristic. However, it fails to analyze higher order chirp waveforms and is unable to estimate their parameters. To solve this problem, a generalized time-frequency transform (GTFT) based generalized fractional AF (GFAF), and generalized fractional Wigner-Ville distribution (GFWVD) are proposed. GFAF is also a generalization of the Fourier transform based ambiguity function, and the fractional Fourier transform based ambiguity function. The uncertainty principle for GFAF and GFWVD is derived. Examples are presented to demonstrate the effectiveness of GFAF in analyzing cubic chirp waveforms and estimating parameters of multicomponent cubic chirps. The superiority of GFAF is demonstrated by comparing the mean square error to Cramer-Rao lower bound and high-order ambiguity function under different input signal to noise ratio conditions. The robustness is demonstrated by comparing the signal to noise ratio gain to that of the time domain matched filtering and other ambiguity functions. Finally, 4^{th} order parameters of a real bat echolocation signal are estimated.

4.1 Introduction

The ambiguity function (AF) is a crucial time-frequency analysis tool to estimate signal parameters in radar applications. It can be used effectively and reliably to analyze radar waveform

properties like the peak to side-lobe ratio, time delay resolution, Doppler resolution, and Doppler tolerance characteristic. In most of the radar, sonar, and biomedical applications, a chirp signal is transmitted to hit a target, and the reflected signal is received and estimated to know the characteristics of the radar target. These reflected chirp signals are of the higher order, and hence there is a need to estimate the parameters of the received radar signal and thereby the characteristics of the target [6, 12, 32, 45, 84, 107].

Many transforms have been proposed to estimate parameters of higher order frequency modulated signals based on computation complexity and parameter estimation accuracy. Some linear transforms are proposed to estimate the parameter of higher order chirps such as polynomial Fourier transform [32], local polynomial Fourier transform [59], polynomial chirplet transform, generalized parametric time frequency transform [130, 132, 133], generalized time-frequency transform [92–94], maximum likelihood estimator [16, 31], QML [30] and QML with reduce coarse search method [104]. All these higher order linear transforms give better parameter estimation accuracy, and they do not produce cross-terms during multicomponent signal analysis. However, the estimation of higher order parameters are possible, but computational complexity increases drastically with the increase of polynomial phase order.

Some non-linear transforms are proposed to reduce the computational complexity to estimate the parameter of higher order chirp signal such as cubic phase function [31], linear canonical transform-based ambiguity function [19, 111], linear canonical transform-based Wigner Ville Distribution (WVD) [91, 106], unified Wigner ambiguity function [140, 141], high-resolution time-frequency rate representation [144]. All these transforms are capable of estimating parameters with reduced computational complexity as compared to higher order linear transforms. However, they produce cross-terms during the multicomponent signal. So they can not give good estimation accuracy in low signal to noise ratio (SNR) condition. A new AF based on LCT called generalized LCT (GLCT) has been developed and shown to have better performances in terms of SNR [105]. Sparse fractional ambiguity function further reduces the computational complexity of fractional Fourier transform based ambiguity function [63].Similarly segmented sparse discrete polynomial phase transform [62, 64] and sparse cubic phase function based methods [65] proposed to detect chirp in low SNR conditions. However, all these transforms are capable of estimating parameters up to a third-order phase and capable to estimate parameters of polynomial phase signals only. These transforms [62–65], along with the results obtained in this paper, could be used to provide a basis for generalizing these results to higher order frequency

modulated signals.

Some higher order non-linear transforms have been proposed to estimate higher order chirp parameters (phase order≥ 3) such as higher order ambiguity function (HAF), polynomial WVD. These produce cross-terms due to the non-linear nature of transform. Each correlation or phase differentiation in HAF increases the SNR threshold by 6dB and degrade parameter estimation accuracy. To reduce cross-terms during multicomponent signal analysis, product higher order ambiguity function (PHAF), and integrated generalized ambiguity function (IGAF), HAF-CPF is proposed [12, 102]. However, these higher order non-linear transforms are capable of estimating parameter up to some higher order in low SNR condition due to the use of multiple correlations. IGAF is very accurate, but it is computationally intensive to analyze polynomial phase signals [105]. Furthermore, these higher order non-linear transforms can estimate only the polynomial phase signal.

The generalized time-frequency transform (GTFT) has been shown to analyze any higher order polynomial chirp signals [92–94]. In this chapter, the GTFT based GFAF and GFWVD is proposed to analyze a large variety of multicomponent frequency modulated signals with reduced computational complexity. GFAF follows the property of index additivity of angle (similar to fractional Fourier transform (FrFT) based AF), thereby giving computational efficiency to GFAF. GFAF can analyze a variety of signals by appropriate selection of the parametric function in the GTFT kernel. Furthermore, GFAF with the appropriately selected kernel can be used to analyze or estimate parameters of hybrid sinusoidal frequency modulated-polynomial phase signals. GFAF estimates higher order chirp parameters with reduced computational complexity because of a single correlation. GFAF is capable of analyzing radar waveform properties, and thereby it is useful to select the suitable radar waveform based on application. GFAF can provide better SNR threshold as compared to high-order ambiguity function (HAF), and other multi-lag phase differentiation transforms due to the use of a single correlation. A combination of correlation and higher order GTFT kernel in GFAF can be used to analyze any higher order chirp with reasonable computational complexity. Product of different lag GFAF or product-GFAF (PGFAF) can be used to reduce cross-terms during multicomponent polynomial phase signal analysis. The computational complexity of GFAF is lesser than generalized CPF, maximum likelihood, and QML estimator for estimating higher order chirp parameters. These properties make GFAF superior to other transforms.

The remaining part of the chapter is organized in the following manner. In section 4.2,

FrFT and GTFT are explained briefly along with some useful formulae. In sections 4.3 and 4.4, GFAF, GFWVD, and their properties are proposed. Section 4.5 presents the derivations of the uncertainty principle for the GFAF and GFWVD. Section 4.6 presents the analysis of a multicomponent cubic chirp waveform and its parameter estimation using GFAF. In section 4.8, the mathematical derivation and simulation results of multicomponent cubic chirps for SNR gain, mean square error (MSE), and its comparison with other transforms are presented. In section 4.9, phase parameters of real multicomponent bat signal till fourth order of phase are estimated, and it is compared with the estimated parameter of FrFT based AF. Finally, conclusions are drawn, and future work is outlined.

4.2 Preliminaries: Different time-frequency transforms

4.2.1 Linear Canonical Transform (LCT)

The LCT of a signal $x(t)$ with parameter matrix $A = (a, b, c, d) \in \mathbb{R}$ satisfying $ad - bc = 1$, is defined as

$$X_A(u) = \begin{cases} \int_{-\infty}^{\infty} x(t) K_A(u,t) dt, & b \neq 0, \\ \sqrt{d} e^{(\frac{icd}{2} u^2)} x(du), & b = 0, \end{cases} \tag{4.1}$$

where $K_A(u,t) = \frac{1}{\sqrt{i2\pi b}} exp\left(i\frac{d}{2b}u^2 - i\frac{ut}{b} + i\frac{a}{2b}t^2\right)$.

Under some special cases, by adjusting the parameter matrix A, the LCT reduces to Fourier transform (FT), fractional Fourier transform (FrFT) and Fresnel transform [19, 111].

4.2.2 Generalized time-frequency transform

If a signal $x(t)$ has a finite absolute sum (finite L^1 norm), then its Generalized time-frequency transform (GTFT) evaluated at parameters (α, λ) is given by

$$X_{\alpha,\lambda}(f) = \int_{-\infty}^{+\infty} x(t) \cdot K_{\alpha,\lambda}(t, f) dt, \tag{4.2}$$

where $K_{\alpha,\lambda}(t,f)$ is the kernel of GTFT and it is defined as [92–94]

$$K_{\alpha,\lambda}(t,f) = \begin{cases} \sqrt{1-icot\alpha}\cdot exp\Big(i\pi t_0^2 f^2 cot\alpha + i\pi f_0^2 t^2 cot\alpha \\ -i2\pi f t \text{cosec}\alpha + i\cdot h(\lambda,t_0 f) - i\cdot h(\lambda,f_0 t)\Big), & \text{if } \alpha \text{ is not a multiple of } \pi \\ \delta(f_0 t - t_0 f), & \text{if } \alpha \text{ is a multiple of } 2\pi \\ \delta(f_0 t + t_0 f), & \text{if } \alpha+\pi \text{ is a multiple of } 2\pi \end{cases}$$

where $h(\cdot)$ is a real valued dimensionless function, α, λ are the real valued GTFT parameters and t_0,f_0 are dimensional normalisation factors, $t_0^2 = \frac{T_{max}}{f_s}$, $f_0^2 = \frac{f_s}{T_{max}}$, $t_0^2 f_0^2 = 1$, T_{max} is the window length during GTFT and f_s is the sampling frequency. The unit of t_0 is sec and unit of f_0 is Hz.

One speciality of the GTFT kernel is that it follows the property of index additivity of angle [2, 93], i.e

$$\int_{-\infty}^{\infty} K_{\alpha_1,\lambda}(t,f) K_{\alpha_2,\lambda}(f,u) df = K_{(\alpha_1+\alpha_2),\lambda}(t,u). \tag{4.3}$$

The inverse GTFT is defined as [94]

$$x(t) = \int_{-\infty}^{\infty} X_{\alpha,\lambda}(f)\cdot K^*_{\alpha,\lambda}(t,f) df. \tag{4.4}$$

The GTFT can be used to analyze a much wider variety of frequency modulated signals by varying $h(\cdot)$ in the GTFT kernel. Cubic-kernel-GTFT (ck-GTFT) may be defined by substituting the parametric function $h(\cdot)$ as

$$h(\lambda,z) = \pi\lambda z^3. \tag{4.5}$$

It is to be noted that ck-GTFT is similar to the 3$^{\text{rd}}$ order polynomial Fourier transform (PFT) [32], with the added advantage of possessing the property of index additivity of angle.

Sinusoidal-kernel-GTFT may be defined by substituting a multiparametric function $h(\cdot)$ as

$$h(A,\phi,\lambda,z) = A\sin(\pi\lambda z + \phi), \tag{4.6}$$

where A, ϕ and λ are the variable parameters, which can be tuned to match the kernel with signal for estimating parameters. This can be a useful transform to analyze certain micro-Doppler effects in radar for the classification of rotating and vibrating targets [20, 21].

4.2.3 Ambiguity function and its variants

- **Ambiguity function**

  For a given signal $x(t)$, the classical ambiguity function (AF) is defined as

$$A_x(\tau,\omega) = \int_{-\infty}^{\infty} x(t+\frac{\tau}{2})x^*(t-\frac{\tau}{2})e^{-i\omega t}dt. \tag{4.7}$$

  If $X(\omega)$ is the FT of $x(t)$, then the AF is also defined as

$$A_X(v,\tau) = \int_{-\infty}^{\infty} X(\omega+\frac{v}{2})X^*(\omega-\frac{v}{2})e^{i\omega\tau}d\omega. \tag{4.8}$$

- **Wigner-Ville distribution**

  For a given signal $x(t)$, the Wigner-Ville distribution (WVD) is defined as

$$W_x(t,\omega) = \int_{-\infty}^{\infty} x(t+\frac{\tau}{2})x^*(t-\frac{\tau}{2})e^{-i\omega\tau}d\tau. \tag{4.9}$$

- **Relation between AF and WVD**

  The WVD can be expressed in terms of AF as

$$W_x(t,\omega) = \frac{1}{2\pi}\int_{-\infty}^{\infty}\int_{-\infty}^{\infty} A_x(\tau,v)e^{-i(\omega\tau-vt)}dvd\tau. \tag{4.10}$$

- **Fractional Fourier transform or linear canonical transform based ambiguity function**

  Fractional Fourier transform or linear canonical transform (LCT) based ambiguity function $AF_x^A(\tau,f)$, of signal $x(t)$ is defined as [19, 22, 86, 111]

$$AF_x^A(\tau,f) = \int_{-\infty}^{\infty} x(t+\frac{\tau}{2})x^*(t-\frac{\tau}{2})K_\alpha(t,f)dt. \tag{4.11}$$

  Similarly, the WVD based on LCT $WVD_x^A(t,f)$ of signal $x(t)$ is defined as [91]

$$WVD_x^A(t,f) = \int_{-\infty}^{\infty} x(t+\frac{\tau}{2})x^*(t-\frac{\tau}{2})K_\alpha(t,f)d\tau. \tag{4.12}$$

  where $K_\alpha(t,f)$ is FrFT kernel and it is a special case of LCT kernel.

4.2.4 Useful Formulae

Gaussian integral:

$$\int_{-\infty}^{+\infty} e^{-At^2 \pm 2Bt + C} dt = \sqrt{\frac{\pi}{A}} e^{\frac{B^2}{A} + C}, \tag{4.13}$$

where A, B, $C \in \mathbb{C}$, $A \neq 0$, and $Re(A) \geq 0$, [115].

Principle of stationary phase:

The principle of stationary phase (PSP) is used to obtain an approximate closed-form expression for the integral of a function, whose amplitude $A(t)$ varies very slowly in comparison to the phase $\phi(t)$. Over the interval where the phase varies rapidly compared to amplitude, the contribution to the integral is negligible because positive and negative parts of the phase cancel each other. Hence, the non-zero contribution comes mainly from the stationary phase point 't_0' [107] which implies

$$\int_{-\infty}^{+\infty} A(t) \cdot e^{i\phi(t)} \cdot dt \approx \sqrt{\frac{2\pi}{\phi''(t_0)}} \cdot A(t_0) e^{i\phi(t_0)} \cdot e^{\frac{i\pi}{4}}, \tag{4.14}$$

where $\phi''(t)$ is second derivative of the phase function $\phi(t)$ and 't_0' is the point where derivative of the phase function becomes equal to 0 ($\phi'(t_0) = 0$). At this point phase of the signal $\phi(t)$ is considered to be 'stationary'. If t_0, $t_1 ... t_n$ are the solutions of $\phi'(t) = 0$, then the integral can be approximated as

$$\int_{-\infty}^{+\infty} A(t) \cdot e^{i\phi(t)} \cdot dt \approx \sum_{k=0}^{n} \sqrt{\frac{2\pi}{\phi''(t_k)}} \cdot A(t_k) e^{i\phi(t_k)} \cdot e^{\frac{i\pi}{4}}. \tag{4.15}$$

This stationary phase approximation is accurate for high time-bandwidth products [27]. If a_0 is the coefficient of t in the phase function $\phi(t)$, then PSP is valid for $|a_0| >> 0$.

4.2.5 The ambiguity function: approaches in literature

Ambiguity function based on the linear canonical transform:

R. Tao, et al. [111] and Tian-Wen Che et al. [19] proposed an AF based on the LCT (LCTAF) to estimate the monocomponent cubic phase signal and also to transform non band-limited signals to the LCT domain and process them using band-limited theory. In addition, properties like symmetry, conjugation, and shifting property of the LCTAF and its relationship with

other time-frequency analysis tools are also derived. Simulations demonstrated to estimate a monocomponent quadratic frequency modulated signal using LCTAF gave satisfactory results.

For a given signal $x(t)$, the LCTAF with parameter $A = (a, b, c, d)$ is defined as

$$AF_x^A(\tau, u) = \int_{-\infty}^{\infty} k_x(t, \tau) K_A(u, t) dt, \tag{4.16}$$

where

$$k_x(t, \tau) = x(t + \frac{\tau}{2}) x^*(t - \frac{\tau}{2}),$$
$$K_A(u, t) = \frac{1}{\sqrt{i2\pi b}} exp\left(i\frac{d}{2b}u^2 - i\frac{ut}{b} + i\frac{a}{2b}t^2\right).$$

Similarly, the cross-LCTAF of two signals $x(t)$ and $y(t)$ is defined as

$$AF_{x,y}^A(\tau, u) = \int_{-\infty}^{\infty} x(t + \frac{\tau}{2}) y^*(t - \frac{\tau}{2}) K_A(u, t) dt. \tag{4.17}$$

Similarly, the WVD based on LCT of signal $x(t)$ is defined as [91]

$$WVD_x^A(t, u) = \int_{-\infty}^{\infty} x(t + \frac{\tau}{2}) x^*(t - \frac{\tau}{2}) K_A(u, \tau) d\tau. \tag{4.18}$$

New integral transforms for generalizing the Wigner distribution and ambiguity function:

Zhichao Zhang and Maokang Luo [140] proposed a new integral transform which under special conditions, yields several other time-frequency tools such as LCAF, linear canonical Wigner-Ville distribution (LCWVD), LCTAF, and WVD based on LCT (LCTWVD). It is also shown that this transformation offers better performance under low SNR as compared to the other, as mentioned earlier.

For a given signal $x(t)$, the new AF and WVD are defined as

$$AF_{A_1,A_2}^A(\tau, \omega) = \int_{-\infty}^{\infty} R_{A_1,A_2}(t, \tau) K_A(\omega, t) dt, \tag{4.19}$$

$$W_{A_1,A_2}^A(t, \omega) = \int_{-\infty}^{\infty} R_{A_1,A_2}(t, \tau) K_A(\omega, \tau) d\tau, \tag{4.20}$$

where

$$R_{A_1,A_2}(t, \tau) = X_{A_1}(t + \frac{\tau}{2}) X_{A_2}^*(t - \frac{\tau}{2}).$$

Simulation has been done to estimate a monocomponent LFM signal and the results obtained indicate that a weak LFM signal embedded in noise can be precisely detected, when compared with LCWVD, LCAF, LCTWVD, and LCTAF.

Algorithm based on the linear canonical transform for QFM signal parameters estimation:

In this study, Yu E. Song et al. [105] proposed a new kind of LCT called generalized LCT (GLCT) to estimate a quadratic frequency modulated (QFM) signal. Simulation results show that the GLCT is better than the other time-frequency analysis tools.

For a given signal $x(t)$, GLCT with parameter $A = (a, b, c, d)$ is defined as

$$GL_x^A(t,u) = \int_{-\infty}^{\infty} k'_x(t,\tau) K_A(u,\tau) d\tau, \tag{4.21}$$

where

$$k'_x(t,\tau) = x(t+\tau)x(t-\tau)x^*(-t+\tau)x^*(-t-\tau),$$
$$K_A(u,\tau) = \frac{1}{\sqrt{i2\pi b}} exp\left(i\frac{d}{2b}u^2 - i\frac{u\tau}{b} + i\frac{a}{2b}\tau^2\right).$$

Simulation results show that the GLCT is better than the other time-frequency analysis tools. It is also shown that this algorithm is computationally efficient compared to other algorithms.

4.3 Proposed definitions

4.3.1 Generalized fractional ambiguity function and generalized fractional Wigner-Ville distribution

All the above-stated algorithms can only estimate parameters of the chirp signals by compromising in computation complexity or parameter estimation accuracy and capable of analyzing only polynomial phase signals. But, in the synthetic aperture radar system during imaging of moving targets, ground-based radar, and sonar system, the reflected waveforms are required to be modeled as chirp signals with higher order polynomial phase [6, 12, 32, 45, 84, 107]. Therefore, a new kind of AF associated with GTFT called generalized fractional ambiguity function (GFAF) has been introduced.

For a given signal $x(t)$ with finite L^2 norm,

- The proposed GFAF associated with GTFT is defined as

$$AF^{G}_{x(t),\alpha,\lambda}(\tau, f) = \int_{-\infty}^{\infty} x(t+\tau/2)x^{*}(t-\tau/2)K_{\alpha,\lambda}(t, f)dt. \tag{4.22}$$

- The proposed generalized fractional Wigner-Ville distribution(GFWVD) associated with GTFT is defined as

$$WDF^{G}_{x(t),\alpha,\lambda}(t, f) = \int_{-\infty}^{\infty} x(t+\tau/2)x^{*}(t-\tau/2)K_{\alpha,\lambda}(\tau, f)d\tau. \tag{4.23}$$

Here $K_{\alpha,\lambda}(t, f)$ is the kernel of GTFT. Cubic-kernel-GFAF (ck-GFAF) is defined as cubic-kernel-GTFT (ck-GTFT) based ambiguity function. Similarly, cubic-kernel-GFWVD (ck-GFWVD) is defined as ck-GTFT based WVD.

For two given signals $x(t)$ and $y(t)$ with finite L^2 norm,

- The proposed cross GFAF associated with GTFT is defined as

$$AF^{G}_{x(t),y(t),\alpha,\lambda}(\tau, f) = \int_{-\infty}^{\infty} x(t+\tau/2)y^{*}(t-\tau/2)K_{\alpha,\lambda}(t, f)dt. \tag{4.24}$$

- The proposed cross GFWVD associated with GTFT is defined as

$$WDF^{G}_{x(t),y(t),\alpha,\lambda}(t, f) = \int_{-\infty}^{\infty} x(t+\tau/2)y^{*}(t-\tau/2)K_{\alpha,\lambda}(\tau, f)d\tau. \tag{4.25}$$

GFAF can perform waveform analysis and parameter estimation of a variety of signals (polynomial, sinusoidal frequency modulated, etc.) by appropriate selection of the parametric function $h(\cdot)$ in the GTFT kernel. For example, GFAF can use polynomial phase GTFT kernel to analyze multicomponent polynomial phase signals. Cubic-kernel-GFAF (ck-GFAF) may be defined by using cubic-kernel GTFT to analyze multicomponent cubic frequency modulated signals. On the other hand, GFAF can use sinusoidal-kernel GTFT to analyze multicomponent sinusoidal frequency modulated phase signals. Furthermore, GFAF with the appropriately selected kernel can be used to analyze or estimate parameters of hybrid sinusoidal frequency modulated-polynomial phase signals. Similarly, parametric function $h(\cdot)$ of GTFT kernel can be appropriately selected for other types of signals.

4.3.2 Relation between GFAF and GFWVD

From the definition of the GFAF and inverse transform property of GTFT, we have

$$x(t+\tau/2)x^*(t-\tau/2) = \int_{-\infty}^{\infty} AF^G_{x(t),\alpha,\lambda}(\tau,f)K^*_{\alpha,\lambda}(t,f)df.$$

Hence from the definition of GFWVD, we get

$$WDF^G_{x(t),\alpha,\lambda}(t,f') = \iint_{-\infty}^{\infty} AF^G_{x(t),\alpha,\lambda}(\tau,f)K^*_{\alpha,\lambda}(t,f)K_{\alpha,\lambda}(\tau,f')d\tau df,$$

where $K_{\alpha,\lambda}$ is the GTFT kernel.

4.4 Properties of generalized fractional ambiguity function

4.4.1 Relation with other ambiguity functions

- If $h(\cdot) = 0$, then the GTFT kernel reduces to the fractional Fourier transform kernel, and therefore the GFAF reduces to FrFT based AF, and it is not linear.
- If $\alpha = 90°$, $h(\cdot) = 0$, then the GTFT kernel reduces to the Fourier transform kernel, and therefore the GFAF reduces to classical AF, and it is not linear.

4.4.2 Inverse and uniqueness property of GFAF

If $x(t)$ has finite and non-zero L^2 norm, then there exists an a such that $x(a) \neq 0$. Additionally if the $AF^G_{x(t),\alpha,\lambda}(\tau,f)$ has finite L^1 norm, we can define the unique inverse for GFAF as follows

$$x(t) = \frac{1}{x^*(a)} \int_{-\infty}^{\infty} AF^G_{x(t),\alpha,\lambda}(t-a,f)K^*_{\alpha,\lambda}((t+a)/2,f)df. \tag{4.26}$$

Proof:

We know that

$$x(t+\tau/2)x^*(t-\tau/2) = \int_{-\infty}^{\infty} AF^G_{x(t),\alpha,\lambda}(\tau,f)K^*_{\alpha,\lambda}(t,f)df. \tag{4.27}$$

Let $\tau/2 = t - a$, then Eq. (4.27) can be written as

$$x(2t-a)x^*(a) = \int_{-\infty}^{\infty} AF^G_{x(t),\alpha,\lambda}(2(t-a),f)K^*_{\alpha,\lambda}(t,f)df, \tag{4.28}$$

Now, substitute $t = t/2 + a/2$, thus we get

$$x(t) = \frac{1}{x^*(a)} \int_{-\infty}^{\infty} AF^G_{x(t),\alpha,\lambda}(t-a,f)K^*_{\alpha,\lambda}\left(\frac{t+a}{2},f\right)df. \tag{4.29}$$

Hence from Eq. (4.29), it is easy to see that for any non-zero $x(a)$, the inverse is unique for particular $x(t)$.

Also noteworthy is the case for $a = 0$; the form we obtain for the inverse in this case is

$$x(t) = \frac{1}{x^*(0)} \int_{-\infty}^{\infty} AF^G_{x(t),\alpha,\lambda}(t,f)K^*_{\alpha,\lambda}(t/2,f)df. \tag{4.30}$$

4.4.3 Non linearity

If multicomponent signal $z(t)$ is the sum of two multicomponent signals $x(t)$ and $y(t)$ respectively ($z(t) = x(t) + y(t)$), then GFAF of $z(t)$ can be expressed as:

$$\begin{aligned} AF^G_{z(t),\alpha,\lambda}(\tau,f) = AF^G_{x(t),\alpha,\lambda}(\tau,f) + AF^G_{y(t),\alpha,\lambda}(\tau,f) \\ +AF^G_{x(t),y(t),\alpha,\lambda}(\tau,f) + AF^G_{y(t),x(t),\alpha,\lambda}(\tau,f), \end{aligned} \tag{4.31}$$

Here, as GFAF is a non linear transform, we can see that it produced cross terms such as $AF^G_{x(t),y(t),\alpha,\lambda}(\tau,f)$ and $AF^G_{y(t),x(t),\alpha,\lambda}(\tau,f)$ during multicomponent signal analysis.

4.4.4 Total energy bound

Suppose that $x(t)$ has finite and non-zero L^2 norm, then we have

$$|AF^G_{x(t),\alpha,\lambda}(\tau,f)| \leq |\sqrt{\mathrm{cosec}\alpha}| \int_{-\infty}^{\infty} |x(t)|^2 dt. \tag{4.32}$$

Proof:

We know that

$$\left|AF^{G}_{x(t),\alpha,\lambda}(\tau,f)\right| = \left|\int_{-\infty}^{\infty} x(t+\tau/2)x^{*}(t-\tau/2)K_{\alpha,\lambda}(t,f)dt\right|. \tag{4.33}$$

By the Cauchy-Bunyakovsky-Schwarz inequality,

$$\left|\int_{-\infty}^{\infty} x(t+\tau/2)x^{*}(t-\tau/2)K_{\alpha,\lambda}(t,f)dt\right| \leq \left(\int_{-\infty}^{\infty} |x(t+\tau/2)|^{2}\, dt\cdot\right. \tag{4.34}$$

$$\left.\int_{-\infty}^{\infty} \left|x^{*}(t-\tau/2)K_{\alpha,\lambda}(t,f)\right|^{2} dt\right)^{\frac{1}{2}}, \tag{4.35}$$

$$\implies \left|AF^{G}_{x(t),\alpha,\lambda}(\tau,f)\right| \leq \left|\sqrt{\text{cosec}\alpha}\right| \cdot \left(\int_{-\infty}^{\infty} \left|x(t)^{2}\right| dt\right)^{2.\frac{1}{2}}, \tag{4.36}$$

$$|AF^{G}_{x(t),\alpha,\lambda}(\tau,f)| \leq |\sqrt{\text{cosec}\alpha}| \int_{-\infty}^{\infty} |x(t)|^{2} dt. \tag{4.37}$$

So the maximum value of GFAF is bounded by energy or L^2 norm of signal, and fractional Fourier angle. This property can be proved using Cauchy Schwarz inequality.

4.4.5 Total energy invariant property

If $\alpha = 90^{\circ}$ and $\lambda = 0$, then GFAF gives the energy of signal $x(t)$ at origin i.e.

$$AF^{G}_{x(t),\alpha=\frac{\pi}{2}\lambda=0,}(0,0) = \int_{-\infty}^{\infty} |x(t)|^{2} dt. \tag{4.38}$$

4.4.6 Finite time delay Support

If $x(t)$ is zero for all t $\notin [t_1, t_2]$, then $AF^{G}_{x(t),\alpha,\lambda}(\tau,f)$ is zero for all $\tau > t_2 - t_1$.

4.4.7 Symmetry and conjugation properties

The following properties can be proved:

Symmetry properties:

- $AF^G_{x(t),\alpha,\lambda}(-\tau,f) = \left[AF^G_{x(t),-\alpha,-\lambda}(\tau,f)\right]^*$, if $h(\lambda,\cdot)$ is an odd function of λ
- $AF^G_{x(t),\alpha,\lambda}(-\tau,-f) = \left[AF^G_{x(t),-\alpha,-\lambda}(\tau,-f)\right]^*$, if $h(\lambda,\cdot)$ is an odd function of λ

Conjugation Properties:

- $AF^G_{x^*(t),\alpha,\lambda}(\tau,f) = \left[AF^G_{x(t),-\alpha,-\lambda}(\tau,f)\right]^*$, if $h(\lambda,\cdot)$ is an odd function of λ
- $AF^G_{x(-t),\alpha,\lambda}(\tau,f) = \begin{cases} AF^G_{x(t),\alpha,\lambda}(\tau,-f), & \text{if } h(\lambda,\cdot) \text{ is an even function of } t,\ f \\ AF^G_{x(t),\alpha,-\lambda}(\tau,-f), & \text{if } h(\cdot,\cdot) \text{ is an odd function of } t,\ f \\ & \text{and } \lambda \end{cases}$
- $AF^G_{x^*(-t),\alpha,\lambda}(\tau,f) = \begin{cases} \left[AF^G_{x(t),-\alpha,-\lambda}(\tau,-f)\right]^*, & \text{if } h(\cdot,\cdot) \text{ is an even function of } t \\ & \text{and } f \text{ and an odd function of } \lambda \\ \left[AF^G_{x(t),-\alpha,\lambda}(\tau,-f)\right]^* & \text{if } h(\cdot,\cdot) \text{ is an odd function of } t, \\ & f \text{ and } \lambda \end{cases}$

In particular, these properties are useful for ck-GFAF, since for ck-GFAF, the GTFT kernel is odd function of λ. Proof of above mentioned properties are as follows:

Symmetry properties:

- $$AF^G_{x(t),\alpha,\lambda}(-\tau,f) = \int_{-\infty}^{\infty} x(t-\frac{\tau}{2})x^*(t+\frac{\tau}{2})K_{\alpha,\lambda}(t,f)dt,$$
$$= \left[\int_{-\infty}^{\infty} x(t+\frac{\tau}{2})x^*(t-\frac{\tau}{2})K^*_{\alpha,\lambda}(t,f)dt\right]^*.$$

If $h(\lambda,\cdot)$ is odd function of λ, then $K^*_{\alpha,\lambda}(t,f) = K_{-\alpha,-\lambda}(t,f)$.

$$\therefore AF^G_{x(t),\alpha,\lambda}(-\tau,f) = [AF^G_{x(t),-\alpha,-\lambda}(\tau,f)]^*. \tag{4.39}$$

- $$AF^G_{x(t),\alpha,\lambda}(-\tau,-f) = \int_{-\infty}^{\infty} x^*(t+\frac{\tau}{2})x(t-\frac{\tau}{2})K_{\alpha,\lambda}(t,-f)dt,$$
$$= \left[\int_{-\infty}^{\infty} x(t+\frac{\tau}{2})x^*(t-\frac{\tau}{2})K^*_{\alpha,\lambda}(t,-f)dt\right]^*.$$

If $h(\lambda,\cdot)$ is odd function of λ, then $K^*_{\alpha,\lambda}(t,f) = K_{-\alpha,-\lambda}(t,f)$.

$$\therefore AF^G_{x(t),\alpha,\lambda}(-\tau,-f) = \left[AF^G_{x(t),-\alpha,-\lambda}(\tau,-f)\right]^*. \tag{4.40}$$

Conjugation Properties:

- $$AF^G_{x^*(t),\alpha,\lambda}(\tau,f) = \int_{-\infty}^{\infty} x^*(t+\frac{\tau}{2})x(t-\frac{\tau}{2})K_{\alpha,\lambda}(t,f)dt,$$
$$= \left[\int_{-\infty}^{\infty} x(t+\frac{\tau}{2})x^*(t-\frac{\tau}{2})K^*_{\alpha,\lambda}(t,f)dt\right]^*,$$

If $h(\lambda,\cdot)$ is odd function of λ, then $K^*_{\alpha,\lambda}(t,f) = K_{-\alpha,-\lambda}(t,f)$ and

$$AF^G_{x^*(t),\alpha,\lambda}(\tau,f) = \left[\int_{-\infty}^{\infty} x(t+\frac{\tau}{2})x^*(t-\frac{\tau}{2})K_{-\alpha,-\lambda}(t,f)dt\right]^*.$$

$$\therefore AF^G_{x^*(t),\alpha,\lambda}(\tau,f) = \left[AF^G_{x(t),-\alpha,-\lambda}(\tau,f)\right]^*. \tag{4.41}$$

- $$AF^G_{x(-t),\alpha,\lambda}(\tau,f) = \int_{-\infty}^{\infty} x(-t+\frac{\tau}{2})x^*(-t-\frac{\tau}{2})K_{\alpha,\lambda}(t,f)dt.$$
$$put\ -t = t'$$
$$= \int_{-\infty}^{\infty} x(t'+\frac{\tau}{2})x^*(t'-\frac{\tau}{2})K_{\alpha,\lambda}(-t',f)dt',$$
$$= \sqrt{1-i\cot\alpha}\int_{-\infty}^{\infty} x(t'+\frac{\tau}{2})x^*(t'-\frac{\tau}{2})\cdot exp[i\pi(f_0^2t'^2\cot\alpha+$$
$$t_0^2f^2\cot\alpha + 2ft'\mathrm{cosec}\alpha) - ih(\lambda,-f_0t') + ih(\lambda,t_0f)]dt'.$$

Case 1: If $h(\lambda,\cdot)$ is an even function in the second parameter i.e. $h(\lambda,-f_0t) = h(\lambda,f_0t)$ and $h(\lambda,-t_0f) = h(\lambda,t_0f)$, then

$$AF^G_{x(-t),\alpha,\lambda}(\tau,f) = \sqrt{1-i\cot\alpha}\int_{-\infty}^{\infty} x(t'+\frac{\tau}{2})x^*(t'-\frac{\tau}{2})\cdot exp[i\pi(f_0^2t'^2\cot\alpha+$$
$$t_0^2f^2\cot\alpha - 2(-f)t'\mathrm{cosec}\alpha) - ih(\lambda,f_0t') + ih(\lambda,-t_0f)]dt',$$
$$= \int_{-\infty}^{\infty} x(t'+\frac{\tau}{2})x^*(t'-\frac{\tau}{2})K_{\alpha,\lambda}(t',-f)dt'.$$

$$\therefore AF^{G}_{x(-t),\alpha,\lambda}(\tau,f) = AF^{G}_{x(t),\alpha,\lambda}(\tau,-f). \tag{4.42}$$

Case 2: If $h(\lambda,\cdot)$ is an odd function (as in case of ck-GTFT) in the second parameter i.e. $h(\lambda,-f_0t) = -h(\lambda,f_0t)$ and $h(\lambda,-t_0f) = -h(\lambda,t_0f)$, then

$$AF^{G}_{x(-t),\alpha,\lambda}(\tau,f) = \sqrt{1-i\text{cot}\alpha}\int_{-\infty}^{\infty} x(t'+\frac{\tau}{2})x^*(t'-\frac{\tau}{2})\cdot exp[i\pi(f_0^2t'^2\text{cot}\alpha + t_0^2f^2\text{cot}\alpha - 2(-f)t'\text{cosec}\alpha) + ih(\lambda,f_0t') - ih(\lambda,-t_0f)]dt'.$$

If $h(\lambda,\cdot)$ is odd function of λ, then $h(-\lambda,\cdot) = -h(\lambda,\cdot)$

$$\begin{aligned} AF^{G}_{x(-t),\alpha,\lambda}(\tau,f) &= \sqrt{1-i\text{cot}\alpha}\int_{-\infty}^{\infty} x(t'+\frac{\tau}{2})x^*(t'-\frac{\tau}{2})\cdot exp[i\pi(f_0^2t'^2\text{cot}\alpha \\ &\quad + t_0^2f^2\text{cot}\alpha - 2(-f)t'\text{cosec}\alpha) - ih(-\lambda,f_0t') + ih(-\lambda,-t_0f)]dt' \\ &= \int_{-\infty}^{\infty} x(t'+\frac{\tau}{2})x^*(t'-\frac{\tau}{2})K_{\alpha,-\lambda}(t',-f)dt'. \end{aligned}$$

$$\therefore AF^{G}_{x(-t),\alpha,\lambda}(\tau,f) = AF^{G}_{x(t),\alpha,-\lambda}(\tau,-f). \tag{4.43}$$

- $AF^{G}_{x^*(-t),\alpha,\lambda}(\tau,f) = \int_{-\infty}^{\infty} x^*(-t+\frac{\tau}{2})x(-t-\frac{\tau}{2})K_{\alpha,\lambda}(t,f)dt$

  $put\ -t = t'$

  $$= \int_{-\infty}^{\infty} x^*(t'+\frac{\tau}{2})x(t'-\frac{\tau}{2})K_{\alpha,\lambda}(-t',f)dt',$$

  $$= \sqrt{1-i\text{cot}\alpha}\int_{-\infty}^{\infty} x^*(t'+\frac{\tau}{2})x(t'-\frac{\tau}{2})\cdot exp[i\pi(f_0^2t'^2\text{cot}\alpha + t_0^2f^2\text{cot}\alpha + 2ft'\text{cosec}\alpha) - ih(\lambda,-f_0t') + ih(\lambda,t_0f)]dt.$$

Case 1: If $h(\lambda,\cdot)$ is an even function in the second parameter i.e. $h(\lambda,-f_0t) = h(\lambda,f_0t)$ and

$h(\lambda, -t_0 f) = h(\lambda, t_0 f)$, then

$$AF^G_{x^*(-t),\alpha,\lambda}(\tau, f) = \sqrt{1 - i\cot\alpha} \int_{-\infty}^{\infty} x^*(t' + \frac{\tau}{2}) x(t' - \frac{\tau}{2}) \cdot exp[i\pi(f_0^2 t'^2 \cot\alpha + t_0^2 f^2 \cot\alpha - 2(-f)t' \mathrm{cosec}\alpha) - ih(\lambda, f_0 t') + ih(\lambda, -t_0 f)]dt',$$

$$= \int_{-\infty}^{\infty} x^*(t' + \frac{\tau}{2}) x(t' - \frac{\tau}{2}) K_{\alpha,\lambda}(t', -f)dt'.$$

If $h(\lambda, \cdot)$ is odd function of λ, then $K^*_{\alpha,\lambda}(t, f) = K_{-\alpha,-\lambda}(t, f)$ and

$$AF^G_{x^*(-t),\alpha,\lambda}(\tau, f) = \left[\int_{-\infty}^{\infty} x(t' + \frac{\tau}{2}) x^*(t' - \frac{\tau}{2}) K_{-\alpha,-\lambda}(t', -f)dt' \right]^*.$$

$$\therefore AF^G_{x^*(-t),\alpha,\lambda}(\tau, f) = \left[AF^G_{x(t),-\alpha,-\lambda}(\tau, -f) \right]^*. \tag{4.44}$$

Case 2: If $h(\lambda, \cdot)$ is an odd function (as in the case of ck-GTFT) in the second parameter i.e. $h(\lambda, -f_0 t) = -h(\lambda, f_0 t)$ and $h(\lambda, -t_0 f) = -h(\lambda, t_0 f)$, then

$$AF^G_{x^*(-t),\alpha,\lambda}(\tau, f) = \sqrt{1 - i\cot\alpha} \int_{-\infty}^{\infty} x^*(t' + \frac{\tau}{2}) x(t' - \frac{\tau}{2}) \cdot exp[i\pi(f_0^2 t'^2 \cot\alpha + t_0^2 f^2 \cot\alpha - 2(-f)t' \mathrm{cosec}\alpha) + ih(\lambda, f_0 t') - ih(\lambda, -t_0 f)]dt'.$$

If $h(\lambda, \cdot)$ is odd function of λ, then $h(-\lambda, \cdot) = -h(\lambda, \cdot)$, $K^*_{\alpha,\lambda}(t, f) = K_{-\alpha,-\lambda}(t, f)$ and

$$AF^G_{x^*(-t),\alpha,\lambda}(\tau, f) = \sqrt{1 - i\cot\alpha} \int_{-\infty}^{\infty} x^*(t' + \frac{\tau}{2}) x(t' - \frac{\tau}{2}) \cdot exp[i\pi(f_0^2 t'^2 \cot\alpha + t_0^2 f^2 \cot\alpha - 2(-f)t' \mathrm{cosec}\alpha) - ih(-\lambda, f_0 t') + ih(-\lambda, -t_0 f)]dt',$$

$$= \int_{-\infty}^{\infty} x^*(t' + \frac{\tau}{2}) x(t' - \frac{\tau}{2}) K_{\alpha,-\lambda}(\tau, -f)dt',$$

$$= \left[\int_{-\infty}^{\infty} x(t' + \frac{\tau}{2}) x^*(t' - \frac{\tau}{2}) K_{-\alpha,\lambda}(\tau, -f)dt' \right]^*.$$

$$\therefore AF^G_{x^*(-t),\alpha,\lambda}(\tau, f) = [AF^G_{x(t),-\alpha,\lambda}(\tau, -f)]^*. \tag{4.45}$$

4.4.8 Time delay property

If ck-GFAF of $x(t)$ is $AF^G_{x(t),\beta,\lambda}(\tau, f)$, then ck-GFAF of time delayed signal $x_1(t) = x(t - t_d)$ is given by

$$AF^G_{x_1(t),\alpha,\lambda}(\tau, f) = \int_{-\infty}^{\infty} x_1(t + \frac{\tau}{2}) x_1^*(t - \frac{\tau}{2}) K_{\alpha,\lambda}(t, f) dt,$$

$$\text{where} \quad x_1(t) = x(t - t_d).$$

$$AF^G_{x_1(t),\alpha,\lambda}(\tau, f) = \int_{-\infty}^{\infty} x(t - t_d + \frac{\tau}{2}) x^*(t - t_d - \frac{\tau}{2}) K_{\alpha,\lambda}(t, f) dt,$$

$$\text{Put} \quad t - t_d = t_1, \quad \Longrightarrow \; t_1 + t_d = t,$$

$$AF^G_{x_1(t),\alpha,\lambda}(\tau, f) = \int_{-\infty}^{\infty} x(t_1 + \frac{\tau}{2}) x^*(t_1 - \frac{\tau}{2}) K_{\alpha,\lambda}(t_1 + t_d, f) dt_1.$$

Put $t_1 = t$, for simplicity and consider $K_{\alpha,\lambda}(t, f)$ as a ck-GTFT kernel

$$\begin{aligned} AF^G_{x_1(t),\alpha,\lambda}(\tau, f) = \sqrt{1 - i\text{cot}\alpha} \int_{-\infty}^{\infty} x(t + \frac{\tau}{2}) x^*(t - \frac{\tau}{2}) \cdot exp(i\pi[f_0^2 t^2 \text{cot}\alpha + f_0^2 t_d^2 \text{cot}\alpha \\ + 2f_0^2 t t_d \text{cot}\alpha + t_0^2 f^2 \text{cot}\alpha - 2tf\,\text{cosec}\alpha - 2f t_d \text{cosec}\alpha \\ - f_0^3(\lambda t^3 + \lambda t_d^3 + 3\lambda t_d^2 t + 3\lambda t^2 t_d) + \lambda t_0^3 f^3])dt, \end{aligned}$$

$$\begin{aligned} AF^G_{x_1(t),\alpha,\lambda}(\tau, f) = \sqrt{1 - i\text{cot}\alpha} \int_{-\infty}^{\infty} x(t + \frac{\tau}{2}) x^*(t - \frac{\tau}{2}) \cdot exp(i\pi[-\lambda f_0^3 t^3 \\ + f_0^2 t^2(\text{cot}\alpha - 3\lambda f_0 t_d) - 2t(f\,\text{cosec}\alpha - f_0^2 t_d \text{cot}\alpha + \frac{3}{2}\lambda f_0^3 t_d^2) \\ + (t_0^2 f^2 \text{cot}\alpha + f_0^2 t_d^2 \text{cot}\alpha - 2f t_d \text{cosec}\alpha - \lambda f_0^3 t_d^3 + \lambda t_0^3 f^3)])dt. \end{aligned} \tag{4.46}$$

Put $\text{cot}\alpha - 3\lambda f_0 t_d = \text{cot}\beta$, and $f\,\text{cosec}\alpha - f_0^2 t_d \text{cot}\alpha + \frac{3}{2}\lambda f_0^3 t_d^2 = f'\text{cosec}\beta$,

$$\begin{aligned} AF^G_{x_1(t),\alpha,\lambda}(\tau, f) = \frac{\sqrt{1 - i\text{cot}\alpha}}{\sqrt{1 - i\text{cot}\beta}} \int_{-\infty}^{\infty} x(t + \frac{\tau}{2}) x^*(t - \frac{\tau}{2}) K_{\beta,\lambda}(t, f') \cdot exp(i\pi[-\lambda t_0^3 f'^3 \\ - t_0^2 f'^2 cot\beta + t_0^2 f^2 \text{cot}\alpha + f_0^2 t_d^2 cot\alpha - 2f t_d \text{cosec}\alpha \\ - \lambda f_0^3 t_d^3 + \lambda t_0^3 f^3])dt, \end{aligned} \tag{4.47}$$

$$AF^G_{x_1(t),\alpha,\lambda}(\tau, f) = C_0(f, \alpha, \lambda, t_d) \cdot AF^G_{x(t),\beta,\lambda}(\tau, f'), \tag{4.48}$$

where

$$\cot\beta = \cot\alpha - 3\lambda f_0 t_d,\ f' = \frac{f\,\mathrm{cosec}\alpha - f_0^2 t_d \cot\alpha + \frac{3}{2}\lambda f_0^3 t_d^2}{\mathrm{cosec}\beta} \text{ and}$$

$$C_0(f,\alpha,\lambda,t_d) = \frac{\sqrt{1-i\cot\alpha}}{\sqrt{1-i\cot\beta}} \cdot exp\left(i\pi\left[-\lambda t_0^3 f'^3 - t_0^2 f'^2 \cot\beta + t_0^2 f^2 \cot\alpha \right.\right.$$
$$\left.\left. + f_0^2 t_d^2 \cot\alpha - 2 f t_d \mathrm{cosec}\alpha - \lambda f_0^3 t_d^3 + \lambda t_0^3 f^3\right]\right).$$

Case 1: When $\lambda = 0$ in Eq. (4.46), then we can get relationship equivalent to time delay property of FrFT based ambiguity function

$$\begin{aligned} AF^G_{x_1(t),\alpha,\lambda=0}(\tau,f) &= \sqrt{1-i\cot\alpha} \int_{-\infty}^{\infty} x(t+\frac{\tau}{2}) x^*(t-\frac{\tau}{2}) \cdot exp(i\pi[f_0^2 t^2 \cot\alpha - 2t\mathrm{cosec}\alpha \\ &\quad \cdot (f - f_0^2 t_d cos\alpha) + t_0^2 f^2 \cot\alpha + f_0^2 t_d^2 \cot\alpha - 2 f t_d \mathrm{cosec}\alpha])dt, \\ &= \int_{-\infty}^{\infty} x(t+\frac{\tau}{2}) x^*(t-\frac{\tau}{2}) K_\alpha(t, f - f_0^2 t_d cos\alpha) exp(i\pi[-f_0^2 t_d^2 cos^2\alpha \cot\alpha \\ &\quad + 2 f t_d cos\alpha \cot\alpha + f_0^2 t_d^2 \cot\alpha - 2 f t_d \mathrm{cosec}\alpha])dt, \\ &= \int_{-\infty}^{\infty} x(t+\frac{\tau}{2}) x^*(t-\frac{\tau}{2}) K_\alpha(t, f - f_0^2 t_d cos\alpha) \\ &\quad exp(i\pi[f_0^2 t_d^2 sin^2\alpha \cot\alpha - 2 f t_d \mathrm{cosec}\alpha(1-\cos^2\alpha)])dt, \end{aligned}$$

$$AF^G_{x_1(t),\alpha,\lambda=0}(\tau,f) = AF_{x(t),\alpha}(\tau, f - f_0^2 t_d cos\alpha) \cdot exp(i\pi[f_0^2 t_d^2 cos\alpha \sin\alpha - 2 f t_d sin\alpha]]), \quad (4.49)$$

where $AF_{x(t),\alpha}$ is the ambiguity function in FrFT domain. Thus, a delay in time translates to the ambiguity function with a changed frequency. *Case 2*: When $\alpha = \frac{\pi}{2}$ and $\lambda = 0$ in Eq. (4.49), then we can get a relationship similar to Fourier transform ambiguity function

$$AF^G_{x_1(t),\alpha=\frac{\pi}{2},\lambda=0}(\tau,f) = AF_{x(t),\frac{\pi}{2}}(\tau,f) e^{-i2\pi f t_d}, \quad (4.50)$$

where $AF_{x(t),\frac{\pi}{2}}(\tau,f)$ is Fourier transform based ambiguity function of signal $x(t)$.

4.4.9 Frequency delay property

If GFAF of $x(t)$ is $AF^{G}_{x(t),\alpha,\lambda}(\tau, f)$, then GFAF of the frequency modulated signal $x_1(t) = x(t)e^{i\omega_d t}$ is given by

$$
\begin{aligned}
AF^{G}_{x_1(t),\alpha,\lambda}(\tau, f) &= \int_{-\infty}^{\infty} x_1(t+\frac{\tau}{2}) x_1^*(t-\frac{\tau}{2}) K_{\alpha,\lambda}(t, f)dt, \\
AF^{G}_{x_1(t),\alpha,\lambda}(\tau, f) &= \int_{-\infty}^{\infty} x(t+\frac{\tau}{2}) e^{i\omega_d(t+\frac{\tau}{2})} x^*(t-\frac{\tau}{2}) e^{-i\omega_d(t-\frac{\tau}{2})} K_{\alpha,\lambda}(t, f)dt, \\
AF^{G}_{x_1(t),\alpha,\lambda}(\tau, f) &= \int_{-\infty}^{\infty} x(t+\frac{\tau}{2}) x^*(t-\frac{\tau}{2}) e^{i\omega_d\tau} K_{\alpha,\lambda}(t, f)dt, \\
AF^{G}_{x_1(t),\alpha,\lambda}(\tau, f) &= e^{i\omega_d\tau} AF^{G}_{x(t),\lambda,\alpha}(\tau, f).
\end{aligned} \tag{4.51}
$$

Case 1 : When $\lambda = 0$ in Eq. (4.51), then we will get a relationship similar to that of a FrFT based AF.

$$
\begin{aligned}
AF^{G}_{x_1(t),\alpha,\lambda=0}(\tau, f) &= \int_{-\infty}^{\infty} x(t+\frac{\tau}{2}) x^*(t-\frac{\tau}{2}) e^{i\omega_d\tau} K_{\alpha}(t, f)dt, \\
&= AF_{x(t),\alpha}(\tau, f) e^{i\omega_d\tau},
\end{aligned}
$$

where $AF_{x(t),\alpha}$ is the ambiguity function in FrFT domain.

Case 2 : When $\lambda = 0$ and $\alpha = \frac{\pi}{2}$ in Eq. (4.51), we get a relationship similar to that of a classical AF.

$$
\begin{aligned}
AF^{G}_{x_1(t),\alpha=\frac{\pi}{2},\lambda=0}(\tau, f) &= \int_{-\infty}^{\infty} x(t+\frac{\tau}{2}) x^*(t-\frac{\tau}{2}) e^{i\omega_d\tau} e^{-i2\pi f t} dt, \\
AF^{G}_{x_1(t),\alpha=\frac{\pi}{2},\lambda=0}(\tau, f) &= AF_{x(t),\frac{\pi}{2}}(\tau, f) e^{i\omega_d\tau},
\end{aligned}
$$

where $AF_{x(t),\frac{\pi}{2}}(\tau, f)$ is the ambiguity function in Fourier domain.

4.4.10 Time scaling property

If ck-GFAF of $x(t)$ is $AF^G_{x(t),\beta,\lambda}(\tau, f)$, then ck-GFAF of $x_1(t) = \sqrt{a}x(at)$ is given by

$$AF^G_{x_1(t),\alpha,\lambda}(\tau, f) = \int_{-\infty}^{\infty} x_1(t + \frac{\tau}{2})x_1^*(t - \frac{\tau}{2})K_{\alpha,\lambda}(t, f)dt,$$

$$= a\int_{-\infty}^{\infty} x(at + \frac{a\tau}{2})x^*(at - \frac{a\tau}{2})K_{\alpha,\lambda}(t, f)dt.$$

Put $t' = at, \quad \implies dt' = adt, \quad and \quad \frac{t'}{a} = t,$

$$AF^G_{x_1(t),\alpha,\lambda}(\tau, f) = \int_{-\infty}^{\infty} x(t' + \frac{a\tau}{2})x^*(t' - \frac{a\tau}{2})K_{\alpha,\lambda}(\frac{t'}{a}, f)dt'.$$

Put $t' = t$ for simplicity and consider $K_{\alpha,\lambda}(t, f)$ as a ck-GTFT kernel

$$AF^G_{x_1(t),\alpha,\lambda}(\tau, f) = \sqrt{1 - i\text{cot}\alpha}\int_{-\infty}^{\infty} x(t + \frac{a\tau}{2})x^*(t - \frac{a\tau}{2})$$
$$exp\left(i\pi\left[\frac{f_0^2t^2\text{cot}\alpha}{a^2} + t_0^2f^2.\text{cot}\alpha - \frac{2t.f.\text{cosec}\alpha}{a} - \frac{\lambda f_0^3t^3}{a^3} + \lambda t_0^3f^3\right]\right)dt,$$

Put $\quad \text{cot}\beta = \frac{\text{cot}\alpha}{a^2} \quad and \quad \frac{\lambda}{a^3} = \gamma_1, \quad \implies \lambda = a^3\gamma_1\ .$

$$AF^G_{x_1(t),\alpha,\lambda}(\tau, f) = \sqrt{1 - i\text{cot}\alpha}\int_{-\infty}^{\infty} x(t + \frac{a\tau}{2})x^*(t - \frac{a\tau}{2}) \cdot exp(i\pi[f_0^2t^2\text{cot}\beta - \gamma_1 f_0^3t^3,$$
$$- \frac{2t.f.\text{cosec}\alpha}{a.\text{cosec}\beta}\text{cosec}\beta + \left(\frac{t_0f.\text{cosec}\alpha}{a.\text{cosec}\beta}\right)^2\text{cot}\beta + \gamma_1.a^3.t_0^3f^3 + t_0^2f^2\text{cot}\alpha$$
$$+ \gamma_1\left(\frac{t_0f\,cosec\alpha}{a.\text{cosec}\beta}\right)^3 - \left(\frac{t_0f.\text{cosec}\alpha}{a.\text{cosec}\beta}\right)^2\text{cot}\beta - \gamma_1\left(\frac{t_0f.\text{cosec}\alpha}{a.\text{cosec}\beta}\right)^3])dt.$$

Put $\quad \frac{f\,cosec\alpha}{\text{cosec}\beta} = f' \quad \implies \quad f = \frac{f'\text{cosec}\beta}{\text{cosec}\alpha}$

$$AF^G_{x_1(t),\alpha,\lambda}(\tau, f) = \sqrt{1 - i\text{cot}\alpha}\int_{-\infty}^{\infty} x(t + \frac{a\tau}{2})x^*(t - \frac{a\tau}{2}) \cdot exp(i\pi[f_0^2t^2\text{cot}\beta - \gamma_1 f_0^3t^3$$
$$- 2t\left(\frac{f'}{a}\right)\text{cosec}\beta + \left(\frac{t_0f'}{a}\right)^2\text{cot}\beta + \gamma_1\left(\frac{t_0f'}{a}\right)^3 - \left(\frac{t_0f'}{a}\right)^2\text{cot}\beta$$
$$+ \gamma_1a^3\left(\frac{t_0f'\text{cosec}\beta}{\text{cosec}\alpha}\right)^3 - \gamma_1\left(\frac{t_0f'}{a}\right)^3 + \left(\frac{t_0f'\text{cosec}\beta}{\text{cosec}\alpha}\right)^2\text{cot}\alpha])dt,$$

$$AF^{G}_{x_1(t),\alpha,\lambda}(\tau,f)=\frac{\sqrt{1-i\cot\alpha}}{\sqrt{1-i\cot\beta}}\int_{-\infty}^{\infty}x(t+\frac{a\tau}{2})x^{*}(t-\frac{a\tau}{2})\cdot exp\left(i\pi\left[-\left(\frac{t_0f'}{a}\right)^2\cot\beta+\right.\right.$$
$$\left.\left.\gamma_1.a^3\left(\frac{t_0f'\mathrm{cosec}\beta}{\mathrm{cosec}\alpha}\right)^3-\gamma_1\left(\frac{t_0f'}{a}\right)^3+\left(\frac{t_0f'\mathrm{cosec}\beta}{\mathrm{cosec}\alpha}\right)^2\cot\alpha\right]\right)K_{\beta,\gamma_1}(t,\frac{f'}{a})dt,$$

$$AF^{G}_{x_1(t),\alpha,\lambda}(\tau,f)=\frac{\sqrt{1-i\cot\alpha}}{\sqrt{1-i\cot\beta}}\int_{-\infty}^{\infty}x(t+\frac{a\tau}{2})x^{*}(t-\frac{a\tau}{2})K_{\beta,\gamma_1}(t,\frac{f'}{a})\cdot exp\left(i\pi\left(\frac{\gamma_1t_0^3f'^3}{a^3}\right.\right.$$
$$\left.\left.\cdot\left[a^6\left(\frac{\mathrm{cosec}\beta}{\mathrm{cosec}\alpha}\right)^3-1\right]+\left(\frac{t_0f'}{a}\right)^2\left[a^2\left(\frac{\mathrm{cosec}\beta}{\mathrm{cosec}\alpha}\right)^2\cot\alpha-\cot\beta\right]\right)\right)dt, \quad (4.52)$$

$$AF^{G}_{x_1(t),\alpha,\lambda}(\tau,f)=C_0(f,\alpha,\lambda,a)\cdot AF^{G}_{x(t),\beta,\lambda}\left(a\tau,\frac{f'}{a}\right), \quad (4.53)$$

where $\cot\beta=\frac{\cot\alpha}{a^2}$, $f'=\frac{fcosec\alpha}{\mathrm{cosec}\beta}$, $\gamma_1=\frac{\lambda}{a^3}$ and

$$C_0(f,\alpha,\lambda,a)=\frac{\sqrt{1-i\cot\alpha}}{\sqrt{1-i\cot\beta}}\cdot exp\left(i\pi\left(\frac{\gamma_1t_0^3f'^3}{a^3}\left[a^6\left(\frac{\mathrm{cosec}\beta}{\mathrm{cosec}\alpha}\right)^3-1\right]+\right.\right.$$
$$\left.\left.\left(\frac{t_0f'}{a}\right)^2\left[a^2\left(\frac{\mathrm{cosec}\beta}{\mathrm{cosec}\alpha}\right)^2\cdot\cot\alpha-\cot\beta\right]\right)\right).$$

Case 1: If $\lambda=0\implies\gamma_1=0$ in equation (4.52), then we get a relationship like that of the FrFT based ambiguity function

$$AF^{G}_{x_1(t),\alpha,\lambda=0}(\tau,f)=\frac{\sqrt{1-i\cot\alpha}}{\sqrt{1-i\cot\beta}}\cdot exp\left(i\pi\left(\frac{t_0f'}{a}\right)^2\left[a^2\left(\frac{\mathrm{cosec}\beta}{\mathrm{cosec}\alpha}\right)^2cot\alpha-\cot\beta\right]\right)$$
$$\left[\int_{-\infty}^{\infty}x(t+\frac{a\tau}{2})x^{*}(t-\frac{a\tau}{2})K_{\beta}(t,\frac{f'}{a})dt\right],$$

where $K_\beta(t,\frac{f'}{a})$ is an FrFT kernel at angle β.

$$AF^{G}_{x_1(t),\alpha,\lambda=0}(\tau,f)=\frac{\sqrt{1-i\cot\alpha}}{\sqrt{1-i\cot\beta}}\cdot exp\left(i\pi\left(\frac{t_0f'}{a}\right)^2\left[a^2\left(\frac{\mathrm{cosec}\beta}{\mathrm{cosec}\alpha}\right)^2cot\alpha-\cot\beta\right]\right)$$
$$AF_{x(t),\beta}(a\tau,\frac{f'}{a}),$$

where $AF_{x(t),\beta}(\tau,f')$ is fractional Fourier transform based ambiguity function at an angle β of signal $x(t)$.

Case 2: When $\alpha=\frac{\pi}{2}$, $\beta=\frac{\pi}{2}$, $\lambda=0$ and $\gamma_1=0$, then the result will be similar to that of a

Fourier transform based AF.

$$AF^{G}_{x_1(t),\alpha=\frac{\pi}{2},\lambda=0}(\tau,f)=\int_{-\infty}^{\infty}x(t+\frac{a\tau}{2})x^{*}(t-\frac{a\tau}{2})\cdot exp\left(-i2\pi\left(\frac{f}{a}\right)t\right)dt,$$

$$AF^{G}_{x_1(t),\alpha=\frac{\pi}{2},\lambda=0}(\tau,f)=AF_{x(t),\frac{\pi}{2}}(a\tau,\frac{f}{a}),$$

where $AF_{x(t),\frac{\pi}{2}}(\tau,f)$ is Fourier transform based ambiguity function of signal $x(t)$.

4.4.11 GFAF in terms of GTFT of signal x(t)

If ck-GFAF of $x(t)$ is $AF^{G}_{x(t),\alpha,\lambda}(\tau,f)$, then ck-GFAF in terms of GTFT is given by

$$AF^{G}_{x(t),\alpha,\lambda}(\tau,f)=\int_{-\infty}^{\infty}x(t+\frac{\tau}{2}).x^{*}(t-\frac{\tau}{2})K_{\alpha,\lambda}(t,f)dt. \tag{4.54}$$

Put $t'=t+\frac{\tau}{2}\implies t=t'-\frac{\tau}{2}$

$$AF^{G}_{x(t),\alpha,\lambda}(\tau,f)=\int_{-\infty}^{\infty}x(t')x^{*}(t'-\tau)K_{\alpha,\lambda}(t'-\frac{\tau}{2},f)dt. \tag{4.55}$$

Put $x(t')=\int_{-\infty}^{\infty}X_{\alpha,\lambda}(f_1)K^{*}_{\alpha,\lambda}(t',f_1)df_1$, where $X_{\alpha,\lambda}(f_1)$ is the GTFT of $x(t')$

$$AF^{G}_{x(t),\alpha,\lambda}(\tau,f)=\iint_{-\infty}^{\infty}X_{\alpha,\lambda}(f_1)K^{*}_{\alpha,\lambda}(t',f_1)x^{*}(t'-\tau)K_{\alpha,\lambda}(t'-\frac{\tau}{2},f)dt'df_1. \tag{4.56}$$

Put $t'-\tau=t''\implies t'=t''+\tau$

$$AF^{G}_{x(t),\alpha,\lambda}(\tau,f)=\iint_{-\infty}^{\infty}X_{\alpha,\lambda}(f_1)K^{*}_{\alpha,\lambda}(t''+\tau,f_1)x^{*}(t'')K_{\alpha,\lambda}(t''+\frac{\tau}{2},f)dt''df_1. \tag{4.57}$$

Put $t''=t$ for simplicity and consider $K_{\alpha,\lambda}(t,f)$ as a ck-GTFT kernel

$$\begin{aligned}AF^{G}_{x(t),\alpha,\lambda}(\tau,f)=|\text{cosec}\alpha|\iint_{-\infty}^{\infty}X_{\alpha,\lambda}(f_1)x^{*}(t)exp(i\pi[&-f_0^2t^2cot\alpha-f_0^2\tau^2cot\alpha\\&-2f_0^2t\tau\text{cot}\alpha+2tf_1\text{cosec}\alpha+2\tau f_1\text{cosec}\alpha-t_0^2f_1^2cot\alpha+f_0^2t^2\text{cot}\alpha\\&+\frac{f_0^2\tau^2}{4}\text{cot}\alpha+f_0^2t\tau\text{cot}\alpha-2tf\text{cosec}\alpha-\tau f\text{cosec}\alpha+t_0^2f^2\text{cot}\alpha\\&+\lambda f_0^3t^3+\lambda f_0^3\tau^3+3\lambda f_0^3t^2\tau+3\lambda f_0^3t\tau^2-\lambda t_0^3f_1^3-\lambda f_0^3t^3-\lambda\frac{f_0^3\tau^3}{8}\\&-\frac{3\lambda f_0^3t^2\tau}{2}-\frac{3\lambda f_0^3t\tau^2}{4}+\lambda t_0^3f^3])dtdf_1,\end{aligned} \tag{4.58}$$

$$= |\text{cosec}\alpha| \iint_{-\infty}^{\infty} X_{\alpha,\lambda}(f_1)x^*(t) \cdot exp(i\pi[f_0^3t^2\left(\frac{3\lambda\tau}{2}\right) - 2t\left(\frac{f_0^2\tau}{2}\text{cot}\alpha - f_1\text{cosec}\alpha\right.$$

$$\left. + f\text{cosec}\alpha - \frac{9\lambda f_0^3\tau^2}{8}\right) + (2\tau f_1\text{cosec}\alpha - t_0^2f_1^2cot\alpha - \tau f\text{cosec}\alpha + t_0^2f^2\text{cot}\alpha \tag{4.59}$$

$$+ \lambda t_0^3f^3 - \lambda t_0^3f_1^3 - \frac{3f_0^2\tau^2cot\alpha}{4} + \frac{7\lambda f_0^3\tau^3}{8})])dtdf_1,$$

Put $\frac{3f_0\lambda\tau}{2} = -\text{cot}\beta \quad and \quad \frac{f_0^2\tau}{2}\text{cot}\alpha - f_1\text{cosec}\alpha + f\text{cosec}\alpha - \frac{9\lambda f_0^3\tau^2}{8} = -f'\text{cosec}\beta,$

$$AF^G_{x(t),\alpha,\lambda}(\tau, f) = |\text{cosec}\alpha| \iint_{-\infty}^{\infty} X_{\alpha,\lambda}(f_1)x^*(t) \cdot exp(i\pi[-f_0^2t^2\text{cot}\beta + 2tf'\text{cosec}\beta - t_0^2f'^2\text{cot}\beta])$$

$$exp(i\pi[t_0^2f'^2\text{cot}\beta - \frac{3f_0^2\tau^2\text{cot}\alpha}{4} + 2\tau f_1\text{cosec}\alpha - t_0^2f_1^2\text{cot}\alpha$$

$$- \tau f\text{cosec}\alpha + t_0^2f^2\text{cot}\alpha + \lambda t_0^3f^3 - \lambda t_0^3f_1^3 + \frac{7\lambda f_0^3\tau^3}{8}])dtdf_1,$$

$$Put \quad X_\beta(f') = \int_{-\infty}^{\infty} x(t)K_{\beta,\lambda=0}(t, f')dt = FrFT \quad of \quad x(t) \quad at \quad angle \quad \beta$$

$$AF^G_{x(t),\alpha,\lambda}(\tau, f) = \frac{|\text{cosec}\alpha|}{\sqrt{1 - i\text{cot}\beta}} \int_{-\infty}^{\infty} X_{\alpha,\lambda}(f_1)X^*_\beta(f') \cdot exp(i\pi[t_0^2f'^2\text{cot}\beta + f_0^2(-\tau^2 + \left(\frac{\tau}{2}\right)^2)\text{cot}\alpha$$

$$-2\tau(f/2 - f_1)\text{cosec}\alpha + t_0^2(f^2 - f_1^2)\text{cot}\alpha - \lambda f_0^3(-\tau^3 + \left(\frac{\tau}{2}\right)^3) + \lambda t_0^3(f^3 - f_1^3)]df_1,$$

$$AF^G_{x(t),\alpha,\lambda}(\tau, f) = \frac{1}{\sqrt{1 - i\text{cot}\beta}} \int_{-\infty}^{\infty} X_{\alpha,\lambda}(f_1)X^*_\beta(f')K^*_{\alpha,\lambda}(\tau, f_1)K_{\alpha,\lambda}(\tau/2, f) \cdot e^{i\pi t_0^2f'^2\text{cot}\beta}df_1, \tag{4.60}$$

where $\frac{3f_0\lambda\tau}{2} = -\text{cot}\beta$ and $f' = \frac{-1}{\text{cosec}\beta}\left[\frac{f_0^2\tau}{2}\text{cot}\alpha - f_1\text{cosec}\alpha + f\text{cosec}\alpha - \frac{9\lambda f_0^3\tau^2}{8}\right]$, and $X_\beta(f')$ is the FrFT of $x(t)$ at angle β.

Case 1: If $\lambda = 0$ then $\beta = \frac{\pi}{2}$ so the GFAF becomes the ambiguity function in fractional Fourier domain.

$$AF^G_{x(t),\alpha,\lambda=0}(\tau, f) = \int_{-\infty}^{\infty} X_{\alpha,\lambda=0}(f_1)X^*_{\frac{\pi}{2}}\left(-\frac{f_0^2\tau}{2}\text{cot}\alpha + f_1\text{cosec}\alpha - f\text{cosec}\alpha\right)K^*_{\alpha,\lambda=0}(\tau, f_1)$$

$$K_{\alpha,\lambda=0}(\tau/2, f)df_1.$$

Case 2: If $\alpha = \frac{\pi}{2}$ and $\lambda = 0$, GFAF is the ambiguity function in Fourier domain i.e,

$$AF^{G}_{x(t),\alpha=\frac{\pi}{2},\lambda=0}(\tau, f) = \int_{-\infty}^{\infty} X_{\frac{\pi}{2}}(f_1) X^{*}_{\frac{\pi}{2}}(f_1 - f) e^{i2\pi\tau(f_1 - \frac{f}{2})} df_1,$$

$$Let \quad f_1 = U + \frac{f}{2},$$

$$\therefore AF^{G}_{x(t),\alpha=\frac{\pi}{2},\lambda=0}(\tau, f) = \int_{-\infty}^{\infty} X_{\frac{\pi}{2}}(U + \frac{f}{2}) X^{*}_{\frac{\pi}{2}}(U - \frac{f}{2}) e^{i2\pi\tau U} dU,$$

where $X_{\frac{\pi}{2}}(\cdot)$ is Fourier transform of signal $x(t)$.

4.4.12 Relationship of GFAF with STFrFT

If ck-GFAF of $x(t)$ is $AF^{G}_{x(t),\alpha,\lambda}(\tau, f)$, then ck-GFAF is related to short time FrFT is given by

$$AF^{G}_{x(t),\alpha,\lambda}(\tau, f) = \int_{-\infty}^{\infty} x(t + \frac{\tau}{2}).x^{*}(t - \frac{\tau}{2}) K_{\alpha,\lambda}(t, f) dt.$$

Put $t + \frac{\tau}{2} \implies t = t' - \frac{\tau}{2}$

$$AF^{G}_{x(t),\alpha,\lambda}(\tau, f) = \int_{-\infty}^{\infty} x(t') x^{*}(t' - \tau) K_{\alpha,\lambda}(t' - \frac{\tau}{2}, f) dt.$$

Put $t' = t$ for simplicity

$$AF^{G}_{x(t),\alpha,\lambda}(\tau, f) = \int_{-\infty}^{\infty} x(t) x^{*}(t - \tau) K_{\alpha,\lambda}(t - \tau + \frac{\tau}{2}, f) dt.$$

Consider $K_{\alpha,\lambda}(t, f)$ as a ck-GTFT kernel

$$= \sqrt{1 - i\cot\alpha} \cdot exp\left(i\pi \left[\frac{-3\tau^2 f_0^2 cot\alpha}{4} + t_0^2 f^2 \cot\alpha + f\tau \operatorname{cosec}\alpha + \lambda t_0^3 f^3 \right.\right.$$
$$\left.\left. - \frac{7\lambda f_0^3 \tau^3}{8} \right] \right) \int_{-\infty}^{\infty} x(t) x^{*}(t - \tau) exp\left(-i\pi\lambda f_0^3 (t - \tau)^3 \right) exp\left(i\pi (t - \tau)^2 f_0^2 \cot\alpha \right)$$
$$exp\left(i\pi \left[\frac{-3\lambda f_0^3 t^2 \tau}{2} - 2t \left[-\frac{\tau f_0^2 \cot\alpha}{2} + f \operatorname{cosec}\alpha - \frac{9\lambda f_0^3 \tau^2}{8} \right] \right] \right) dt,$$

$$= \sqrt{1-i\cot\alpha}\cdot exp\left(i\pi\left[\frac{-3\tau^2 f_0^2 cot\alpha}{4}+t_0^2 f^2\cot\alpha+f\tau\,\mathrm{cosec}\alpha+\lambda t_0^3 f^3\right.\right.$$
$$\left.\left.-\frac{7\lambda f_0^3\tau^3}{8}+\tau^2 f_0^2\cot\alpha\right]\right)\int_{-\infty}^{\infty}x(t)\left[x(t-\tau)\cdot exp\left(i\pi\lambda f_0^3(t-\tau)^3\right)\right]^*$$
$$exp\left[i\pi t^2(f_0^2\cot\alpha-\frac{3\lambda f_0^3\tau}{2})\right]exp\left(-i2\pi t\left[-\frac{\tau f_0^2\cot\alpha}{2}+f\,\mathrm{cosec}\alpha\right.\right.$$
$$\left.\left.-\frac{9\lambda f_0^3\tau^2}{8}+\tau f_0^2\cot\alpha\right]\right)dt, \tag{4.61}$$

$$Put\quad f'\mathrm{cosec}\beta = f\,\mathrm{cosec}\alpha-\frac{9\lambda f_0^3\tau^2}{8}+\frac{f_0^2\tau\cot\alpha}{2},$$
$$f_0^2\cot\beta = f_0^2\cot\alpha-\frac{3\lambda f_0^3\tau}{2},\quad g(t)=x(t)exp\left(i\pi\lambda f_0^3 t^3\right),$$
$$AF^G_{x(t),\alpha,\lambda}(\tau,f)=\frac{\sqrt{1-i\cot\alpha}}{\sqrt{1-i\cot\beta}}\cdot exp\left(i\pi\left[\frac{\tau^2.f_0^2\cot\alpha}{4}+t_0^2f^2\cot\alpha+f\tau\,\mathrm{cosec}\alpha+\lambda t_0^3f^3\right.\right.$$
$$\left.\left.-\frac{7\lambda f_0^3\tau^3}{8}\right]\right)\int_{-\infty}^{\infty}x(t)g^*(t-\tau)K_\beta(t,f')dt\cdot e^{-i\pi t_0^2 f'^2\cot\beta},$$
$$AF^G_{x(t),\alpha,\lambda}(\tau,f)=C_0(\tau,f,\alpha,\lambda)\cdot X^g_\beta(\tau,f'), \tag{4.62}$$

where $X^g_\beta(\tau,f')$ is STFrFT at angle β with window function

$$g(t)=x(t)\cdot exp(i\pi\lambda f_0^3t^3),\ f'=\frac{1}{\mathrm{cosec}\beta}\cdot\left[f\,\mathrm{cosec}\alpha-\frac{9\lambda f_0^3\tau^2}{8}+\frac{f_0^2\tau\cot\alpha}{2}\right]\text{ and}$$
$$C_0(\tau,f,\alpha,\lambda)=\frac{\sqrt{1-i\cot\alpha}}{\sqrt{1-i\cot\beta}}\cdot exp\left(i\pi\left[\frac{\tau^2.f_0^2\cot\alpha}{4}+t_0^2f^2\cot\alpha+f\tau\,\mathrm{cosec}\alpha+\lambda t_0^3f^3\right.\right.$$
$$\left.\left.-\frac{7\lambda f_0^3\tau^3}{8}\right]\right).$$

Put $\lambda=0$, in Eq. (4.61) to get relation of fractional Fourier based AF with STFT

$$AF^G_{x(t),\alpha,\lambda=0}(\tau,f)=\sqrt{1-i\cot\alpha}\cdot exp\left(i\pi\left[\frac{-3\tau^2f_0^2\cot\alpha}{4}+t_0^2f^2\cot\alpha+f\tau\,\mathrm{cosec}\alpha\right]\right)$$
$$\int_{-\infty}^{\infty}x(t)\left[x(t-\tau)exp\left(-i\pi(t-\tau)^2f_0^2\cot\alpha\right)\right]^*$$
$$exp\left(-i2\pi t\left[-\frac{\tau f_0^2\cot\alpha}{2}+f\,\mathrm{cosec}\alpha\right]\right)dt,$$

$$AF^{G}_{x(t),\alpha,\lambda=0}(\tau,f) = C_1(\tau,f,\alpha)\cdot X^{g_1}_{\frac{\pi}{2}}\left(\tau,-\frac{\tau f_0^2\cot\alpha}{2}+f\,\mathrm{cosec}\alpha\right),$$

where $X^{g_1}_{\frac{\pi}{2}}\left(\tau,-\frac{\tau f_0^2\cot\alpha}{2}+f\,\mathrm{cosec}\alpha\right)$ is STFT at angle $\pi/2$ with window function

$$g_1(t,\alpha) = x(t)\cdot exp\left(-i\pi t^2 f_0^2\cot\alpha\right),$$
$$C_1(\tau,f,\alpha) = \sqrt{1-i\cot\alpha}\cdot exp\left(i\pi\left[\frac{-3\tau^2 f_0^2 cot\alpha}{4}+t_0^2 f^2\cot\alpha+f\tau\,\mathrm{cosec}\alpha\right]\right).$$

4.4.13 Moyal property

$$\iint_{-\infty}^{\infty} AF^{G}_{x(t),\alpha,\lambda}(\tau,f)\cdot\left[AF^{G}_{y(t),\alpha,\lambda}(\tau,f)\right]^{*}d\tau df$$
$$= \iint_{-\infty}^{\infty}\left[\int_{-\infty}^{\infty} x(t+\frac{\tau}{2})x^{*}(t-\frac{\tau}{2})K_{\alpha,\lambda}(t,f)dt\right]$$
$$\left[\int_{-\infty}^{\infty} y(t'+\frac{\tau}{2})y^{*}(t'-\frac{\tau}{2})K_{\alpha,\lambda}(t',f)dt'\right]^{*}d\tau df,$$
$$= \iiint_{-\infty}^{\infty} x(t+\frac{\tau}{2}).x^{*}(t-\frac{\tau}{2})y^{*}(t'+\frac{\tau}{2})y(t'-\frac{\tau}{2})$$
$$\int_{-\infty}^{\infty} K_{\alpha,\lambda}(t,f)K^{*}_{\alpha,\lambda}(t',f)df\,d\tau dt dt',$$

$$= \iint_{-\infty}^{\infty} x(t+\frac{\tau}{2}).x^{*}(t-\frac{\tau}{2})y^{*}(t'+\frac{\tau}{2})y(t'-\frac{\tau}{2})$$
$$\int_{-\infty}^{\infty}\delta(t-t')d\tau dt dt',$$

where $\delta(\cdot)$ is impulse function,

$$= \iint_{-\infty}^{\infty} x(t+\frac{\tau}{2}).x^{*}(t-\frac{\tau}{2})y^{*}(t+\frac{\tau}{2})y(t-\frac{\tau}{2})dt d\tau,$$
$$Put\quad u = t-\frac{\tau}{2}\quad\Longrightarrow\quad t = u+\frac{\tau}{2},$$
$$= \left[\int_{-\infty}^{\infty} x(u)y^{*}(u)du\right]^{*}\left[\int_{-\infty}^{\infty} x(u+\tau)y^{*}(u+\tau)d\tau\right].$$

$$
\begin{aligned}
Now \quad put \quad t_1 = u + \tau \quad &\Longrightarrow \quad dt_1 = d\tau, \\
&= \left[\int_{-\infty}^{\infty} x(u)y^*(u)du\right]^* \left[\int_{-\infty}^{\infty} x(t_1)y^*(t_1)dt_1\right], \\
&= \left|\left[\int_{-\infty}^{\infty} x(u)y^*(u)du\right]\right|^2, \\
&= |< x \cdot y >|^2,
\end{aligned}
$$

where $< x \cdot y >$ is the standard inner product of the functions $x(\cdot)$ and $y(\cdot)$. GFAF follows total energy property and total energy of GFAF is equal to total energy of signal. Thus, the inner product of the two AFs can be found conveniently by using the value of inner product of the signals.

4.4.14 Multiplication property

If signals $x(t)$ and $y(t)$ have respective ck-GFAFs $AF^G_{x(t),\alpha,\lambda}(\tau, f_1)$ and $AF^G_{y(t),\alpha,\lambda}(\tau, f_1)$, then a signal $z(t) = x(t)y(t)$ has an ck-GFAF $AF^G_{z(t),\alpha,\lambda}(\tau, f)$ given by

$$
\begin{aligned}
AF^G_{z(t),\alpha,\lambda}(\tau, f) &= \int_{-\infty}^{\infty} z(t + \frac{\tau}{2}).z^*(t - \frac{\tau}{2})K_{\alpha,\lambda}(t, f)dt, \\
AF^G_{z(t),\alpha,\lambda}(\tau, f) &= \int_{-\infty}^{\infty} x(t + \frac{\tau}{2})y(t + \frac{\tau}{2}).x^*(t - \frac{\tau}{2})y^*(t - \frac{\tau}{2})K_{\alpha,\lambda}(t, f)dt, \qquad (4.63)
\end{aligned}
$$

Now,

$$
\begin{aligned}
AF^G_{x(t),\alpha,\lambda}(\tau, f_1) &= \int_{-\infty}^{\infty} x(t + \frac{\tau}{2})x^*(t - \frac{\tau}{2})K_{\alpha,\lambda}(t, f_1)dt, \\
\Longrightarrow \; x(t + \frac{\tau}{2})x^*(t - \frac{\tau}{2}) &= \int_{-\infty}^{\infty} AF^G_{x(t),\alpha,\lambda}(\tau, f_1)K^*_{\alpha,\lambda}(t, f_1)df_1, \qquad (4.64)
\end{aligned}
$$

substituting Eq.(4.64) in Eq. (4.63), we get

$$
AF^G_{z(t),\alpha,\lambda}(\tau, f) = \iint_{-\infty}^{\infty} AF^G_{x(t),\alpha,\lambda}(\tau, f_1)K^*_{\alpha,\lambda}(t, f_1)y(t + \frac{\tau}{2})y^*(t - \frac{\tau}{2})K_{\alpha,\lambda}(t, f)df_1\,dt.
$$

Consider $K_{\alpha,\lambda}(t,f)$ as a ck-GTFT kernel

$$
\begin{aligned}
&= |\text{cosec}\alpha| \iint_{-\infty}^{\infty} \Big[AF^{G}_{x(t),\alpha,\lambda}(\tau, f_1) y(t+\frac{\tau}{2}) y^*(t-\frac{\tau}{2}) \\
&\qquad exp\Big(i\pi \left[-2t\text{cosec}\alpha(f-f_1) + t_0^2 cot\alpha(f^2-f_1^2) + \lambda t_0^3 (f^3-f_1^3) \right] \Big) \Big] df_1 dt, \\
&= |\text{cosec}\alpha| \int_{-\infty}^{\infty} AF^{G}_{x(t),\alpha,\lambda}(\tau, f_1) e^{i\pi[t_0^2 \text{cot}\alpha(f^2-f_1^2)+\lambda t_0^3(f^3-f_1^3)]} df_1 \\
&\qquad \int_{-\infty}^{\infty} y(t+\frac{\tau}{2}) y^*(t-\frac{\tau}{2}) e^{-i2\pi t \text{cosec}\alpha(f-f_1)} dt. \qquad (4.65)
\end{aligned}
$$

Now, as we know that,

$$
\int_{-\infty}^{\infty} y(t+\frac{\tau}{2}) y^*(t-\frac{\tau}{2}) e^{-i2\pi t \text{cosec}\alpha(f-f_1)} dt = AF_{y(t),\frac{\pi}{2}}(\tau, (f-f_1)\text{cosec}\alpha), \qquad (4.66)
$$

where $AF_{y(t),\frac{\pi}{2}}(\tau,(f-f_1)\text{cosec}\alpha)$ is Fourier transform based ambiguity function. After substituting Eq. (4.66) in Eq. (4.65), we get

$$
\begin{aligned}
\implies AF^{G}_{z(t),\alpha,\lambda}(\tau,f) = |\text{cosec}\alpha| \int_{-\infty}^{\infty} [& AF_{x(t),\alpha,\lambda}(\tau,f_1).AF_{y(t),\frac{\pi}{2}}(\tau,(f-f_1)\text{cosec}\alpha) \\
& e^{i\pi[t_0^2 \text{cot}\alpha(f^2-f_1^2)+\lambda t_0^3(f^3-f_1^3)]}] df_1. \qquad (4.67)
\end{aligned}
$$

where $AF_{y(t),\frac{\pi}{2}}(\tau,(f-f_1)\text{cosec}\alpha) = \int_{-\infty}^{\infty} y(t+\frac{\tau}{2}) y^*(t-\frac{\tau}{2}) e^{-i2\pi t \text{cosec}\alpha(f-f_1)} dt$, is Fourier transform based ambiguity function. Thus, the ambiguity function of the multiplication of two signals such as $z(t)$ can be computed in a convenient way by using the ambiguity functions of $x(t)$ and $y(t)$.

When $\lambda = 0$ & $\alpha = 90°$, Eq. (4.67) reduces to FT based ambiguity function

$$
\begin{aligned}
AF^{G}_{z(t),\alpha=\frac{\pi}{2},\lambda=0}(\tau,f) &= \int_{-\infty}^{\infty} AF_{x(t),\frac{\pi}{2}}(\tau,f_1).AF_{y(t),\frac{\pi}{2}}(\tau,(f-f_1)) df_1, \\
&= AF_{x(t),\frac{\pi}{2}}(\tau,f) *_f AF_{y(t),\frac{\pi}{2}}(\tau,f),
\end{aligned}
$$

where $*_f$ is convolution over f.

4.4.15 Time marginal property

The time marginal property of the GFAF can be expressed by

$$AF^{G}_{x(t),\alpha,\lambda}(0,f) = \int_{-\infty}^{\infty} |x(t)|^2 K_{\alpha,\lambda}(t,f)dt. \tag{4.68}$$

4.4.16 Frequency marginality property

The frequency marginal property of the GFAF can be expressed by

$$AF^{G}_{x(t),\alpha,\lambda}(\tau,0) = \int_{-\infty}^{\infty} x(t+\tau/2)x^*(t-\tau/2)K_{\alpha,\lambda}(t,0)dt. \tag{4.69}$$

4.4.17 Cubic phase shift property

If cubic kernel cross generalized fractional ambiguity function of $x(t)$ and $y(t)$ is $AF^{G}_{x(t),y(t),\alpha,\lambda}(\tau,f)$, and it is defined as follows:

$$AF^{G}_{x(t),y(t),\alpha,\lambda}(\tau,f) = \int_{-\infty}^{\infty} x(t+\frac{\tau}{2})y^*(t-\frac{\tau}{2})K_{\alpha,\lambda}(t,f)dt$$

If $y(t) = x(t)\cdot exp\left(i\pi[a_3t^3 + a_2t^2 + a_1t]\right)$, then assuming $-a_3 = f_0^3\lambda$ and $\frac{3a_3\tau}{2} + a_2 = f_0^2 cot\alpha$, $AF^{G}_{x(t),y(t),\alpha,\lambda}(\tau,f)$ is given by

$$AF^{G}_{x(t),y(t),\alpha,\lambda}(\tau,f) = c_0(\tau,f,\alpha,\lambda)\cdot AF_{x(t),\frac{\pi}{2}}\left(\tau, f\,\mathrm{cosec}\alpha + \frac{a_1}{2} + \frac{3\tau^2a_3}{8} - \frac{a_2\tau}{2}\right), \tag{4.70}$$

where $AF_{x(t),\frac{\pi}{2}}(\tau,f)$ is the Fourier transform based ambiguity function and $c_0(\tau,f,\alpha,\lambda) = \sqrt{1-icot\alpha}\cdot exp\left(i\pi\left[\frac{-a_3\tau^3}{8} - \frac{a_2\tau^2}{4} + \frac{a_1\tau}{2} + \lambda t_0^3 f^3 + t_0^2 f^2 cot\alpha\right]\right)$.

Proof:

If cubic kernel cross generalized fractional ambiguity function of $x(t)$ and $y(t)$ is $AF^{G}_{x(t),y(t),\alpha,\lambda}(\tau,f)$, and it is defined as follows

$$AF^{G}_{x(t),y(t),\alpha,\lambda}(\tau,f) = \int_{-\infty}^{\infty} x(t+\frac{\tau}{2})y^*(t-\frac{\tau}{2})K_{\alpha,\lambda}(t,f)dt.$$

If $y(t) = x(t)e^{i\pi(a_3t^3+a_2t^2+a_1t)}$

$$AF^G_{x(t),y(t),\alpha,\lambda}(\tau,f) = \int_{-\infty}^{\infty} x(t+\frac{\tau}{2})x^*(t-\frac{\tau}{2})e^{-i\pi(a_3(t-\frac{\tau}{2})^3+a_2(t-\frac{\tau}{2})^2+a_1(t-\frac{\tau}{2}))}K_{\alpha,\lambda}(t,f)dt.$$

Consider $K_{\alpha,\lambda}(t,f)$ as a ck-GTFT kernel

$$AF^G_{x(t),y(t),\alpha,\lambda}(\tau,f) = \sqrt{1-i\text{cot}\alpha}\int_{-\infty}^{\infty} x(t+\frac{\tau}{2})x^*(t-\frac{\tau}{2})\cdot exp\left(i\pi\left[(-a_3-f_0^3\lambda)t^3 + \left(\frac{3a_3\tau}{2}-a_2+f_0^2\text{cot}\alpha\right)t^2 + \left(-\frac{3\tau^2a_3}{4}+a_2\tau-a_1-2f\text{cosec}\alpha\right)t + \left(\frac{a_3\tau^3}{8}-\frac{a_2\tau^2}{4}+\frac{a_1\tau}{2}+\lambda t_0^3f^3+t_0^2f^2\text{cot}\alpha\right)\right]\right)dt.$$

Assume $-a_3 = f_0^3\lambda$ and $\frac{-3a_3\tau}{2}+a_2 = f_0^2\text{cot}\alpha$ and $c_0(\tau,f,\alpha,\lambda) = \sqrt{1-i\text{cot}\alpha}$
$\cdot\, e^{i\pi\left[\left(\frac{a_3\tau^3}{8}-\frac{a_2\tau^2}{4}+\frac{a_1\tau}{2}+\lambda t_0^3f^3+t_0^2f^2\text{cot}\alpha\right)\right]}$,

$$AF^G_{x(t),y(t),\alpha,\lambda}(\tau,f) = c_0(\tau,f,\alpha,\lambda)\cdot\int_{-\infty}^{\infty} x(t+\frac{\tau}{2})x^*(t-\frac{\tau}{2})\cdot e^{-i2\pi t\left[\frac{3\tau^2a_3}{8}-\frac{a_2\tau}{2}+\frac{a_1}{2}+f\text{cosec}\alpha\right]}dt,$$

$$AF^G_{x(t),y(t),\alpha,\lambda}(\tau,f) = c_0(\tau,f,\alpha,\lambda)\cdot AF_{x(t),\frac{\pi}{2}}\left(\tau, f\text{cosec}\alpha+\frac{a_1}{2}+\frac{3\tau^2a_3}{8}-\frac{a_2\tau}{2}\right),$$

where $AF_{x(t),\frac{\pi}{2}}(\tau,f)$ is Fourier transform based ambiguity function

Now if $x(t) = 1$ and $y(t) = e^{i\pi(a_3t^3+a_2t^2+a_1t)}$, then $y(t)$ is a quadratic frequency modulated signal and cross ambiguity function is defined as follows:

$$AF^G_{x(t),y(t),\alpha,\lambda}(\tau,f) = \int_{-\infty}^{\infty} e^{-i\pi(a_3(t-\frac{\tau}{2})^3+a_2(t-\frac{\tau}{2})^2+a_1(t-\frac{\tau}{2}))}K_{\alpha,\lambda}(t,f)dt,$$

$$= \sqrt{1-i\text{cot}\alpha}\int_{-\infty}^{\infty} exp\left(i\pi\left[\left(-a_3-f_0^3\lambda\right)t^3+\left(\frac{3a_3\tau}{2}-a_2+f_0^2\text{cot}\alpha\right)t^2 + \left(\frac{-3\tau^2a_3}{4}+a_2\tau-a_1-2f\text{cosec}\alpha\right)t + \left(\frac{3a_3\tau^3}{8}-\frac{a_2\tau^2}{4}+\frac{a_1\tau}{2}+\lambda t_0^3f^3+t_0^2f^2\text{cot}\alpha\right)\right]\right)dt.$$

Assume $-a_3 = f_0^3\lambda$ and $\frac{-3a_3\tau}{2}+a_2 = f_0^2\text{cot}\alpha$ and $c_0(\tau,f,\alpha,\lambda) = \sqrt{1-i\text{cot}\alpha}$
$\cdot\, e^{i\pi\left(\frac{3a_3\tau^3}{8}-\frac{a_2\tau^2}{4}+\frac{a_1\tau}{2}+\lambda f^3+f^2\text{cot}\alpha\right)}$.

$$= c_0(\tau, f, \alpha, \lambda) \cdot \int_{-\infty}^{\infty} e^{-2i\pi.t\left(\frac{3a_3\tau^2}{8} - \frac{a_2\tau}{2} + \frac{a_1}{2} + \frac{2f\,\mathrm{cosec}\alpha}{2}\right)} dt,$$

$$= c_0(\tau, f, \alpha, \lambda) \cdot \delta\left(f.\mathrm{cosec}\alpha + \frac{3a_3\tau^2}{8} - \frac{a_2.\tau}{2} + \frac{a_1}{2}\right),$$

$$= \frac{c_0(\tau, f, \alpha, \lambda)}{|\mathrm{cosec}\alpha|} \cdot \delta\left(f + \frac{a_1}{2}\sin\alpha - \frac{a_2\tau.\sin\alpha}{2} + \frac{3\tau^2.a_3.\sin\alpha}{8}\right),$$

where $\delta(\cdot)$ is impulse response. If $\alpha = \pi/2$, then

$$AF^G_{x(t),y(t),\alpha,\lambda}(\tau, f) = c_0(\tau, f, \alpha = \frac{\pi}{2}, \lambda) \cdot \delta\left(f + a_1 - \frac{a_2\tau}{2} + \frac{3\tau^2.a_3}{8}\right),$$

where $c_0(\tau, f, \alpha = \frac{\pi}{2}, \lambda) = e^{i\pi\left[\frac{3a_3\tau^3}{8} - \frac{a_2\tau^2}{4} + \frac{a_1\tau}{2} + \lambda t_0^3 f^3\right]}$.

4.4.18 Computational complexity of digital GFAF

GFAF is the GTFT of the auto-correlation of a signal. The computational requirement of the GTFT for an N length quadratic chirp signal is $O(N\log_2 N)$. With the correlation of the signal added, the digital computational complexity of GFAF becomes $O(N^2\log_2 N)$ [16, 30, 41, 105]. Comparison of computational complexity of different higher order transform are shown in Table (4.1). As shown in Table (4.1), computational complexity of GFAF is lesser than generalized cubic phase function (GCPF), maximum likelihood, and QML estimator for estimating higher order chirp parameters.

Table 4.1: Comparison of computational complexity of different higher order transforms

Higher order transform	**GFAF**	ML	HAF	GCPF	Hybrid CPF-HAF	QML
Computational complexity	$O(N^2\log_2 N)$	$O(N^{P+1})$	$O(PN\log_2 N)$	$O(N^3)$	$O(N^2)$	$O(N^3)$

4.4.19 Property of index additivity of angle for GFAF

The GFAF follows the property of index additivity of angle. Hence, GFAF is computationally efficient, i.e.

$$AF^G_{x(t),\alpha+\beta,\lambda}(\tau, u) = \int_{-\infty}^{+\infty} AF^G_{x(t),\alpha,\lambda}(\tau, f) K_{\beta,\lambda}(f, u) df. \tag{4.71}$$

Proof:

$$AF^{G}_{x(t),\alpha+\beta,\lambda}(\tau,u) = \int_{-\infty}^{+\infty} x(t+\frac{\tau}{2})x^{*}(t-\frac{\tau}{2})K_{\alpha+\beta,\lambda}(t,u)dt,$$

$$\int_{-\infty}^{+\infty} AF^{G}_{x(t),\alpha,\lambda}(\tau,f)K_{\beta,\lambda}(f,u)df = \iint_{-\infty}^{+\infty} x(t+\frac{\tau}{2})x^{*}(t-\frac{\tau}{2})K_{\alpha,\lambda}(t,f)K_{\beta,\lambda}(f,u)dtdf,$$

$$= \int_{-\infty}^{+\infty} x(t+\frac{\tau}{2})x^{*}(t-\frac{\tau}{2}) \int_{-\infty}^{+\infty} \left[K_{\alpha,\lambda}(t,f)K_{\beta,\lambda}(f,u)df\right] dt,$$

Here, equation (4.71) is valid iff

$$K_{\alpha+\beta,\lambda}(t,u) = \int_{-\infty}^{+\infty} K_{\alpha,\lambda}(t,f)K_{\beta,\lambda}(f,u)df. \tag{4.72}$$

Above mentioned equality in Eq. (4.72) is already proved in Eq. (2.12) of chapter 2.

4.5 Uncertainty principle for GFAF

Consider a unit energy signal $x(t)$ and its GTFT $X_{\alpha,\lambda}(\cdot)$. Let τ_{mean} be mean time and f_{mean} be mean frequency of $x(t)$.

$$\int_{-\infty}^{\infty} |x(\tau)|^2 d\tau = 1, \text{ and } \int_{-\infty}^{\infty} |X_{\alpha,\lambda}(f)|^2 df = 1,$$

$$\int_{-\infty}^{\infty} \tau|x(\tau)|^2 d\tau = \tau_{mean}, \text{ and } \int_{-\infty}^{\infty} f|X_{\alpha,\lambda}(f)|^2 df = f_{mean}.$$

Now consider time variance of GFAF is $\sigma^2_{t_{GFAF}}$

$$\sigma^2_{t_{GFAF}} = \iint_{-\infty}^{\infty} (\tau-\tau_{mean})^2 |AF^{G}_{x(t),\alpha,\lambda}(\tau,f)|^2 d\tau df,$$

$$= \int_{-\infty}^{\infty} (\tau-\tau_{mean})^2 \int_{-\infty}^{\infty}\int_{-\infty}^{\infty} x(t+\tau/2)x^{*}(t-\tau/2)$$

$$x^{*}(t'+\tau/2)x(t'-\tau/2).\left[\int_{-\infty}^{\infty} K_{\alpha,\lambda}(t,f)^{*}K_{\alpha,\lambda}(t',f)df\right] dtdt'd\tau,$$

$$= \iint_{-\infty}^{\infty} (\tau-\tau_{mean})^2 |x(t+\tau/2)|^2 |x(t-\tau/2)|^2 d\tau dt.$$

Put $t + \tau/2 = m$, $t - \tau/2 = n$, If $x(t)$ is real and zero mean, then $\tau_{mean} = 0$. Hence, the time-variance is given

$$\sigma^2_{t_{GFAF}} = \iint_{-\infty}^{\infty} (m-n)^2 |x(m)|^2 |x(n)|^2 dmdn = 2\int_{-\infty}^{\infty} m^2 |x(m)|^2 dm. \tag{4.73}$$

Now consider frequency variance of GFAF is $\sigma^2_{f_{GFAF}}$

$$\begin{aligned}
\sigma^2_{f_{GFAF}} &= \iint_{-\infty}^{\infty} (f - f_{mean})^2 |AF^G_{X_{\alpha,\lambda}(u),\alpha,\lambda}(f,\tau)|^2 d\tau df, \\
&= \int_{-\infty}^{\infty} (f - f_{mean})^2 \int_{-\infty}^{\infty} X_{\alpha,\lambda}(u + f/2) X^*_{\alpha,\lambda}(u - f/2) \\
&\qquad \int_{-\infty}^{\infty} X^*_{\alpha,\lambda}(u' + f/2) X_{\alpha,\lambda}(u' - f/2). \left[\int_{-\infty}^{\infty} K_{\alpha,\lambda}(u,\tau)^* K_{\alpha,\lambda}(u',\tau) d\tau \right] du du' df, \\
&= \iint_{-\infty}^{\infty} (f - f_{mean})^2 |X_{\alpha,\lambda}(u + f/2)|^2 |X_{\alpha,\lambda}(u - f/2)|^2 du df.
\end{aligned}$$

Put $u + f/2 = w$, $u - f/2 = v$, If $x(t)$ is real and zero mean, then $f_{mean} = 0$. Hence, the frequency-variance is given

$$\sigma^2_{f_{GFAF}} = \iint_{-\infty}^{\infty} (w-v)^2 |X_{\alpha,\lambda}(w)|^2 |X_{\alpha,\lambda}(v)|^2 dwdv = 2\int_{-\infty}^{\infty} w^2 |X_{\alpha,\lambda}(w)|^2 dw. \tag{4.74}$$

From Eq. (4.73) and Eq. (4.74), square of time bandwidth product (TBP) can be written

$$\sigma^2_{t_{GFAF}} \sigma^2_{f_{GFAF}} = 4\int_{-\infty}^{\infty} m^2 |x(m)|^2 dm \int_{-\infty}^{\infty} w^2 |X_{\alpha,\lambda}(w)|^2 dw = 4 \cdot \sigma^2_{t_{GTFT}} \sigma^2_{f_{GTFT}},$$

where $\sigma^2_{t_{GTFT}}$ is time variance and $\sigma^2_{f_{GTFT}}$ is frequency variance of GFAF and their product is always greater than or equal to $\sin^2 \alpha/4$ [93].

$$\sigma^2_{t_{GFAF}} \cdot \sigma^2_{f_{GFAF}} \geq 4 \cdot \frac{\sin^2 \alpha}{4},$$

$$\therefore \sigma_{t_{GFAF}} \cdot \sigma_{f_{GFAF}} \geq |\sin \alpha|. \tag{4.75}$$

Similarly, we can also derive the uncertainty principle or TBP for generalized fractional Wigner-Ville distribution.

$$\sigma_{t_{GFWVD}} \cdot \sigma_{f_{GFWVD}} \geq \frac{|\sin \alpha|}{4}. \tag{4.76}$$

where $\sigma^2_{t_{GFWVD}}$ and is time variance and $\sigma^2_{f_{GFWVD}}$ is frequency variance of GFWVD.

4.6 Pulsed cubic chirp waveform analysis using ck-GFAF

4.6.1 Mathematical derivation of pulsed cubic chirp waveform analysis using ck-GFAF

Unmatched case

Consider a signal

$$x(t) = A \cdot rect\left(\frac{t}{T}\right) \cdot exp[i\pi(a_1 t + a_2 t^2 + a_3 t^3 + a_4 t^4)]. \tag{4.77}$$

where

$$rect\left(\frac{t}{T}\right) = \begin{cases} 1, & -\frac{T}{2} \leq t \leq \frac{T}{2} \\ 0, & \text{otherwise} \end{cases}$$

Then its instantaneous correlation becomes

$$x(t+\tau/2)x^*(t-\tau/2) = |A|^2 \cdot rect\left(\frac{t}{T-|\tau|}\right) \cdot exp\left[i\pi\left(4a_4\tau t^3 + 3a_3\tau t^2 + (2a_2\tau + a_4\tau^3)t + a_1\tau + \frac{a_3\tau^3}{4}\right)\right],$$

Consider the ck-GTFT kernel given by equation (4.5) taking $h(\lambda, t_0 f) = i\pi\lambda(t_0 f)^3$ and $h(\lambda, f_0 t) = i\pi\lambda(f_0 t)^3$ to be

$$\begin{aligned} K_{\alpha,\lambda}(t,f) = (\sqrt{1 - i.\cot\alpha}) \cdot exp[i\pi(t_0^2 f^2 \cot\alpha + f_0^2 t^2 \cot\alpha - 2ft\,\mathrm{cosec}\alpha \\ + \lambda(t_0 f)^3 - \lambda(f_0 t)^3)]. \end{aligned} \tag{4.78}$$

Then, the GFAF of the signal $x(t)$ becomes

$$\begin{aligned}
AF^{G}_{x(t),\alpha,\lambda}(\tau,f) &= \int_{-\infty}^{\infty} x(t+\tau/2)x^{*}(t-\tau/2)K_{\alpha,\lambda}(t,f)dt, \\
&= |A|^2\sqrt{1-i\text{cot}\alpha}\int_{-\infty}^{\infty} rect\left(\frac{t}{T-|\tau|}\right)\cdot exp[i\pi(4a_4\tau t^3+3a_3\tau t^2 \\
&\quad +(2a_2\tau+a_4\tau^3)t+a_1\tau+\frac{a_3\tau^3}{4}+t_0^2f^2\text{cot}\alpha+f_0^2t^2\text{cot}\alpha \\
&\quad -2ft\text{cosec}\alpha+\lambda(t_0f)^3-\lambda(f_0t)^3)]dt, \\
&= |A|^2\sqrt{1-i\text{cot}\alpha}\int_{-\infty}^{\infty} rect\left(\frac{t}{T-|\tau|}\right)\cdot exp[i\pi((4a_4\tau-f_0^3\lambda)t^3 \\
&\quad +(3a_3\tau+f_0^2\text{cot}\alpha)t^2+(2a_2\tau+a_4\tau^3-2f\text{cosec}\alpha)t \\
&\quad +t_0^2f^2\text{cot}\alpha+\lambda(t_0f)^3+a_1\tau+\frac{a_3\tau^3}{4})]dt.
\end{aligned} \tag{4.79}$$

Assume

$$\begin{aligned}
A_0 &= |A|^2\sqrt{1-i\text{cot}\alpha}, \\
\phi_0(f) &= \pi\left(t_0^2f^2\text{cot}\alpha+\lambda(t_0f)^3+a_1\tau+\frac{a_3\tau^3}{4}\right), \\
c' &= 4a_4\tau-f_0^3\lambda, \\
a' &= 3a_3\tau+f_0^2\text{cot}\alpha, \\
f' &= a_2\tau+\frac{a_4\tau^3}{2}-f\text{cosec}\alpha.
\end{aligned}$$

The GFAF magnitude becomes

$$\left|AF^{G}_{x(t),\alpha,\lambda}(\tau,f)\right| = |A_0||e^{i\phi_0(f)}|\left|\int_{-\infty}^{\infty} rect\left(\frac{t}{T-|\tau|}\right)\cdot exp[i\pi(c't^3+a't^2+2f't)]dt\right|. \tag{4.80}$$

Now, consider the integral

$$I_0 = \int_{-\infty}^{\infty} rect\left(\frac{t}{T-|\tau|}\right)\cdot exp[i\pi(c't^3+a't^2+2f't)]dt, \tag{4.81}$$

where,

$$\begin{aligned}
x(t) &= rect\left(\frac{t}{T-|\tau|}\right), \\
\phi_1(t) &= \pi(c't^3+a't^2+2f't).
\end{aligned}$$

we can use the principle of stationary phase (PSP) to approximate this integral. The stationary points ($t_{1,2}$) are obtained by solving the following equation.

$$\begin{aligned} \phi_1^{'}(t) &= \pi(3c't^2 + 2a't + 2f') = 0, \\ \implies t_{1,2} &= \underbrace{\frac{-a'}{3c'}}_{\alpha_0} \pm \underbrace{\frac{\sqrt{a'^2 - 6c'f'}}{3c'}}_{\beta_0}. \end{aligned} \tag{4.82}$$

At these points, the rate of change of frequency becomes

$$\phi_1''(t) = 6\pi c't + 2\pi a'.$$

$$\therefore \phi_1''(t_1) = 6\pi c'\beta_0, \quad \phi_1''(t_2) = -6\pi c'\beta_0.$$

Therefore, the stationary approximation of I_0 becomes

$$\begin{aligned} I_0 &\approx \sqrt{\frac{\pi}{3\pi c'\beta_0}} e^{i\phi_1(t_1)} e^{i\pi/4} x(t_1) + \sqrt{\frac{-\pi}{3\pi c'\beta_0}} e^{i\phi_1(t_2)} e^{i\pi/4} x(t_2), \\ &= \sqrt{\frac{1}{3c'\beta_0}} e^{i\pi/4} \left[e^{i\phi_1(t_1)} x(t_1) + i e^{i\phi_1(t_2)} x(t_2) \right], \\ &= \sqrt{\frac{1}{3c'\beta_0}} e^{i\pi/4} e^{i\phi_{10}} \left[e^{i\phi_{20}} x(t_1) + i e^{-i\phi_{20}} x(t_2) \right], \end{aligned} \tag{4.83}$$

where

$$\begin{aligned} \phi_{10} &= \pi \left[c'(\alpha_0^3 + 3\alpha_0\beta_0^2) + a'(\alpha_0^2 + \beta_0^2) + 2f^{'}\alpha_0 \right], \\ \phi_{20} &= \pi \left[c'(\beta_0^3 + 3\beta_0\alpha_0^2) + 2a'\alpha_0\beta_0 + 2f^{'}\beta_0 \right]. \\ \phi_1(t_1) &= \phi_{10} + \phi_{20},\ \phi_1(t_2) = \phi_{10} - \phi_{20}. \end{aligned} \tag{4.84}$$

Hence,

$$|I_0| \approx \left| \sqrt{\frac{1}{3c'\beta_0}} e^{i\phi_{10}} \left[e^{i\phi_{20}} x(t_1) + i e^{-i\phi_{20}} x(t_2) \right] \right|. \tag{4.85}$$

Therefore, from equation (4.85), equation (4.80) and substituting β_0, we have

$$\begin{aligned} \left| AF^G_{x(t),\alpha,\lambda}(\tau, f) \right| = \Bigg| \sqrt{\frac{|A|^2 \mathrm{cosec}\alpha}{\sqrt{\left(3a_3\tau + f_0^2\cot\alpha\right)^2 - 6\left(4a_4\tau - f_0^3\lambda\right)\left(a_2\tau + \frac{a_4\tau^3}{2} - f\mathrm{cosec}\alpha\right)}}} \\ \cdot \left[e^{i\phi_{20}} \cdot rect\left(\frac{t_1}{T - |\tau|}\right) + i e^{-i\phi_{20}} \cdot rect\left(\frac{t_2}{T - |\tau|}\right) \right] \Bigg|. \end{aligned}$$

Cubic phase matched case

If $4a_4\tau = f_0^3\lambda$ and $3a_3\tau \neq -f_0^2\cot\alpha$, then

$$AF^G_{x(t),\alpha,\lambda}(\tau,f) = |A|^2\sqrt{1-i\cot\alpha}\int_{-\infty}^{\infty} rect\left(\frac{t}{T-|\tau|}\right)\cdot exp\left[i\pi\left((3a_3\tau + f_0^2\cot\alpha)t^2 + (2a_2\tau + a_4\tau^3 - 2f\,\mathrm{cosec}\alpha)t + t_0^2f^2\cot\alpha + \lambda(t_0f)^3 + a_1\tau + \frac{a_3\tau^3}{4}\right)\right]dt.$$

Let $C_0(\tau,f,\alpha) = 2a_2\tau + a_4\tau^3 - 2f\,\mathrm{cosec}\alpha$ and $C_1(\tau,\alpha) = 3a_3\tau + f_0^2\cot\alpha$.

$$\left|AF^G_{x(t),\alpha,\lambda}(\tau,f)\right| = |A|^2\sqrt{\mathrm{cosec}\alpha}\left|\int_{-\infty}^{\infty} rect\left(\frac{t}{T-|\tau|}\right)\cdot exp\left[i\pi\left(C_1t^2 + C_0t\right)\right]dt\right|.$$

Applying PSP approximation,

$$\left|AF^G_{x(t),\alpha,\lambda}(\tau,f)\right| \approx |A|^2\sqrt{\frac{\mathrm{cosec}\alpha}{C_1}}, \qquad -\frac{T-|\tau|}{2} \leq -\frac{C_0}{2C_1} \leq \frac{T-|\tau|}{2}. \tag{4.86}$$

Cubic and quadratic phase matched case

If $4a_4\tau = f_0^3\lambda$, $3a_3\tau = -f_0^2\cot\alpha$ and $2a_2\tau + a_4\tau^3 \neq 2f\,\mathrm{cosec}\alpha$, then

$$AF^G_{x(t),\alpha,\lambda}(\tau,f) = |A|^2\sqrt{1-i\cot\alpha}\int_{-\infty}^{\infty} rect\left(\frac{t}{T-|\tau|}\right)\cdot exp[i\pi((2a_2\tau + a_4\tau^3 - 2f\,\mathrm{cosec}\alpha)t + t_0^2f^2\cot\alpha + \lambda(t_0f)^3 + a_1\tau + \frac{a_3\tau^3}{4})]dt.$$

$$\left|AF^G_{x(t),\alpha,\lambda}(\tau,f)\right| = |A|^2\sqrt{\mathrm{cosec}\alpha}\int_{-\frac{T-|\tau|}{2}}^{\frac{T-|\tau|}{2}} exp[i\pi(2a_2\tau + a_4\tau^3 - 2f\,\mathrm{cosec}\alpha)t]dt.$$

$$= |A|^2\sqrt{\mathrm{cosec}\alpha}\cdot\frac{exp\left[\frac{i\pi C_0(T-|\tau|)}{2}\right] - exp\left[-\frac{i\pi C_0(T-|\tau|)}{2}\right]}{i\pi C_0},$$

where $C_0(\tau,f,\alpha) = 2a_2\tau + a_4\tau^3 - 2f\,\mathrm{cosec}\alpha$,

$$\left|AF^G_{x(t),\alpha,\lambda}(\tau,f)\right| = 2|A|^2\sqrt{\mathrm{cosec}\alpha}\cdot\frac{\sin\left[\frac{\pi C_0(T-|\tau|)}{2}\right]}{\pi C_0}.$$

$$\left|AF^G_{x(t),\alpha,\lambda}(\tau,f)\right| = 2|A|^2\sqrt{\mathrm{cosec}\alpha}\cdot\frac{\sin\left[\frac{\pi(2a_2\tau+a_4\tau^3-2f\,\mathrm{cosec}\alpha)(T-|\tau|)}{2}\right]}{\pi(2a_2\tau + a_4\tau^3 - 2f\,\mathrm{cosec}\alpha)}, \quad -T \leq \tau \leq T \tag{4.87}$$

From Eq. (4.87), the zero-Doppler response can be given by

$$\left|AF^{G}_{x(t),\alpha,\lambda}(\tau,0)\right| = 2|A|^2\sqrt{\text{cosec}\alpha}\cdot\frac{\sin\left[\frac{\pi(2a_2\tau+a_4\tau^3)(T-|\tau|)}{2}\right]}{\pi(2a_2\tau+a_4\tau^3)}, \qquad -T\le\tau\le T \tag{4.88}$$

With the zero range and zero Doppler responses, we can find range and Doppler resolutions as follows:

From Eq. (4.88), the first zero occurs when

$$T = |\tau| + \frac{2}{2a_2\tau + a_4\tau^3}. \tag{4.89}$$

Hence range resolution $\Delta R = c\tau_0/2$, where τ_0 is the smallest positive root of Eq. (4.89) and 'c' is the velocity of light.

From Eq. (4.87), the zero-delay response is given by

$$\left|AF^{G}_{x(t),\alpha,\lambda}(0,f)\right| = |A|^2\sqrt{\text{cosec}\alpha}\cdot\frac{\sin\left[\pi T f\,\text{cosec}\alpha\right]}{\pi f\,\text{cosec}\alpha}. \tag{4.90}$$

From Eq. (4.90), the first zero occurs when $f = \frac{1}{T\text{cosec}\alpha}$ and hence Doppler resolution $\Delta F_D = \frac{1}{T\text{cosec}\alpha}$.

4.6.2 Waveform analysis using different GFAFs

Multicomponent chirp signal $x(t) = x_1(t) + x_2(t)$ is considered, where

$$x_1(t) = e^{i\pi\left(a_1t+a_2t^2+a_3t^3+a_4t^4\right)}, \qquad -2 \le \text{t} < 2 \text{ (in seconds)} \tag{4.91}$$

$$x_2(t) = e^{i\pi\left(b_1t+b_2t^2+b_3t^3+b_4t^4\right)}, \qquad -2 \le \text{t} < 2 \text{ (in seconds)} \tag{4.92}$$

are two 4^{th} order chirp signals.

Simulations have been done to analyze multicomponent cubic chirp signals and the respective AF plots are obtained by focusing at each individual component and also focusing at both the components. The parameters used for the above simulation are $a_1 = 4$, $a_2 = 4$, $a_3 = 4$, $a_4 = 4$, $\lambda_a = 18.7880$ and $\alpha_a = 0.8087$, for the first component and $b_1 = 20$, $b_2 = 15$, $b_3 = 10$, $b_4 = 5$, $\lambda_b = 20$ and $\alpha_b = -1$ for the second component. Here, α_a, λ_a and α_b, λ_b are the matched ck-GTFT kernel parameters for first and second components respectively. We consider $f_s = 200\ Hz$ as the sampling frequency. At the matched condition, the GFAF should produce an impulse, which can be seen in Fig. 4.1 and Fig. 4.2.

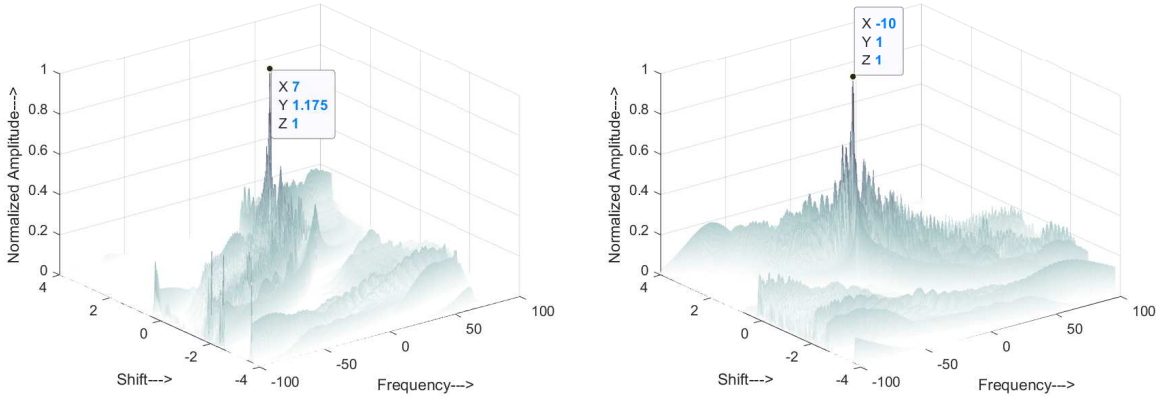

(a) First Component (b) Second Component

Figure 4.1: The cubic kernel GTFT based GFAF plot for multicomponent cubic chirp signal focused at individual components

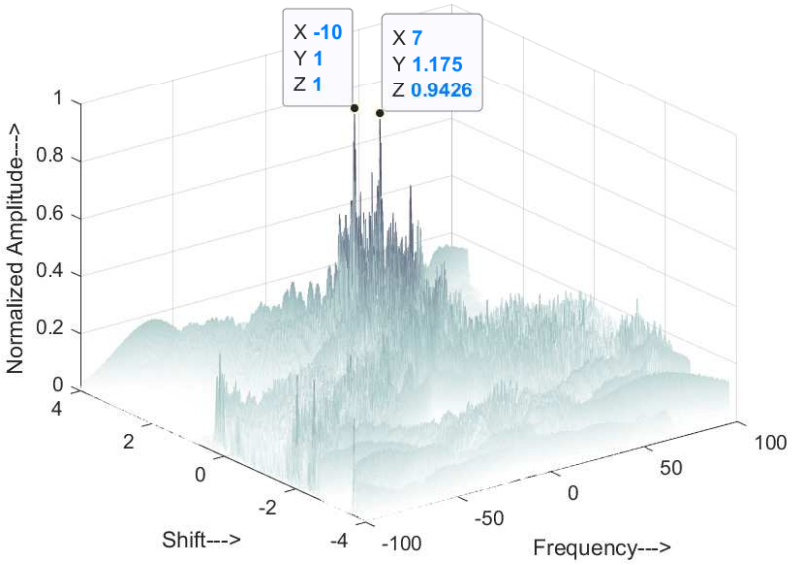

Figure 4.2: The cubic kernel GTFT based GFAF plot for multicomponent cubic chirp signal

4.7 Extraction of 4th order chirp parameters using ck-GFAF

4.7.1 Proposed Method

Consider a signal $x(t) = A_0 \cdot exp\left(i\pi\left[a_1 t + a_2 t^2 + a_3 t^3 + a_4 t^4\right]\right)$. Now its instantaneous correlation is

$$x(t)x^*(t-\tau) = |A_0|^2 \cdot exp\left(i\pi\left[4a_4\tau t^3 + (3a_3\tau - 6a_4\tau^2)t^2 + (2a_2\tau - 3a_3\tau^2 + a_4\tau^3)t\right]\right).$$

Now considering ck-GTFT, the kernel then becomes

$$K_{\alpha,\lambda}(t,f) = (\sqrt{1-icot\alpha}) \cdot exp\Big(i\pi t_0^2 f^2 cot\alpha + i\pi f_0^2 t^2 cot\alpha - i \cdot 2\pi f t \text{cosec}\alpha \\ +i\pi\lambda t_0^3 f^3 - i\pi\lambda f_0^3 t^3\Big). \tag{4.93}$$

Now if the GFAF has to show an impulse in the delay-Doppler domain, two conditions have to be satisfied, so that the cubic and quadratic phase coefficients will be matched to cubic and quadratic phase coefficients of GTFT kernel.

$$4a_4\tau = f_0^3\lambda. \tag{4.94}$$

$$3a_3\tau - 6a_4\tau^2 = -f_0^2 cot\alpha. \tag{4.95}$$

The location on frequency axis of the impulse is given by the following equation

$$2a_2\tau - 3a_3\tau^2 + a_4\tau^3 = 2f\text{cosec}\alpha. \tag{4.96}$$

The method used for estimating the parameters is as follows:

1. Iterate τ over the range $(-T_{max}, T_{max})$, where T_{max} is the length of the signal. Initially rough estimation of λ range $(\lambda_{min}, \lambda_{max})$, and α range $(\alpha_{min}, \alpha_{max})$ can be obtained using STFT estimation. STFT cannot provide excellent parameter estimation due to the dispersive nature of cubic chirp in the Fourier domain.

   (a) Perform fine search for $\alpha \in (\alpha_{min}, \alpha_{max})$, $\lambda \in (\lambda_{min}, \lambda_{max})$, and find optimum $\hat{\alpha}_{opt}$ and optimum $\hat{\lambda}_{opt}$ which gives the maximum peak amplitude of GFAF for each τ.

   (b) Estimate parameters a_4^{est}, a_3^{est} and a_2^{est} using optimum $\hat{\alpha}_{opt}$and optimum $\hat{\lambda}_{opt}$.

   (c) Multiply the signal with $e^{-i\pi(\hat{a_4}^{est}t^4 + \hat{a_3}^{est}t^3 + \hat{a_2}^{est}t^2)}$ which reduces the signal to be of the form $e^{i\pi(a_1 t + err)}$, where err is the error in conjugate multiplication as a result of errors in estimating a_4, a_3 and a_2.

   (d) Find the maximum amplitude (say A_τ) of the Fourier transform of the resultant signal.

2. Repeat step 1(a-d) for all τ.

3. Now, take the τ value which gives the maximum of all A_τ values as τ_{opt} and the corresponding $\hat{\alpha}_{opt}$, $\hat{\lambda}_{opt}$ as α_{opt}^{est}, λ_{opt}^{est}.

4. Finally, the chirp parameters a_4^{est}, a_3^{est},a_2^{est} and a_1^{est} are estimated using α_{opt}^{est}, λ_{opt}^{est} .

4.7.2 Simulation for parameter estimation using GFAF

To demonstrate the effectiveness of ck-GFAF, amplitude modulated cubic chirp x(t) is considered, which is a sum of two amplitude modulated cubic chirps $x_1(t)$ and $x_2(t)$.

$$\begin{aligned} x_1(t) &= exp\Big(i\pi(a_1 t + a_2 t^2 + a_3 t^3 + a_4 t^4)\Big) \qquad -1 \leq \text{t} < 1 \text{ (in seconds)}, \\ x_2(t) &= exp\Big(i\pi(b_1 t + b_2 t^2 + b_3 t^3 + b_4 t^4)\Big) \qquad -1 \leq \text{t} < 1 \text{ (in seconds)}, \end{aligned} \tag{4.97}$$

$$x(t) = 2e^{-0.08t} \cdot x_1(t) + 1.5e^{-0.04t} \cdot x_2(t). \tag{4.98}$$

Simulations have been done to estimate the parameters of a 4^{th} order chirp using GFAF. The GFAF technique has proven to be successful in estimating chirp parameters from signals containing multiple chirps. Here a_4, a_3, a_2 and a_1 are cubic rate, quadratic rate, chirp rate and Doppler frequency of first component of multicomponent cubic chirp. Similarly b_4, b_3, b_2 and b_1 are cubic rate, quadratic rate, chirp rate and Doppler frequency of second component of multicomponent cubic chirp. In the case of multicomponent signals, a good separation of various components present in the signal in the GFAF domain is required for effective parameter estimation.

Short time Fourier transform is used to find a rough estimation of parameters of the multicomponent signal. STFT cannot provide excellent parameter estimation due to the dispersive nature of cubic chirp in the Fourier domain. Parameters estimation of a multicomponent signal is obtained by fine search or focusing near to optimum parameter of individual component in a multicomponent chirp signal. Generally, the cross-terms has a different optimum angle as compared to the optimum angle of auto-terms, so it can not give impulse at GFAF optimum angle α and optimum λ. So the effect of cross-terms can be reduced in GFAF. Parameters estimation of multicomponent cubic frequency modulated signal is presented in Table 4.2.

Table 4.2: Parameter estimation of an amplitude modulated chirp having multiple components

Parameter Values	Chirp parameters							
	a_1	a_2	a_3	a_4	b_1	b_2	b_3	b_4
Actual	4	4	5	4	20	15	10	5
Estimated	4	4.1630	5.0067	3.8097	20	15	10	5

Furthermore, the signal $x_1(t)$ given by Eq. (4.97) is considered to analyze the effect of amplitude modulation in parameter estimation in the presence of noise. It is observed that parameter estimation fails below SNR of -5 dB.

4.8 SNR gain and mean error analysis of ck-GFAF

4.8.1 GFAF SNR gain analysis

Consider a cubic chirp signal $x(t) = A \cdot exp[i\pi(a_1 t + a_2 t^2 + a_3 t^3 + a_4 t^4)]$. The GFAF of the signal $x(t)$ is defined as:

$$\begin{aligned} AF^{G}_{x(t),\alpha,\lambda}(\tau, f) &= \int_{-\infty}^{\infty} x(t+\tau/2)x^*(t-\tau/2)K_{\alpha,\lambda}(t,f)dt, \\ &= |A|^2\sqrt{1-i\cot\alpha}\int_{-\infty}^{\infty} exp[i\pi((4a_4\tau - f_0^3\lambda)t^3 + (3a_3\tau + f_0^2\cot\alpha)t^2 \\ &\quad + (2a_2\tau + a_4\tau^3 - 2f\,\mathrm{cosec}\alpha)t + t_0^2 f^2\cot\alpha + \lambda(t_0 f)^3 \\ &\quad + a_1\tau + \frac{a_3\tau^3}{4})]dt. \end{aligned} \tag{4.99}$$

The approximate analytical expression for the GFAF magnitude spectrum of a signal $x(t)$ denoted by $|AF^{G}_{x(t),\alpha,\lambda}(\tau, f)|^2$, using the stationary phase approximation for unmatched cubic phase condition, where $|2a_2\tau + a_4\tau^3 - 2f\,\mathrm{cosec}(\alpha)| >> 0$ is

$$\begin{aligned} \left|AF^{G}_{x(t),\alpha,\lambda}(\tau, f)\right| \approx 2 \cdot & \sqrt{\frac{|A|^4\mathrm{cosec}\alpha}{\sqrt{\left(3a_3\tau + f_0^2\cot\alpha\right)^2 - 6\left(4a_4\tau - f_0^3\lambda\right)\left(a_2\tau + \frac{a_4\tau^3}{2} - f\,\mathrm{cosec}\alpha\right)}}} \\ & \cos\left(\frac{\pi\sqrt{\left(3a_3\tau + f_0^2\cot\alpha\right)^2 - 6\left(4a_4\tau - f_0^3\lambda\right)(a_2\tau + \frac{a_4\tau^3}{2} - f\,\mathrm{cosec}\alpha)}}{27\left(4a_4\tau - f_0^3\lambda\right)^2}\right. \\ & \left. \cdot\left[12\left(4a_4\tau - f_0^3\lambda\right)(a_2\tau + \frac{a_4\tau^3}{2} - f\,\mathrm{cosec}\alpha) - 2\left(3a_3\tau + f_0^2\cot\alpha\right)^2\right] - \frac{\pi}{4}\right). \end{aligned} \tag{4.100}$$

At GFAF matched condition, ($4a_4\tau = f_0^3\lambda$ and $3a_3\tau = -f_0^2\cot\alpha$) we get an impulse at $f = a_2\tau\sin\alpha + \frac{a_4\tau^3}{2}\sin\alpha$ with area $|A|^2||A_\alpha|$, where $|A_\alpha|$ is the amplitude of GTFT kernel.

SNR gain analysis at GFAF matched condition has been derived as follows, considering input signal $x(t)$ corrupted by additive white Gaussian noise $n(t)$ of variance σ_n^2. SNR of the output signal $y(t) = x(t) + n(t)$ is given by [8, 61, 114, 142]

$$SNR^{GFAF} = \frac{|AF^{G}_{x(t),\alpha,\lambda}(\tau, f)|^2}{Var\left[|AF^{G}_{y(t),\alpha,\lambda}(\tau, f)|\right]}, \tag{4.101}$$

where $|AF^{G}_{x(t),\alpha,\lambda}(\tau, f)|$ is peak modulus of GFAF of the signal $x(t)$ and $Var\left[|AF^{G}_{y(t),\alpha,\lambda}(\tau, f)|\right]$ is variance of the peak of the modulus of GFAF of received signal $y(t)$. It can be expressed as

$$Var\left[|AF^{G}_{y(t),\alpha,\lambda}(\tau, f)|\right] = \mathbb{E}\left[\left|AF^{G}_{y(t),\alpha,\lambda}(\tau, f)\right|^2\right] - \mathbb{E}^2\left[\left|AF^{G}_{y(t),\alpha,\lambda}(\tau, f)\right|\right]. \tag{4.102}$$

Since the signal and noise are uncorrelated and noise is having zero mean,

$$\mathbb{E}\left[\left|AF^{G}_{y(t),\alpha,\lambda}(\tau, f)\right|\right] = \int_{-\infty}^{+\infty} \mathbb{E}\left(\left[x(t+\frac{\tau}{2}) + n(t+\frac{\tau}{2})\right]\left[x^*(t-\frac{\tau}{2}) + n^*(t-\frac{\tau}{2})\right]\right)$$

$$K_{\alpha,\lambda}(t, f)dt.$$

$$\therefore \mathbb{E}\left[\left|AF^{G}_{y(t),\alpha,\lambda}(\tau, f)\right|\right] = |A|^2|A_\alpha|T^2 + \sigma_n^2|A_\alpha|T, \tag{4.103}$$

where T is the time duration of $x(t)$.

Similarly,

$$\mathbb{E}\left[\left|AF^{G}_{y(t),\alpha,\lambda}(\tau, f)\right|^2\right] = \iint_{-\infty}^{+\infty} \mathbb{E}\left(\left[x\left(t_1+\frac{\tau}{2}\right) + n\left(t_1+\frac{\tau}{2}\right)\right]\left[x^*\left(t_1-\frac{\tau}{2}\right) + n^*\left(t_1-\frac{\tau}{2}\right)\right]\right.$$
$$\left.\left[x^*\left(t_2+\frac{\tau}{2}\right) + n^*\left(t_2+\frac{\tau}{2}\right)\right]\left[x\left(t_2-\frac{\tau}{2}\right) + n\left(t_2-\frac{\tau}{2}\right)\right]\right)$$
$$K_{\alpha,\lambda}(t_1, f)K^*_{\alpha,\lambda}(t_2, f)dt_1dt_2.$$

$$\therefore \mathbb{E}\left[\left|AF^{G}_{y(t),\alpha,\lambda}(\tau, f)\right|^2\right] = |A_\alpha|^2\left[|A|^4T^4 + 2T^2\sigma_n^4 + 4T^3|A|^2\sigma_n^2\right]. \tag{4.104}$$

Hence variance is given by

$$Var|AF^{G}_{y(t),\alpha,\lambda}(\tau, f)| = |A_\alpha|^2\left[\sigma_n^4T^2 + 2T^3|A|^2\sigma_n^2\right]. \tag{4.105}$$

Therefore GFAF SNR and SNR gain are given by

$$SNR^{GFAF} = \frac{|A_\alpha|^2|A|^4T^4}{|A_\alpha|^2\left[\sigma_n^4T^2 + 2T^3|A|^2\sigma_n^2\right]} = \frac{T^2SNR_t^2}{2TSNR_t + 1}, \tag{4.106}$$

$$\frac{SNR^{GFAF}}{SNR_t} \approx \frac{T}{2}, \tag{4.107}$$

where SNR_t is input SNR, defined as A^2/σ_n^2. In discrete case, SNR gain is given by

$$\frac{SNR^{GFAF,discrete}}{SNR_t} \approx D\frac{N}{K}, \tag{4.108}$$

where D is a constant, K is the number of components and N is the number of samples during signal pulse time T.

4.8.2 SNR gain simulation

Consider a signal for SNR gain and mean error under different SNR conditions (Monte Carlo simulation) as

$$s(t) = x_1(t) + x_2(t) + n(t), \tag{4.109}$$

where $n(t)$ is an additive white Gaussian noise (AWGN). $x_1(t)$ and $x_2(t)$ are 4^{th} order chirp signals defined by

$$\begin{aligned} x_1(t) &= exp\left(i\pi(4t^4 + 4t^3 + 5t^2 + 4t)\right), \qquad -1 \leq \text{t} < 1 \text{ (in seconds)}, \\ x_2(t) &= exp\left(i\pi(20t^4 + 15t^3 + 10t^2 + 5t)\right), \qquad -1 \leq \text{t} < 1 \text{ (in seconds)}, \end{aligned} \tag{4.110}$$

Monte Carlo simulation for 200 noise realizations has been performed to compare the SNR gain of GFAF and time domain matched filtering for individual cubic chirp components $x_1(t)$ and $x_2(t)$. The search range for the quadratic rate of the kernel (λ) is considered to be (-13.4 : 0.001: -13.42) and (19.99: 0.001: 20.01) for first and second component respectively. Similarly, the search range of GTFT optimum angle (α) is considered (0.7991 : 0.001 : 0.8291) and (-0.99 : 0.001 : -1) for first and second component respectively.

As shown in Fig. 4.3, time domain matched filtering gives the highest SNR in case of additive white Gaussian noise (AWGN), and it is equivalent to N_1, where N_1 is the product of the bandwidth and the pulse width. GFAF is observed to have a lesser SNR gain compared to that of time domain matched filtering but performed better than FrFT based AF and AF.

4.8.3 Mean square error analysis simulation

Monte Carlo simulation for 200 noise realisations has been performed to compare mean square errors in estimating cubic chirp parameters using GFAF of individual quadratic chirp components $x_1(t)$ and $x_2(t)$ as mentioned in Eq. (4.110). The search range of quadratic rate and GTFT optimum angle are considered similar to the search range for SNR gain analysis for first and

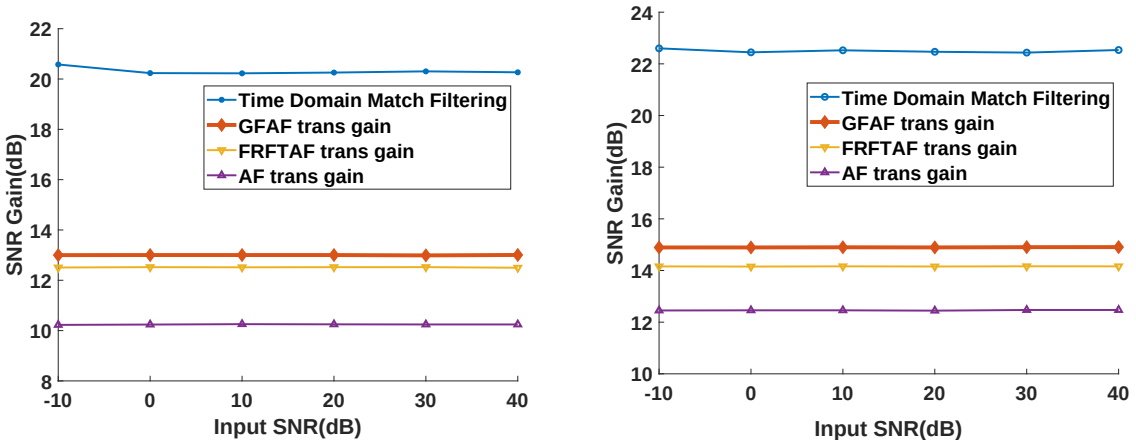

(a) SNR gain comparison of first component

(b) SNR gain comparison of second component

Figure 4.3: Monte Carlo Simulation to estimate the performance of GFAF in SNR gain

second components. Fig. 4.4(a) shows the MSE in the estimation of first component $x_1(t)$ parameters in the presence of second component $x_2(t)$ and AWGN noise $n(t)$. Similarly Fig. 4.4(b) shows the MSE in the estimation of second component $x_2(t)$ parameters in presence of first component $x_1(t)$ and AWGN noise $n(t)$. Finally, as shown in Fig. 4.4 as SNR increases, GFAF does better at parameter estimation and has lesser MSE in the estimations.

GFAF based parameter estimation is a non-linear transform and produces cross-terms during multicomponent chirp signals. So it will not work satisfactorily at low SNR condition in case of multicomponent chirp signals. Furthermore, reduction in cross-terms can be achieved by using the product of different lag GFAF or product-GFAF(PGFAF) during multicomponent polynomial phase signal analysis. Lag of GFAF in PGFAF need to be selected in such a way that it increase the auto-terms amplitude and degrade cross-terms amplitude. Some smoothening filter can be explored to remove cross-terms of GFAF for multicomponent weak or low SNR signals detection.

Many real-world systems' noise, such as radar clutter, radar jamming, and interference, atmospheric noise are non-Gaussian in nature. Many systems produce the wrong results in the presence in non-Gaussian noise. [55, 56, 109, 110]. Sigmoid based fractional Fourier transform, sigmoid based fractional Fourier ambiguity function and sigmoid based fractional Fourier Wigner-Ville distribution are proposed to overcome the effect of impulsive noise in parameter estimation of chirp signal. These sigmoid based transforms do not require any prior knowledge of impulsive noise [55, 56]. Similar to sigmoid based fractional Fourier based ambiguity function, a sigmoid based GFAF and sigmoid based GFWVD approach can be proposed to reduce

the effect of impulse noise on parameter estimation.

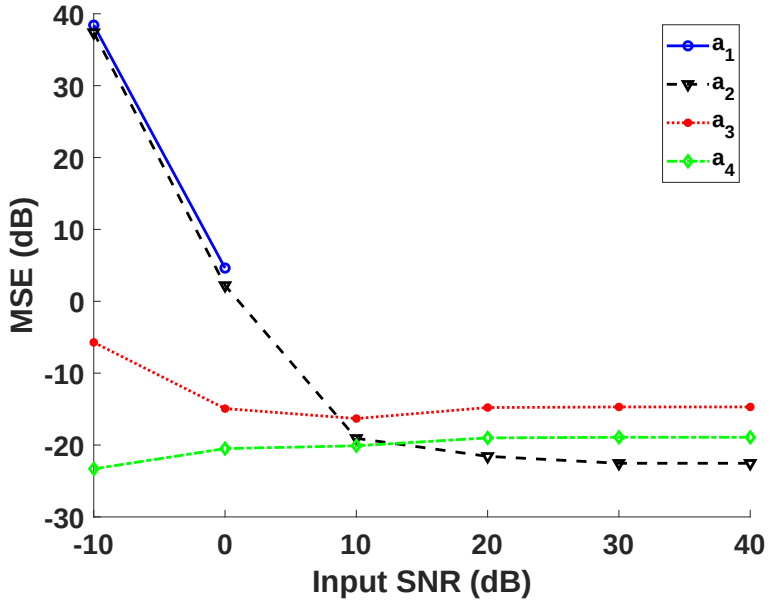

(a) MSE in parameter estimation of first component

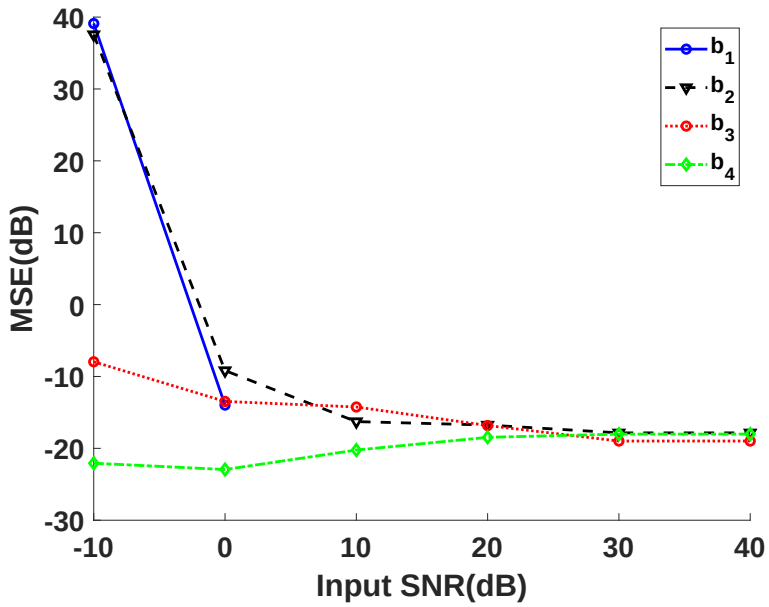

(b) MSE in parameter estimation of second component

Figure 4.4: MSE in parameter estimation for cubic chirps using GFAF

4.8.4 Comparison of MSE in parameter estimation with different transforms

The GFAF method is compared with different estimators such as HAF and Cramer-Rao lower bound (CRLB) [12, 102]. Here, we consider a chirp signal $x(t)$ given by

$$x(t) = exp\left(i\pi(20t^4 + 15t^3 + 10t^2 + 5t)\right), \text{ -1} \leq \text{t} < 1 \text{ (in seconds)}. \tag{4.111}$$

Monte Carlo simulation has been performed for 100 iterations to obtain the MSE in the estimation of the parameters a_3 and a_4 in case of a single component chirp signal. The comparison results are as shown in Fig. 4.5. Each phase differentiation or correlation increases the SNR threshold by approximately 6 dB [12]. GFAF performs only one de-chirping or phase differentiation for estimating the fourth order phase coefficient a_4, whereas HAF performs multiple de-chirpings to estimate the fourth order phase coefficient. As shown in Fig. 4.5(a), GFAF performs better than HAF transform for estimating the higher order phase coefficient a_4. Also, error propagation from higher to lower order phase coefficient a_3 is very less as compared to HAF, due to single de-chirping operation. As opposite to HAF, GFAF estimates more parameters of cubic chirp at ones, so error propagation is less in GFAF. As shown in Fig. 4.5(b), GFAF performs better than HAF transform for estimating the lower order phase coefficient a_3. As shown in both the diagrams in Fig. 4.5, at higher SNR, the GFAF estimated parameters follow CRLB estimated parameters.

A combination of correlation and higher order GTFT kernel in GFAF can be used to analyze any frequency-modulated chirp. As the number of correlation increases, the SNR threshold increases, and as the order of GTFT kernel increases, computational complexity increases. So GFAF gives the flexibility to choose the number of correlations and order of GTFT kernel based on SNR threshold and computational complexity requirement for analyzing any higher order chirp signals. These properties make GFAF superior to other transforms.

In the case of higher order chirp signals with low SNR and very high phase order, GFAF needs to use multiple correlators to reduce computational complexity during parameter estimation. Each correlation increases the SNR threshold by approximately 6 dB and also increases cross-terms. In such a condition, GFAF can not estimate the parameter of low SNR, higher order chirp signals.

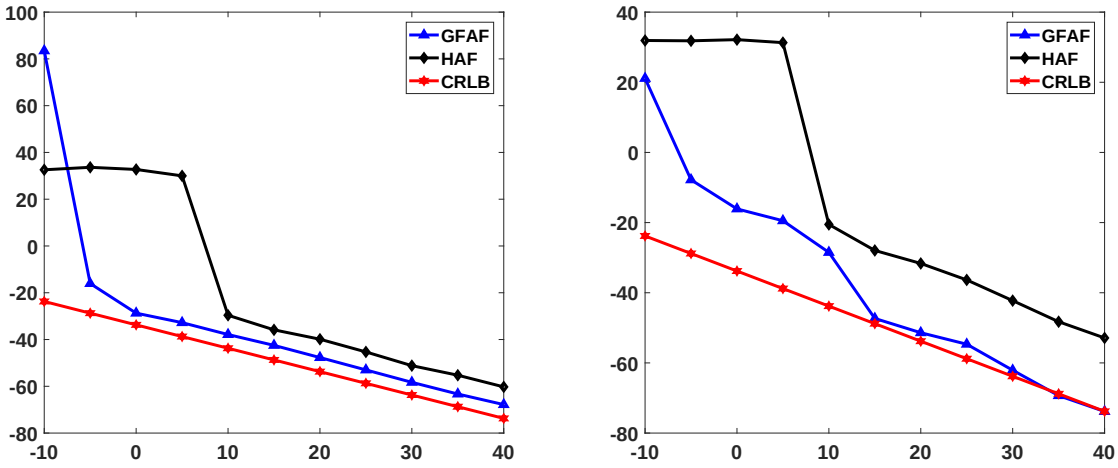

(a) MSE in a_3 parameter estimation

(b) MSE in a_4 parameter estimation

Figure 4.5: Comparison of MSE in parameter estimation with different transforms

4.9 Real multicomponent Bat echolocation signal analysis

The real echolocation signal of a large brown bat [7] is considered to estimate its parameters. It is a multicomponent chirp signal with a sampling frequency of $142,000Hz$ with 400 samples. As mentioned in [18], this signal contains four components at different time-intervals, whose parameters are reported in the Table 4.3 & Table 4.4.

Table 4.3: Parameter estimation of a bat echolocation signal having multiple components of 3^{rd} order

Signal	Sample range	Estimated parameters		
		a_3	a_2	a_1
1^{st} component	1:150	9.9467×10^9	-3.5058×10^7	8.7093×10^4
2^{nd} component	121:280	2.5174×10^9	-1.8906×10^7	9.7625×10^4
3^{rd} component	226:385	-8.7099×10^9	-5.6132×10^6	7.2775×10^4
4^{th} component	141:280	4.1639×10^9	-2.0173×10^7	9.3314×10^4

The parameters of this signal are estimated by focusing on four components of a multi-component bat signal using the algorithm mentioned in section 4.7.2. As shown in Table 4.3, the signal is considered to be a chirp of 3^{rd} order, and FrFT based AF is applied to estimate its parameters. As shown in Table 4.4, the signal is considered to be a chirp of 4^{rd} order, and ck-GFAF is applied to estimate its parameters up to 4^{th} order. For both cases, the estimated parameters for different components until 3^{rd} order are found to be similar.

Table 4.4: Parameter estimation of a bat echolocation signal having multiple components of 4^{th} order

Signal	Sample range	Estimated parameters			
		a_4	a_3	a_2	a_1
1^{st} component	1:150	-5.0493×10^{10}	1.1832×10^{10}	-3.8411×10^{7}	8.8987×10^{4}
2^{nd} component	121:280	8.9772×10^{10}	2.7342×10^{9}	-1.9232×10^{7}	9.7625×10^{4}
3^{rd} component	226:385	6.3435×10^{12}	-1.3906×10^{10}	-5.7777×10^{6}	7.2775×10^{4}
4^{th} component	141:280	-3.7566×10^{11}	4.427×10^{9}	-2.0173×10^{7}	9.3314×10^{4}

4.10 Conclusion

A new kind of AF and WDF based on GTFT to estimate the parameter of higher order chirp signals and to analyze higher order radar waveforms are proposed. GFAF can be used to analyze various waveform properties of higher order chirp signals for its suitability as radar waveform. GFAF and GFWVD can be used to estimate a large variety of multicomponent higher order chirp signals by choosing appropriate $h(\cdot)$ function in GTFT kernel. GFAF follows the property of index additivity of angle (similar to FrFT); hence, GFAF is computationally efficient. The computational complexity of GFAF is lesser than generalized CPF, maximum likelihood, and QML estimator for estimating higher order chirp parameters. GFAF is computationally efficient as compared to the GTFT for estimating the same higher order chirp. But as the chirp order increases, the computational complexity for parameter estimation using GFAF increases. In such cases, a combination of correlation and higher order GTFT kernel in GFAF can be used

to analyze any higher order chirp with reasonable computational complexity. SNR gain of ck-GFAF for multicomponent cubic frequency modulated signal is less than time domain matched filter but is more than that of FrFT based AF and classical AF. At higher SNR, GFAF estimated parameters follow CRLB estimated parameters. GFAF can provide better SNR threshold as compared to HAF, and other multi-lag phase differentiation transforms due to the use of a single de-chirping operation. Ck-GFAF is capable of estimating 4^{th} order parameters of all the four components of the real multicomponent bat signal, and it is comparable with estimated parameters of FrFT based AF. Parameter estimation and waveform analysis of chirp signal using GFAF and GFWVD can be used in applications such as radar, sonar, and biomedical signal processing.

In the future, GFAF application on SAR ground moving target detection and imaging will be explored further and compared with different techniques. GFAF application can be explored for analyzing properties of different waveforms such as hyperbolic chirp and sinusoidal frequency modulated waveform. PGFAF with different lag can be used to reduce the effect of cross-terms during multicomponent signal analysis. Some smoothening filter can be explored to remove cross-terms of GFAF during multicomponent analysis. Sigmoid based GFAF and sigmoid based GFWVD approach can be proposed to reduce the effect of impulse noise on parameter estimation and performance of sigmoid based GFAF, and sigmoid based GFWVD can be compared with GFAF and GFWVD.

Chapter 5

Generalized fractional matched filter and its applications

Time domain matched filtering is a classic method used in radar and sonar applications to maximize signal to noise ratio (SNR) gain, estimate time delay, and improve range resolution. Fractional Fourier transforms, and fractional Fourier transform based matched filtering are used extensively to overcome the drawbacks of time domain matched filtering and are shown to have improved performance for the linear chirp. This chapter presents a generalized time-frequency transform domain based matched filter or generalized fractional matched filtering (GFMF) for estimating higher order chirp parameters. It is shown to provide SNR gain equivalent to time domain matched filtering. A novel method to minimize SNR gain degradation due to the range-Doppler coupling effect of quadratic chirps for a high-speed target using GFMF is presented. The performance of GFMF is compared to a conventional time domain matched filter in case of varying Doppler frequency. Finally, a new waveform named double quadratic chirp is proposed to estimate time delay, velocity, acceleration, and jerk of the moving target simultaneously using GFMF.

5.1 Introduction

Time domain matched filtering correlates a known signal (replica of the transmitted signal) with an unknown signal (received signal) [34]. Time domain matched filter gives the highest SNR gain, improves range resolution, and is useful for estimating time delay of high SNR (strong) as well as low SNR (weak) moving targets in radar and sonar application. However, it gives SNR

gain degradation due to range Doppler coupling effect and is unable to estimate higher order motion parameters.

The fractional Fourier domain matched filter was proposed for linear chirps, and it was shown to perform better than time-domain matched filtering in the presence of chirp noise [53]. FrFT (fractional Fourier transform) and FrFT domain matched filtering also provide better sidelobe suppression as compared to time-domain matched filtering for linear chirps [34, 136, 137]. Matched filter theory for higher order polynomial chirp and its comparison with time-domain matched filtering, and other transforms have not been addressed sufficiently in the existing literature. The first section of this chapter describes GFMF, and its SNR gain is shown to be comparable to time domain matched filtering and shown to provide better SNR gain for higher order chirps. Simulation results are presented to demonstrate the superiority of GFMF with other transforms in the case of a quadratic chirp.

In the case of linear chirps, time-domain matched filtering gives SNR gain degradation due to a significant mismatch between the transmitted and received waveforms. When the Doppler frequency of the received waveform is large with respect to waveform bandwidth, then time-domain matched filtering produces significant degradation in output SNR [66, pp. 803-806]. FrFT performs better than time-domain matched filtering for linear chirps in the presence of Doppler frequency because it depends on the chirp rate [54]. However, GFMF provides better SNR gain as compared to FrFT. The second section of this chapter describes applications of GFMF to solve SNR gain degradation due to the range-Doppler coupling effect in quadratic chirps.

In the case of high-speed targets such as ballistic missiles, the received radar echo is modeled as higher order phase and contains information regarding jerk, acceleration, velocity, and time delay of moving target [28, 46]. So, estimation of the joint parameters from the received radar echo signal is essential. In the case of FrFT or FrFT domain matched filtering, peak shift is a function of time delay and Doppler frequency [67]. Joint estimation of time delay and Doppler frequency was proposed using the sum of two linear chirps transmitting waveform by FrFT domain correlation [71]. FrFT matched filtering, or FrFT domain correlation provides good target detection in case of low SNR, and FrFT domain matched filtering performs over FrFT owing to superior noise performance of FrFT domain matched filtering [1, 71, 125]. However, it cannot be used for detecting higher order motion parameters. The last section of the chapter describes a novel quadratic chirp based radar waveform (sum of two quadratic chirps)

design for joint estimation of jerk, acceleration, velocity, and time delay for weak moving targets using GFMF. Simulations and mathematical derivations are presented to support the proposed approach.

5.2 Preliminaries

5.2.1 Time domain matched filtering

A conventional matched filter or time domain matched filtering is commonly used in radar systems, where the transmitted signal is known. Matched filtering in the radar system involves cross-correlation of a received signal with a known transmitted waveform in the time domain. Match filtering or more commonly known as pulse compression techniques are performed in radar systems to improve the SNR and range resolution. SNR gain of the matched filter is equal to the product of pulse width and bandwidth of the chirp waveform.

5.3 Generalized fractional matched filter

5.3.1 Impulse response and maximum SNR gain of the GFMF

Let $S_{\alpha,\lambda}(f_{\alpha,\lambda})$ represent the GTFT domain power spectral density at (α, λ) for input time domain additive white Gaussian noise (AWGN), where α and λ are parameters of ck-GTFT kernel. GTFT power spectrum is a generalization of the fractional power spectral density [112]. Let $H_{\alpha,\lambda}(f_{\alpha,\lambda})$ be the transfer function of the matched filter in GTFT domain at parameters (α, λ). Output noise power spectral density $S^{op}_{\alpha,\lambda}(f_{\alpha,\lambda})$ at (α, λ) is given by:

$$S^{op}_{\alpha,\lambda}(f_{\alpha,\lambda}) = |H_{\alpha,\lambda}(f_{\alpha,\lambda})|^2 \cdot S_{\alpha,\lambda}(f_{\alpha,\lambda}) \tag{5.1}$$

Thus, total output noise power at $(\alpha, \lambda) = \int_{-\infty}^{+\infty} S^{op}_{\alpha,\lambda}(f_{\alpha,\lambda}) df_{\alpha,\lambda}$.
From conservation of energy along any angle in FrFT (analogous to Parseval's theorem), we have

$$\int_{-\infty}^{+\infty} S^{op}_{\alpha,\lambda}(f_{\alpha,\lambda}) df_{\alpha,\lambda} = \int_{-\infty}^{+\infty} S^{op}_{\alpha+\pi/2,\lambda}(f_{\alpha+\pi/2,\lambda}) df_{\alpha+\pi/2,\lambda}. \tag{5.2}$$

Let $X_{\alpha,\lambda}(f_{\alpha,\lambda}), Y_{\alpha,\lambda}(f_{\alpha,\lambda})$ be the input and the output of the GFMF at parameters (α, λ) respectively.

$$\text{Output SNR of GFMF at } (\alpha, \lambda) = \frac{\text{Peak signal power in GTFT domain at } (\alpha, \lambda)}{\text{Total noise power in GTFT domain at } (\alpha, \lambda)}.$$

The output signal $Y_{\alpha,\lambda}(f_{\alpha,\lambda})$ at (α,λ) is given by $F^{\frac{-\pi}{2}}\left[X_{\alpha+\frac{\pi}{2},\lambda}(f_{\alpha+\frac{\pi}{2},\lambda})\cdot H_{\alpha+\frac{\pi}{2},\lambda}(f_{\alpha+\frac{\pi}{2},\lambda})\right]$, where $F^{\frac{-\pi}{2}}$ is the inverse Fourier transform operator. Assume $\alpha+\pi/2=\beta$, then the output SNR of the GFMF is:

$$= \frac{max\left|\int_{-\infty}^{\infty} X_{\beta,\lambda}(f_{\beta,\lambda})H_{\beta,\lambda}(f_{\beta,\lambda})e^{i2\pi f_{\alpha,\lambda}f_{\beta,\lambda}}df_{\beta,\lambda}\right|^2}{\int_{-\infty}^{\infty} S_{\beta,\lambda}(f_{\beta,\lambda})|H_{\beta,\lambda}(f_{\beta,\lambda})|^2 df_{\beta,\lambda}}, \tag{5.3}$$

where $F^{\frac{-\pi}{2}}$ is the inverse Fourier transform operator. Let numerator is highest at $f_{\alpha,\lambda}=f'_{\alpha,\lambda}$, then output SNR is

$$= \frac{\left|\int_{-\infty}^{\infty} \frac{X_{\beta,\lambda}(f_{\beta,\lambda})\sqrt{S_{\beta,\lambda}(f_{\beta,\lambda})}}{\sqrt{S_{\beta,\lambda}(f_{\beta,\lambda})}}H_{\beta,\lambda}(f_{\beta,\lambda})e^{i2\pi f'_{\alpha,\lambda}f_{\beta,\lambda}}df_{\beta,\lambda}\right|^2}{\int_{-\infty}^{\infty} S_{\beta,\lambda}(f_{\beta,\lambda})|H_{\beta,\lambda}(f_{\beta,\lambda})|^2 df_{\beta,\lambda}}. \tag{5.4}$$

From Cauchy-Schwartz inequality,

$$\begin{aligned} &\leq \left[\frac{\left[\int_{-\infty}^{\infty}\frac{|X_{\beta,\lambda}(f_{\beta,\lambda})|^2}{S_{\beta,\lambda}(f_{\beta,\lambda})}df_{\beta,\lambda}\right]\cdot\left[\int_{-\infty}^{\infty} S_{\beta,\lambda}(f_{\beta,\lambda})|H_{\beta,\lambda}(f_{\beta,\lambda})|^2 df_{\beta,\lambda}\right]}{\int_{-\infty}^{\infty} S_{\beta,\lambda}(f_{\beta,\lambda})|H_{\beta,\lambda}(f_{\beta,\lambda})|^2 df_{\beta,\lambda}}\right], \\ &= \left[\int_{-\infty}^{\infty}\frac{|X_{\beta,\lambda}(f_{\beta,\lambda})|^2}{S_{\beta,\lambda}(f_{\beta,\lambda})}df_{\beta,\lambda}\right]. \end{aligned} \tag{5.5}$$

Equality holds when,

$$\left[\frac{X_{\beta,\lambda}(f_{\beta,\lambda})}{\sqrt{S_{\beta,\lambda}(f_{\beta,\lambda})}}\right]^* = k.\left[\sqrt{S_{\beta,\lambda}(f_{\beta,\lambda})}\cdot H_{\beta,\lambda}(f_{\beta,\lambda})e^{i2\pi f'_{\alpha,\lambda}f_{\beta,\lambda}}\right], \tag{5.6}$$

where k is a real constant and * is the conjugate operator.

$$\implies H_{\beta,\lambda}(f_{\beta,\lambda}) = \frac{X^*_{\beta,\lambda}(f_{\beta,\lambda})\cdot e^{-i2\pi f'_{\alpha,\lambda}f_{\beta,\lambda}}}{k.S_{\beta,\lambda}(f_{\beta,\lambda})}. \tag{5.7}$$

$$\text{Maximum output SNR at } (\alpha,\lambda) = \int_{-\infty}^{\infty}\frac{|X_{\beta,\lambda}(f_{\beta,\lambda})|^2}{S_{\beta,\lambda}(f_{\beta,\lambda})}df_{\beta,\lambda}. \tag{5.8}$$

Let $n(t)$ be AWGN. Then, the GTFT domain power spectral density of $n(t)$ at parameters (β, λ) can be written as

$$\begin{aligned} S_{\beta,\lambda}(f_{\beta,\lambda}) &= E\left[\left|\int n(\tau)K_{\beta,\lambda}(\tau, f_{\beta,\lambda})d\tau\right|^2\right], \\ &= \int\int\int n(\tau_1)n^*(\tau_2)K_{\beta,\lambda}(\tau_1, f_{\beta,\lambda})K^*_{\beta,\lambda}(\tau_2, f_{\beta,\lambda})d\tau_1 d\tau_2 df_{\beta,\lambda}, \\ &= \int\int\int n(\tau_1)n^*(\tau_2)|\text{cosec}\beta|exp[i\pi\text{cot}\beta f_0^2 \cdot (\tau_1^2 - \tau_2^2) \\ &\quad + i2\pi f_{\beta,\lambda}\text{cosec}\beta(\tau_2 - \tau_1) + i \cdot h(\lambda, f_0\tau_2) - i \cdot h(\lambda, f_0\tau_1)]d\tau_1 d\tau_2 df_{\beta,\lambda}. \end{aligned} \tag{5.9}$$

$$S_{\beta,\lambda}(f_{\beta,\lambda}) = \int |n(\tau)|^2 d\tau = \frac{\eta}{2}. \tag{5.10}$$

The above value of input noise power spectrum density at β is substituted in Eq. (5.8) to get the expression for maximum SNR gain of the GTFT matched filter. Considering a unit amplitude signal, we get

$$\begin{aligned} \text{GFMF SNR gain at } (\alpha, \lambda) &= \frac{\text{output SNR at } (\alpha, \lambda)}{\text{input SNR at } (\alpha, \lambda)}, \\ &= \frac{2.\tau/\eta}{2/\eta} = \tau. \end{aligned} \tag{5.11}$$

where τ is pulse width and input SNR at (α, λ) is $\frac{1}{\eta/2}$, so the SNR gain of GFMF at (α, λ) is equal to time domain matched filter, as demonstrated in Eq. (5.11). Now, from Eq. (5.7), impulse response of GFMF is given as:

$$H_{\beta,\lambda}(f_{\beta,\lambda}) = \frac{X^*_{\beta,\lambda}(f_{\beta,\lambda})e^{-i2\pi f'_{\alpha,\lambda} f_{\beta,\lambda}}}{k \cdot \frac{\eta}{2}}, \tag{5.12}$$

$$H_{\alpha,\lambda}(f_{\alpha,\lambda}) = \frac{2X^*_{\alpha,\lambda}(f'_{\alpha,\lambda} - f_{\alpha,\lambda})}{k \cdot \eta}. \tag{5.13}$$

Without loss of generality we can assume $k = 1$ (as k is a proportionality constant) and $f'_{\alpha,\lambda} = 0$. Then, we get

$$H_{\alpha,\lambda}(f_{\alpha,\lambda}) = \frac{2X^*_{\alpha,\lambda}(-f_{\alpha,\lambda})}{\eta}. \tag{5.14}$$

5.3.2 GFMF of pulsed chirp at matched cubic phase condition

As an example, GFMF is presented for quadratic chirp using ck-GTFT kernel. GFMF for higher order chirp can be evaluated by considering higher order polynomial phase GTFT kernel.

ck-GTFT of the transmitted chirp pulse

Consider a quadratic chirp transmission waveform $x^{tr}(t)$ for pulse Doppler radar as:

$$x^{tr}(t) = rect\left(\frac{t}{\tau}\right) e^{ia\pi t^2 + ic\pi t^3}, \tag{5.15}$$

where a is chirp rate and c is quadratic rate. GTFT of transmitted waveform $x(t)$, $X^{tr}_{\alpha,\lambda}(f_{\alpha,\lambda})$ considering a cubic kernel is given by:

$$X^{tr}_{\alpha,\lambda}(f_{\alpha,\lambda}) = (\sqrt{1 - i.\cot\alpha}) \int_{-\infty}^{+\infty} rect\left(\frac{t}{\tau}\right) \cdot exp\big[ia\pi t^2 + ic\pi t^3 + i\pi t_0^2 f_{\alpha,\lambda}^2 \cot\alpha + i\pi f_0^2 t^2 \cot\alpha - i \cdot 2\pi f_{\alpha,\lambda} t \operatorname{cosec}\alpha + i\lambda\pi t_0^3 f_{\alpha,\lambda}^3 - i\lambda\pi t^3 f_0^3\big] dt.$$

Applying principle of stationary phase to the above and at Matched GTFT of cubic phase, $\lambda_{opt} = ct_0^3$, we get

$$\left|X^{tr}_{\alpha,\lambda}(f_{\alpha,\lambda})\right| \approx \sqrt{\frac{1}{a\sin\alpha + f_0^2\cos\alpha}}\, rect\left[\frac{f_{\alpha,\lambda}}{a\tau\sin\alpha + f_0^2\tau\cos\alpha}\right]. \tag{5.16}$$

ck-GTFT of the received pulsed chirp waveform

Received waveform $x^{recv}(t)$ with time delay t_d, positive Doppler f_d, acceleration a_r and jerk parameter J_r, for narrow band signal, considering radar echo model, is given by

$$\begin{aligned} x^{recv}(t) &= x(t - t_d).e^{i2\pi f_d t + i\pi a_r t^2 + i\pi J_r t^3} \\ &= rect\left[\frac{t - t_d}{\tau}\right] e^{ic\pi(t-t_d)^3 + ia\pi(t-t_d)^2} e^{i2\pi f_d t + i\pi a_r t^2 + i\pi J_r t^3}. \end{aligned} \tag{5.17}$$

GTFT of received waveform $x_{recv}(t)$, $X_{recv}(t, f_{\alpha,\lambda})$ is given by:

$$X^{recv}_{\alpha,\lambda}(t, f_{\alpha,\lambda}) = (\sqrt{1 - i.\cot\alpha}) \int_{-\infty}^{+\infty} rect\left[\frac{t - t_d}{\tau}\right] exp\Big[i\pi\Big(c(t-t_d)^3 + a(t-t_d)^2 + 2f_d t + a_r t^2 + J_r t^3 + t_0^2 f_{\alpha,\lambda}^2 \cot\alpha + f_0^2 t^2 \cot\alpha - 2f_{\alpha,\lambda}.t\operatorname{cosec}\alpha + \lambda t_0^3 f_{\alpha,\lambda}^3 - \lambda t^3 f_0^3\Big)\Big] dt.$$

Applying Principle of stationary phase and at Matched GTFT of cubic phase, $\lambda_{opt} = (c + J_r)t_0^3$, we get

$$\left|X^{recv}(f_{\alpha,\lambda})\right| \approx \sqrt{\frac{1}{(a + a_r)\sin\alpha - 3ct_d\sin\alpha + f_0^2\cos\alpha}} .rect\left[\frac{f_{\alpha,\lambda} - f^p_{\alpha,\lambda}}{\tau[(a + a_r)\sin\alpha + f_0^2\cos\alpha - 3ct_d\sin\alpha]}\right], \tag{5.18}$$

where $f^p_{\alpha,\lambda} = f_0^2 t_d\cos\alpha + f_d\sin\alpha - 1.5ct_d^2\sin\alpha + a_r t_d\sin\alpha$.

5.3.3 Envelope correlation in GTFT domain

GTFT of transmit wave at parameters (α, λ_{opt}) is taken from Eq. (5.16), and GTFT of the received wave at parameters (α, λ_{opt}) is taken from Eq. (5.18). In this method, cross correlation of known transmitted waveform and the unknown received waveform is performed, without considering the phase component. Using Eq. (5.16) and Eq. (5.18), Envelope correlation $X^{corr}(\epsilon)$ in GTFT domain at parameters (α, λ_{opt}) can be given as:

$$X^{corr}(\epsilon) = \int_{-\infty}^{\infty} |X^{tr}(f_{\alpha,\lambda} - \epsilon)| \cdot |X^{recv}(f_{\alpha,\lambda})| df_{\alpha,\lambda},$$

$$= \int_{-\infty}^{\infty} \left[\frac{-1}{\sqrt{(a\sin\alpha + f_0^2\cos\alpha).[(a+a_r)\sin\alpha + 3ct_d\sin\alpha + f_0^2\cos\alpha]}} rect\left[\frac{f_{\alpha,\lambda} - \epsilon}{a\tau\sin\alpha + f_0^2\tau\cos\alpha}\right] \cdot rect\left[\frac{f_{\alpha,\lambda} - f^p_{\alpha,\lambda}}{\tau[(a+a_r)\sin\alpha + f_0^2\cos\alpha - 3ct_d\sin\alpha]}\right]\right] df_{\alpha,\lambda}. \tag{5.19}$$

To evaluate the above expression, we consider the following integral:

$$\int_{-\infty}^{\infty} rect\left(\frac{f-\tau}{f_2}\right) \cdot rect\left(\frac{f-f_1}{f_3}\right) df. \tag{5.20}$$

Thus,

$$max(\tau - f_2/2, f_1 - f_3/2) \leq f \leq min(\tau + f_2/2, f_1 + f_3/2), \tag{5.21}$$

Considering 4 cases, we get:

1. Consider the conditions that

$$\tau - f_2/2 \geq f_1 - f_3/2, \tau + f_2/2 \leq f_1 + f_3/2. \tag{5.22}$$

Thus, we get that

$$\tau - f_2/2 \leq f \leq \tau + f_2/2. \tag{5.23}$$

So we get that, in this case,

$$rect\left(\frac{f-\tau}{f_2}\right).rect\left(\frac{f-f_1}{f_3}\right) = rect\left(\frac{f-\tau}{f_2}\right). \tag{5.24}$$

Thus, we get that

$$\int_{-\infty}^{\infty} rect\left(\frac{f-\tau}{f_2}\right) df = f_2. \tag{5.25}$$

This holds for

$$f_1 + f_2/2 - f_3/2 \leq \tau \leq f_1 - f_2/2 + f_3/2. \tag{5.26}$$

2. Consider the conditions that

$$\tau - f_2/2 \leq f_1 - f_3/2, \tau + f_2/2 \leq f_1 + f_3/2. \tag{5.27}$$

Thus, we get that

$$f_1 - f_3/2 \leq f \leq \tau + f_2/2. \tag{5.28}$$

So we get that, in this case,

$$rect\left(\frac{f-\tau}{f_2}\right).rect\left(\frac{f-f_1}{f_3}\right) = rect\left(\frac{f-\tau/2-f_2/4-f_1/2+f_3/4}{\tau-f_1+f_2/2+f_3/2}\right). \tag{5.29}$$

Thus, we get that

$$\int_{-\infty}^{\infty} rect\left(\frac{f-\tau/2-f_2/4-f_1/2+f_3/4}{\tau-f1+f_2/2+f_3/2}\right) df = \tau + f_2/2 - f_1 + f_3/2. \tag{5.30}$$

. This holds for

$$\tau \leq f_1 + f_2/2 - f_3/2, \& \tau \leq f_1 - f_2/2 + f_3/2. \tag{5.31}$$

3. Consider the conditions that

$$\tau - f_2/2 \geq f_1 - f_3/2, \tau + f_2/2 \geq f_1 + f_3/2. \tag{5.32}$$

Thus, we get that

$$\tau - f_2/2 \leq f \leq f_1 + f_3/2. \tag{5.33}$$

So we get that, in this case,

$$rect\left(\frac{f-\tau}{f_2}\right).rect\left(\frac{f-f_1}{f_3}\right) = rect\left(\frac{f-\tau/2-f_1/2+f_2/4-f_3/4}{-\tau+f_1+f_2/2+f_3/2}\right). \tag{5.34}$$

Thus, we get that

$$\int_{-\infty}^{\infty} rect\left(\frac{f-\tau/2-f_1/2+f_2/4-f_3/4}{-\tau+f_1+f_2/2+f_3/2}\right) df = -\tau + f_1 + f_2/2 + f_3/2. \tag{5.35}$$

This holds for

$$\tau \geq f_1 + f_2/2 - f_3/2, \& \tau \geq f_1 - f_2/2 + f_3/2. \tag{5.36}$$

4. Consider the conditions that

$$\tau - f_2/2 \leq f_1 - f_3/2, \tau + f_2/2 \geq f_1 + f_3/2. \tag{5.37}$$

Thus, we get that

$$f_1 - f_3/2 \leq f \leq f_1 + f_3/2. \tag{5.38}$$

So we get that, in this case,

$$rect\left(\frac{f-\tau}{f_2}\right) \cdot rect\left(\frac{f-f_1}{f_3}\right) = rect\left(\frac{f-f_1}{f_3}\right). \tag{5.39}$$

Thus, we get that

$$\int_{-\infty}^{\infty} rect\left(\frac{f-f_1}{f_3}\right) df = f_3. \tag{5.40}$$

This holds for

$$f_1 - f_2/2 + f_3/2 \leq \tau \leq f_1 + f_2/2 - f_3/2. \tag{5.41}$$

The resulting waveform would be a trapezoid. Practically these individual rects would fall off smoothly at the ends. Hence, for the sake of practicality, we take the center of the trapezoid to find the peak shift in frequency. There are a few cases to consider, to find the center of the trapezoid. The maximum is either of f_2 or f_3. Consider these cases:

1. If $f_2 \geq f_3$, then the center point of the trapezium can be taken as :

$$f_1 = f_0^2 \cdot t_d cos\alpha + f_d \cdot \sin\alpha - 1.5c \cdot t_d^2 \sin\alpha + a_r \cdot t_d \sin\alpha. \tag{5.42}$$

2. If $f_3 \geq f_2$, then the center point of the trapezium can be taken as:

$$f_1 = f_0^2 \cdot t_d cos\alpha + f_d \cdot \sin\alpha - 1.5c \cdot t_d^2 \sin\alpha + a_r \cdot t_d \sin\alpha \tag{5.43}$$

Thus, in both cases, we get the same result. Only one of the cases will exist depending on whether $f_2 \geq f_3$ or the opposite. This will also be correspondingly the peak amplitude of the trapezium, multiplied by the constant factor. Resulting waveform would be a trapezoid. The center of the trapezoid can be considered to find peak shift in frequency.

$$\Delta d_{GFMF} = f_0^2 t_d cos\alpha + f_d \sin\alpha - 1.5ct_d^2 \sin\alpha + a_r t_d \sin\alpha, \tag{5.44}$$

Where Δd_{GFMF} is peak shift of output of GFMF.

5.3.4 Dimension normalization in GTFT matched filter output

Matched filtering in ck-GTFT domain of transmitted wave and received wave gives the peak at $(f_d \sin\alpha + f_0^2 \cdot t_d \cos\alpha - 1.5c \cdot t_d^2 \sin\alpha + a_r \cdot t_d \sin\alpha)$.

$$\Delta d_{GFMF} = f_0^2 \cdot t_d cos\alpha + f_d \cdot \sin\alpha - 1.5c \cdot t_d^2 \sin\alpha + a_r \cdot t_d \sin\alpha \tag{5.45}$$

Δd_{GFMF} is the relative distance between transmitted and received waves in GTFT domain. After normalization, the samples are spaced $\frac{1}{\Delta x} = \frac{1}{\sqrt{\Delta t \Delta f}}$ apart in GTFT domain; so to get the actual sample difference, we have to multiply distance Δd_{GFMF} with Δx and t_0. After performing dimensional normalization in GTFT domain, expression of peak shift of output of GFMF can be given by:

$$\begin{aligned}\Delta d_{GFMFnorm} &= \Delta x \Delta d_{GFMF} \cdot t_0, \\ &= \left[\sqrt{T_{max} f_s}\right] \cdot \sqrt{\frac{T_{max}}{f_s}} \left[t_d \cos\alpha \cdot \frac{f_s}{T_{max}} + f_d \sin\alpha - 1.5c \cdot t_d^2 \sin\alpha + a_r \cdot t_d \sin\alpha\right],\end{aligned} \tag{5.46}$$

Where $\Delta d_{GFMFnorm}$ is peak shift of output of GFMF.

$$\Delta d_{GFMFnorm} = f_s t_d \cos\alpha + (f_d - 1.5ct_d^2 + a_r t_d) T_{max} \sin\alpha. \tag{5.47}$$

5.4 Simulation results: SNR gain variation of GTFT domain matched filter for single quadratic chirp

Monte Carlo simulation of 100 iterations has been performed to compare SNR gain of GFMF with SNR gain of time domain matched filtering, FrFT, and GTFT. Fig. 5.1(a) shows SNR gain comparison in the presence of AWGN noise and zero Doppler frequency of quadratic chirp. Similarly, Fig. 5.1(b) shows SNR gain comparison in the presence of AWGN noise and 10Hz Doppler frequency.

As shown in Fig. 5.1(a), SNR gain of GFMF is almost equal to that of time domain matched filtering. This result strengthens our mathematical derivation of the SNR gain of GFMF in Eq. (5.11). GFMF is useful as compared to time domain matched filtering, because it can detect higher order chirp parameters with equivalent SNR gain of time domain matched filtering. However, time domain matched filtering can estimate only time delay. As shown in

Fig. 5.1(b), GFMF gives better performance than time domain matched filtering, FrFT, and GTFT in the presence of non-zero Doppler frequency. SNR gain in the FrFT domain will be almost independent of Doppler frequency because it depends on the chirp rate. So the reduction in SNR gain is not significant in the FrFT domain, but the reduction in SNR gain is higher in time domain matched filtering [54]. The reduction of SNR in time domain happens due to a large mismatch between transmitted and received waveforms [66, pp. 803-806]. Reduction of SNR gain in GTFT domain filtering is less as compared to time domain matched filtering, because SNR gain in GTFT domain is independent of Doppler frequency. GFMF outperforms time domain matched filtering, FrFT, and GTFT in terms of SNR gain and target detectability. The parameters for the simulation are $fd_1 = 0\ Hz$ and $fd_2 = 10\ Hz$, pulse width = 1 sec, SNR

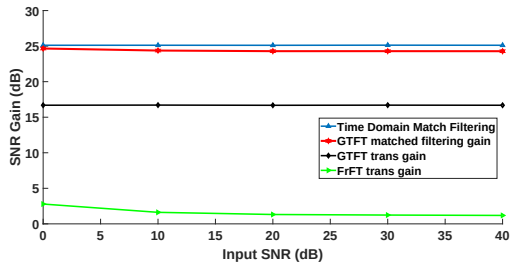

(a) SNR gain comparison at 0 Hz Doppler frequency

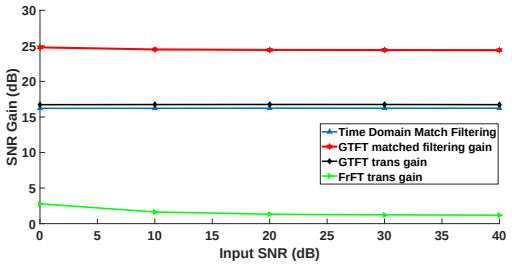

(b) SNR gain comparison at 10 Hz Doppler frequency

Figure 5.1: SNR gain comparison of GTFT domain matched filter

variation = (0:10:40) dB, $f_s = 1000\ Hz$, $T_{max} = 3$ sec, $t_d = 1$ sec, chirp rate = 100 Hz^3, bandwidth = 325 Hz, quadratic rate = 150 Hz^3.

5.5 GFMF applications: range-Doppler coupling effect

In this section, Monte Carlo simulation of 100 iterations has been performed to compare the effects of Doppler variation on performance in time domain matched filtering and GFMF.

5.5.1 Effect on SNR gain due to varying Doppler frequency

SNR gain decreases with an increase in Doppler frequency in time domain matched filtering. Simulation results of SNR gain with respect to Doppler frequency are shown in Fig. (5.2). SNR gain in the GFMF also reduces with an increase in Doppler frequency, but the reduction in

SNR gain is significantly higher in conventional or time domain matched filtering. Reduction in SNR gain is observed in the time domain due to the large mismatch between transmitted and received waveform. The reduction of SNR gain in GFMF is less compared to that of time domain matched filtering because peak amplitude depends on α and λ of GTFT kernel and is independent of Doppler frequency. GFMF gives better target SNR gain and detectability as compared to time domain matched filtering for the same Doppler frequency variation.

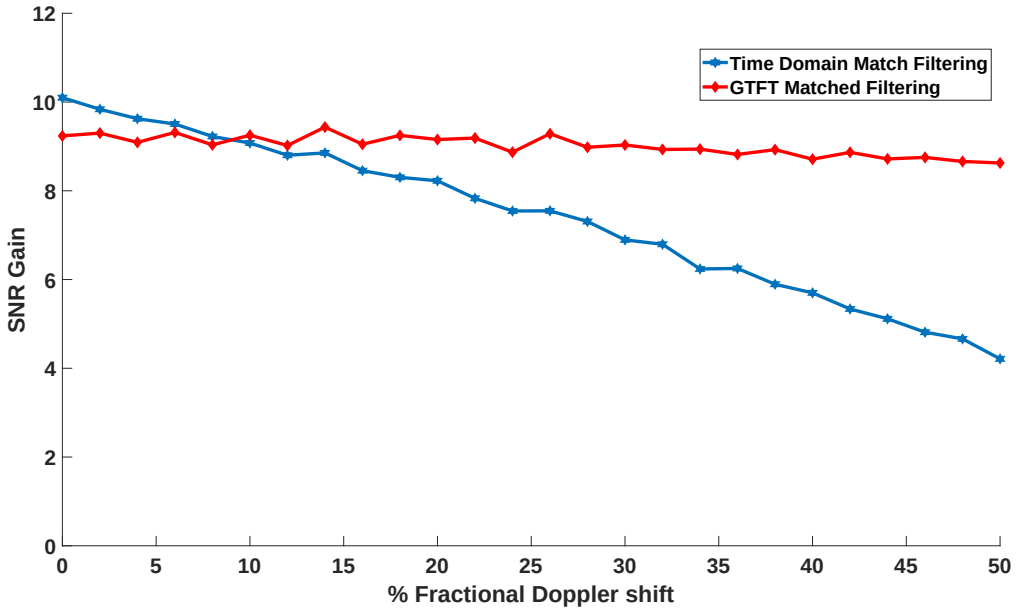

Figure 5.2: SNR gain variation w.r.t percentage fractional Doppler shift

The simulation is shown in Fig. (5.2) compares the SNR of matched filters in both domains. In the simulation, Doppler frequency is varied in the percentage of signal bandwidth, and it is denoted as a percentage fractional Doppler shift. Parameters selected for simulation are as follows: pulse width = 0.1ms, sampling frequency = 500,750 Hz, Doppler shift is varying from 0 to 50 percentage of signal bandwidth, bandwidth = 100,150 Hz and target range = 15,000 km.

5.6 GFMF applications: Double quadratic chirp

5.6.1 Mathematical derivation for joint estimation of velocity, acceleration, time delay using double quadratic chirp

The transmitted signal x^{tr} is a double quadratic chirp and is given by:

$$x^{tr}(t) = rect\left(\frac{t}{\tau}\right).[e^{ic_1\pi t^3+ia_1\pi t^2} + e^{ic_2\pi t^3+ia_2\pi t^2}], \tag{5.48}$$

Then, the received signal $x^{recv}(t)$ is given by:

$$\begin{aligned} x^{recv}(t) &= x(t-t_d).e^{i2\pi f_d t+i\pi a_r t^2+i\pi J_r t^3} \\ &= rect\left[\frac{t-t_d}{\tau}\right].\left[e^{ic_1\pi(t-t_d)^3+ia_1\pi(t-t_d)^2} + e^{i.c_2\pi(t-t_d)^3+ia_2\pi(t-t_d)^2}\right] \\ &\quad \cdot e^{i2\pi f_d\pi t+i\pi a_r t^2+i\pi J_r t^3}, \end{aligned} \tag{5.49}$$

where a_r is radial acceleration, t_d is time delay, f_d is Doppler frequency and J_r is radial jerk of the moving target. Now, applying GTFT we get:

$$X^{recv}_{\alpha,\lambda}(t,f) = \int_{-\infty}^{+\infty} K_{\alpha,\lambda}(t,f)x_r(t)dt,$$

Here $K_{\alpha,\lambda}(t,f)$ is kernel of GTFT and it is defined as shown in Eq. (5.50) [6-7]

$$K_{\alpha,\lambda}(t,f) = A_\alpha \cdot exp[i\pi t_0^2 f^2\cot\alpha + i\pi f_0^2 t^2\cot\alpha - i\cdot 2\pi ft\,\mathrm{cosec}\alpha + i\lambda\pi t_0^3 f^3 - i\lambda\pi t^3 f_0^3],$$

where $A_\alpha = \sqrt{1-icot\alpha}$. Hence,

$$\begin{aligned} X^{recv}_{\alpha,\lambda}(t,f) = \int_{-\infty}^{+\infty} & rect\left[\frac{t-t_d}{\tau}\right]\left[e^{ic_1\pi(t-t_d)^3+ia_1\pi(t-t_d)^2} + e^{ic_2\pi(t-t_d)^3+ia_2\pi(t-t_d)^2}\right] \\ & \cdot e^{i2\pi f_d t+i\pi a_r t^2+i\pi J_r t^3} K_{\alpha,\lambda}(t,f)dt, \end{aligned} \tag{5.50}$$

If $\lambda f_0^3 = c + J_r$, the cubic phase term is zeroed out. Thus, we get:

$$\begin{aligned} = A_\alpha \int_{-\infty}^{+\infty} & rect\left[\frac{t-t_d}{\tau}\right] exp\Big[i\pi[\cancel{ct^3} - ct_d^3 - 3ct^2t_d + 3ctt_d^2 + at^2 + at_d^2 - 2att_d + 2f_d t \\ & + a_r t^2 + \cancel{J_r t^3} + t_0^2 f^2\cot\alpha + f_0^2 t^2\cot\alpha - 2ft\,\mathrm{cosec}\alpha + \lambda t_0^3 f^3 - \cancel{\lambda t^3 f_0^3}\Big] dt. \end{aligned} \tag{5.51}$$

Thus, optimum λ (for each wave) is obtained through the cubic matching condition :

$$\lambda = \frac{c+J_r}{f_0^3} = \frac{(c+J_r).T_{max}^{3/2}}{f_s^{3/2}}. \tag{5.52}$$

Equations of optimum λ_1 and λ_2 corresponding to first and the second chirp are given by:

$$\lambda_1 = \frac{c_1 + J_r}{f_0^3} = \frac{(c_1 + J_r)T_{max}^{3/2}}{f_s^{3/2}}, \tag{5.53}$$

$$\lambda_2 = \frac{c_2 + J_r}{f_0^3} = \frac{(c_2 + J_r)T_{max}^{3/2}}{f_s^{3/2}}. \tag{5.54}$$

Optimum GTFT angle (obtained using quadratic chirp matching at optimum α):

$$\tan\alpha_1 = \frac{f_s}{T_{max}[3c_1t_d - (a_1 + a_r)]}, \tag{5.55}$$

Similarly,

$$\tan\alpha_2 = \frac{f_s}{T_{max}[3c_2t_d - (a_2 + a_r)]}. \tag{5.56}$$

Thus, we can calculate a_r from Eq. (5.55) and Eq. (5.56).

The two cubic frequency modulated waveform are considered and Eq. (5.57) and Eq. (5.58) can be obtained from Eq. (5.47) at two different optimum angle α_1, α_2 and matched λ_1, λ_2

$$\Delta d_{1GTFT} = f_s t_d \cos\alpha_1 + (f_d + a_r t_d - 1.5c_1 t_d^2)T_{max}\sin\alpha_1, \tag{5.57}$$

$$\Delta d_{2GTFT} = f_s t_d \cos\alpha_2 + (f_d + a_r t_d - 1.5c_2 t_d^2)T_{max}\sin\alpha_2. \tag{5.58}$$

f_d and t_d can be calculated from the above two equations, Eq. (5.57) and Eq. (5.58) with the use of estimated jerk and estimated acceleration parameter.

As we had 6 equations and 4 unknowns, then mean of the estimated parameters obtained by the separate equations from each quadratic chirp can be taken to reduce the parameter estimation error.

Case 1: a = 0, only cubic term in transmitted chirp is non zero.

$$\tan\alpha = \frac{f_s}{T_{max}[3ct_d - (a_r)]} \tag{5.59}$$

If a_r is zero,

$$\tan\alpha = \frac{f_s}{T_{max}[3ct_d]} \tag{5.60}$$

Eq. (5.60) holds if $a_r = 0$; i.e, α depends on cubic rate and time delay.

Case 2: $a_r = 0, a \neq 0, c \neq 0$:

$$\tan\alpha = \frac{f_s}{T_{max}[3ct_d - (a)]} \tag{5.61}$$

If 'c' is of the same order as 'a'

$$\tan\alpha = \frac{f_s}{T_{max}[(3t_d - 1)a]} = \frac{f_s\tau}{BT_{max}(3t_d - 1)} \tag{5.62}$$

So as t_d increases, α decreases.

Case 3: $a_r = 0, a \neq 0, c = 0$:

$$\tan\alpha = \frac{f_s\tau}{T_{max}B} \tag{5.63}$$

5.6.2 Double quadratic chirp waveform: Estimation error

As we have two equations to estimate J_r, we use both of them. This minimizes the error in estimating J_r due to errors in estimating λ_1 and λ_2 . Thus, we have

$$J_r = \frac{(\lambda_1 + \lambda_2) \cdot f_o^3 - (c_1 + c_2)}{2} \tag{5.64}$$

The error in estimating J_r is calculated by considering errors in the estimated parameters i.e λ_1 and λ_2.

$$\delta J_r = \frac{(\delta\lambda_1 + \delta\lambda_2) \cdot f_o^3}{2} \tag{5.65}$$

Variance of the parameter is an accurate error estimation metric. Assuming errors in λ are Gaussian random variables $N(0, \sigma^2)$, variance in J_r is calculated as:

$$var(J_r) = \frac{\sigma^2 \cdot f_o^6}{2} \tag{5.66}$$

We can calculate a_r and t_d from Eq. (5.55) or from Eq. (5.56). Thus, we get,

$$t_d = \frac{(\cot\alpha_1 - \cot\alpha_2) \cdot f_o^2 + (a_1 - a_2)}{3 \cdot (c_1 - c_2)} \tag{5.67}$$

Error in t_d depends on the estimation errors of α_1 and α_2. Assuming they are $N(0, \sigma^2)$ random variables, we get

$$var(t_d) = \frac{(\mathrm{cosec}^4\alpha_2 + \mathrm{cosec}^4\alpha_1) \cdot \sigma^2 \cdot f_o^4}{9 \cdot (c_1 - c_2)^2} \tag{5.68}$$

Similarly, we get,

$$a_r = \frac{(c_2 \cdot \cot\alpha_1 - c_1 \cdot \cot\alpha_2) \cdot f_o^2 + (a_1 \cdot c_2 - a_2 \cdot c_1)}{(c_1 - c_2)} \tag{5.69}$$

And thus the error in a_r is

$$var(a_r) = \frac{(c_1^2 \cdot \text{cosec}^4\alpha_2 + c_2^2 \cdot \text{cosec}^4\alpha_1) \cdot \sigma^2 \cdot f_o^4}{(c_1 - c_2)^2} \tag{5.70}$$

The variance in f_d can also be calculated along similar lines. Assuming error in t_d, a_r is negligible (for simplicity of calculation) while calculating variance in f_d, we obtain

$$var(f_d) = \frac{\sigma^2 \cdot (\text{cosec}^2\alpha_1 + \text{cosec}^2\alpha_2 + u_1^2 \cdot \text{cosec}^2\alpha_1 \cdot \cot^2\alpha_1 + u_2^2 \cdot \text{cosec}^2\alpha_2 \cdot \cot^2\alpha_2)}{(2 \cdot T_{max})^2} + \frac{f_s^2 \cdot (\cot\alpha_1 + \cot\alpha_2)^2 + \sigma^2 \cdot (f_s^2 \cdot t_d^2(\text{cosec}^4\alpha_1 + \text{cosec}^4\alpha_2))}{(2 \cdot T_{max})^2} \tag{5.71}$$

Thus, it is observed from Eq.(5.71), that the calculated error expressions, will be minimum, when the optimum fractional Fourier angles (α_1 and α_2) will be near to $\pm 90^0$.

5.6.3 Mean square estimation simulation: double quadratic chirp

Results of a Monte Carlo simulation of 100 iterations for mean square estimation (MSE) of a single target's time delay (t_d) of $1sec$, Doppler frequency (f_d) of $10Hz$, jerk (J_r) of $2Hz^3$ and acceleration (a_r) of $5Hz^2$ using a double quadratic chirp are presented in Fig. (5.3). Here, the double quadratic chirp $x(t) = rect(\frac{t}{\tau})[e^{i(-20)\pi t^3 + i(-110)\pi t^2} + e^{i20\pi t^3 + i100\pi t^2}]$, is considered as the transmitting waveform with pulse width of $1sec$. Input SNR is varied from -15 dB to 9 dB. Assuming estimation errors in $\alpha_1, \alpha_2, \lambda_1, \lambda_2, u_1, u_2$ to be independent and identical random variables with variance σ^2, the optimum fractional Fourier angles (α_1 and α_2) can be considered to be near to $\pm 90^0$ (as discussed in the previous section), so optimum fractional Fourier angle of first and second quadratic chirp in simulation is taken to be -86.56^0 and 86.56^0 respectively. The mean of the estimated parameters obtained by the separate equations from each quadratic chirp is taken to reduce the parameter estimation error. Similarly, multiple pulses of radar can be added non-coherently to detect weaker targets, using this method [135].

5.7 Conclusion

In this chapter, the theory and application of the GTFT domain matched filter are presented. SNR gain and impulse response of GFMF are derived. GTFT based generalized fractional matched filtering (GFMF) is proposed to detect higher order target parameters with equivalent SNR gain of time domain matched filtering. Simulations of SNR gain comparison are demonstrated to

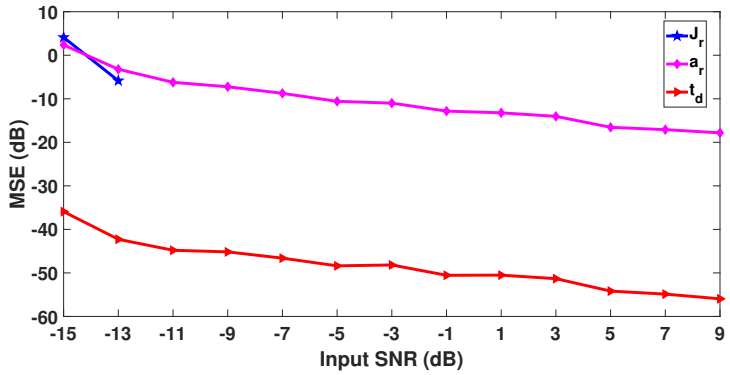

(a) MSE in estimation of jerk, acceleration, time delay

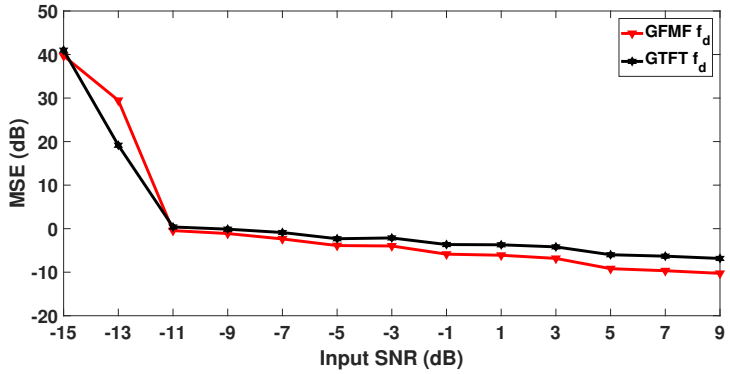

(b) MSE comparison in the estimation of Doppler frequency using GTFT and GFMF method

Figure 5.3: MSE in the estimation of a jerk, acceleration, time delay, and Doppler frequency

show the superior noise performance of GFMF as compared to time domain matched filtering, FrFT, and GTFT in the case of quadratic chirps. Simulation results are presented to show that GFMF gives lesser SNR degradation than time-domain matched filtering for high-speed targets. The double quadratic chirp waveform provides a method for joint estimation of time delay, velocity, acceleration, and jerk with a reasonable accuracy using GFMF. Finally, error analysis in parameter estimation is done for finding appropriate quadratic chirp waveforms to reduce parameter estimation errors.

In the future, higher order waveforms can be analyzed using GFMF by appropriate selection of $h(\cdot)$ in the kernel. Higher order chirp waveforms can be used for joint estimation of target parameters using GFMF. The superiority of GFMF compared to time-domain matched filter can be further demonstrated in case of noise in the form of higher order terms.

Chapter 6

Conclusion and future works

In this thesis, we focused on higher order time-frequency methods, and its application in synthetic aperture radar and conventional ground-based radar for representation, extraction, characterization, and parameter estimation of multicomponent frequency modulated signals. The proposed methods can be applied in different applications such as sonar and biomedical signal processing. Concluding remarks and future work of this thesis are summarized below.

In chapter 2, novel AGFS based on STGTFT is proposed, which can provide a high concentration, high resolution, and cross term free TFD. Matched ck-AGFS at optimum window length resolves the components more precisely than STFT and other TFDs. The TBP of STGTFT for quadratic chirp is shown to be less than the TBP of STFrFT, STFT, and lower bound of TBP of FrAF. The extraction algorithm is demonstrated for signals having closely spaced amplitude-modulated quadratic chirps whose parameters change during the duration of the signal, and ck-AGFS performs better as compared to STFT based spectrogram. AGFS can be used to analyze a large variety of multicomponent frequency-modulated chirp signals by choosing the appropriate $h(\cdot)$ parameter in GTFT kernel. A mathematical derivation of the SNR gain of ck-AGFS for analyzing multicomponent quadratic chirps shows that it is higher than those of GTFT, FrAF, and STFT, and the same was corroborated in simulations. Ck-AGFS based parameter estimation is demonstrated to be better than GTFT and FrAF based parameter estimation by reporting mean errors in parameter estimation. The superiority of LO-ck-AGFS is demonstrated as compared to locally optimized STFrFT based spectrogram for the representation of closely spaced long and short overlapping chirps. LO-ck-AGFS outperformed other well-known TFDs in representing a real multicomponent bat signal. Local optimum window and global optimum window based STGTFT follows the property of index additivity of angle (similar to FrFT),

hence it is computationally efficient. An application of AGFS to estimate higher polynomial phase components in SAR ground moving target imaging is presented, and it can be applied to similar applications, such as radar, sonar, and bio-medical signal processing for representation, extraction, and parameter estimation of multicomponent frequency modulated signals. In the future, AGFS can be used for the representation of a different variety of signals by appropriate selection of the parametric function $h(\cdot)$ in the GTFT kernel. Adaptive time-frequency varying window and different types of window based AGFS can be analyzed for frequency modulated signals. Sigmoid based AGFS can be proposed to work under impulsive noise.

In chapter 3, the proposed method for SAR imaging of moving target gives a decent performance during the non-negligible third order azimuthal phase of the SAR. It successfully corrects the range migrations and generates a focused image of the point target and is able to estimate velocity and tangential acceleration parameters of the SAR moving target. The superiority of ck-AGFS based approach as compared to ck-GTFT based approach is demonstrated, in terms of point target impulse response, SNR Gain, mean estimation error, and target detection probability. In the future, this approach can be validated using real SAR data. Extension of this approach can be explored to correct fourth order range cell migration and estimate higher order parameters of the SAR moving target.

In chapter 4, GFAF and GFWDF, new kind of AF and WDF based on GTFT to estimate the parameter of higher order chirp signals and to analyze higher order radar waveforms are proposed. GFAF can be used to analyze various waveform properties of higher order chirp signals for its suitability as radar waveform. GFAF and GFWVD can be used to estimate a large variety of multicomponent higher order chirp signals by choosing appropriate $h(\cdot)$ function in GTFT kernel. GFAF follows the property of index additivity of angle (similar to FrFT); hence, GFAF is computationally efficient. The computational complexity of GFAF is lesser than generalized CPF, maximum likelihood, and QML estimator for estimating higher order chirp parameters. GFAF is computationally efficient as compared to the GTFT for estimating the same higher order chirp. But as the chirp order increases, the computational complexity for parameter estimation using GFAF increases. In such cases, a combination of correlation and higher order GTFT kernel in GFAF can be used to analyze any higher order chirp with reasonable computational complexity. SNR gain of ck-GFAF for multicomponent cubic frequency modulated signal is less than time domain matched filter but is more than that of FrFT based AF and classical AF. At higher SNR, GFAF estimated parameters follow CRLB estimated parameters. GFAF can provide

better SNR threshold as compared to HAF, and other multi-lag phase differentiation transforms due to the use of a single de-chirping operation. Ck-GFAF is capable of estimating 4^{th} order parameters of all the four components of the real multicomponent bat signal. In the future, GFAF application on SAR ground moving target detection and imaging will be explored further and compared with different techniques. GFAF application can be explored for analyzing properties of different waveforms such as hyperbolic chirp, and sinusoidal frequency modulated waveform. PGFAF with different lag can be used to reduce the effect of cross-terms during multicomponent signal analysis. Smoothening filters can be explored to remove cross-terms of GFAF during multicomponent analysis. Sigmoid based GFAF and sigmoid based GFWVD approach can be proposed to reduce the effect of impulse noise on parameter estimation. Performance of sigmoid based GFAF and sigmoid based GFWVD can be compared with GFAF and GFWVD in the presence of impulsive noise.

In chapter 5, the theory and application of the GTFT domain matched filter are presented. GTFT based generalized fractional matched filtering (GFMF) is proposed to detect higher order target parameters with equivalent SNR gain of time domain matched filtering. Simulations of SNR gain comparison are demonstrated to show the superior noise performance of GFMF as compared to time domain matched filtering, FrFT, and GTFT in the case of quadratic chirps. Simulations are demonstrated to show that GFMF gives lesser SNR degradation than time-domain matched filtering for a high-speed target. Finally, The double quadratic chirp waveform provides a method for joint estimation of time delay, velocity, acceleration, and jerk with a reasonable accuracy using GFMF. Finally, error analysis in parameter estimation is done for finding appropriate double quadratic chirp waveform to reduce parameter estimation errors. In the future, higher order waveform can be analyzed using GTFT domain matched filtering by appropriate selection of $h(\cdot)$ in GTFT kernel. Higher order double chirp waveform can be used for joint estimation of target parameters using GTFT matched filtering. The superiority of generalized fractional matched filter as compared to time-domain matched filter can be demonstrated in the case of higher order chirp noise. Generalized fractional matched filtering based parameter estimation techniques can be analyzed during multiple targets and multiple PRTs scenarios. In the future, higher order waveform can be analyzed using GTFT domain matched filtering by appropriate selection of $h(\cdot)$ in GTFT kernel. Higher order double chirp waveform can be used for joint estimation of target parameters using GTFT matched filtering. The superiority of generalized fractional matched filter as compared to time-domain matched

filter can be demonstrated in the case of higher order chirp noise. Generalized fractional matched filtering based parameter estimation techniques can be analyzed during multiple targets and multiple PRTs scenarios.

List of Publications from the work

Journal paper

[1] Peeyush Sahay, B. S. Teza , Pranav Kulkarni , P. Radhakrishna ,Vikram M. Gadre “Adaptive Generalised Fractional Spectrogram and its Applications”, Circuits, Systems, and Signal Processing, Springer. (Under Revision)

[2] Peeyush Sahay, Izaz Ahamed Shaik Rasheed , Pranav Kulkarni, Shubham Anand Jain , P. Radhakrishna ,Vikram M. Gadre “Generalized Fractional Ambiguity Function and its Applications”, Circuits, Systems, and Signal Processing, Springer. (Under Revision)

Conference paper

[3] Peeyush Sahay, Ameya Anjarlekar, Shubham Anand Jain, P. Radhakrishna, Vikram M. Gadre “Generalized Fractional Matched Filtering and its Applications”, National Conference on Communications. (Under Review)

References

[1] O. Akay and E. Erozden. Use of fractional autocorrelation in efficient detection of pulse compression radar signals. In *First International Symposium on Control, Communications and Signal Processing, 2004.*, pages 33–36, 2004.

[2] Luis B Almeida. The fractional Fourier transform and time-frequency representations. *IEEE Transactions on signal processing*, 42(11):3084–3091, 1994.

[3] François Auger, Patrick Flandrin, Yu-Ting Lin, Stephen McLaughlin, Sylvain Meignen, Thomas Oberlin, and Hau-Tieng Wu. Time-frequency reassignment and synchrosqueezing: An overview. *IEEE Signal Processing Magazine*, 30(6):32–41, 2013.

[4] Md Awal. *Design and optimisation of time-frequency analysis for multichannel neonatal EEG background features in term neonates with hypoxic ischaemic encephalopathy: characterisation, classification and neurodevelopmental outcome prediction*. PhD thesis, University of Queensland, Brisbane, Australia, 2018.

[5] Md Abdul Awal, Samir Ouelha, Shiying Dong, and Boualem Boashash. A robust high-resolution time–frequency representation based on the local optimization of the short-time fractional Fourier transform. *Digital Signal Processing*, 70:125–144, 2017.

[6] X Bai, R Tao, L-J Liu, and J Zhao. Autofocusing of SAR images using STFRFT-based preprocessing. *Electronics Letters*, 48(25):1622–1624, 2012.

[7] R. Baraniuk. Bat echolation chirp. *TX, Houston:DSP Group, Rice University, [online] Available: http://dsp.rice.edu/software/bat-echolocation-chirp*, 2009,.

[8] S. Barbarossa and V. Petrone. Analysis of polynomial-phase signals by the integrated generalized ambiguity function. *IEEE Transactions on Signal Processing*, 45(2):316–327, 1997.

[9] S. Barbarossa, A. Scaglione, and G. B. Giannakis. Product high-order ambiguity function for multicomponent polynomial-phase signal modeling. *IEEE Transactions on Signal Processing*, 46(3):691–708, 1998.

[10] B. Barkat and B. Boashash. Design of higher order polynomial Wigner-Ville distributions. *IEEE Transactions on Signal Processing*, 47(9):2608–2611, 1999.

[11] Braham Barkat and Karim Abed-Meraim. Algorithms for blind components separation and extraction from the time-frequency distribution of their mixture. *EURASIP Journal on Advances in Signal Processing*, 2004(13):2025–2033, 2004.

[12] Boualem Boashash. *Time-Frequency Signal Analysis and Processing: a comprehensive reference*. Academic Press, Orlando, FL, USA, 2015.

[13] Boualem Boashash, Nabeel Ali Khan, and Taoufik Ben-Jabeur. Time-frequency features for pattern recognition using high-resolution TFDs: A tutorial review. *Digital Signal Processing*, 40:1–30, 2015.

[14] Boualem Boashash and Samir Ouelha. Designing high-resolution time–frequency and time–scale distributions for the analysis and classification of non-stationary signals: a tutorial review with a comparison of features performance. *Digital Signal Processing*, 77:120–152, 2018.

[15] S.C. Bradford. *Time-Frequency Analysis of Systems with Changing Dynamic Properties*. PhD thesis, California Institute of Technology,, Pasadena, California, 2006.

[16] Runqing Cao, Ming Li, Lei Zuo, Zeyu Wang, and Yunlong Lu. A new method for parameter estimation of high-order polynomial-phase signals. *Signal Processing*, 142:212–222, 2018.

[17] C Capus and K Brown. Fractional Fourier transform of the gaussian and fractional domain signal support. *IEE Proceedings-Vision, Image and Signal Processing*, 150(2):99–106, 2003.

[18] Chris Capus and Keith Brown. Short-time fractional Fourier methods for the time-frequency representation of chirp signals. *The Journal of the Acoustical Society of America*, 113(6):3253–3263, 2003.

[19] Che Tian-Wen, and Li Bing-Zhao, and Xu Tian-Zhou. The ambiguity function associated with the linear canonical transform. *EURASIP Journal on Advances in Signal Processing*, 2012(1):1–14, 2012.

[20] Victor C Chen. *The Micro-Doppler effect in Radar*. Artech House, Norwood, MA, 2019.

[21] Victor C Chen, David Tahmoush, and William J Miceli. *Radar Micro-Doppler Signatures: Processing and Applications*. Institution of Engineering and Technology, Herts, UK, 2014.

[22] Xiaolong Chen, Yong Huang, Ningbo Liu, Jian Guan, and You He. Radon-fractional ambiguity function-based detection method of low-observable maneuvering target. *IEEE Transactions on Aerospace and Electronic systems*, 51(2):815–833, 2015.

[23] H. . Choi and W. J. Williams. Improved time-frequency representation of multicomponent signals using exponential kernels. *IEEE Transactions on Acoustics, Speech, and Signal Processing*, 37(6):862–871, 1989.

[24] T.A.C.M. Claasen and WFG Mecklenbrauker. The Wigner distribution-A tool for time-frequency signal analysis. *Philips Journal of Research*, 35(3):217–250, 1980.

[25] L. Cohen. Time-frequency distributions-a review. *Proceedings of the IEEE*, 77(7):941–981, 1989.

[26] Leon Cohen. *Time-frequency analysis: theory and applications*. Prentice hall, Englewood Cliffs, NJ, 1995.

[27] Ian G Cumming and Frank H Wong. *Digital processing of Synthetic Aperture Radar data*. Artech house, Norwood, MA, 2005.

[28] P. Cunsuo and R. Tao. A high speed target detection approach based on STFrFT. In *2011 First International Conference on Instrumentation, Measurement, Computer, Communication and Control*, pages 744–747, 2011.

[29] I Djurović, Cornel Ioana, Thayananthan Thayaparan, L Stanković, Pu Wang, V Popović, and M Simeunović. Cubic-phase function evaluation for multicomponent signals with application to SAR imaging. *IET Signal Processing*, 4(4):371–381, 2010.

[30] Igor Djurović and Marko Simeunović. Review of the quasi-maximum likelihood estimator for polynomial phase signals. *Digital Signal Processing*, 72:59–74, 2018.

[31] Igor Djurović, Marko Simeunović, and Pu Wang. Cubic phase function: A simple solution to polynomial phase signal analysis. *Signal Processing*, 135:48–66, 2017.

[32] Igor Djurovic, Thayananthan Thayaparan, and LJubiša Stankovic. SAR imaging of moving targets using polynomial Fourier transform. *IET Signal Processing*, 2(3):237–246, 2008.

[33] MG El-Mashed, Osama Zahran, Moawad I Dessouky, Mohammed El-Kordy, and FE Abd El-Samie. Synthetic aperture radar imaging with fractional Fourier transform and channel equalization. *Digital Signal Processing*, 23(1):151–175, 2013.

[34] S. A. Elgamel, C. Clemente, and J. J. Soraghan. Radar matched filtering using the fractional Fourier transform. In *Sensor Signal Processing for Defence (SSPD 2010)*, pages 1–5, 2010.

[35] D. Gabor. Theory of communication. *Journal of the Institution of Electrical Engineers - Part I: General*, 93(73):429–441, 1947.

[36] S. Golden and B. Friedlander. A modification of the discrete polynomial transform. *IEEE Transactions on Signal Processing*, 46(5):1452–1455, 1998.

[37] F. Hlawatsch and G. F. Boudreaux-Bartels. Linear and quadratic time-frequency signal representations. *IEEE Signal Processing Magazine*, 9(2):21–67, 1992.

[38] Hong-Bo Sun, Guo-Sui Liu, Hong Gu, and Wei-Min Su. Application of the fractional Fourier transform to moving target detection in airborne SAR. *IEEE Transactions on Aerospace and Electronic Systems*, 38(4):1416–1424, 2002.

[39] P. Huang, G. Liao, Z. Yang, Y. Shu, and W. Du. Approach for space-based radar manoeuvring target detection and high-order motion parameter estimation. *IET Radar, Sonar Navigation*, 9(6):732–741, 2015.

[40] P. Huang, G. Liao, Z. Yang, X. Xia, J. Ma, and J. Ma. Long-time coherent integration for weak maneuvering target detection and high-order motion parameter estimation based on keystone transform. *IEEE Transactions on Signal Processing*, 64(15):4013–4026, 2016.

[41] P. Huang, G. Liao, Z. Yang, X. Xia, J. Ma, and X. Zhang. A fast SAR imaging method for ground moving target using a second-order WVD transform. *IEEE Transactions on Geoscience and Remote Sensing*, 54(4):1940–1956, 2016.

[42] P. Huang, G. Liao, Z. Yang, X. Xia, J. Ma, and X. Zhang. An approach for refocusing of ground moving target without target motion parameter estimation. *IEEE Transactions on Geoscience and Remote Sensing*, 55(1):336–350, 2017.

[43] P. Huang, X. Xia, G. Liao, and Z. Yang. Ground moving target imaging based on keystone transform and coherently integrated CPF with a single-channel SAR. *IEEE Journal of Selected Topics in Applied Earth Observations and Remote Sensing*, 10(12):5686–5694, 2017.

[44] P. Huang, X. Xia, G. Liao, Z. Yang, J. Zhou, and X. Liu. Ground moving target refocusing in SAR imagery using scaled GHAF. *IEEE Transactions on Geoscience and Remote Sensing*, 56(2):1030–1045, 2018.

[45] Penghui Huang, Guisheng Liao, Zhiwei Yang, Xiang-Gen Xia, Jingtao Ma, and Jibin Zheng. Ground maneuvering target imaging and high-order motion parameter estimation based on second-order keystone and generalized Hough-HAF transform. *IEEE Transactions on Geoscience and Remote Sensing*, 55(1):320–335, 2017.

[46] H. Huiling and P. Cunsuo. The impact of high-order phase in ballistic missiles detection. In *Third International Conference on Measuring Technology and Mechatronics Automation*, pages 827–830, 2011.

[47] Dmytro Iatsenko, Peter VE McClintock, and Aneta Stefanovska. Linear and synchrosqueezed time–frequency representations revisited: Overview, standards of use, resolution, reconstruction, concentration, and algorithms. *Digital Signal Processing*, 42:1–26, 2015.

[48] Jianyu Yang, Pu Wang, and Jintao Xiong. An algorithm for parameter estimation of multicomponent chirp signals. In *2006 IEEE International Conference on Acoustics Speech and Signal Processing Proceedings*, pages III–III. IEEE, 2006.

[49] Douglas L Jones and Thomas W Parks. A high resolution data-adaptive time-frequency representation. *IEEE Transactions on Acoustics, Speech, and Signal Processing*, 38(12):2127–2135, 1990.

[50] V. Katkovnik. A new form of the Fourier transform for time-varying frequency estimation. In *Proceedings of ISSE'95 - International Symposium on Signals, Systems and Electronics*, pages 179–182, 1995.

[51] Nabeel Ali Khan and Boualem Boashash. Instantaneous frequency estimation of multicomponent nonstationary signals using multiview time-frequency distributions based on the adaptive fractional spectrogram. *IEEE Signal Processing Letters*, 20(2):157–160, 2013.

[52] L. Kong, X. Li, G. Cui, W. Yi, and Y. Yang. Coherent integration algorithm for a maneuvering target with high-order range migration. *IEEE Transactions on Signal Processing*, 63(17):4474–4486, 2015.

[53] Sanjay Kumar and Rajiv Saxena. FrMF: Fractional Fourier matched filter. *Circuits, Systems, and Signal Processing*, 37(1):49–80, 2018.

[54] Mika Levonen and McLaughlin Stephen. Fractional Fourier transform techniques applied to active sonar. In *Oceans 2003. Celebrating the Past ... Teaming Toward the Future (IEEE Cat. No.03CH37492)*, pages 1894 – 1899, 2003.

[55] Li Li and Tianshuang Qiu. A novel phase parameter estimation method of quadratic FM signal based on Sigmoid fractional ambiguity function in impulsive noise environment. *AEU-International Journal of Electronics and Communications*, 93:268–276, 2018.

[56] Li Li, Nicolas H Younan, and Xiaofei Shi. Joint estimation of Doppler stretch and time delay of wideband echoes for LFM pulse radar based on Sigmoid-FRFT transform under the impulsive noise environment. *Electronics*, 8(2):121, 2019.

[57] X. Li, G. Cui, W. Yi, and L. Kong. Fast coherent integration for maneuvering target with high-order range migration via TRT-SKT-LVD. *IEEE Transactions on Aerospace and Electronic Systems*, 52(6):2803–2814, 2016.

[58] Xiumei Li, Guoan Bi, and Yingtuo Ju. Quantitative SNR analysis for ISAR imaging using LPFT. *IEEE Transactions on Aerospace and Electronic Systems*, 45(3):1241–1248, 2009.

[59] Xiumei Li, Guoan Bi, Srdjan Stankovic, and Abdelhak M Zoubir. Local polynomial Fourier transform: A review on recent developments and applications. *Signal Processing*, 91(6):1370–1393, 2011.

[60] A. Liu, L. Chen, F. Zhao, and G. Kuang. A novel multi-channel SAR-GMTI algorithm based on raw data. In *3rd International Congress on Image and Signal Processing*, pages 1489–1493, 2010.

[61] Jian-Guo Liu and Bing-Cheng Yuan. The analysis and simulation of the detectors based on FRFT statistic performance. In *2008 Asia Simulation Conference-7th International Conference on System Simulation and Scientific Computing*, pages 1543–1548, 2008.

[62] Shengheng Liu, Yahui Ma, and Tao Shan. Segmented discrete polynomial-phase transform with coprime sampling. *The Journal of Engineering*, 2019(19):5619–5621, 2019.

[63] Shengheng Liu, Tao Shan, Ran Tao, Yimin D Zhang, Guo Zhang, Feng Zhang, and Yue Wang. Sparse discrete fractional Fourier transform and its applications. *IEEE Transactions on Signal Processing*, 62(24):6582–6595, 2014.

[64] Shengheng Liu, Tao Shan, Yimin D Zhang, Ran Tao, and Yuan Feng. A fast algorithm for multi-component LFM signal analysis exploiting segmented DPT and SDFrFT. In *2015 IEEE Radar Conference (RadarCon)*, pages 1139–1143, 2015.

[65] Shengheng Liu, Yimin D Zhang, and Tao Shan. Detection of weak astronomical signals with frequency-hopping interference suppression. *Digital Signal Processing*, 72:1–8, 2018.

[66] J. A. Scheer M. A. Richards and W. A. Holm. *Principles of Modern Radar: Basic Principles*. Scitech Publishing, Raleigh, NC, 2010.

[67] Y. Ma and Y. Kong. FRFT based on joint estimation time delay and radial velocity of underwater target. In *Third International Congress on Image and Signal Processing*, pages 4074–4078, Oct 2010.

[68] Stphane Mallat. *A Wavelet Tour of Signal Processing, Third Edition: The Sparse Way*. Academic Press, Inc., 2008.

[69] Alfred Mertins. *Signal Analysis: Wavelets, Filter Banks, Time-Frequency Transforms and Applications*. John Wiley & Sons, Inc., 1999.

[70] A. Moreira, P. Prats-Iraola, M. Younis, G. Krieger, I. Hajnsek, and K. P. Papathanassiou. A tutorial on synthetic aperture radar. *IEEE Geoscience and Remote Sensing Magazine*, 1(1):6–43, 2013.

[71] X. Ning, L. Guo, and X. Sha. Joint time delay and frequency offset estimation based on fractional Fourier transform. In *2012 International Conference on ICT Convergence (ICTC)*, pages 318–322, 2012.

[72] P. O'Shea. A fast algorithm for estimating the parameters of a quadratic FM signal. *IEEE Transactions on Signal Processing*, 52(2):385–393, 2004.

[73] Haldun M Ozaktas, Orhan Arikan, M Alper Kutay, and Gozde Bozdagt. Digital computation of the fractional Fourier transform. *IEEE Transactions on signal processing*, 44(9):2141–2150, 1996.

[74] S. Pei and J. Ding. Relations between gabor transforms and fractional Fourier transforms and their applications for signal processing. *IEEE Transactions on Signal Processing*, 55(10):4839–4850, 2007.

[75] Soo-Chang Pei and Shih-Gu Huang. STFT with adaptive window width based on the chirp rate. *IEEE Transactions on Signal Processing*, 60(8):4065–4080, 2012.

[76] S. Peleg and B. Friedlander. The discrete polynomial-phase transform. *IEEE Transactions on Signal Processing*, 43(8):1901–1914, 1995.

[77] S. Peleg and B. Porat. Estimation and classification of polynomial-phase signals. *IEEE Transactions on Information Theory*, 37(2):422–430, 1991.

[78] S. Peleg and B. Porat. Linear FM signal parameter estimation from discrete-time observations. *IEEE Transactions on Aerospace and Electronic Systems*, 27(4):607–616, 1991.

[79] Ramona Pelich, Nicolas Longépé, Grégoire Mercier, Guillaume Hajduch, and René Garello. Vessel refocusing and velocity estimation on SAR imagery using the fractional

Fourier transform. *IEEE Transactions on Geoscience and Remote Sensing*, 54(3):1670–1684, 2016.

[80] Bo Peng, Xizhang Wei, Bin Deng, Haowen Chen, Zhen Liu, and Xiang Li. A sinusoidal frequency modulation Fourier transform for radar-based vehicle vibration estimation. *IEEE Transactions on Instrumentation and Measurement*, 63(9):2188–2199, 2014.

[81] Bo Peng, Xizhang Wei, Bin Deng, Haowen Chen, Zhen Liu, and Xiang Li. A sinusoidal frequency modulation Fourier transform for radar-based vehicle vibration estimation. *IEEE Transactions on Instrumentation and Measurement*, 63(9):2188–2199, 2014.

[82] RP Perry, RC Dipietro, and RL Fante. SAR imaging of moving targets. *IEEE Transactions on Aerospace and Electronic Systems*, 35(1):188–200, 1999.

[83] Gaurav Pooniwala. The generalised time frequency transform: Properties and application. B.tech. thesis, Indian Institute of Technology, Bombay, Mumbai, India, 2014.

[84] Vesna Popović, Igor Djurović, LJubiša Stanković, Thayananthan Thayaparan, and Miloš Daković. Autofocusing of SAR images based on parameters estimated from the PHAF. *Signal Processing*, 90(5):1382–1391, 2010.

[85] B. Porat and B. Friedlander. Asymptotic statistical analysis of the high-order ambiguity function for parameter estimation of polynomial-phase signals. *IEEE Transactions on Information Theory*, 42(3):995–1001, 1996.

[86] Tian-Shuang Qiu and Li Li. A novel joint parameter estimation method based on fractional ambiguity function in bistatic multiple-input multiple-output radar system. *Computers & Electrical Engineering*, 39(4):1248–1259, 2013.

[87] P. Rao and F. J. Taylor. Estimation of instantaneous frequency using the discrete Wigner distribution. *Electronics Letters*, 26(4):246–248, 1990.

[88] B. Ristic and B. Boashash. Kernel design for time-frequency signal analysis using the Radon transform. *IEEE Transactions on Signal Processing*, 41(5):1996–2008, 1993.

[89] B. Ristic and B. Boashash. Instantaneous frequency estimation of quadratic and cubic FM signals using the cross polynomial Wigner-Ville distribution. *IEEE Transactions on Signal Processing*, 44(6):1549–1553, 1996.

[90] A Roenko, I Djurović, V Lukin, and A Zelensky. Accuracy improvement of the Wigner distribution estimate in non-Gaussian noise environment by means of clipping technique application. In *2008 International Conference on" Modern Problems of Radio Engineering, Telecommunications and Computer Science"(TCSET)*, pages 362–365, 2008.

[91] Bing-Zhao Li Rui-Feng Bai and Qi-Yuan Cheng. Wigner-Ville distribution associated with the linear canonical transform. *Journal of Applied Mathematics*, pages 1–14, 2012.

[92] Shishir Sahay, Deepak Pande, Naval Wing, Vikram Gadre, and Prashant Sohani. A novel generalized time-frequency transform inspired by the fractional Fourier transform for higher order chirps. In *International Conference on Signal Processing and Communications (SPCOM)*, pages 1–5, 2012.

[93] Shishir B Sahay, T Meghasyam, Rahul K Roy, Gaurav Pooniwala, Sasank Chilamkurthy, and Vikram Gadre. Parameter estimation of linear and quadratic chirps by employing the fractional Fourier transform and a generalized time frequency transform. *Sadhana*, 40(4):1049–1075, 2015.

[94] Shishir Brijendra Sahay. *Parameter Estimation of Chirp Signals*. PhD thesis, Indian Institute of Technology, Bombay, Mumbai, India, 2015.

[95] E. Sejdic, I. Djurovic, and L. Stankovic. Quantitative performance analysis of scalogram as instantaneous frequency estimator. *IEEE Transactions on Signal Processing*, 56(8):3837–3845, 2008.

[96] E. Sejdic, L. Stankovic, M. Dakovic, and J. Jiang. Instantaneous frequency estimation using the s-transform. *IEEE Signal Processing Letters*, 15:309–312, 2008.

[97] Ervin Sejdić, Igor Djurović, and Jin Jiang. Time–frequency feature representation using energy concentration: An overview of recent advances. *Digital Signal Processing*, 19(1):153–183, 2009.

[98] Ervin Sejdić, Igor Djurović, and LJubiša Stanković. Fractional Fourier transform as a signal processing tool: An overview of recent developments. *Signal Processing*, 91(6):1351–1369, 2011.

[99] J. J. Sharma, C. H. Gierull, and M. J. Collins. The influence of target acceleration on velocity estimation in dual-channel SAR-GMTI. *IEEE Transactions on Geoscience and Remote Sensing*, 44(1):134–147, 2006.

[100] Sudarshan Shinde and Vikram M Gadre. An uncertainty principle for real signals in the fractional Fourier transform domain. *IEEE Transactions on Signal Processing*, 49(11):2545–2548, 2001.

[101] Shujuan Peng, Debao Ma, and Jianlin Lin. Fractional Fourier transform for moving target detection and location in spaceborne SAR. In *International Conference on Information and Automation*, pages 485–488, 2008.

[102] M. Simeunovic and I. Djurovic. CPF-HAF estimator of polynomial-phase signals. *Electronics Letters*, 47(17):965–966, 2011.

[103] Marko Simeunović, Slobodan Djukanović, and Igor Djurović. A fine search method for the cubic-phase function-based estimator. In *2012 Proceedings of the 20th European Signal Processing Conference (EUSIPCO)*, pages 924–928, 2012.

[104] Marko Simeunović and Igor Djurović. A method for efficient maximization of PPS estimation functions. *Digital Signal Processing*, 84:38–45, 2019.

[105] Y. E. Song, C. Wang, and P. Shi. Algorithm based on the linear canonical transform for QFM signal parameters estimation. *IET Signal Processing*, 10(3):318–324, 2016.

[106] Yu-E Song, Xiao-Yan Zhang, Chun-Heng Shang, Hong-Xia Bu, and Xiao-Yan Wang. The Wigner-Ville distribution based on the linear canonical transform and its applications for QFM signal parameters estimation. *Journal of Applied Mathematics*, pages 1–8, 2014.

[107] Ljubisa Stankovic, Milos Dakovic, and Thayannathan Thayaparan. *Time-Frequency Signal Analysis with Applications*. Artech house, Norwood, MA, USA, 2014.

[108] Sebastian Starosielec and Daniel Hägele. Discrete-time windows with minimal rms bandwidth for given rms temporal width. *Signal Processing*, 102:240–246, 2014.

[109] Vladimir Stojanovic and Vojislav Filipovic. Adaptive input design for identification of output error model with constrained output. *Circuits, Systems, and Signal Processing*, 33(1):97–113, 2014.

[110] Vladimir Stojanovic and Novak Nedic. Robust Kalman filtering for nonlinear multivariable stochastic systems in the presence of non-Gaussian noise. *International Journal of Robust and Nonlinear Control*, 26(3):445–460, 2016.

[111] R. Tao, Y. E. Song, Z. J. Wang, and Y. Wang. Ambiguity function based on the linear canonical transform. *IET Signal Processing*, 6(6):568–576, 2012.

[112] R. Tao, F. Zhang, and Y. Wang. Fractional power spectrum. *IEEE Transactions on Signal Processing*, 56(9):4199–4206, 2008.

[113] Ran Tao, Bing Deng, Wei-Qiang Zhang, and Yue Wang. Sampling and sampling rate conversion of band limited signals in the fractional Fourier transform domain. *IEEE Transactions on Signal Processing*, 56(1):158–171, 2008.

[114] Ran Tao, Xue-Mei Li, Yan-Lei Li, and Yue Wang. Time-delay estimation of chirp signals in the fractional Fourier domain. *IEEE Transactions on Signal Processing*, 57(7):2852–2855, 2009.

[115] Ran Tao, Yan-Lei Li, and Yue Wang. Short-time fractional Fourier transform and its applications. *IEEE Transactions on Signal Processing*, 58(5):2568–2580, 2010.

[116] Thayananthan Thayaparan, LJ Stankovic, Chris Wernik, and Miloš Dakovic. Real-time motion compensation, image formation and image enhancement of moving targets in ISAR and SAR using s-method-based approach. *IET Signal Processing*, 2(3):247–264, 2008.

[117] K. Tomiyasu. Tutorial review of synthetic-aperture radar (SAR) with applications to imaging of the ocean surface. *Proceedings of the IEEE*, 66(5):563–583, May 1978.

[118] P. Wang, H. Li, I. Djurovic, and B. Himed. Integrated cubic phase function for linear FM signal analysis. *IEEE Transactions on Aerospace and Electronic Systems*, 46(3):963–977, 2010.

[119] Wen-Qin Wang. Moving target indication via three-antenna SAR with simplified fractional Fourier transform. *EURASIP Journal on Advances in Signal Processing*, 2011(1):117–127, 2011.

[120] K. M. Wong and Q. Jin. Estimation of the time-varying frequency of a signal: the Cramer-Rao bound and the application of Wigner distribution. *IEEE Transactions on Acoustics, Speech, and Signal Processing*, 38(3):519–536, 1990.

[121] J. Wu, Y. Jiang, G. Kuang, J. Lu, and Z. Li. Parameter estimation for SAR moving target detection using fractional Fourier transform. In *2014 IEEE Geoscience and Remote Sensing Symposium*, pages 596–599, 2014.

[122] Xiang-Gen Xia, Genyuan Wang, and Victor C Chen. Quantitative SNR analysis for ISAR imaging using joint time-frequency analysis-short time Fourier transform. *IEEE Transactions on Aerospace and Electronic systems*, 38(2):649–659, 2002.

[123] Zhao Xinghao, Tao Ran, and Deng Bing. Practical normalization methods in the digital computation of the fractional Fourier transform. In *Proceedings of 7th International Conference on Signal Processing*, pages 105–108, 2004.

[124] Manman Xu and Wei Tang. Multi-component LFM signal filtering based on the short-time fractional Fourier transform. In *Proceedings of the 32nd Chinese Control Conference*, pages 4507–4512, 2013.

[125] Z. Yan, J. Zhang, F. Fan, S. Che, and H. Zhao. Parameters extraction of linear FM signal using fractional autocorrelation. In *2010 International Conference on Intelligent Control and Information Processing*, pages 102–105, 2010.

[126] J. Yang, Y. Zhang, and X. Kang. A doppler ambiguity tolerated algorithm for airborne SAR ground moving target imaging and motion parameters estimation. *IEEE Geoscience and Remote Sensing Letters*, 12(12):2398–2402, 2015.

[127] Jian Yang. *Study on Ground Moving Target Indication and Imaging Technique of Airborne SAR*. PhD thesis, Chinese Academy of Sciences, China, 2017.

[128] Jian Yang, Chang Liu, and Yanfei Wang. Detection and imaging of ground moving targets with real SAR data. *IEEE Transactions on Geoscience and Remote Sensing*, 53(2):920–932, 2015.

[129] Jiefang Yang and Yunhua Zhang. An airborne SAR moving target imaging and motion parameters estimation algorithm with azimuth-dechirping and the second-order keystone

transform applied. *IEEE Journal of Selected Topics in Applied Earth Observations and Remote Sensing*, 8(8):3967–3976, 2015.

[130] Y Yang, ZK Peng, XJ Dong, WM Zhang, and G Meng. General parameterized time-frequency transform. *IEEE Transactions on Signal Processing*, 62(11):2751–2764, 2014.

[131] Yang Yang, Zhike Peng, Xingjian Dong, Wenming Zhang, and Guang Meng. Application of parameterized time-frequency analysis on multicomponent frequency modulated signals. *IEEE Transactions on Instrumentation and Measurement*, 63(12):3169–3180, 2014.

[132] Yang Yang, Zhike Peng, Wenming Zhang, and Guang Meng. Parameterised time-frequency analysis methods and their engineering applications: A review of recent advances. *Mechanical Systems and Signal Processing*, 119:182–221, 2019.

[133] Yang Yang, Wenming Zhang, Zhike Peng, and Guang Meng. Multicomponent signal analysis based on polynomial chirplet transform. *IEEE Transactions on Industrial Electronics*, 60(9):3948–3956, 2013.

[134] Ahmed I Zayed. A convolution and product theorem for the fractional Fourier transform. *IEEE Signal processing letters*, 5(4):101–103, 1998.

[135] L. Zhan, Z. Tang, and Z. Zhu. Application of FRFT in the detection and parameter estimation of accelerating weak targets. In *IEEE 12th International Conference on Computer and Information Technology*, pages 470–476, Oct 2012.

[136] F. Zhang, R. Tao, and Y. Wang. Analysis and processing for chirp pulse with matched FRFT. In *2012 Second International Conference on Instrumentation, Measurement, Computer, Communication and Control*, pages 5–9, 2012.

[137] F. Zhang, R. Tao, and Y. Wang. Matched filtering in fractional Fourier domain. In *2012 Second International Conference on Instrumentation, Measurement, Computer, Communication and Control*, pages 1–4, 2012.

[138] J. Zhang, T. Su, J. Zheng, and X. He. Novel fast coherent detection algorithm for radar maneuvering target with jerk motion. *IEEE Journal of Selected Topics in Applied Earth Observations and Remote Sensing*, 10(5):1792–1803, 2017.

[139] W. Zhang, R. Tao, and Y. Li. A novel method of SAR multiple moving targets detection and parameter estimation. In *2nd Asian-Pacific Conference on Synthetic Aperture Radar*, pages 193–196, 2009.

[140] Z. Zhang and M. Luo. New integral transforms for generalizing the Wigner distribution and ambiguity function. *IEEE Signal Processing Letters*, 22(4):460–464, 2015.

[141] Zhi-Chao Zhang. Novel Wigner distribution and ambiguity function associated with the linear canonical transform. *Optik - International Journal for Light and Electron Optics*, 127(12):4995 – 5012, 2016.

[142] Jian-dong Zhu, Jin-liang Li, Xiang-dong Gao, Li-Bang Ye, and Huan-yao Dai. Adaptive threshold detection and estimation of linear frequency-modulated continuous-wave signals based on periodic fractional Fourier transform. *Circuits, Systems, and Signal Processing*, 35(7):2502–2517, 2016.

[143] S. Zhu, G. Liao, D. Yang, and H. Tao. A new method for radar high-speed maneuvering weak target detection and imaging. *IEEE Geoscience and Remote Sensing Letters*, 11(7):1175–1179, 2014.

[144] Lei Zuo, Ming Li, Zheng Liu, and Lin Ma. A high-resolution time-frequency rate representation and the cross-term suppression. *IEEE Transactions on Signal Processing*, 64(10):2463–2474, 2016.